REPORT NO. FAA-RD-76-20-I

# AN ANALYSIS OF RADIO FREQUENCY SURVEILLANCE SYSTEMS FOR AIR TRAFFIC CONTROL
## Volume I: Text

Louis A. Kleiman


FEBRUARY 1976
FINAL REPORT





Prepared for
U.S. DEPARTMENT OF TRANSPORTATION
FEDERAL AVIATION ADMINISTRATION
Systems Research and Development Service
Washington DC 20591

# DISCLAIMER NOTICE

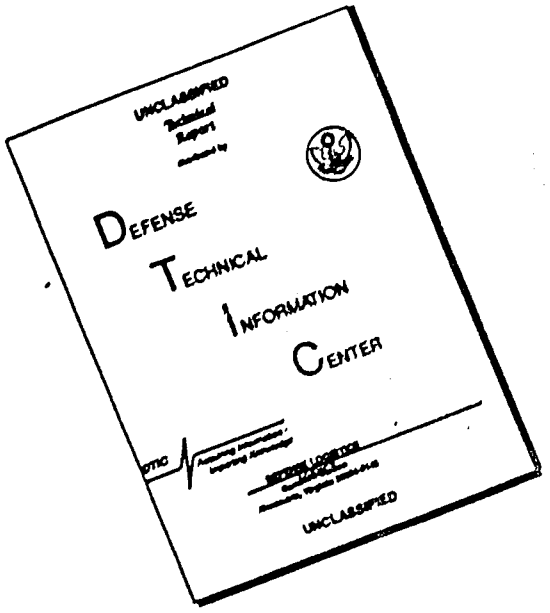


THIS DOCUMENT IS BEST QUALITY AVAILABLE. THE COPY FURNISHED TO DTIC CONTAINED A SIGNIFICANT NUMBER OF PAGES WHICH DO NOT REPRODUCE LEGIBLY.

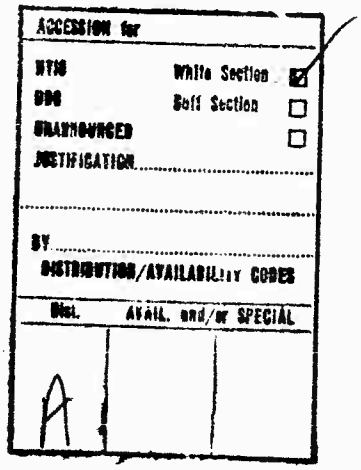

TECHNICAL REPORT STANDARD TITLE PAGE

| 1. Report No. | 2. Government Accession No. | 3. Recipient's Catalog No. |
|---|---|---|
| FAA-RD-76-20-Vol-1 | | |

4. Title and Subtitle
AN ANALYSIS OF RADIO FREQUENCY SURVEILLANCE SYSTEMS FOR AIR TRAFFIC CONTROL
Volume I: Text

5. Report Date
Feb 1976

6. Performing Organization Code

7. Author(s)
Louis A. Kleiman

8. Performing Organization Report No.
TSC-FAA-75-10-Vol-1

9. Performing Organization Name and Address
U.S. Department of Transportation
Transportation Systems Center
Kendall Square
Cambridge MA 02142

10. Work Unit No.
FA510/R6117

11. Contract or Grant No.

12. Sponsoring Agency Name and Address
U.S. Department of Transportation
Federal Aviation Administration
Systems Research and Development Service
Washington DC 20591

13. Type of Report and Period Covered
Final Report.
Sep 1974 — May 1975

14. Sponsoring Agency Code

15. Supplementary Notes
*This report is a doctoral thesis by the author.

225 p.

16. Abstract

Performance criteria that afford quantitative evaluation of a variety of current and proposed configurations of the Air Traffic Control Radar Beacon System (ATCRBS) are described in detail. Two analytic system models are developed to allow application of these performance criteria. A simple system model, based on the assumption of a flat earth, enables closed-form analytic expressions for some of the performance criteria to be developed for a wide range of desired areas of coverage. An extremely accurate complex system model provides a tool for simulation of operating characteristics that would be observed in the course of actual flight tests. The complex model includes a new solution for the grazing angle of radiation over a spherical earth that is shown to be more accurate than the commonly-used solution of Fishback. Applications and limitations of both models in the evaluation of four new ATCRBS antennas and of the proposed receiver side-lobe suppression feature are discussed. Both numerical results and a computer-generated representation of an air traffic controller's display are presented.

| 17. Key Words | 18. Distribution Statement |
|---|---|
| ATCRBS, Air Traffic Control, Radar Beacons, Surveillance, Radar, Propagation, Simulation | DOCUMENT IS AVAILABLE TO THE PUBLIC THROUGH THE NATIONAL TECHNICAL INFORMATION SERVICE, SPRINGFIELD, VIRGINIA 22161 |

| 19. Security Classif. (of this report) | 20. Security Classif. (of this page) | 21. No. of Pages | 22. Price |
|---|---|---|---|
| Unclassified | Unclassified | 224 | |

Form DOT F 1700.7 (8-69)

## PREFACE

This report was submitted as a thesis to the Department of Aeronautics and Astronautics at the Massachusetts Institute of Technology (MIT) in partial fulfillment of the requirements for the degree of Doctor of Science in Instrumentation. Dr. Kleiman's thesis research was sponsored by the Transportation Systems Center (TSC) in support of the continuing effort of the Federal Aviation Administration to improve the performance of the Air Traffic Control Radar Beacon System. The thesis, published with the permission of MIT, is directly applicable to many of the projects with which the author was involved at TSC prior to graduate study.

The author is grateful to his thesis committee, Dr. Thomas J. Goblick, Jr. of the MIT Lincoln Laboratory, Prof. Robert W. Simpson, and Prof. Walter Wrigley, for specific advice in their respective fields of expertise and for general suggestions regarding organization of the thesis. He is especially grateful to Prof. Walter M. Hollister, thesis committee chairman, whose enthusiastic support and day-to-day guidance proved invaluable. The practical advice, inspiration, and facilities provided by Prof. Winston R. Markey are also very much appreciated.

James E. Kuhn of TSC provided many enlightening technical discussions in the course of research. Both he and Paul E. Manning of TSC provided the author with the opportunity to remain abreast of those activities that might affect, or be affected by, the results of the thesis.

# TABLE OF CONTENTS


| CHAPTERS | VOLUME I | PAGE |
|---|---|---|
| 1 | INTRODUCTION | |
| | 1.1 Recent Developments in Air Traffic Control | 17 |
| | 1.2 Related Efforts in the Field of the Thesis | 24 |
| | 1.3 Objectives of the Thesis | 26 |
| | 1.4 Summary of the Contents of the Thesis | 28 |
| 2 | DESCRIPTION OF THE AIR TRAFFIC CONTROL RADAR BEACON SYSTEM | |
| | 2.1 References | 30 |
| | 2.2 General Description | 30 |
| | 2.3 Interrogator Operation | 31 |
| | 2.4 Transponder Operation | 34 |
| | 2.5 Receiver Operation | 37 |
| | 2.6 Operating Problems | 38 |
| 3 | DEVELOPMENT OF PERFORMANCE CRITERIA | |
| | 3.1 Introduction | 42 |
| | 3.2 System Coverage | 43 |
| | 3.3 Contribution to System Interference | 50 |
| | 3.4 Susceptibility to External Interference | 53 |
| | 3.5 Susceptibility to Self-Interference | 55 |
| | 3.6 Target Quality | 57 |

| CHAPTERS | | PAGE |
|---|---|---|
| 4 | A SIMPLE FLAT-EARTH MODEL OF ATCRBS OPERATION | |
| | 4.1 Introduction | 59 |
| | 4.2 Ray Propagation over a Flat Earth | 60 |
| | 4.3 System Coverage Area | 74 |
| | 4.4 Parametric Changes for the Downlink | 79 |
| | 4.5 Receiver Sensitivity-Time Control | 80 |
| | 4.6 The Spherical-Earth-Horizon Barrier | 81 |
| | 4.7 Desired Coverage Boundary | 83 |
| | 4.8 Intersection of Lobing and Coverage Contours | 83 |
| | 4.9 Desired Coverage Area | 85 |
| 5 | A COMPLEX SPHERICAL-EARTH MODEL OF ATCRBS OPERATION | |
| | 5.1 Introduction | 86 |
| | 5.2 Propagation over a Spherical Earth | 87 |
| | 5.3 Reflection Coefficient | 91 |
| | 5.4 The Grazing Angle | 93 |
| | 5.5 Indirect Path Length | 100 |
| | 5.6 Lower Limit of Grazing Angle | 100 |
| | 5.7 Surface Roughness | 101 |
| | 5.8 Transponder Operation | 104 |
| | 5.9 Receiver Side-Lobe Suppression | 106 |
| | 5.10 Aircraft Flight Profiles | 109 |

| CHAPTERS | | PAGE |
|---|---|---|
| 6 | APPLICATIONS OF THE MODELS | |
| | 6.1 Introduction | 112 |
| | 6.2 Inputs to the Models | 113 |
| | 6.3 Model Validation | 116 |
| | 6.4 Antenna Performance in a Standard En Route Configuration | 130 |
| | 6.5 Antenna Performance in a Standard Terminal Configuration | 162 |
| | 6.6 Antenna Performance in an Adjusted Terminal Configuration | 192 |
| | 6.7 Performance of Receiver Side-Lobe Suppression | 212 |
| 7 | CONCLUSIONS AND RECOMMENDATIONS | |
| | 7.1 Conclusions Concerning Methods of the Thesis | 217 |
| | 7.2 Conclusions Concerning Applications of the Thesis | 220 |
| | 7.3 Specific Contributions of the Thesis | 221 |
| | 7.4 Recommendations for Further Study | 222 |

| APPENDICES | VOLUME II | |
|---|---|---|
| A | PROCEDURE TO DETERMINE A LEAST-SQUARES FIT FOR ANTENNA PATTERNS | 225 |
| B | DERIVATION OF MAGNITUDE AND PHASE OF THE COMPLEX REFLECTION COEFFICIENT | 231 |
| C | RADIATION PATTERNS USED IN APPLICATIONS OF THE MODELS | 234 |
| REFERENCES | | 294 |

FIGURES VOLUME I PAGE


| | | |
|---|---|---|
| 3.1 | Typical Vertical Lobing Contours | 45 |
| 3.2 | False Suppression of a Valid Target | 47 |
| 4.1 | Geometry of Ray Propagation over a Flat Earth | 60 |
| 4.2 | Flow Diagram for ATCRBS Interrogations | 62 |
| 4.3 | Free-Space Vertical Radiation Pattern of Standard ATCRBS Antenna | 64 |
| 4.4 | Vector Sum of Direct and Reflected Rays | 66 |
| 4.5 | Distance to the Horizon over a Spherical Earth | 82 |
| 5.1 | Geometry of Ray Propagation over a Spherical Earth | 87 |
| 6.1 | 5000-Ft Flight Test, FA-8043 Antenna, Low Interrogator Power | 118 |
| 6.2 | Simulated 5000-Ft Flight, FA-8043 Antenna, Low Interrogator Power | 119 |
| 6.3 | 5000-Ft Flight Test, FA-8043 Antenna, High Interrogator Power | 122 |
| 6.4 | Simulated 5000-Ft Flight, FA-8043 Antenna, High Interrogator Power | 123 |
| 6.5 | 5000-Ft Flight Test, FA-8043 Antenna, Showing Target Detail Inside 25 NM | 125 |
| 6.6 | 5000-Ft Flight Test, Hazeltine Antenna, Low Interrogator Power | 126 |
| 6.7 | Simulated 5000-Ft Flight, Hazeltine Antenna, Low Interrogator Power | 127 |
| 6.8 | 5000-Ft Flight Test, Hazeltine Antenna, High Interrogator Power | 128 |
| 6.9 | Simulated 5000-Ft Flight, Hazeltine Antenna, High Interrogator Power | 129 |

FIGURES PAGE


| | | |
|---|---|---|
| 6.10 | Simulated 5000-Ft Flight, FA-8043 Antenna, Roughness Parameter H=10 Ft | 131 |
| 6.11 | Vertical Lobing Contours, System 1 | 134 |
| 6.12 | Vertical Lobing Contours, System 2 | 135 |
| 6.13 | Vertical Lobing Contours, System 3 | 136 |
| 6.14 | Vertical Lobing Contours, System 4 | 137 |
| 6.15 | Vertical Lobing Contours, System 5 | 138 |
| 6.16 | False Suppression Contours, System 1 | 139 |
| 6.17 | False Suppression Contours, System 2 | 140 |
| 6.18 | False Suppression Contours, System 3 | 141 |
| 6.19 | False Suppression Contours, System 4 | 142 |
| 6.20 | False Suppression Contours, System 5 | 143 |
| 6.21 | Simulated Flight at 12,000 Ft, System 1 | 147 |
| 6.22 | Simulated Flight at 12,000 Ft, System 2 | 148 |
| 6.23 | Simulated Flight at 12,000 Ft, System 3 | 149 |
| 6.24 | Simulated Flight at 12,000 Ft, System 4 | 150 |
| 6.25 | Simulated Flight at 12,000 Ft, System 5 | 151 |
| 6.26 | Simulated Flight at 40,000 Ft, System 1 | 152 |
| 6.27 | Simulated Flight at 40,000 Ft, System 2 | 153 |
| 6.28 | Simulated Flight at 40,000 Ft, System 3 | 154 |
| 6.29 | Simulated Flight at 40,000 Ft, System 4 | 155 |
| 6.30 | Simulated Flight at 40,000 Ft, System 5 | 156 |
| 6.31 | Vertical Lobing Contours, System 6 | 165 |
| 6.32 | Vertical Lobing Contours, System 7 | 166 |

FIGURES PAGE


| | | |
|---|---|---|
| 6.33 | Vertical Lobing Contours, System 8 | 167 |
| 6.34 | Vertical Lobing Contours, System 9 | 168 |
| 6.35 | False Suppression Contours, System 6 | 169 |
| 6.36 | False Suppression Contours, System 7 | 170 |
| 6.37 | False Suppression Contours, System 8 | 171 |
| 6.38 | False Suppression Contours, System 9 | 172 |
| 6.39 | Simulated Flight at 2000 Ft, System 6 | 175 |
| 6.40 | Simulated Flight at 2000 Ft, System 7 | 176 |
| 6.41 | Simulated Flight at 2000 Ft, System 8 | 177 |
| 6.42 | Simulated Flight at 2000 Ft, System 9 | 178 |
| 6.43 | Simulated Flight at 2000 Ft, System 10 | 179 |
| 6.44 | Simulated Flight at 5000 Ft, System 8 | 180 |
| 6.45 | Simulated Flight at 5000 Ft, System 9 | 181 |
| 6.46 | Simulated Flight at 5000 Ft, System 10 | 182 |
| 6.47 | Simulated Flight at 10,000 Ft, System 6 | 183 |
| 6.48 | Simulated Flight at 10,000 Ft, System 7 | 184 |
| 6.49 | Simulated Flight at 10,000 Ft, System 8 | 185 |
| 6.50 | Simulated Flight at 10,000 Ft, System 9 | 186 |
| 6.51 | Similated Flight at 10,000 Ft, System 10 | 187 |
| 6.52 | Simulated Power Levels for 5000-Ft Flight, System 6 | 194 |
| 6.53 | Simulated Power Levels for 5000-Ft Flight, System 7 | 195 |
| 6.54 | Simulated Power Levels for 5000-Ft Flight, System 8 | 196 |

| FIGURES | VOLUME II | PAGE |
|---|---|---|
| 6.55 | Simulated Power Levels for 5000-Ft Flight, System 9 | 197 |
| 6.56 | Simulated Flight at 5000 Ft, System 13 | 200 |
| 6.57 | Simulated Flight at 5000 Ft, System 14 | 201 |
| 6.58 | Simulated Flight at 5000 Ft, System 11, Sensitive, High-Power Transponder | 205 |
| 6.59 | Simulated Flight at 5000 Ft, System 12, Sensitive, High-Power Transponder | 206 |
| 6.60 | Simulated Flight at 5000 Ft, System 13, Sensitive, High-Power Transponder | 207 |
| 6.61 | Simulated Flight at 5000 Ft, System 14, Sensitive, High-Power Transponder | 208 |
| 6.62 | False Suppression Contours, Integral SLS | 211 |
| 6.63 | Simulated Flight at 5000 Ft, Integral SLS | 213 |
| C.1 | 1030 MHz Azimuth Pattern, FA-8043 Antenna, $-180^{\circ}$ to $+180^{\circ}$ | 236 |
| C.2 | 1030 MHz Azimuth Pattern, FA-8043 Antenna, $-12^{\circ}$ to $+12^{\circ}$ | 237 |
| C.3 | 1090 MHz Azimuth Pattern, FA-8043 Antenna, $-180^{\circ}$ to $+180^{\circ}$ | 238 |
| C.4 | 1090 MHz Azimuth Pattern, FA-8043 Antenna, $-12^{\circ}$ to $+12^{\circ}$ | 239 |
| C.5 | 1030 MHz Elevation Pattern, FA-8043 Antenna | 240 |
| C.6 | 1090 MHz Elevation Pattern, FA-8043 Antenna | 241 |
| C.7 | 1030 MHz Elevation Pattern, FA-8044 Antenna | 242 |
| C.8 | 1030 MHz Elevation Pattern, FA-8045 Antenna | 243 |
| C.9 | 1030 MHz Azimuth Pattern, Hazeltine Antenna, $-180^{\circ}$ to $+180^{\circ}$ | 244 |

FIGURES PAGE


C.10 1030 MHz Azimuth Pattern, Hazeltine Antenna, -12° to +12° 245

C.11 1090 MHz Azimuth Pattern, Hazeltine Antenna, -180° to +180° 246

C.12 1090 MHz Azimuth Pattern, Hazeltine Antenna, -12° to +12° 247

C.13 1030 MHz Elevation Pattern, Hazeltine Antenna 248

C.14 1090 MHz Elevation Pattern, Hazeltine Antenna 249

C.15 1030 MHz Azimuth Pattern, Hazeltine Omni Antenna 250

C.16 1030 MHz Elevation Pattern, Hazeltine Omni Antenna 251

C.17 1030 MHz Azimuth Pattern, ARSR Beacon Feed, -180° to +180° 252

C.18 1030 MHz Azimuth Pattern, ARSR Beacon Feed, -12° to +12° 253

C.19 1090 MHz Azimuth Pattern, ARSR Beacon Feed, -180° to +180° 254

C.20 1090 MHz Azimuth Pattern, ARSR Beacon Feed, -12° to +12° 255

C.21 1030 MHz Elevation Pattern, ARSR Beacon Feed 256

C.22 1090 MHz Elevation Pattern, ARSR Beacon Feed 257

C.23 1030 MHz Azimuth Pattern, ARSR Omni Antenna 258

C.24 1030 MHz Elevation Pattern, ARSR Omni Antenna 259

C.25 1030 MHz Azimuth Pattern, TI Separate Rotator, -180° to +180° 260

C.26 1030 MHz Azimuth Pattern, TI Separate Rotator, -12° to +12° 261

C.27 1090 MHz Azimuth Pattern, TI Separate Rotator, -180° to +180° 262

FIGURES


| | | PAGE |
|---|---|---|
| C.28 | 1090 MHz Azimuth Pattern, TI Separate Rotator, $-12^{o}$ to $+12^{o}$ | 263 |
| C.29 | 1030 MHz Elevation Pattern, TI Separate Rotator | 264 |
| C.30 | 1090 MHz Elevation Pattern, TI Separate Rotator | 265 |
| C.31 | 1030 MHz Azimuth Pattern, TI Separate Rotator Omni | 266 |
| C.32 | 1030 MHz Elevation Pattern, TI Separate Rotator Omni | 267 |
| C.33 | 1030 MHz Azimuth Pattern, Westinghouse Antenna, $-180^{o}$ to $+180^{o}$ | 268 |
| C.34 | 1030 MHz Azimuth Pattern, Westinghouse Antenna, $-12^{o}$ to $+12^{o}$ | 269 |
| C.35 | 1090 MHz Azimuth Pattern, Westinghouse Antenna, $-180^{o}$ to $+180^{o}$ | 270 |
| C.36 | 1090 MHz Azimuth Pattern, Westinghouse Antenna, $-12^{o}$ to $+12^{o}$ | 271 |
| C.37 | 1030 MHz Elevation Pattern, Westinghouse Antenna | 272 |
| C.38 | 1090 MHz Elevation Pattern, Westinghouse Antenna | 273 |
| C.39 | 1030 MHz Azimuth Pattern, Westinghouse Omni | 274 |
| C.40 | 1030 MHz Elevation Pattern, Westinghouse Omni | 275 |
| C.41 | 1030/1090 MHz Elevation Pattern, Ideal Antenna | 276 |
| C.42 | Least-Squares Fit, 1030 MHz Elevation Pattern, FA-8043 Antenna | 278 |
| C.43 | Least-Squares Fit, 1090 MHz Elevation Pattern, FA-8043 Antenna | 279 |
| C.44 | Least-Squares Fit, 1030 MHz Elevation Pattern, FA-8044 Antenna | 280 |
| C.45 | Least-Squares Fit, 1030 MHz Elevation Pattern, FA-8045 Antenna | 281 |

FIGURES


| | | PAGE |
|---|---|---|
| C.46 | Least-Squares Fit, 1030 MHz Elevation Pattern, Hazeltine Antenna | 282 |
| C.47 | Least-Squares Fit, 1090 MHz Elevation Pattern, Hazeltine Antenna | 283 |
| C.48 | Least-Squares Fit, 1030 MHz Elevation Pattern, Hazeltine Omni Antenna | 284 |
| C.49 | Least-Squares Fit, 1030 MHz Elevation Pattern, ARSR Beacon Feed | 285 |
| C.50 | Least-Squares Fit, 1090 MHz Elevation Pattern, ARSR Beacon Feed | 286 |
| C.51 | Least-Squares Fit, 1030 MHz Elevation Pattern, ARSR Omni Antenna | 287 |
| C.52 | Least-Squares Fit, 1030 MHz Elevation Pattern, TI Separate Rotator | 288 |
| C.53 | Least-Squares Fit, 1090 MHz Elevation Pattern, TI Separate Rotator | 289 |
| C.54 | Least-Squares Fit, 1030 MHz Elevation Pattern, TI Separate Rotator Omni | 290 |
| C.55 | Least-Squares Fit, 1030 MHz Elevation Pattern, Westinghouse Antenna | 291 |
| C.56 | Least-Squares Fit, 1090 MHz Elevation Pattern, Westinghouse Antenna | 292 |
| C.57 | Least-Squares Fit, 1030 MHz Elevation Pattern, Westinghouse Omni Antenna | 293 |


TABLES

VOLUME I


| | | |
|---|---|---|
| 6.1 | En Route Antenna Systems Modeled | 132 |
| 6.2 | En Route Antenna System Characteristics | 133 |
| 6.3 | En Route Antenna System Performance, Simple Model | 144 |
| 6.4 | En Route Antenna System Performance, Complex Model, 12,000-Ft Flight | 158 |

TABLES


| | | PAGE |
|---|---|---|
| 6.5 | En Route Antenna System Performance, Complex Model, 40,000-Ft Flight | 160 |
| 6.6 | Terminal Antenna Systems Modeled | 162 |
| 6.7 | Terminal Antenna System Characteristics | 163 |
| 6.8 | Terminal Antenna System Performance, Simple Model | 164 |
| 6.9 | Terminal Antenna System Performance, Complex Model, 2000-Ft Flight | 189 |
| 6.10 | Terminal Antenna System Performance, Complex Model, 5000-Ft Flight | 190 |
| 6.11 | Terminal Antenna System Performance, Complex Model, 10,000-Ft Flight | 191 |
| 6.12 | Characteristics of Adjusted Terminal Systems | 199 |
| 6.13 | Adjusted Terminal Antenna System Performance, Complex Model, 5000-Ft Flight | 202 |
| 6.14 | Adjusted Terminal Antenna System Performance, Simple Model | 203 |
| 6.15 | Adjusted Terminal Antenna System Performance, Complex Model, 5000-Ft Flight, 500-watt/77-dBm Transponder | 209 |
| 6.16 | Integral SLS Antenna System Performance, Simple Model | 210 |
| 6.17 | RSLS Performance as a Function of Interference | 214 |
| 6.18 | RSLS Performance as a Function of Antenna Systems | 215 |

# CHAPTER 1

# INTRODUCTION

## 1.1 Recent Developments in Air Traffic Control

Air Traffic control technology is undergoing a rapid and essential transition. As new air traffic control (ATC) system components continue to be introduced by the Federal Aviation Administration (FAA) throughout the country, the so-called Third Generation of ATC comes ever-closer to completion. This Third Generation semiautomatic system is now assisting air traffic controllers by performing such tasks as printing flight strips, determining aircraft altitude and identity, and tagging targets on the controllers' displays. These tasks, performed manually throughout ATC's Second Generation, are carried out in the terminal area by a variety of electronic subsystems, known collectively as ARTS (Automatic Radar Control Terminal System), whose activities are coordinated by a Univac computer. The Third Generation's first stage in en route air traffic control, NAS (National Airspace System) Stage A, consists also of a variety of electronic subsystems integrated by a central computer, in this case an IBM 9020.

Even the Third Generation System, however, is not expected to be able to handle the air traffic loads projected for the 1980's. Accordingly, an Upgraded Third Generation System was recommended in 1969 by the U.S. Department of Transportation's

(DOT's) Air Traffic Control Advisory Committee (ATCAC) in an effort to improve the present safety record and to minimize trip times[1]. The various features proposed for the Upgraded Third Generation System include improved terminal navigation devices and landing aids such as scanning beam microwave instrument landing systems, high-capacity airports, improved en route navigation including use of area navigation, a Discrete Address Beacon System (DABS) with data link, automatic Intermittent Positive Control (IPC) in regions of high air traffic density, expanded automation and functional responsibility of the NAS and ARTS, and ground-to-air transmission of control information via data link.

The ATCAC went still further in its report, however, to recommend a Fourth Generation System for the 1990's and beyond. Such a system would accommodate a total U.S. fleet of one million aircraft, ten per cent of which might be airborne at peak times. The elements of the Fourth Generation System could involve satellite systems, time-frequency technology, fourth generation computers, or an intricate combination of such elements. Regardless of the configuration of the system, its operation must be highly automated. To provide ATC services efficiently for so many thousands of aircraft will require the automation of such functions as conflict prediction and resolution (collision avoidance), spacing, sequencing, and metering, as well as the incorporation of weather changes, wind shifts, runway blockages, aircraft emergencies, ATC equipment failures, and other anomalies as inputs to

the automated system. In such a complex control loop, man remains the chief strategist, particularly in unusual emergency situations, but he must relinquish his former responsibility for direct control of several discrete aircraft. Rather, he must become the manager of a highly-automated air traffic control system which in turn takes responsibility for the individual aircraft.

The Third Generation ATC System being completed by the FAA, and the Upgraded Third and Fourth Generation Systems now in various stages of design and development, are extremely complex. Their successful implementation requires both numerous technical developments and analytical efforts, and sound systems engineering management.

This thesis is concerned with one aspect of these complex ATC systems — radio frequency surveillance. In particular the thesis treats the Air Traffic Control Radar Beacon System (ATCRBS), a surveillance system based on World War II technology to allow identification of friend or foe (IFF). Although the ATCRBS has been used to control air carrier and general aviation aircraft since the late 1950's, various improvements and modifications will extend the useful life of beacon-based systems to the 1990's. The greatest innovation yet in beacon system technology is the Discrete Address Beacon System (DABS), whose initial development and specification has been completed recently by MIT's Lincoln Laboratory[2]. Many interim improvements in ATCRBS

hardware, software, and system management are part of a formal FAA program[3] that should ensure safe and efficient surveillance of aircraft until the DABS becomes operational.

Whereas expanded system capacity, more services, and better system performance are inherent in the basic features of DABS, the improvement of present ATCRBS performance has been directed more toward compatibility with Third Generation automation. Although the present radar beacon system, and indeed the entire air traffic control system, has proven to be safe and reliable, it does experience problems that can be amplified as the Third Generation System comes into more widespread use. Although the air traffic controller has learned through intensive training and many years of experience to identify such problems as weak, missing, or false indications of aircraft on his radar display, it is difficult to program a computer to identify and cope with these same problems. It becomes extremely important, then, to ensure that the best data possible is supplied by the ATCRBS sensors to the air traffic control computers.

One of the most recent advances in improvement of the quality of surveillance data has been the development of four prototypic ATCRBS antennas by DOT's Transportation Systems Center (TSC) for the FAA. Although the antennas were designed for experimental evaluation in the laboratory and the field, one antenna has successfully completed its experimental tests and was commissioned by the FAA at Albuquerque International Airport, which

it has served since December 1974. The new "open-array" antenna has reduced the occurrence of false targets seen with the old antenna at Albuquerque, according to reports from air traffic controllers and regional personnel, by up to 90%.

Since the results of TSC's antenna development efforts are the inputs to many of the applications of the techniques developed in the thesis, a description of the antenna development program is included here. The objective of the program, which was begun in 1972, was to develop modification kits for the standard ATCRBS antenna to reduce the occurrence of false and missing targets on a controller's display. These problems are caused primarily by reflected low-angle (below the local horizontal plane) radiation that bounces off nearby buildings and the surrounding terrain either at the same azimuth as the direct signal, thus resulting in missing targets due to signal phase cancellation on arrival at the aircraft, or at a different azimuth, which results in false targets at the azimuth of the reflecting surface. Although the missing target or vertical lobing problem is usually dealt with at operational sites by turning up radar power until coverage gaps are eliminated, the very process of increasing power aggravates such other problems as susceptibility to false targets from reflection.

To minimize these problems, TSC's specification for improved ATCRBS antennas included two important changes from the present antenna: an increased vertical aperture (taller antenna than the

standard one, which is 18-in high) to enable low-angle radiation to be reduced substantially; and an omnidirectional antenna for transmission of side-lobe suppression pulses whose vertical radiation pattern matches that of the directional interrogator antenna. To ensure the achievement of suitable technical solutions with minimum risk, wide application, and the lowest possible production cost, TSC structured its antenna development program to include three basic approaches.

For the terminal area, the Hazeltine Corporation designed and built a direct replacement for the standard ATCRBS antenna. The 4-ft by 27-ft open phased-array antenna is nearly equal in weight to the existing antenna and induces approximately the same shaft torsion and overturning moment that the present antenna induces in the presence of strong winds; that is, the replacement produces the same static and dynamic loads as the present antenna. This requirement, which allows the new antenna to be mounted on top of the primary skin-tracking radar or Airport Surveillance Radar (ASR) without a radome, eliminates the necessity for a separate pedestal for the new, larger antenna in the terminal area.

For en route application (200-nm range rather than 60 nm tor the terminal area), Texas Instruments (TI) Incorporated designed and built a beacon-feed modification for the primary Air Route Surveillance Radar (ARSR). This approach involves the use of beacon feed elements clustered around the existing ARSR feed horn

and utilizes the existing 22-ft by 44-ft ARSR dish. Its production cost is therefore very low.

For both terminal and en route application, TI and Westinghouse Electric Corporation have each built a "separate rotator" antenna that requires its own tower, pedestal, and drive mechanism because of its large size. TI's antenna, a 10-ft by 30-ft reflector fed with three horns, and the Westinghouse antenna, an 8-ft by 28-ft phased array, will be located in the terminal area on their own pedestals separate from the ASR, to which their rotation will be slaved, but close enough to allow sharing of the ASR's equipment building and to minimize the separation of primary radar and beacon information on the controller's display. In addition to allowing a large, high-performance antenna to be used in the terminal area, the separate rotator configuration provides a fail-soft mode of operation by continuing beacon coverage even though the ASR is stopped. Also, the present beacon antenna could be left in place atop the ASR to serve as a back-up in case of failure of the separate rotator.

In an en route environment, either of the separate rotators could be mounted on a 75-ft tower independent of a primary radar. Almost all en route aircraft, of course, are equipped with transponders that enable them to respond to ATCRBS interrogations. In the terminal area, smaller aircraft without transponders can only be detected by the primary radar, which senses signal reflections from the skin of the aircraft.

All these antennas were designed to minimize their impact on other systems such as the primary radar, target processing computers, and displays. Despite this ground rule that emphasized taking "one step at a time", all four antennas were built with the capability of receiving information in a difference mode, a feature necessary for the monopulse processing required by DABS.

Another application of the techniques developed in the thesis concerns a concept called receiver side-lobe suppression (RSLS). This concept, also a part of the National Improvement Program for ATCRBS, involves a comparison of signals received on the ground through both a directional and an omnidirectional antenna. Such a concept tends to reduce both random interference and reflected replies that result in false targets. RSLS is explained in more detail in Chapter 2.

Although the techniques developed in the thesis are applied in Chapter 6 primarily to the evaluation of the new antennas and of the RSLS concept described above, these applications were chosen merely as important and representative ones. The potential applications of the methods of the thesis are restricted neither to current nor beacon-based systems, and may well include systems and problems as yet unforeseen.

## 1.2 Related Efforts in the Field of the Thesis

Clearly, the improvements discussed in the previous section would be unnecessary in the absence of a variety of problems that arise in the day-to-day operation of the ATCRBS. These problems,

which are described in Chapter 2, have prompted analytical efforts to be undertaken by several organizations in support of the FAA. Most of the efforts to date have concentrated on system interference problems involving the interaction of many ground interrogator/receiver sites and many transponder-equipped aircraft. The U.S. Department of Defense Electromagnetic Compatibility Analysis Center, for instance, has developed a performance prediction model for the ATCRBS that allows evaluation of many of its features in a statistical sense[4]. The ECAC model allows the assessment of environments consisting of hundreds of interrogators and aircraft with a reasonable amount of computer time, but at some expense in detail. The Transportation Systems Center has developed a much more detailed simulation of the ATCRBS than the model of ECAC[5]. The level of detail provided by TSC affords the capability for computer generation of the display that would be seen by an air traffic controller. The cost of simulation detail, of course, is computer execution time which escalates rapidly as interrogator-aircraft products increase.

Still other assessments of ATCRBS performance have been performed by the MITRE Corporation[6] using statistical analysis and by Lincoln Laboratory[7,8] using a process of thorough examination and analysis of data tapes obtained from several sites throughout the country where Third Generation automation has been installed. The efforts of Lincoln Laboratory described in References 7 and 8 address many of the problems peculiar to individual

sites which tend to be related more to such environmental factors as terrain and buildings than to the existence of many interrogators and aircraft. Lincoln's activites, certainly the most current and prolific in the field, continue in two project areas: development of a Discrete Address Beacon System[9,10] and ATC surveillance/communication analysis and planning[11]. Reference 9 describes detailed simulations of ATCRBS phenomena undertaken by Lincoln in relation to their DABS development efforts.

Another recent study of the antennas described previously has been performed by the University of Michigan Radiation Laboratory for TSC[12,13]. This study enables coverage diagrams and zones of side-lobe punch-through and false main-beam suppression to be plotted given analytic approximations to the various antenna patterns. A flat earth is assumed for purposes of this study.

## 1.3 Objectives of the Thesis

Despite the variety and the outstanding quality of work being performed in the field of analysis and improvement of the ATCRBS, it was evident that until this thesis was undertaken there was no concerted effort to develop specific performance criteria by which the relative merits of various configurations of beacon system hardware and operating conditions could be judged. Certainly there are various means of telling that one system is better than another, but just how much better and in what specific respects is it better, are questions that appeared

likely to go unanswered.

The frustration of hardware development schedules, test aircraft availability, adverse weather, and limited manpower were perhaps the primary motivational factors for the second thesis objective. The cost and difficulty of executing experimental flight tests of the four antennas developed under contracts with TSC made the prospect of a detailed simulation of ATCRBS propagation effects that cause vertical lobing appear to be a worthwhile venture. If developed the detailed simulation could be used to validate some of the performance criteria that might be developed in ways other than simulation. Ultimately, the flight test results, when completed, would serve to validate the simulation itself. Furthermore, once validated, the simulation would provide a convenient means for investigating a variety of phenomena such as the effect of main-beam interference on RSLS performance that involved principally a single ground site and a single aircraft.

Thus evolved the two primary objectives of the thesis:

1) to develop system performance criteria that could be expressed in closed-form over a wide range of system coverage using a simple flat-earth model; and
2) to develop a complex, spherical-earth simulation of the interaction between an interrogator/receiver and an aircraft making as few simplifying assumptions as possible and using actual antenna pattern data.

Hopefully, the simple flat-earth model would allow the derivation of the equation for the area under a vertical lobing contour. Upon that derivation could be built a series of performance criteria that could be evaluated quickly and simply for a variety of test configurations over a wide range of airspace.

The complex, spherical-earth simulation, on the other hand, would provide a tool for detailed investigation of specific propagation characteristics over a single flight profile. If developed with the level of detail included in TSC's pulse-by-pulse simulation of ATCRBS inter-site interference, this intra-site simulation of propagation characteristics could also produce a computer-generated representation of the controller's, or test director's, display. Combined with an interference generator, such a simulation could be used for the investigation of a wide variety of phenomena whose sensitivity to adjustments at a single ground site was of interest.

## 1.4 Summary of the Contents of the Thesis

In Chapter 2 a brief description of the operation of the Air Traffic Control Radar Beacon System and some of its problems is accompanied by a list of references with more detailed descriptions. Chapter 3 describes the various performance criteria upon which it is proposed to base the quantitative assessment of several ATCRBS configurations. Chapters 4 and 5 include the derivations of equations used in the simple flat-earth propagation model and the complex, spherical-earth simulation, respectively.

Applications of both the simple model and the simulation to evaluation of the performance of the four antennas discussed previously and of receiver side-lobe suppression are presented in Chapter 6. The data presented is both tabular and graphical in nature, and includes computer-generated representations of an air traffic control display for several representative tests. Photographs of the display used in actual tests of two antennas at the National Aviation Facilities Experimental Center in Atlantic City, New Jersey, are correlated with the computer-generated displays as one means of validation. Finally, conclusions based on findings during the development of the model and the simulation, and on the applications of both to the problems discussed in Chapter 6, are included in Chapter 7. A summary of the contributions of the thesis and several recommendations for further study are also included in the final chapter.

# CHAPTER 2

# DESCRIPTION OF THE AIR TRAFFIC CONTROL RADAR BEACON SYSTEM

## 2.1 References

A brief description of the ATCRBS is included in this chapter for the convenience of the reader. Further details are covered well in the open literature. The most comprehensive account of ATCRBS currently available has been compiled by Drouilhet[14]. In his paper Drouilhet describes the entire history of ATCRBS, its functional characteristics and operating problems, and the next generation of beacon system, DABS, whose development he has directed at Lincoln Laboratory.

Two other references are noteworthy. A concise general description of ATCRBS operation and problems, and an extensive bibliography of ATCRBS-related material is contained in a paper by Ashley et al.[15] Also, the U.S. National Standard for ATCRBS[16] contains the many details with which both ground-based and airborne equipment should comply. The National Standard is well-written and easy to understand, and should not discourage the reader looking for an answer to an exacting question.

## 2.2 General Description

Both the Second Generation and semiautomatic Third Generation ATC systems described in Chapter 1 depend primarily on the

ATCRBS to provide information for air traffic controllers about the position and identification of transponder-equipped aircraft. When used in conjunction with either the en route portion (NAS Stage A) or terminal portion (ARTS) of the Third Generation System, the ATCRBS makes possible automatic reporting and display of altitude and identity. This automatic reporting capability is essential for the efficient operation of the Third Generation System, whose objective is to provide safer and faster air traffic control services despite increasing air traffic density.

The ATCRBS is based on the technology of the military Mark X System used during World War II to identify aircraft as friend or foe (IFF). Very simply, the ATCRBS can be described as a ground-based radar which interrogates an airborne transponder and then listens for a reply. Aircraft altitude and identity are encoded in the reply pulses from the transponder, while slant range is determined from the time between interrogation and receipt of response.

## 2.3 Interrogator Operation

More than 90 en route interrogator/receiver sites and 125 terminal sites are currently operated by the FAA throughout the United States. The en route sites provide surveillance information for Air Route Traffic Control Centers (ARTCCs) and have ranges of approximately 200 nm. Terminal sites are operated principally at major airports and can detect aircraft as far away as 60 nm. Although a new age of operation of ATCRBS interroga-

tors without a primary radar for en route coverage is nearly upon us, the beacon system operates in conjunction either with an Air Route Surveillance Radar (ARSR) or an Airport Surveillance Radar (ASR). These primary radars, which are becoming secondary in importance to the beacon system as automation continues to be introduced throughout the country, provide coverage of aircraft, generally small and relatively-inexpensive aircraft, that are not equipped with transponders. They operate by detecting the echo of signals transmitted from the radar site in the direction of the aircraft. Ironically, the smaller aircraft without transponders tend to provide weaker primary radar echoes than larger aircraft, most of which are transponder-equipped. In addition to the ATCRBS sites operated by the FAA, the military runs several hundred sites within the United States, and at least several hundred more throughout the world. This abundance of beacon interrogators is one cause of the interference that occurs at many sites.

The interrogators transmit time-coded pulses at a fixed rate from a rotating directional antenna. This fixed interrogation rate is generally about 400 interrogations per second for terminal interrogators and 360 interrogations per second at en route sites. The rate is varied intentionally by the FAA for interrogators within a few hundred miles of each other, however, to help reduce inter-site interference. The directional antenna is approximately 16-in high and 28-ft long, and is sometimes

referred to as a "hog trough" for reasons obvious to those with agrarian backgrounds. The ATCRBS antenna is mounted atop either the ARSR, which generally rotates at 6 rpm, or the ASR, which rotates between 12 and 15 rpm. The en route facility is usually enclosed in a radome.

The time-coded pulses transmitted by the interrogator determine the information with which the aircraft will reply. A pulse pair spacing of 8 microseconds (Mode A) is a request for aircraft identity, while a 21-microsecond spacing (Mode C) evokes an altitude reply. Modes B and D are also assigned to the FAA, but are currently used only for special purposes such as experimentation. The military denotes its interrogation modes as 1, 2, 3, and 4, in contrast to the FAA's A, B, C, and D. Military Mode 3 is identical (an 8-microsecond pulse pair) to FAA Mode A and is commonly referred to as Mode 3/A.

A third pulse is transmitted by ATCRBS sites from an omnidirectional antenna located on a mast at the corner of ASR towers or usually suspended from the top of the radome at ARSR sites. This third pulse, transmitted 2 microseconds after the first pulse of the interrogation pair from the directional antenna, serves as a reference level for the transponder. The operation of this side-lobe suppression system is described further in the next section on transponder operation. Still another variation of side-lobe suppression (SLS) involves transmission of the first interrogation pulse both on the directional and on the omnidirec-

tional antennas. Called improved side-lobe suppression, this technique tends to eliminate false targets that result from reflections by ensuring that the first interrogation pulse is received by aircraft at all azimuths with respect to the antenna and up to at least several tens of miles away.

The interrogation pulses described in the foregoing have been given specific names by the National Standard. $P_1$ is the first interrogation pulse and is always transmitted on the directional antenna and sometimes on the omnidirectional antenna (when a site is equipped with improved SLS). $P_2$ is the second pulse transmitted in time; it is radiated on the omnidirectional antenna and is also referred to as the suppression pulse. $P_3$ is the second pulse transmitted from the directional antenna and completes the interrogation pair that specifies the interrogation mode.

## 2.4 Transponder Operation

There are more than 90,000 transponder-equipped aircraft currently operating in the United States. Although nearly every air carrier aircraft is transponder-equipped (most carry two or more transponders), air carriers account for only about 2,500 aircraft. Approximately 30,000 military aircraft carry transponders (most of the total), while about 60,000 of 140,000 general aviation aircraft are equipped.

The transponder decodes the interrogations received at the omnidirectional antenna mounted in most cases somewhere on the

belly of the aircraft. Depending upon the mode of interrogation detected by the transponder, it transmits a 12-bit pulse train between two "framing pulses" spaced 20.3 microseconds. A Mode A interrogation initiates the transmission of a pulse train corresponding to a 4-octal-digit code selected by the pilot at the request of the air traffic controller. A Mode C interrogation causes the transponder to respond with aircraft altitude encoded from a barometric altimeter input. For those aircraft not equipped with an altimeter digitizer, usually only the framing pulses are transmitted to the ground. Pulses transmitted from the aircraft leave it with peak powers of the order of 500 watts, approximately the same as the amplitude of interrogation pulses that enter the directional antenna at a terminal site. Interrogation pulses of 1500 watts into the antenna are generally necessary to ensure en route coverage.

Besides responding to encoded interrogations, the transponder performs a number of other actions to enhance its performance. It compares the amplitude of the $P_2$ pulse with that of $P_1$ before it decides whether or not to reply. If $P_2$ exceeds $P_1$, the transmission must have come from a side lobe of the interrogator antenna, and the transponder suppresses its receiver for approximately 35 microseconds. If $P_2$ is at least 9 dB below the level of $P_1$, the interrogation is almost surely on the main beam, and the transponder initiates a reply. Within the 9-dB deadband, the transponder may either suppress or reply. Any time a trans-

ponder replies, it suppresses its receiver for up to 125 microseconds after the transmission of the last reply pulse. Usually this "dead time" lasts about the same length of time as the sidelobe suppression cycle (35 microseconds).

The transponder also undergoes two types of reduction in sensitivity to reduce some of the interference effects that occur within the ATCRBS. Upon receipt of any single pulse, the transponder desensitizes to the level of that pulse or within 9 dB of it. That is, the transponder can detect no pulse with amplitude 9 dB or more lower than the amplitude of a pulse just received if the second pulse arrives shortly after the first. This "echo suppression" desensitization eliminates many of the garbled interrogations that would be received by transponders flying over mountains or other areas where reflected interrogations occur.

The other sensitivity reduction is due to the action of the reply rate limit control. When the rate of interrogations from all ground sites equals a nominal level, usually 1200 interrogations per second, the transponder begins to desensitize until the rate decreases. If the interrogation rate exceeds 150% of the nominal rate, the transponder desensitizes by at least 30 dB. Such a process, of course, discriminates against the farthest interrogator, whose signal is likely to be the weakest one arriving at the transponder. This is not necessarily a desirable characteristic for an air carrier or general aviation aircraft to have if it flies near military facilities with many operating

interrogators that cause it to deny replies to FAA interrogators.

## 2.5 Receiver Operation

The ATCRBS receives 1090-MHz replies from the aircraft on the same antenna from which it transmits 1030-MHz interrogation pairs. The maximum sensitivity of the receiver is approximately -88 dBm, but this is modified by the action of the sensitivity-time control circuit (STC). The STC reduces receiver sensitivity initially by about 36 dB at terminal sites and 42 to 45 dB at en route facilities. The time of initial reduction is 15.36 microseconds after the transmission of the $P_3$ pulse, which allows a radar signal to travel 1 nm to the aircraft and 1 nm back to the interrogator with a 3-microsecond delay at the transponder. Since the ATCRBS is required to operate from 1 nm out to its coverage range, this initial time of receiver desensitization merely corresponds to the "start time" corresponding to 1 nm on the controller's display. After this inital desensitization, the receiver recovers sensitivity at the rate of 6 dB for every doubling of range (and hence of time) from the interrogator.

The STC effectively compensates for the free space loss of signals received from extreme ranges. Otherwise, aircraft near the receiver would cause power levels 40 or 50 dB greater than those from distant aircraft to be received. By requiring the aircraft at long range to be sensed on the main beam, nearby aircraft would then be detected on most of the side lobes as well. The STC thus causes the effective receive beamwidth to be approximately

the same for all aircraft independent of range.

Another means of suppressing downlink interference is being considered by the FAA. Called receiver side-lobe suppression (RSLS) this technique would entail comparison of the replies from aircraft as received both on the directional and on the ground-based omnidirectional antennas. Just as in interrogator side-lobe suppression, RSLS would reject replies as side-lobe signals if the omnidirectional power level exceeded the directional level. An evaluation of this technique is included in Chapter 6.

## 2.6 Operating Problems

Evidence of problems with the operation of ATCRBS appears in several ways on a controller's display. Indications of aircraft or "targets" can be missing, weak or broken, or false. Furthermore, there can be interference such as "ring-around" or "fruit" that affects large areas of the display.

Missing targets are generally caused either by shielding of the path of propagation by an aircraft wing, landing gear, or fuselage, or by a phenomenon called vertical lobing which results from cancellation of the direct signal by a reflected signal of nearly equal amplitude that arrives out of phase. Shielding occurs most often in the terminal area where aircraft are more apt to have their gear down and to be performing a variety of maneuvers that can impose a structural member between the ground antenna and the aircraft antenna. Vertical lobing is the subject

of most of the remainder of this thesis and will be addressed in detail in subsequent chapters.

Weak or narrow targets can be caused by insensitive or low-power transponders, aircraft antenna shielding, or improper side-lobe suppression circuitry in the transponder. Broken targets are generated for the most part by asynchronous interference resulting in the capturing of a transponder by an interrogator/receiver other than the one of interest. If an aircraft replies to an interrogator, it can reply to no other generally for 35 microseconds, its dead time. Or it may be suppressed due to the SLS or improved SLS action of another ground site. In either case, an interrogation that arrives during a transponder's time of insensitivity, will not be answered. If the interfering interrogation is not present on the subsequent interrogation by the site of interest, then normal replies are resumed. This process leaves a "hole" in the target. In regions of high interrogator density, these holes accumulate and tend to break up the target into sections.

False targets occur primarily because of reflections of the directional antenna signal from buildings and terrain. A poor antenna can also cause false targets as a direct result of interrogation by a high side lobe. Malfunctioning side lobe suppression circuits in a transponder or mismatches in the vertical lobes of directional and omnidirectional antennas can also cause false targets.

Ring-around generally occurs at ranges close to the antenna and, when seen, usually consists of complete or partially broken concentric circles about the center of the display. It results from both interrogation and reply on all side lobes of the directional antenna usually as a result of malfunctioning SLS equipment, particularly that on the aircraft, or too shallow (small) a reduction in the STC. If a particular aircraft is observed to "ring", the problem can generally be traced to a bad transponder or, particularly in the case of some older military transponders, to no SLS circuits at all.

Fruit is observed on a display as "snow" or single replies from aircraft often arranged in spirals about the center of the display. The shape of the spiral is actually a measure of the interrogation repetition frequency of the interfering interrogator relative to that of the interrogator of interest. Fruit is caused by reception of replies that were elicited by some other interrogator, generally operating at a different rate of interrogation. When a fruit reply arrives at the same time as a valid reply, it can garble the real target because of the overlapping of the pulse trains. Still another garbling mechanism occurs when two aircraft are in the main beam of one interrogator and within 1.65 nm apart as measured at the receiver (slant range). In this case, the two 20.3-microsecond reply pulse trains overlap and cause difficulty in the decoding of their separate responses. This phenomenon, called synchronous garble, occurs most often in

holding patterns or "stacks" of aircraft. It will occur more often in en route and terminal airspace, however, as traffic densities continue to increase. DABS is an effective means of eliminating synchronous garble.

The many efforts described in the National Improvement Program for ATCRBS are designed to reduce or eliminate most of these operational problems. The pages that follow describe several techniques that should also prove useful in the analysis, evaluation, and improvement of the Air Traffic Control Radar Beacon System.

# CHAPTER 3

# DEVELOPMENT OF PERFORMANCE CRITERIA

## 3.1 Introduction

The performance criteria discussed in this chapter involve system coverage, contributions of an interrogator to system interference, susceptibility of a receiver to external interference, susceptibility of an interrogator/receiver to self-interference, and target quality. Ideally, a cooperative surveillance system will guarantee detection of all valid targets within some desired coverage volume, but will not interrogate nor suppress nor in any other way interfere with the operation of transponders outside that volume. In addition, such an ideal system will be immune to the effects of other interrogators and will produce only strong, sharp, valid targets. The extent to which particular sites and system configurations actually achieve these goals is a measure of system performance.

In the paragraphs that follow, specific performance criteria are developed to describe each aspect of system operation mentioned above. Thus, the strengths and weaknesses of several system configurations can be evaluated objectively as different items of hardware (interrogator/receiver antennas and receiver side-lobe suppression electronics, for example) are introduced, and as various operating characteristics (such as pulse power, antenna heights, and sensitivity-time control levels) are

adjusted.

All the performance criteria are associated either with the simple, flat-earth system model developed in Chapter 4, or with the complex, spherical-earth simulation model of Chapter 5. The simple model attempts to give approximate but informative measures of system performance in closed form for a wide range of desired areas of coverage and with a minimum of computational effort. The complex simulation model, on the other hand, affords a precise assessment of system performance over a specific flight profile.

## 3.2 System Coverage

To ensure detection of all aircraft of interest, coverage is usually specified in terms of a maximum slant range and a service ceiling within which and beneath which the display of all valid targets is desired. Although most terminal operations occur within 30 nm of the interrogator, terminal area coverage is generally desired out to 60 nm. Similarly, handoffs from an ARTCC to the approach controller may occur at altitudes of 10,000 to 12,000 ft, but the capability of detecting targets up to 40,000 ft may be desired in case of en route declaration of emergency or to provide redundant coverage of heavily-traveled air routes. (One of the two terminal radars at Los Angeles International Airport functions primarily as a short-range sensor of en route air traffic.)

Generally, an en route facility requires detection to a

slant range of 200 nm and a service ceiling of 40,000 ft, although military aircraft and the SST may impose even more severe requirements. An en route sensor is more sensitive to aircraft altitude than a terminal radar with regard to its long-range coverage, as some aircraft may be over the radar horizon at their cruising altitudes. Specifically, the radar horizon over a spherical earth is approximately 200 nm from an aircraft at 20,000 ft. Below that altitude, such an aircraft must be closer than the desired coverage range to be detected. Mountains, buildings, and atmospheric conditions can further degrade coverage of aircraft at long range.

In the absence of smooth reflecting surfaces in the vicinity of the interrogator, coverage would be determined for the most part by the free-space radiation pattern of the antenna in use. When radiation leaves the antenna at negative elevation angles, however, it can be reflected by such smooth surfaces as runways and flat terrain. When this reflection occurs, the direct and reflected electromagnetic fields combine vectorially to cause regions of both reinforcement and cancellation of the desired direct signal. This phenomenon, called vertical lobing, results in regions of the desired coverage area in which there is insufficient power for interrogation of an aircraft or reception of its reply.

The vertical lobing phenomenon, which will be described in detail in Chapters 4 and 5, is depicted in Figure 3.1. The figure shows three contours: 1) the boundary of a desired coverage area

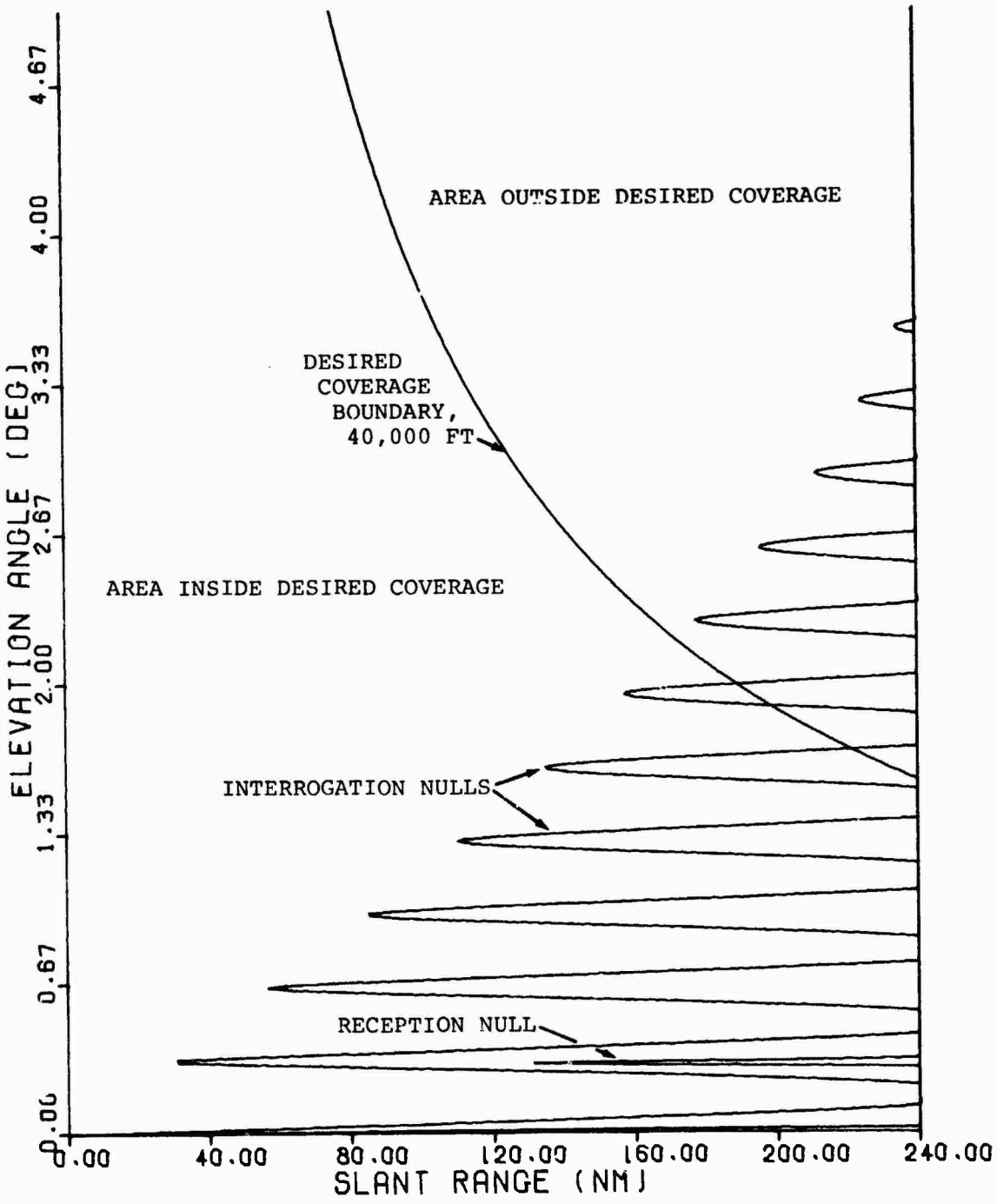


Figure 3.1 Typical Vertical Lobing Contours

with maximum slant range 240 nm up to the elevation angle at which a service ceiling of 40,000 ft is intercepted; 2) a contour of constant interrogation power necessary to trigger a typical ATCRBS transponder; and 3) a contour of constant transponder reply pulse power necessary for reception by a typical ground site. Both power contours are typical vertical cuts through the antenna boresight or direction of maximum power in the azimuthal plane. Since the ground receiver is generally at least 8 dB more sensitive than an airborne transponder, the downlink usually contains fewer "holes" in the coverage area than does the uplink.

The regions in which the nulls of the patterns lie inside the desired coverage boundary are holes in the coverage. The contours of constant power, of course, extend beyond the 240-nm limit of Figure 3.1. In such cases, and outside the curved contour of constant altitude, the constant-power curve bounds a region of excessive interrogation or susceptibility to replies that may result in system interference. That issue is addressed later in this chapter.

Holes in coverage can occur in still another way because of the vertical lobing phenomenon. As shown in Figure 3.2, the omnidirectional pattern, as well as that of the directional antenna, undergoes periodic reinforcement and cancellation. Because the omni is mounted higher than the directional antenna in normal use, its nulls are displaced downward. Eventually, the omni pattern, which should always lie well below the directional

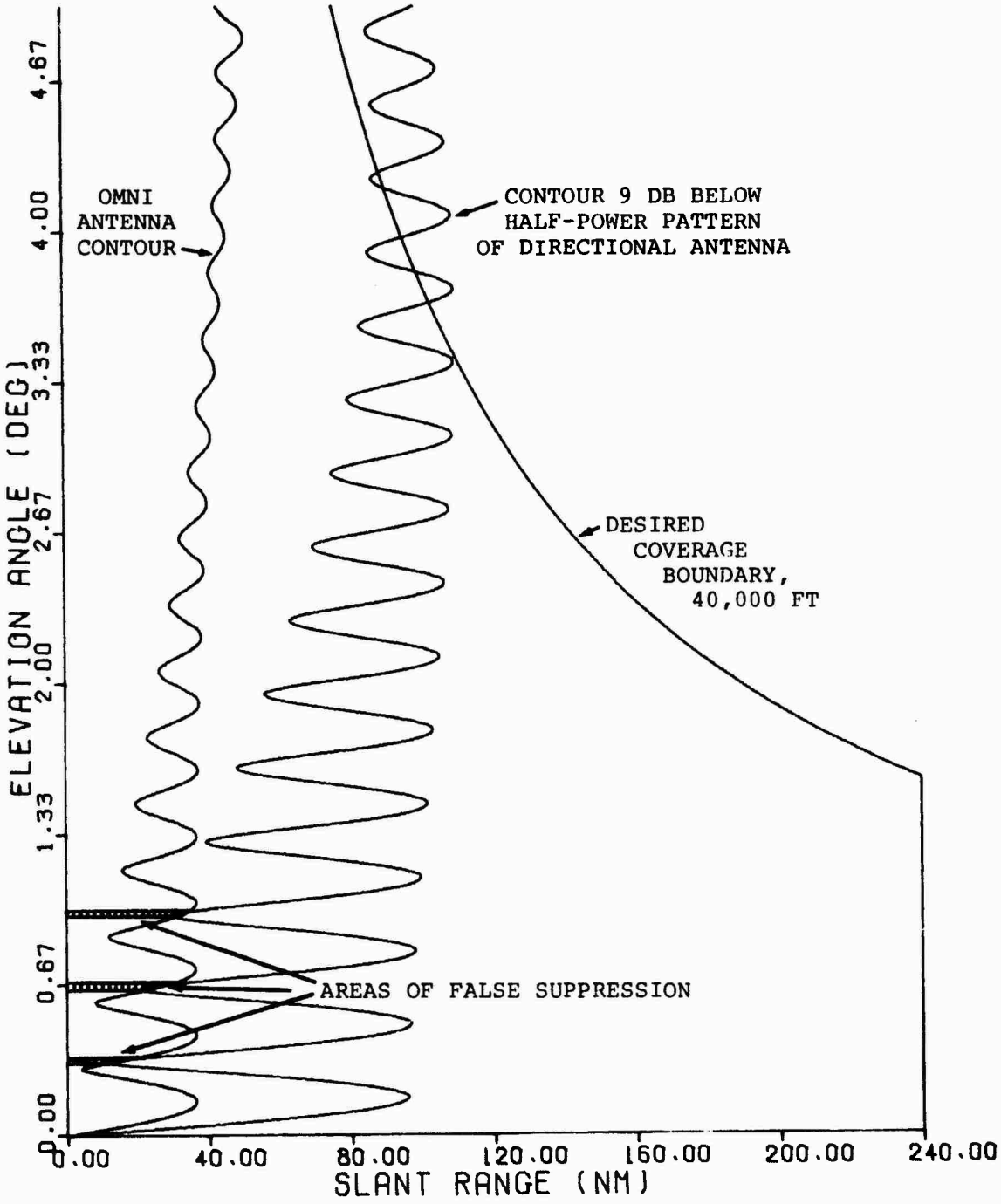


Figure 3.2 False Supression of a Valid Target

pattern in the main beam of the antenna, exceeds that level necessary (9 dB below the power of $P_1$) to initiate side-lobe suppression. Any transponder that enters such a region may be falsely suppressed and therefore lost from coverage.

Insufficient power and false suppression are the two mechanisms that cause deficient coverage. The criteria by which this deficiency can be measured, however, involve not only the vertical radiation pattern but the azimuthal pattern as well. That is, to ensure coverage on boresight is not necessarily to ensure a target of adequate width for validation by either a controller or a computer. Usually, the 3-dB or half-power beamwidth of an antenna is accepted as sufficient in azimuth for target declaration. The half-power beamwidth of a conventional ATCRBS antenna is approximately 2 deg.

As a measure of system coverage one can determine the area under contours of constant power. By subtracting 3 dB from the transmitted power and reducing ground receiver sensitivity by 3 dB, one can incorporate the effect of a half-power beamwidth into the determination of the uplink and downlink coverage areas. Similarly, an area of false suppression is just the area under the omnidirectional power pattern between those pairs of angles where the omni contour crosses the contour that lies 9 dB below the directional half-power pattern.

In Chapter 4 the equations for these areas are derived. It should be emphasized here, however, that the solutions for these

coverage and suppression areas involve several simplifying assumptions whose effect is evaluated in Chapter 6. The objective of using the areas under constant power contours as a means of determining performance criteria is to obtain straightforward closed-form solutions applicable over a wide range of desired coverage areas.

As an alternative to the method of areas derived in Chapter 4, a more accurate simulation model is presented in Chapter 5. Whereas the simpler model using areas applies over a specified range of elevation angles of interest, the more complex simulation model requires the designation of a specific flight profile. The tabulation of interrogations, suppressions, and replies for the duration of this simulated flight thus becomes another means of determining system performance. Minimum transponder sensitivity and output power are assumed in the calculation of all coverage criteria.

The complex model will, of course, provide significantly more information with regard to azimuthal side-lobe interactions and target character as a function of time. (Target quality is addressed later in this chapter.) The major indicator of system coverage obtained from the complex model is the standard deviation of target width from the mean. Many holes in the desired coverage will, of course, contribute significantly to this deviation. The total number of interrogations and replies, tabulated for each flight profile as a function of slant range, is also a means of

comparing different system configurations. Other indicators of system coverage are described in a subsequent section on target quality.

## 3.3 Contribution to System Interference

In the previous section it was mentioned that the contours of constant power may have peaks that extend beyond the desired coverage area. When this occurs, the undesired coverage can in fact cause system interference by generating fruit (unnecessary replies) or by locking out replies to a ground site responsible for covering the area in question. The lock-out phenomenon arises when an interfering interrogator elicits a transponder reply and thus the subsequent dead time. Any valid interrogation that arrives during the dead time is ignored by the transponder until the silent period has expired — up to 125 microseconds after transmission of the reply pulse train. Such interference thus results in an effective hole in the coverage of other interrogators that may vary with time.

In the main beam of the directional antenna, such a phenomenon might be characterized as over-interrogation. Outside the main beam, however, there occurs a contribution to external interference that can be even more consequential. In the absence of side-lobe suppression, any interrogation at all may elicit a transponder response. Outside the main interrogation beam, all such responses cause interference in the same manner as that described above.

But even with side-lobe suppression, an interrogator causes interference in the form of suppression times as long as 45 microseconds. These suppression times can cause transponder lock-out just as dead times due to interrogation cause lock-out. Improved side-lobe suppression, which increases the side-lobe coverage area of the $P_1$ pulse, accordingly raises the suppression time of transponders within range of the $P_1$,$P_2$ pair.

Still another mechanism causes a type of lock-out interference if an interrogator is equipped with improved SLS or, to a greater degree, with standard SLS. This mechanism, referred to hereafter as transponder "hang-up", results from the reception of individual $P_2$ pulses by a transponder when $P_1$ goes undetected. Although the more expensive transponders with delay-line decoders, used primarily by air carriers and high-performance general aviation, are generally immune to hang-up, those economical transponders with active or gate-type decoders are not. Upon receipt of a single pulse, these active decoders assume the pulse to be a potential $P_1$. Then they wait 2, 8, or 21 microseconds for the next pulse which would, of course, be a corresponding $P_2$ or $P_3$. If the second pulse is not received in the proper time interval, the transponder resumes listening for the next potential $P_1$. For every $P_2$ interpreted falsely as a potential $P_1$, therefore, such a transponder hangs up for 21 microseconds. This phenomenon is comparable to the lock-out mechanisms discussed previously.

For a realistic assessment of the detrimental effects of

external interference, the airspace in which interference occurs must be suitably restricted. In particular, it should be noted that over a spherical earth the long-range contributions to interference are in fact very small because the existence of a radar horizon shields most aircraft from over-interrogation. Although it is true that the range of an en route interrogator whose power has been increased to fill holes in its coverage may be 400 nm or more, the sphericity of the earth requires an aircraft to be at an altitude of at least 80,000 ft for interference to occur at such a range. Interference of ground sites with the operation of high-performance military aircraft, spacecraft, and satellites is not considered in this thesis.

It will be shown in Chapter 6 that even in terminal areas, the over-interrogation region of the main beam tends to fill most of the area between the maximum desired slant range and the radar horizon, regardless of adjustments made in the system configuration or of the shape of radiation pattern in the directional antenna. Rather, contributions to system interference can best be controlled by regulating such side-lobe phenomena as suppressions and single $P_2$ hang-ups.

Chapter 4 details a procedure for retaining realism in the flat-earth model by imposition of a spherical-earth-horizon barrier beyond which over-interrogation area is discounted. In the absence of such a barrier, of course, interference areas over the flat earth would extend for hundreds of miles. The area under the

constant power contour outside the maximum desired slant range, beneath the service ceiling, and inside the spherical-earth-horizon barrier is used as the flat-earth model system performance criterion for contribution to interference in the numerical results of Chapter 6. Maximum transponder sensitivity and power are used in the computation of all interference criteria.

Since the complex simulation model contains the details of both directional and omnidirectional antenna side-lobe patterns, it is more suited to evaluation of interference contributions than is the simple model. Single $P_2$ counts and suppression pair counts thus serve as the complex model performance criteria for determination of contributions to interference. Because these pulse counts are recorded scan-by-scan over the flight profile in question, the amount of interference contribution can be determined precisely as a function of slant range. Such knowledge is important in the consideration of the effects of buildings and other large reflecting structures.

## 3.4 Susceptibility to External Interference

Just as the peaks of the uplink radiation pattern extend beyond the desired coverage area and contribute to system interference, so the fingers of the downlink vertical lobing contour reach out to grab replies from aircraft beyond the desired range. The replies received in this manner contribute to the fruit detected by the main beam.

But the side lobes also receive fruit in this case from any

aircraft that replies to an interrogator other than the one of interest. Since the downlink side lobes tend to extend for several tens of miles, the contribution to fruit due to the side lobes can exceed that due to the main beam by a significant margin. High antenna gain, low free-space side lobes, and a sharp STC curve help reduce this external interference.

Another means of reducing external interference is the proposed receiver side-lobe suppression (RSLS) feature discussed in Chapter 2. By comparing signals received on both the directional and omnidirectional antennas, RSLS electronics can usually determine whether or not a reply was received through the side lobes. Main-beam fruit, of course, goes undetected, and the possibility exists that the decision to suppress detection of a strong side-lobe response may mask ("kill") the detection of a valid main-beam reply.

The simulation of RSLS in conjunction with the complex model is described in Chapter 5 and numerical results presented in Chapter 6 for a variety of assumed interference environments. Fruit counts are also tabulated for these environments without RSLS to assess the performance of several system configurations. The ratio of received replies to interrogations is also presented as an indicator of the probability of main-beam kill due to RSLS.

The area under the downlink contours of constant power outside the desired zones of coverage is the simple-model criterion used to assess susceptibility to external interference. Just as

in the determination of contributions to interference, a spherical-earth-horizon barrier is utilized to limit realistically the extent of the area of potential interference over a flat earth.

## 3.5 Susceptibility to Self-Interference

In the context of the performance criteria described above, self-interference is meant here to imply the generation of invalid responses by a ground site through both uplink and downlink phenomena. One example of self-interference is the false-suppression mechanism described in Section 3.2. Such a phenomenon certainly represents a case of an interrogator's interfering with its own operation, the result being loss of coverage.

There is another way, however, in which an interrogator/receiver can contribute to its own degradation independent of the influence of other interrogators or of aircraft outside its domain. If a particular system configuration that otherwise results in acceptable performance tends to produce false targets, its operation may still be impaired seriously. False targets arise for two principal reasons. One is usually referred to as side-lobe "punch-through", a phenomenon analogous to the false suppression mechanism described previously. Punch-through simply involves the rising of a directional antenna side lobe to a level higher than that of the omnidirectional pattern in the same direction. Thus, a reply rather than suppression is initiated. Such a phenomenon becomes likely when directional antenna side lobes are high and when the phase centers of directional and omni antennas

are vertically displaced so as to cause misalignment of nulls of the two vertical lobing patterns. A proposed configuration for alignment of the nulls through use of a common aperture for both antennas is discussed and analyzed in Chapter 6.

The simple model can be used to explore side-lobe regions suspected of being susceptible to punch-through. This is accomplished by assuming the side lobe of interest to be a main beam. The vertical radiation pattern at that particular azimuth is also inserted into the model. Then any coverage area that results is simply the punch-through area, for no coverage would result if the side lobe were covered or suppressed by the omnidirectional pattern.

False targets also arise because of reflections from terrain and buildings. When the relative locations of radar site, aircraft, and reflecting surface are suitable, improved SLS tends to minimize the effect of reflections. All too often, however, the problem geometry or behavior of the transponder (even within the bounds of the U.S. National Standard) causes improved SLS to be ineffective. A good indicator of susceptibility to reflection is provided by the features of the complex model. The extent of the side-lobe reception area, described above as a criterion for measuring susceptibility to external interference, is also a measure of the degree to which replies to reflected main-beam interrogations can be received through the side lobes. The lower the side lobes, the lesser the susceptibility to side-lobe

replies.

## 3.6 Target Quality

The quality of a target deals with the number and distribution of hits received on a particular scan of the radar. Perhaps even more important is a parameter called track quality, which concerns the authenticity of the estimate of an aircraft's motion based on observations of a succession of target declarations. Although a particular target may involve very few hits or returns, it is only when several such poor targets are received on consecutive scans that track quality is likely to degrade to the point of loss of contact.

Clearly, such indications require the detail and features of the complex simulation model, although some qualitative conclusions can be drawn using the simple flat-earth approximation. For example, it is intuitive that if a fixed uncovered area were to be distributed throughout a desired area of coverage, it should be divided into small slivers through which an aircraft would fly quickly. This would minimize the prolonged presence of an aircraft in a hole and maximize track quality. Thus, it is generally preferable to have several thin holes rather than one gaping hole of the same total area. The simple model, as shown in Chapter 6, can indicate this size and distribution of coverage gaps in space.

Of most importance in the indication of target and track quality, however, are the performance criteria provided by the complex model. These criteria include the distribution of the

number of consecutive scans with fewer than some specified number of hits, the total number of scans with fewer than 1 through 10 hits, the average number of replies per scan and standard deviation from the average, and the ratio of received replies to interrogations.

Target and track quality can be degraded both by external interference and by the characteristics of the particular system in question. Although the criteria discussed above are indicative of the extent of degradation, there may be particular flight profiles or special system configurations that require the use of other criteria. For this reason and to provide a physical correlation with the numerical performance criteria, the complex simulation model produces a graphic hit-by-hit representation of the target track both on a standard line printer and on a drum plotter. This feature of the complex simulation model affords a convenient quick-look capability and a tool for demonstrating various performance levels to those whose daily tasks bring them more frequently in contact with a plan position indicator than with computer printout.

# CHAPTER 4

# A SIMPLE FLAT-EARTH MODEL OF ATCRBS OPERATION

## 4.1 Introduction

In this chapter the equations for propagation of radiation between interrogator and aircraft over a flat earth are derived. These equations, after several simplifying assumptions are made, allow slant range for contours of constant interrogator power and receiver sensitivity to be expressed as a single-valued function of the elevation angle of the aircraft. This formulation and a polynomial approximation for vertical antenna radiation above and below the local horizontal plane yield a closed-form expression for the area within a vertical-lobing contour bounded by two arbitrary elevation angles.

The area under the downlink lobing contour is obtained from the uplink equations by a few parametric substitutions and the addition of a term that describes the operation of the ground receiver's sensitivity-time control circuit. Next, the equations describing the spherical-earth-horizon barrier are derived and their use in the flat-earth model discussed. The algorithms used to compute the slant range and elevation angle of intersection of the various lobing and coverage contours are explained in detail. These points of intersection allow the closed-form expressions for coverage area to be evaluated, as the limits of the integral involved are the elevation angles bounding the coverage area.

## 4.2 Ray Propagation over a Flat Earth

The geometry of propagation of rays from a typical ATCRBS interrogator located at I, a height $h_i$ above the ground, to an aircraft transponder located at T, a height $h_t$ above the ground, is shown in Figure 4.1 for a flat earth. (The case of a spheri-

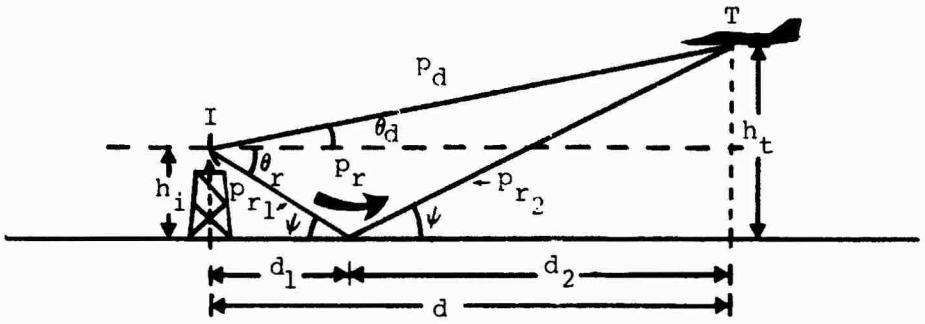


Figure 4.1 Geometry of Ray Propagation over a Flat Earth

cal earth is considered in Chapter 5; it will be shown later that the flat-earth assumption affords the convenience of closed-form expressions for all performance criteria.) The distance between the points on the earth's surface directly beneath the interrogator and transponder is d, while an ATCRBS interrogation traverses a direct path or slant range of length $p_d$ en route to the aircraft.

A signal generally weaker than the direct-path transmission, but whose strength depends upon the physical properties of the terrain surrounding the interrogator site, also arrives at the aircraft by way of the indirect or reflected path, $p_r$. The angle

of incidence or grazing angle $\psi$ of the first portion of the reflected path, $p_{r_1}$, equals the angle of reflection made by the second portion of the reflected path, $p_{r_2}$, with the surface of the earth at the reflection point. The elevation angle $\theta$ of the aircraft with respect to the interrogator is defined positive upward from the local horizontal plane of the interrogator. Any indirect ray leaves the antenna at a negative elevation angle, usually a small negative angle.

For the present only propagation in a vertical plane is of interest, as coverage is determined primarily by interference between the direct and reflected paths. If the two rays arrive at the aircraft antenna with the same phase, their resultant power will be greater than that of either individual signal. On the other hand, they may arrive out of phase and cancel each other, thus causing the target to go undetected; it is this loss of signal due to "vertical lobing" that causes holes or gaps in radar system coverage and that has motivated the development of new ATCRBS antennas by the Transportation Systems Center for the FAA.

The transmission and reception of interrogation pulses in the ATCRBS involve a number of operations as depicted in Figure 4.2. First, interrogation pulses of peak power $P_i$ (watts) are generated and sent through a transmission line to the directional antenna. (The process is analogous for the omnidirectional antenna.) The transmission line causes the signal power to be re-

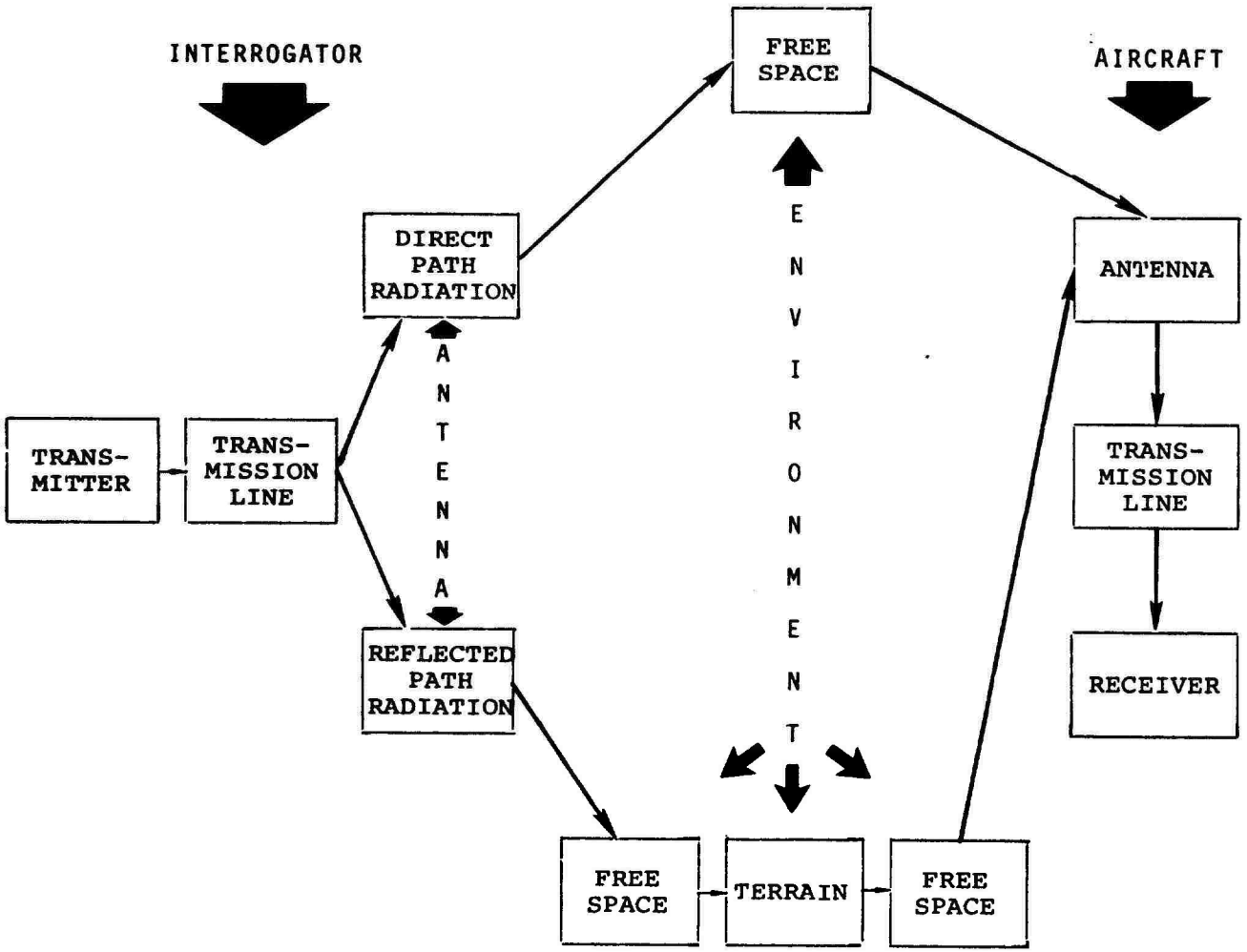


Figure 4.2 Flow Diagram for ATCRBS Interrogations

duced to a factor $L_i$ of its original value. $L_i$ is between 0 and 1, but is usually about 0.5 (a 3-dB line loss).

Once the signal reaches the antenna, it is radiated into space with a power distribution very much dependent on the direction of interest. The free-space vertical radiation pattern of a standard ATCRBS antenna is shown in Figure 4.3. To normalize the power distribution with respect to the boresight or direction of maximum radiation, the antenna gain $G_i$ can be separated from the free-space power pattern factor $A_f(\theta)$. It is assumed here that the azimuthal plane with which we are concerned contains the antenna boresight. Thus there is no attenuation of the signal due to the azimuthal radiation pattern, but merely that caused by the vertical antenna pattern. Depending on the elevation angle with which the ray of interest leaves the antenna, then, the signal power is boosted by a factor $G_i$ ($1<G_i<\infty$), nominally 200 (23 dB) for ATCRBS and then attenuated by the pattern factor $A_f(\theta)$, which is between 0 and 1.

The energy thus radiated $[P_i L_i G_i A_f(\theta)]$ is distributed over a sphere in space that grows in radius r at the speed of light. The power density $\Phi$ thus decreases as the range from the antenna increases according to the following equation:

$$\Phi = \frac{P_i \; L_i \; G_i \; A_f(\theta)}{4\pi r^2} \qquad (4.1)$$

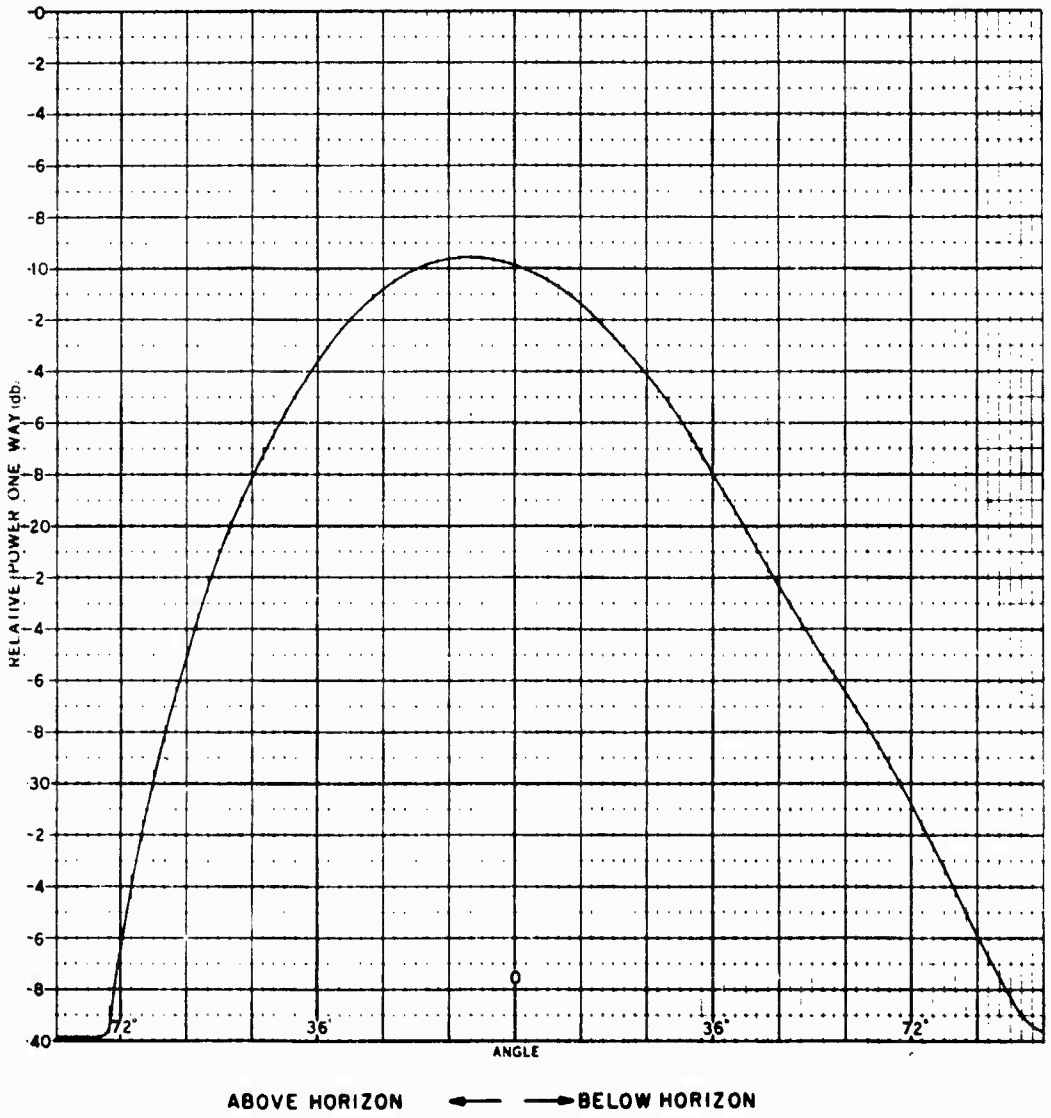


Figure 4.3 Free-Space Vertical Radiation Pattern of Standard ATCRBS Antenna

In the absence of reflections from the ground, equation (4.1) would properly represent the power density at the aircraft with $r=p_d$. However, the indirect ray must be accounted for with great care for several reasons. First, upon striking the ground, both the magnitude and phase of the incident signal are altered according to the electromagnetic properties of the reflecting surface (specifically, the conductivity and relative permittivity of the surface). This alteration of signal magnitude and phase, which depends also on the wavelength and grazing angle of the incident radiation, is generally described by use of a parameter known as the reflection coefficient. Although this matter will be treated in more detail in Chapter 5, the magnitude $C_r$ of the reflection coefficient will be assumed in this flat earth case to be unity, while the phase $\delta$ of the coefficient will be $\pi$. Such an assumption, which is especially valid at low grazing angles over land[5], will again prove crucial in the development of analytical expressions for the performance criteria.

Another slight alteration of the indirect ray is caused by the fact that it undergoes greater attenuation than the direct ray because of its longer path. Again, this factor is assumed negligible for the purposes of Chapter 4.

The most important phenomenon for our consideration is the difference in signal phases upon arrival at the transponder due to the slightly different lengths of the direct and reflected paths. Whereas this slight difference was not significant enough

to contribute to the free-space loss over the indirect path, it is extremely influential in causing phase variations of a signal whose wavelength is approximately one foot. This is true because a variation of just half a wavelength between the direct and reflected paths (just six inches) can mean the difference between addition and subtraction of the two arriving signals. The phase difference $\gamma$ between direct and reflected signals is given by

$$\gamma = \frac{2\pi}{\lambda}(p_r - p_d) \tag{4.2}$$

The vector addition of direct and reflected signals is perhaps best understood by reference to Figure 4.4, which is adapted

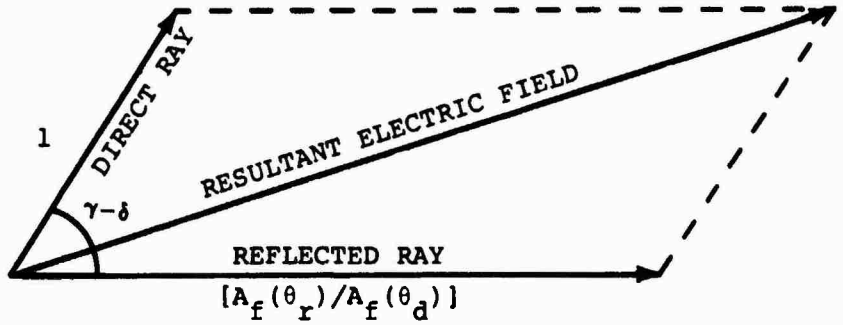


Figure 4.4 Vector Sum of Direct and Reflected Rays

from Reed and Russell[5], p. 110. The electric field intensity vectors, of course, and not the power contained in the signals, are to be added. The direct-path signal is assumed to have unit strength, while the reflected-path signal differs from the direct

by the square root of the ratio of its power pattern factor to that of the direct ray. Since antenna design tends to minimize radiation toward the ground and to keep the signal up where the aircraft are, $A_f(\theta_r)$ is generally less than $A_f(\theta_d)$. It is entirely possible, however, that through a combination of poor antenna design and problem geometry, such as an aircraft passing nearly over the antenna, the reflected signal can exceed the direct signal in magnitude.

The total phase difference between the two vectors is simply the sum of the phase lag $\delta$ of the reflection coefficient and the phase difference $\gamma$ between the two arriving signals. As will be seen in Chapter 5, the magnitude of the reflection coefficient is simply multiplied by the square root of the ratio of the power pattern factors when the coefficient is not unity. If the square of the resultant electric field vector in Figure 4.4 is denoted as $A_v$, a vertical lobing factor, then the law of cosines gives

$$A_v = 1 + \frac{A_f(\theta_r)}{A_f(\theta_d)} + 2\left[\frac{A_f(\theta_r)}{A_f(\theta_d)}\right]^{1/2} \cos(\gamma-\delta) \qquad (4.3)$$

The vertical lobing factor $A_v$ can now be appended to equation (4.1) to complete the mathematical description of power density at some point in space.

One additional factor that will be neglected for the purposes of this thesis is the antenna pattern of the aircraft.

Although the aircraft antenna pattern is of utmost importance, and indeed often the crux of many other analyses, the primary concern here is the proper adjustment of the ground-based interrogator/receiver given a standard airborne system. Since aircraft antennas generally operate in a standard way during air-to-ground transmissions (and vice versa), it is assumed for this analysis that the radiation pattern of the antenna mounted on the aircraft causes no variation in signal attenuation as a function of the angle of arrival of the signal. Rather, it is assumed that the power pattern factor for the aircraft is unity. The times when this assumption becomes invalid are primarily those involving aircraft turns or other maneuvers, and those in which an aircraft flies near the interrogator. These instances can be neglected in the development of the performance criteria described previously.

Although the effect of the aircraft power pattern will be neglected, the aircraft antenna in Figure 4.2 will be represented mathematically by a gain, $G_a$. Another characteristic of the aircraft antenna must be considered, since the antenna is receiving the interrogation. This characteristic is the so-called effective area of the antenna, $A_e$, which actually includes the antenna gain and is given mathematically by

$$A_e = \frac{G_a \lambda^2}{4\pi} \tag{4.4}$$

where $\lambda$ is the wavelength of the incident radiation. The greater

the effective area, of course, the greater the energy received by the antenna for a given power density.

The two blocks remaining to be described in Figure 4.2 are the transmission line and the receiver in the aircraft. The former can be represented by a loss factor $L_a$ analogous to that of the interrogator, while the receiver is characterized by its sensitivity $S_a$ or minimum triggering level (MTL), the weakest detectable signal. Sensitivity is usually expressed in decibels below a milliwatt (-dBm) and is allowed to vary according to the U. S. National Standard for ATCRBS from -72 dBm to -80 dBm.

The power $P_t$ in a pulse arriving at the aircraft receiver can now be described completely:

$$P_t = \Phi A_e$$

$$= \frac{P_i L_i G_i A_f(\theta_d)}{4\pi p_d^2} A_v \frac{G_a \lambda^2}{4\pi}$$

$$= \frac{P_i L_i G_i G_a \lambda^2}{(4\pi)^2} \frac{1}{p_d^2} \left\{ A_f(\theta_d) + A_f(\theta_r) \right.$$

$$\left. - 2 \left[ A_f(\theta_d) A_f(\theta_r) \right]^{1/2} \cos\left[ \frac{2\pi}{\lambda} (p_r - p_d) \right] \right\} \qquad (4.5)$$

In order to detect an incoming signal of power $P_t$, then, the transponder sensitivity $S_a$, expressed in the same units of power

as $P_t$, must satisfy the inequality

$$P_t > S_a$$

One measure of system coverage that appears reasonable is the total area in a vertical plane containing the antenna boresight within which a specified power density is exceeded. That is to say, any aircraft with a specified effective area, line loss, and receiver sensitivity could be guaranteed of receiving interrogation pulses within such an area; outside the area, the power density would fall below that necessary to allow detection by the aircraft transponder. The ratio of this covered area to the desired coverage area would thus be a measure of, for example, a particular antenna's performance.

The determination of this coverage area would be a straightforward task were it not for the presence of $p_d^2$ in the denominator of equation (4.5) and of $p_d$ in the cosine term of the same equation. The presence of $p_d$ in both places precludes a closed-form solution for $p_d$ as a function of interrogator and aircraft characteristics, and the problem geometry. If such a closed-form solution were available, then the area under the contour of constant power could be obtained by integrating $p_d$ in polar coordinates as follows:

$$C = \int_{\theta_1}^{\theta_2} \frac{1}{2} p_d^2 \, d\theta \qquad (4.6)$$

where C is the coverage area, and $\theta_1$ and $\theta_2$ are the lower and upper elevation angles, respectively, within which knowledge of the covered area is desired.

We shall proceed now to reduce equation (4.5) to a form from which $p_d$ can be extracted analytically. In particular, an attempt will be made to eliminate the dependence of the cosine term on $p_d$.

The following equations can be deduced from inspection of Figure 4.1:

$$\tan \psi = \frac{h_i}{d_1} = \frac{h_t}{d_2} \tag{4.7}$$

$$d = d_1 + d_2 = \frac{h_i + h_t}{\tan \psi} \tag{4.8}$$

$$\begin{aligned} p_r = p_{r_1} + p_{r_2} &= \left|h_i^2 + d_1^2\right|^{1/2} + \left|h_t^2 + d_2^2\right|^{1/2} \\ &= h_i\left[1 + \frac{d^2}{(h_i+h_t)^2}\right]^{1/2} + h_t\left[1 + \frac{d^2}{(h_i+h_t)^2}\right]^{1/2} \\ &= \left|(h_i + h_t)^2\right|^{1/2}\left[1 + \frac{d^2}{(h_i + h_t)^2}\right]^{1/2} \\ &= \left|(h_i + h_t)^2 + d^2\right|^{1/2} \end{aligned} \tag{4.9}$$

But it is clear also that

$$d = p_d \cos \theta_d \tag{4.10}$$

and

$$h_t = h_i + p_d \sin \theta_d \tag{4.11}$$

Substituting (4.10) and (4.11) into (4.9), one obtains

$$p_r = \left|(2h_i + p_d \sin \theta_d)^2 + (p_d \cos \theta_d)^2\right|^{1/2}$$

$$= \left|4h_i^2 + 4h_i\, p_d \sin \theta_d + p_d^2\right|^{1/2} \tag{4.12}$$

Equation (4.12) can now be inserted into equation (4.2):

$$\gamma = \frac{2\pi}{\lambda}\left\{\left[4h_i^2 + 4h_i\, p_d \sin \theta_d + p_d^2\right]^{1/2} - p_d\right\}$$

$$= \frac{2\pi}{\lambda}\, p_d\left\{\left[4\frac{h_i^2}{p_d^2} + 4\frac{h_i}{p_d} \sin \theta_d + 1\right]^{1/2} - 1\right\} \tag{4.13}$$

Since, for most aircraft ranges and antenna heights of interest we can make the approximation

$$\frac{h_i^2}{p_d} << 1 \tag{4.14}$$

then $\gamma$ becomes

$$\gamma \simeq \frac{2\pi}{\lambda} p_d \left\{ \left[ 4 \frac{h_i}{p_d} \sin \theta_d + 1 \right]^{1/2} - 1 \right\} \tag{4.15}$$

Since

$$4 \frac{h_i}{p_d} \sin \theta_d << 1 \tag{4.16}$$

the first two terms of the binomial series can be used to approximate the square root in equation (4.15):

$$\gamma \simeq \frac{2\pi}{\lambda} p_d \left\{ 1 + \frac{1}{2} \left( 4 \frac{h_i}{p_d} \sin \theta_d \right) - 1 \right\}$$

$$\simeq \frac{4 \pi h_i \sin \theta_d}{\lambda} \tag{4.17}$$

or for small $\theta_d$

$$\gamma \simeq \frac{4 \pi h_i}{\lambda} \theta_d \tag{4.18}$$

With the expression for $\gamma$ now independent of $p_d$, there remains just one approximation for the solution of equation (4.5). Since the angle $\theta_r$ for the case of a flat earth is just $-\psi$, which is a function of $p_d$, we can assume for the antenna heights and ranges of interest that $\psi \simeq \theta_d$, and thus $\theta_r = -\psi \simeq -\theta_d$. The power pattern factor $A_f(\theta_r)$ can thus be replaced in equation (4.5) by

$A_f(-\theta_d)$. Finally, equation (4.5) becomes

$$P_t = \frac{K}{p_d^2}\left\{A_f(\theta_d) + A_f(-\theta_d) - 2\left[A_f(\theta_d)\ A_f(-\theta_d)\right]^{1/2}\cos\left(\frac{4\pi h_i}{\lambda}\theta_d\right)\right\} \tag{4.19}$$

where

$$K = \frac{P_i\ L_i\ G_i\ G_a\ \lambda^2}{(4\pi)^2} \tag{4.20}$$

## 4.3 System Coverage Area

Before the various performance criteria are derived and described, we shall evaluate the integral of equation (4.6). The closed-form expression we obtain for this integral will become the basis for the performance criteria themselves.

The integral cannot be evaluated merely by solving equation (4.19) for the integrand $p_d^2$. Rather, one must first determine a form for $A_f(\theta_d)$ and $A_f(\theta_r)$ that allows the integral to be evaluated. Furthermore, the form of the power pattern factor must be such as to describe adequately the many antenna radiation patterns that may be evaluated by this technique. The convenient forms that we shall use are as follows:

$$A_f(\theta_d) = (a + b\theta + c\theta^2 + d\theta^3)^2 \tag{4.21}$$

and

$$A_f(\theta_r) = (w + x\theta + y\theta^2 + z\theta^3)^2 \tag{4.22}$$

Since the chosen form is the square of some expression, that expression, which is the square root of the power pattern factor, represents the voltage pattern factor. Since the voltage pattern factor is a third-order polynomial, a least-squares fit to this polynomial may be made easily using empirical data from antenna pattern test ranges. Since power patterns are usually recorded for the test data, the square root of the data points that comprise the power pattern must be inserted into the least squares fit routine. This process is much simpler, however, than that involved in solving the integral with assumed forms for the power pattern factors other than those given in equations (4.21) and (4.22). The procedure used to develop a least squares fit of empirical data to polynomials of the form of (4.21) and (4.22) and thus to determine a, b, c, d, w, x, y, and z, is described in Appendix A.

The accuracy of the least squares fit afforded by the third-order polynomial should be sufficient to describe most antenna patterns that will be encountered in practice. A higher-order polynomial could be employed at the expense of effort, but not ingenuity. Simpler expressions can be obtained from the result that will be derived in the following merely by setting the appropriate higher-order coefficients (d,z,c,y,etc.) to zero.

Two separate forms for the power pattern factor have been allowed to accommodate a sharp slope in the elevation pattern below the horizon. That is, the antenna radiation pattern is

assumed to have two sections: one applicable for elevation angles above the horizon and the other for negative elevation angles. In the case of a flat earth this assumption causes no difficulty because an aircraft flying at a negative elevation angle would be at an altitude less than the height of the antenna (typically 30 feet). Over a spherical earth, of course, aircraft are detected at negative elevation angles when they are flying at extreme ranges near the horizon. Thus, in the flat-earth case, all direct-path radiation occurs at positive elevation angles, while all reflected radiation leaves the interrogator antenna at a negative angle.

Sufficient information is now available to allow evaluation of the coverage area, C:

$$C = \frac{K}{2P_t}\left\{\int_{\theta_1}^{\theta_2} (a+b\theta+c\theta^2+d\theta^3)^2\, d\theta + \int_{\theta_1}^{\theta_2} (w-x\theta+y\theta^2-z\theta^3)^2\, d\theta \right.$$

$$\left. - 2\int_{\theta_1}^{\theta_2} (a+b\theta+c\theta^2+d\theta^3)(w-x\theta+y\theta^2-z\theta^3)\cos(q\theta)\, d\theta\right\} \quad (4.23)$$

where

$$q = \frac{4\pi h_i}{\lambda} \quad (4.24)$$

The third integral in (4.23) is the one that requires a judicious choice of the form of the power pattern factor. If a polynomial

had been chosen for the power pattern instead of the voltage pattern, that third integral would contain the square of the product of two polynomials as well as the cosine term.

Expanding the integrands and denoting the three integrals in equation (4.23) by $I_1$, $I_2$, and $I_3$, respectively, so that

$$C = \frac{K}{2P_t}\left(I_1 + I_2 - 2I_3\right) \tag{4.25}$$

one obtains

$$\begin{aligned} I_1 = {} & a^2(\theta_2-\theta_1) + ab(\theta_2^2-\theta_1^2) + \tfrac{1}{3}(2ac+b^2)(\theta_2^3-\theta_1^3) \\ & + \tfrac{1}{2}(ad+bc)(\theta_2^4-\theta_1^4) + \tfrac{1}{5}(2bd+c^2)(\theta_2^5-\theta_1^5) \\ & + \tfrac{1}{3}cd(\theta_2^6-\theta_1^6) + \tfrac{1}{6}d^2(\theta_2^7-\theta_1^7) \end{aligned} \tag{4.26}$$

$$\begin{aligned} I_2 = {} & w^2(\theta_2-\theta_1) - wx(\theta_2^2-\theta_1^2) + \tfrac{1}{3}(2wy+x^2)(\theta_2^3-\theta_1^3) \\ & - \tfrac{1}{2}(wz+xy)(\theta_2^4-\theta_1^4) + \tfrac{1}{5}(2xz+y^2)(\theta_2^5-\theta_1^5) \\ & - \tfrac{1}{3}yz(\theta_2^6-\theta_1^6) + \tfrac{1}{6}z^2(\theta_2^7-\theta_1^7) \end{aligned} \tag{4.27}$$

The expression for $I_3$ is contained on the next page.

$$I_3 = \frac{aw}{q}[\sin(q\theta_2)-\sin(q\theta_1)] + \frac{(-ax+bw)}{q^2}[\cos(q\theta_2)+q\theta_2\sin(q\theta_2)$$

$$-\cos(q\theta_1)-q\theta_1\sin(q\theta_1)] + \frac{(ay-bx+cw)}{q^3}[2q\theta_2\cos(q\theta_2)$$

$$+(q^2\theta_2^2-2)\sin(q\theta_2)-2q\theta_1\cos(q\theta_1)-(q^2\theta_1^2-2)\sin(q\theta_1)]$$

$$+ \frac{(-az+by-cx+dw)}{q^4}[(3q^2\theta_2^2-6)\cos(q\theta_2)+(q^3\theta_2^3-6q\theta_2)\sin(q\theta_2)$$

$$-(3q^2\theta_1^2-6)\cos(q\theta_1)-(q^3\theta_1^3-6q\theta_1)\sin(q\theta_1)]$$

$$+ \frac{(-bz+cy-dx)}{q^5}[(q^4\theta_2^4-12q^2\theta_2^2+24)\sin(q\theta_2)$$

$$+(4q^3\theta_2^3-24q\theta_2)\cos(q\theta_2)-(q^4\theta_1^4-12q^2\theta_1^2+24)\sin(q\theta_1)$$

$$-(4q^3\theta_1^3-24q\theta_1)\cos(q\theta_1)]$$

$$+ \frac{(-cz+dy)}{q^6}[(5q^4\theta_2^4-60q^2\theta_2^2+120)\cos(q\theta_2)$$

$$+(q^5\theta_2^5-20q^3\theta_2^3+120q\theta_2)\sin(q\theta_2)-(5q^4\theta_1^4-60q^2\theta_1^2+120)\cos(q\theta_1)$$

$$-(q^5\theta_1^5-20q^3\theta_1^3+120q\theta_1)\sin(q\theta_1)] - \frac{dz}{q^7}[(q^6\theta_2^6-30q^4\theta_2^4+360q^2\theta_2^2$$

$$-720)\sin(q\theta_2)+(6q^5\theta_2^5-120q^3\theta_2^3+720q\theta_2)\cos(q\theta_2)-(q^6\theta_1^6-30q^4\theta_1^4$$

$$+360q^2\theta_1^2-720)\sin(q\theta_1)-(6q^5\theta_1^5-120q^3\theta_1^3+720q\theta_1)\cos(q\theta_1)]$$

(4.28)

## 4.4 Parametric Changes for the Downlink

The form of the equations for computation of downlink coverage is the same as that of the uplink. Several parametric substitutions must be made, however. In particular the ground interrogator power $P_i$, loss $L_i$, and antenna gain $G_i$ in equation (4.20) must be replaced by the corresponding parameters for the aircraft transponder, which in the downlink case, of course, becomes the transmitter. Likewise in equation (4.20), $G_a$ must be replaced by the gain of the ground antenna $G_i$, and $\lambda$ should be the wavelength of radiation at the downlink frequency, 1090 MHz. Note that the substitution of $G_a$ for $G_i$ and $G_i$ for $G_a$ nullifies the need for numerical substitution in the model because of preservation of the two factors.

Another substitution required for determination of downlink coverage is that of 1090 MHz antenna pattern data for 1030 MHz data in the procedure of Appendix A used to arrive at the analytic forms of equations (4.21) and (4.22) for positive-angle and negative-angle vertical antenna patterns. This substitution results in the computation of four new coefficients for each of the two polynomials.

Equations (4.24) and (4.25) also require modification. In the former the downlink wavelength must again be used, while in the latter, $P_t$ must be replaced by the sensitivity of the ground receiver.

When an omnidirectional antenna coverage contour is involved

in any of the foregoing computations, similar substitutions are made for the characteristics of the omni system including its line loss, antenna gain and vertical radiation pattern, and peak pulse power. The height of the omni must also be used in place of $h_i$.

## 4.5 Receiver Sensitivity-Time Control

The power received on the ground results in a detected reply when it exceeds the receiver sensitivity, $S_r$, a time-varying parameter. In the ATCRBS, receiver sensitivity involves a maximum value, $S_{max}$, or minimum triggering level (MTL) and a sensitivity-time control (STC) that reduces sensitivity initially (at a time corresponding to 1 nm of slant range) by some adjustable amount $\Delta S$, usually 10 to 50 dB, and subsequently recovers at a nominal rate of 6 dB (power sensitivity) per doubling of range ("per octave"). This is done to compensate for the free space loss in a signal with range; thus, a close-in target is sensed no more easily than one farther away beacuse the receiver is less sensitive to the closer target.

The STC action can be described mathematically by the equation

$$S_{r_{dBm}} = S_{max_{dBm}} + \Delta S_{dB} - 20 \log_{10} p_d \qquad (4.29)$$

where $p_d$ is assumed to be expressed in nm. Equation (4.29) is only applicable up to the range of full recovery; otherwise,

receiver sensitivity could get greater than $S_{max}$. Outside full recovery range, sensitivity simply equals the MTL. The total amount of desensitization from MTL is given by the last two terms of equation (4.29). When determining $p_d(\theta)$ for the downlink, therefore, these desensitization terms must be taken into account.

First, $p_d(\theta)$ is determined using maximum receiver sensitivity and solving the downlink equation of the form (4.19) for $p_d$. As long as the sum of the desensitization terms is negative, which implies full recovery (negative desensitization), the value of $p_d$ is in fact that range from which a downlink signal of specified power can be detected. If, however, there is a positive desensitization, the value of $p_d(\theta)$ is too great for detection and must be reduced by an amount sufficient to allow the increase in power at the shorter range to offset the desensitization. Mathematically, one can accomplish this by replacing $p_d$ with a new value $p_d'$ given by

$$p_d' = p_d \left( \frac{p_d}{10^{.05\Delta S_{dB}}} \right) \tag{4.30}$$

## 4.6 The Spherical-Earth-Horizon Barrier

It was explained in Chapter 3 that the use of a flat-earth model requires a means of limiting radar range to that encountered over a spherical earth. The distance to the horizon over a spherical earth can be determined simply with reference to Figure 4.5. Clearly, the total range $r_{hor}$ is just the sum of the

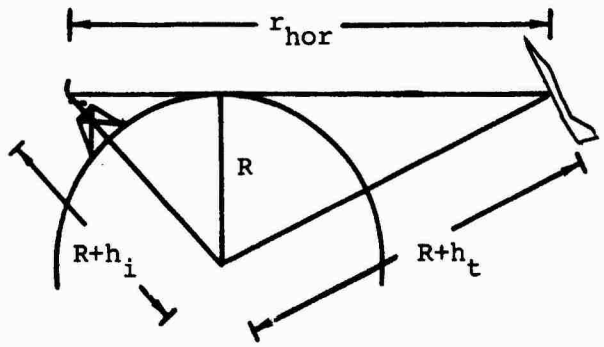


Figure 4.5 Distance to the Horizon Over a Spherical Earth

distance from the horizon to the interrogator and of that from the horizon to the aircraft:

$$r_{hor} = \left|(R+h_i)^2 - R^2\right|^{1/2} + \left|(R+h_t)^2 - R^2\right|^{1/2}$$

$$= \left|2h_iR + h_i^2\right|^{1/2} + \left|2h_tR + h_t^2\right|^{1/2} \qquad (4.31)$$

If the two altitudes are assumed negligible compared to the radius of the earth, then

$$r_{hor} = \left|2h_iR\right|^{1/2} + \left|2h_tR\right|^{1/2} \qquad (4.32)$$

Chapter 5 covers the use of a four-thirds earth radius to account for refraction of rays near the earth's surface. Using a value of 5280 mi for this R and expressing $h_i$ and $h_t$ in ft, one obtains

$$r_{hor_{mi}} = \left|2h_i\right|^{1/2} + \left|2h_t\right|^{1/2} \qquad (4.33)$$

When any value of $p_d$ is determined by the flat-earth model to be greater than $r_{hor}$, the value is reduced to $r_{hor}$ to effect the spherical-earth-horizon barrier.

## 4.7 Desired Coverage Boundary

The desired area of coverage discussed in Chapter 3 has a constant slant range $p_{d_{max}}$ up to the critical angle $\theta_c$ at which a ray from the interrogator intercepts the service ceiling at a height $h_c$. If in Figure 4.1 the aircraft is assumed to be at this extreme corner of coverage at height $h_c$ and slant range $p_{d_{max}}$, the critical angle is seen to be

$$\theta_c = \sin^{-1}\left(\frac{h_c - h_i}{p_{d_{max}}}\right) \tag{4.34}$$

For elevation angles greater than $\theta_c$, the slant range $p_{d_c}$ to the service ceiling is just

$$p_{d_c} = (h_c - h_i) \csc \theta \tag{4.35}$$

## 4.8 Intersection of Lobing and Coverage Contours

The intersections of directional and omnidirectional antenna contours with each other, with the desired coverage curve, and with the spherical-earth-horizon barrier were discussed in Chapter 3. The algorithm used to determine these intersections in the flat-earth model's computational process is fairly straight-

forward.

First, the initial value of $\theta$ is used to compute $p_d(\theta)$ for each of the two curves in question, and the difference in the slant ranges is recorded. The value of $\theta$ is then increased by a prescribable amount, typically 0.1 deg, and the new value of the difference in the slant ranges is recorded. This process is continued until the value of the range difference changes sign; the change, of course, indicates a crossing of the curves.

Upon detection of a crossing, the algorithm halves the size of the increment of $\theta$ and changes its sign. The range difference is recorded again. Each successive cycle involves a halving of the angular increment, but the sign of the increment is changed only when the range difference changes sign. The process continues until the angular increment is less than some specified value (say $10^{-6}$ deg). The accuracy of the algorithm can be increased to the capability of the computer on which it is implemented at a fairly small expense in processing time.

After completion of the solution for the intersection, the algorithm continues with a fixed angular increment until the next crossing is detected. Generally a pair of closely-spaced intersections is found for every null or peak interaction. Thus, the flat-earth model can be used to determine the size of each null or peak of interest.

## 4.9 Desired Coverage Area

Because the critical angle described in Section 4.7 divides the desired coverage area into one region with constant maximum slant range $p_{d_{max}}$ and another region with constant service ceiling $h_c$, the desired coverage area within these regions can be expressed simply. Between any angle $\theta_1$ greater than 0 and any angle $\theta_2$ up to $\theta_c$, the covered area is

$$C_d = \frac{1}{2} p_{d_{max}}^2 \left(\theta_2 - \theta_1\right) \tag{4.36}$$

Between any angle $\theta_1$ greater than $\theta_c$ and any angle $\theta_2$ up to $\pi/2$, the covered area is

$$C_d = \frac{1}{2} \frac{\left(h_c - h_i\right)}{\sin \theta_1} \frac{\left(h_c - h_i\right)}{\sin \theta_2} \sin\left(\theta_2 - \theta_1\right)$$

$$= \frac{1}{2} \left(h_c - h_i\right)^2 \left(\cot \theta_1 - \cot \theta_2\right) \tag{4.37}$$

Between any angle $\theta_1$ greater than 0 and less than $\theta_c$, and any angle $\theta_2$ greater than $\theta_c$ and less than $\pi/2$, the covered area is a combination of the forms (4.36) and (4.37):

$$C_d = \frac{1}{2} p_{d_{max}}^2 \left(\theta_c - \theta_1\right) + \frac{1}{2} \frac{\left(h_c - h_i\right)^2 \sin\left(\theta_2 - \theta_c\right)}{\sin \theta_c \sin \theta_2}$$

$$= \frac{1}{2} \left\{ p_{d_{max}}^2 \left(\theta_c - \theta_1\right) + \left(h_c - h_i\right)^2 \left(\cot \theta_c - \cot \theta_2\right) \right\} \tag{4.38}$$

# CHAPTER 5

# A COMPLEX SPHERICAL-EARTH MODEL OF ATCRBS OPERATION

## 5.1 Introduction

In this chapter, the equations for propagation of radiation between an interrogator and aircraft over a spherical earth are derived. The derivation, which involves very few simplifying assumptions, allows the development of a detailed system simulation, one output of which is a computer-generated representation of a display that would be seen by an air traffic controller observing a particular flight profile of a test aircraft using a specified ATCRBS configuration. The antenna radiation patterns used by the simulation model include both uplink and downlink characteristics for directional and omnidirectional antennas in vertical and horizontal planes. Since the antenna patterns are generated in tabular form, the level of detail is limited only by the capacity of the computer used to implement the simulation and the patience of the user preparing data for input from measured test patterns.

After the general relationships between the propagation equations over the spherical earth and those derived in Chapter 4 for a flat earth are discussed, the more complicated elements of the spherical-earth model are developed. These elements include the vertical lobing factor, the complex reflection coefficient, two new solutions for the grazing angle, and the indirect path

length. Next, a lower limit of the grazing angle and an upper limit based on the roughness of the reflecting surface are presented. A statement of the transponder reply and suppression equations used in the model is followed by a description of the simulation of receiver side-lobe suppression. The RSLS section includes the development of interference and garble models used to investigate the impact of main-beam killing of valid replies on system performance. Finally the equations used to specify three different aircraft flight profiles are derived.

## 5.2 Propagation over a Spherical Earth

The geometry of propagation of rays from a typical ATCRBS interrogator located a height $h_i$ above the ground to an aircraft transponder at a height $h_t$ above the ground is shown in Figure 5.1 for a spherical earth. Although much of the nomenclature is

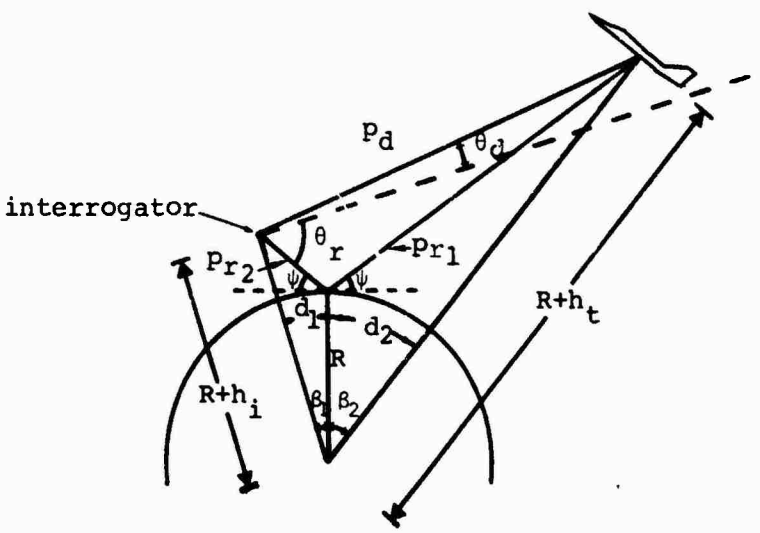


Figure 5.1 Geometry of Ray Propagation over a Spherical Earth

similar to that used for the flat-earth model, the relationships among the various quantities are in fact quite different.

In Figure 5.1, $p_d$ is the direct path length as before. The indirect path length or reflected path $p_r$ is just the sum of the two segments of the indirect path connecting the reflection point:

$$p_r = p_{r_1} + p_{r_2} \tag{5.1}$$

The elevation angles at which the direct and reflected rays leave the antenna are $\theta_d$ and $\theta_r$, respectively, and the angles of incidence and reflection of the indirect ray at the reflection point, also called the grazing angle, are denoted by $\psi$. The angle $\beta_1$ is subtended at the center of the earth by the arc of length $d_1$ along the surface of the earth joining the reflection point and the point directly beneath the interrogator. Similarly $\beta_2$ is subtended at the center of the earth by the arc of length $d_2$ along the surface of the earth joining the reflection point and the point vertically beneath the aircraft. The sum $\beta$ of these two angles will be of interest later:

$$\beta = \beta_1 + \beta_2 \tag{5.2}$$

The earth radius R used in this chapter and throughout the thesis is the so-called "four-thirds earth" radius or equivalent radius, which is used commonly to account for the effect of standard refraction on radio waves propagating through the earth's

atmosphere at shallow angles with respect to the surface[17,18,19]. Qualitatively, the effect of refraction is to cause the rays to bend toward the earth's surface rather than to continue in straight lines. This curvature of the rays allows them to propagate beyond the optical horizon, which, because of the refraction of light in the atmosphere, lies beyond the geometric horizon. In order to allow the curved rays to be considered straight lines in the analysis that follows, one may replace the actual radius of the earth with four-thirds of its actual value. This process effectively flattens the earth and results in a mapping of the curved rays over the actual earth into straight rays over the four-thirds earth.

The power $P_t$ in a pulse arriving at the aircraft receiver can be expressed exactly as in Chapter 4 using equation (4.5):

$$P_t = \frac{P_i L_i G_i G_a A_f(\theta_d) \lambda^2}{(4\pi p_d)^2} A_v \qquad (5.3)$$

For the spherical earth, however, the expression for the vertical lobing factor $A_v$ contains more terms than did equation (4.3):

$$A_v = 1 + \frac{A_f(\theta_r)}{A_f(\theta_d)}\left(\frac{p_d}{p_r}\right)^2 D^2 C_R^2 + 2\left[\frac{A_f(\theta_r)}{A_f(\theta_d)}\right]^{1/2} \frac{p_d}{p_r} D C_R \cos(\gamma-\delta) \qquad (5.4)$$

Whereas over the flat earth it was found that $\theta_r = -\theta_d$, $\theta_r$ must be determined in this case with reference to Figure 5.1 and the triangle whose vertices are the center of the earth, the reflec-

tion point, and the interrogator:

$$\frac{\pi}{2} - \theta_r = \beta_1 + \frac{\pi}{2} + \psi \tag{5.5}$$

Thus,

$$\theta_r = -\beta_1 - \psi \tag{5.6}$$

The terms in equation (5.4) involving $p_d$ and $p_r$ explicitly account for the fact that over the slightly longer reflected path the signal is attenuated by the factor $(p_d/p_r)$. This factor as well as D and $C_R$ would yield equation (5.4) directly if inserted into the geometry shown in Figure 4.4 for the vector addition of direct and reflected signals. The term D is the divergence factor, which accounts for the attenuation of a reflected ray due to the fact that a bundle of rays striking a spherical surface tends to diverge or spread out[17,18]. Divergence goes to zero as the grazing angle of the ray approaches $90^o$ (that is, the divergence factor approaches unity), while as the grazing angle becomes very small, the rays diverge so totally that D tends toward zero. Durlach[20] gives the following exact formula for divergence, which can be derived from Kerr[17], p. 406:

$$D = \left\{ \frac{(R+h_i)(R+h_t)\sin(d/R)}{R(p_{r_1}+p_{r_2})\cos\psi} \left[ 1 + \frac{2\,p_{r_1}p_{r_2}}{R(p_{r_1}+p_{r_2})\sin\psi} \right] \right\}^{-1/2} \tag{5.7}$$

where

$$d = d_1 + d_2 \tag{5.8}$$

To eliminate d from equation (5.7), the Law of Sines can be applied to the large triangle in Figure 5.1 to obtain

$$\left(R+h_t\right) \sin(d/R) = p_d \cos \theta_d \tag{5.9}$$

Then

$$D = \left\{ \frac{\left(R+h_i\right) p_d \cos \theta_d}{R\left(p_{r_1}+p_{r_2}\right) \cos \psi} \left[ 1 + \frac{2 p_{r_1} p_{r_2}}{R\left(p_{r_1}+p_{r_2}\right) \sin \psi} \right] \right\}^{-1/2} \tag{5.10}$$

The phase difference $\gamma$ between direct and reflected rays is the same for the spherical-earth model as it was in equation (4.2) for the flat-earth model. Two new terms in equation (5.4) remain to be discussed, however. They are the magnitude $C_R$ and the phase $\delta$ of the complex reflection coefficient. These parameters are addressed in the next section of this chapter.

Throughout Chapter 5, the same considerations should be made as explained in Section 4.4 regarding substitution of the appropriate parameters, such as wave length, antenna patterns, and transmitter powers, for development of downlink or omnidirectional antenna equations.

## 5.3 Reflection Coefficient

The reflection coefficient accounts for attenuation of the indirect ray due to the electromagnetic properties of the reflecting medium. Reed and Russell[18] give the following equation for the complex reflection coefficient:

$$C_R e^{j\delta} = \frac{n^2 \sin\psi - [n^2 - \cos^2\psi]^{1/2}}{n^2 \sin\psi + [n^2 - \cos^2\psi]^{1/2}} \tag{5.11}$$

where

$$n^2 = \varepsilon_r - jK \tag{5.12}$$

and

$$K = 60\,\sigma_r\,\lambda_{meters} \tag{5.13}$$

The conductivity of the reflecting medium is $\sigma_r$, its relative permittivity $\varepsilon_r$, and the wavelength of the incident radiation in meters $\lambda_{meters}$. A derivation of the solution for $C_R$ and $\delta$ as a function of the independent variables shown above is included as Appendix B. The results of that derivation are as follows:

$$C_R = \left[\frac{W^2 + X^2}{Y^2 + Z^2}\right]^{1/2} \tag{5.14}$$

and

$$\delta = \tan^{-1}(X/W) - \tan^{-1}(Z/Y) \tag{5.15}$$

where

$$W = \varepsilon_r \sin\psi - \left|\left(\varepsilon_r - \cos^2\psi\right)^2 + K^2\right|^{1/4} \cos\left[\frac{1}{2}\tan^{-1}\left(\frac{-K}{\varepsilon_r - \cos^2\psi}\right)\right] \tag{5.16}$$

$$X = -K\sin\psi - \left|\left(\varepsilon_r - \cos^2\psi\right)^2 + K^2\right|^{1/4} \sin\left[\frac{1}{2}\tan^{-1}\left(\frac{-K}{\varepsilon_r - \cos^2\psi}\right)\right] \tag{5.17}$$

$$Y = \varepsilon_r \sin\psi + \left|\left(\varepsilon_r - \cos^2\psi\right)^2 + K^2\right|^{1/4} \cos\left[\frac{1}{2}\tan^{-1}\left(\frac{-K}{\varepsilon_r - \cos^2\psi}\right)\right] \tag{5.18}$$

$$Z = -K \sin\psi + \left[\left(\varepsilon_r - \cos^2\psi\right)^2 + K^2\right]^{1/4} \sin\left[\frac{1}{2}\tan^{-1}\left(\frac{-K}{\varepsilon_r - \cos^2\psi}\right)\right] \qquad (5.19)$$

These expressions for $C_R$ and $\delta$ can now be inserted directly into equation (5.4).

## 5.4 The Grazing Angle

The commonly-used classical solution for the grazing angle over a spherical earth is given by W. T. Fishback in Kerr[17]. This solution, developed nearly thirty years ago, has been used fairly recently by Durlach[20,21] in problems involving tracking near the horizon. Although the exact solution for the grazing angle can be obtained in closed-form by solution of a quartic equation, Fishback's solution is considerably simpler, yet quite accurate. Simplicity, particularly in the era of development of Fishback's solution, can be an important factor in the absence of the services of a digital computer. Fishback's solution results from a cubic equation in $d_2$ (see Figure 5.1) that yields the following:

$$d_2 = \frac{d}{2} + p\cos\left(\frac{\phi+\pi}{3}\right) \qquad (5.20)$$

where

$$p = 2\left[\frac{R\left(h_i+h_t\right) + \frac{d^2}{4}}{3}\right]^{1/2} \qquad (5.21)$$

and

$$\phi = \cos^{-1}\left[\frac{2\,R\,d\,\left(h_i-h_t\right)}{p^3}\right] \qquad (5.22)$$

The apparent lack of recent original research related to solution of the grazing angle motivated the author to undertake such an endeavor. The following analysis is the result.

By inspection of Figure 5.1 and application of the Law of Sines, one can write

$$\frac{R + h_i}{\sin\ (90^o+\psi)} = \frac{R}{\sin[180^o-\beta_1-(90^o+\psi)]} \tag{5.23}$$

or

$$\frac{R + h_i}{\cos\ \psi} = \frac{R}{\cos\beta_1 \cos\ \psi - \sin\beta_1 \sin\psi} \tag{5.24}$$

Similarly,

$$\frac{R + h_t}{\cos\ \psi} = \frac{R}{\cos\beta_2 \cos\ \psi - \sin\beta_2 \sin\psi} \tag{5.25}$$

From equation (5.2) and Figure 5.1 it is known that

$$\beta = \beta_1 + \beta_2 = \frac{d}{R} \tag{5.26}$$

Thus

$$\beta_2 = \frac{d}{R} - \beta_1 \tag{5.27}$$

Rearranging terms and substituting (5.27) into (5.25) one obtains

$$\cos\beta_1 \cos\psi - \sin\beta_1 \sin\psi = \frac{R\cos\psi}{R + h_i} \tag{5.28}$$

and

$$\cos\left(\frac{d}{R} - \beta_1\right)\cos\psi - \sin\left(\frac{d}{R} - \beta_1\right)\sin\psi = \frac{R\cos\psi}{R + h_t} \qquad (5.29)$$

Collecting coefficients of the trigonometric functions of the grazing angle,

$$\left[\cos\beta_1 - \frac{R}{R + h_i}\right]\cos\psi = \sin\beta_1\sin\psi \qquad (5.30)$$

$$\left[\cos\left(\frac{d}{R} - \beta_1\right) - \frac{R}{R + h_t}\right]\cos\psi = \sin\left(\frac{d}{R} - \beta_1\right)\sin\psi \qquad (5.31)$$

Dividing equations (5.30) and (5.31) by $\cos\psi$,

$$\tan\psi = \frac{\cos\beta_1 - \frac{R}{R + h_i}}{\sin\beta_1} = \frac{\cos\left(\frac{d}{R} - \beta_1\right) - \frac{R}{R + h_t}}{\sin\left(\frac{d}{R} - \beta_1\right)} \qquad (5.32)$$

Equation (5.32) is an exact equation for $\psi$ in terms of several given parameters and the unknown $\beta_1$. Equation (5.9) can be solved for d, as is shown later in this section, to give a result in terms of $p_d$, $\theta_d$, $h_t$, and R. A solution of (5.32) for $\beta_1$ is now sought. Cross-multiplying numerators and denominators of the two right-hand portions of equation (5.32) one obtains

$$0 = \sin\left[\beta_1 - \left(\frac{d}{R} - \beta_1\right)\right] + \frac{R}{R + h_i}\sin\left(\frac{d}{R} - \beta_1\right) - \frac{R}{R + h_t}\sin\beta_1 \qquad (5.33)$$

After the substitutions

$$H_i = \frac{R}{R + h_i} \tag{5.34}$$

and

$$H_t = \frac{R}{R + h_t} \tag{5.35}$$

and expanding the terms in (5.34) it follows that

$$2 \sin \frac{d}{R} \sin^2\beta_1 - \left(H_i \cos \frac{d}{R} + H_t\right) \sin \beta_1 - \sin \frac{d}{R} + \left(2 \sin \beta_1 \cos \frac{d}{R} + H_i \sin \frac{d}{R}\right) \cos \beta_1 = 0 \tag{5.36}$$

Equation (5.36) is the foundation of two new solutions for the grazing angle, or rather for the intermediate angle $\beta_1$, from which the grazing angle can be found from equation (5.32). The first of the two new solutions is the solution of the quadratic in $\sin \beta_1$ obtained by assuming

$$\cos \beta_1 \simeq 1 \tag{5.37}$$

and making the appropriate substitution into (5.36):

$$\left[2 \sin \frac{d}{R}\right] \sin^2\beta_1 + \left[\cos \frac{d}{R} \left(2-H_i\right) - H_t\right] \sin \beta_1 + \sin \frac{d}{R}\left(H_i-1\right) = 0 \tag{5.38}$$

The solution of equation (5.38) is

$$\sin \beta_1 = \frac{-\left(2-H_i\right)\cos \frac{d}{R} + H_t + \left\{\left[\left(2-H_i\right)\cos \frac{d}{R} - H_t\right]^2 - 8 \sin^2 \frac{d}{R}\left(H_i-1\right)\right\}^{1/2}}{4 \sin \frac{d}{R}} \tag{5.39}$$

The trigonometric functions of (d/R) in equation (5.39) can be found from the following which are derived from the application of the Law of Sines and Law of Cosines to the triangles in Figure 5.1:

$$\sin \frac{d}{R} = \sin \beta = \frac{p_d \cos \theta_d}{\left[\left(R+h_i\right)^2 + 2\, p_d \sin \theta_d \left(R+h_i\right) + p_d^2\right]^{1/2}} \tag{5.40}$$

$$\cos \frac{d}{R} = \cos \beta = \frac{R+h_i + p_d \sin \theta_d}{\left[\left(R+h_i\right)^2 + 2\, p_d \sin \theta_d \left(R+h_i\right) + p_d^2\right]^{1/2}} \tag{5.41}$$

$$\tan \frac{d}{R} = \tan \beta = \frac{p_d \cos \theta_d}{R + h_i + p_d \sin \theta_d} \tag{5.42}$$

The second solution based on equation (5.36) is the solution of the cubic in $\sin \beta_1$ obtained by assuming

$$\cos \beta_1 \simeq 1 - \frac{1}{2} \sin^2 \beta_1 \tag{5.43}$$

The cubic equation is

$$\sin^3 \beta_1 + p \sin^2 \beta_1 + q \sin \beta_1 + r = 0 \tag{5.44}$$

where

$$p = \left(\frac{H_i}{2} - 2\right) \tan \frac{d}{R} \tag{5.45}$$

$$q = H_i - 2 + H_t \sec \frac{d}{R} \tag{5.46}$$

$$r = \left(1 - H_i\right) \tan \frac{d}{R} \tag{5.47}$$

The solution of the cubic equation (5.44) is

$$\sin \beta_1 = 2\left[\frac{-a}{3}\right]^{1/2} \cos\left(\frac{\phi}{3} + 240^{o}\right) - \frac{p}{3} \tag{5.48}$$

where

$$\phi = \cos^{-1}\left\{\frac{\frac{-b}{2}}{\left[\frac{-a^3}{27}\right]^{1/2}}\right\} \tag{5.49}$$

$$a = q - \frac{p^2}{3} \tag{5.50}$$

$$b = \frac{2}{27} p^3 - \frac{p\,q}{3} + r \tag{5.51}$$

The new solution of the cubic contained in equations (5.48) through (5.51) is the solution used in Chapter 6 to obtain numerical results for the complex spherical-earth simulation model. It was decided to use this solution rather than the solution of Fishback after an analysis of the accuracy of the two cubic solutions as well as the quadratic solution of equation (5.39). All three solutions were programmed in double precision for the CDC 6600 computer, a machine capable of delivering accuracies in double precision up to 25 significant decimal digits. The value of $\beta_1$ determined by each solution was inserted into equation (5.33) and the results printed for antenna heights ($h_i$) of 35, 70, and 105 feet, for slant ranges ($p_d$) from 10 to 100 nm in increments of 10 nm, and for aircraft heights of 5000 to 40000 ft in increments of 5000 ft. An exact solution, of course, would have given a value of 0 when inserted into equation (5.33). Thus the

deviation from 0 would be a measure of the inaccuracy of the solution. In every case, the solution of the cubic derived in this chapter was superior by far both to the quadratic solution and to the solution of Fishback.

The worst performance of the new cubic resulted in a deviation from 0 of $10^{-14}$; its best was $10^{-20}$. Fishback's solution ranged from a most accurate case at $10^{-12}$ to a worst case of $10^{-9}$. Thus, the most favorable geometry for a solution of Fishback's cubic was two orders of magnitude less accurate, by this criterion, than the worst-case geometry for the cubic solution derived in this thesis. The quadratic derived herein had accuracies ranging from $10^{-14}$ to $10^{-7}$. It was thus better in some problem geometries and worse in others than the cubic solution of Fishback. Of the 240 cases run, 170 resulted in a more accurate solution with the quadratic derived in this chapter than with the classical cubic.

Although the derivation of these two new solutions for the grazing angle was incidental to the accomplishment of the primary thesis objectives, it remains one of the major contributions of the thesis itself. The new cubic solution is of the order of $10^6$ times more accurate, by the criterion developed above, than either the new quadratic solution or the classical solution, and is of the same complexity as the classical form. The new quadratic, on the other hand, is simpler than either cubic, yet, on the average, slightly more accurate than the classical solution.

## 5.5 Indirect Path Length

Having solved for $\beta_1$ using the approximate cubic equation derived in the last section, one can now solve exactly for the indirect path length segments needed in the divergence formula and the vertical lobing factor. The exact equation for $p_{r_1}$ is determined by application of the Law of Cosines to the triangle whose vertices are the center of the earth, the interrogator, and the reflection point:

$$p_{r_1}^2 = R^2 + (R+h_i)^2 - 2R(R+h_i)\cos\beta_1 \qquad (5.52)$$

or

$$p_{r_1} = (R+h_i)\left[1 - 2H_i\cos\beta_1 + H_i^2\right]^{1/2} \qquad (5.53)$$

Similarly, the equation for $p_{r_2}$ is determined by application of the Law of Cosines to the triangle whose vertices are the center of the earth, the aircraft, and the reflection point:

$$p_{r_2}^2 = R^2 + (R+h_t)^2 - 2R(R+h_t)\cos\beta_2 \qquad (5.54)$$

or

$$p_{r_2} = (R+h_t)\left[1 - 2H_t\cos(\beta-\beta_1) + H_t^2\right]^{1/2} \qquad (5.55)$$

## 5.6 Lower Limit of Grazing Angle

For several reasons there are restrictions that must be placed on the use of various values of the grazing angle. One

such restriction is a lower limit for the angle. The lower limit restricts the propagation equations to that region in which the assumptions of straight rays made in the derivation of the divergence formula[18] are still valid. The lower limit specified by Reed and Russell is

$$\psi_{min} = \tan^{-1}\left[\left(\frac{\lambda}{2\pi R}\right)^{1/3}\right] = \tan^{-1}\left[\frac{.01777}{f_{MHz}^{1/3}}\right] \quad (5.56)$$

For the ATCRBS, this amounts to approximately 0.1 degree. At most radar sites there is terrain or some combination of structures that obstructs most of the line of sight below 0.1 degree. Furthermore, especially in terminal areas, the area of desired coverage lies above this lower limit for the most part.

The evaluation of radiation strength in the region below this minimum value for the grazing angle yet above the diffraction region, which lies beyond the radio horizon, is a subject which continues to be investigated. Currently, the transition between radiation in these two zones, each of which can be expressed for the most part analytically, is little more than straightforward interpolation. Fortunately for this analysis of the ATCRBS, the so-called intermediate region is of little practical interest.

## 5.7 Surface Roughness

An upper limit on the grazing angle must also be imposed to ensure that the reflections assumed in the foregoing analysis are

indeed specular. When the reflecting surface is to some extent rough, there is an angle above which the reflection becomes diffuse. Actually, there is no specific angle at which an abrupt change from specular to diffuse reflection occurs, but there is an angle below which specular reflection can be expected to be a reasonable description of the physical phenomenon taking place at the surface. When specular reflection no longer holds, of course, the equations derived earlier for the complex reflection coefficient are also invalid.

The inequality that must be satisfied to ensure that specular reflection still occurs is

$$H < \frac{\lambda}{\tau \sin \psi_{max}} \tag{5.57}$$

where $\lambda$ is the wavelength of the incident radiation, $\psi_{max}$ the upper limit of the grazing angle, and H the height of surface irregularities.

Clearly, the very definition of H is sufficient to cast some doubt on the precision of this technique, for the measurement of the height of surface irregularities, even over a reasonably confined area, is an uncertain task at best. But the specification of $\tau$ is even more nebulous. Reed and Russell[18] specify a value of 16, while Kerr[17] endorses a value of 8 while referring to a footnote which justifies values of 16 and 32.

Because of this indecision regarding a criterion for surface

roughness, an effort was undertaken to develop a composite criterion based on available information.

Since at angles above $\psi_{max}$ reflection is diffuse, there should be no vertical lobing, and the following should hold:

$$A_v = 1 \tag{5.58}$$

Noting that equation (5.4) for $A_v$ is of the form

$$A_v = 1 + Q \tag{5.59}$$

one can try the following form for a roughness criterion in an attempt to match the boundary condition (5.58), or at least to approach it:

$$A_v = 1 + e^{-\left(\frac{\psi}{\psi_{max}}\right)^y} Q \tag{5.60}$$

Solving (5.57) for $\psi_{max}$,

$$\psi_{max} = \sin^{-1}\left(\frac{\lambda}{\tau H}\right) \tag{5.61}$$

Arbitrarily, $\psi_{max}$ and y can be chosen such that the exponential term equals 0.99 when $\tau$ equals 32 and 0.01 when $\tau$ is 8. Physically, this means that $\psi_{max}$ will be chosen in such a way that when the grazing angle equals the lowest accepted conventional roughness criterion, 99% of the vertical lobing effect Q will remain; but when $\psi$ proceeds on to a value equal to the largest accepted conventional value for specular reflection, only 1% of the vertical lobing effect Q will remain. Substituting the arbi-

trary values for the exponential term at the extremes of $\tau$,

$$y = \frac{\ln(-\ln .99)}{\ln\left|\sin^{-1}\left(\frac{\lambda}{32H}\right)\right| - \ln \psi_{max}} = \frac{\ln(-\ln .01)}{\ln\left|\sin^{-1}\left(\frac{\lambda}{8H}\right)\right| - \ln \psi_{max}} \tag{5.62}$$

$$\psi_{max} = \exp\left\{\frac{\ln(-\ln .01)\ln\left|\sin^{-1}\left(\frac{\lambda}{32H}\right)\right| - \ln(-\ln .99)\ln\left|\sin^{-1}\left(\frac{\lambda}{8H}\right)\right|}{\ln\left(\frac{\ln .01}{\ln .99}\right)}\right\} \tag{5.63}$$

Equations (5.60), (5.62), and (5.63) constitute the roughness criterion used in the simulation model. A numerical example of the effect of this roughness model is included in Chapter 6.

## 5.8 Transponder Operation

The operation of the aircraft transponder in the simulation model involves the application of the inequalities presented in this section. The transponder is assumed to reply only when

$$P_{t_d} > S_t \tag{5.64}$$

and either

$$P_{t_{d\ dB}} > P_{t_{o\ dB}} + 9 - s_{dB} \tag{5.65}$$

or

$$P_{t_o} < S_t \tag{5.66}$$

$P_{t_d}$ refers to the power received at the transponder from the directional antenna, and $P_{t_o}$ to that received from the omnidirectional antenna. The subscript dB indicates that the quantity with which it is associated should be expressed in decibels or decibels with respect to some reference. $S_t$ is the sensitivity of the transponder which is defined as the lowest level signal power to which the transponder can react. Finally, s is a parameter that accounts for differences from transponder to transponder, and for a given transponder depending upon the level of the input signal, in the relative strengths of $P_1$ and $P_2$ at which the transponder suppresses. This difference of 9 dB allowed by the National Standard for ATCRBS is discussed in Chapter 2. In the simulation model, therefore, s is generally set to some value between 0 and 9. Because coverage is the most critical parameter evaluated in Chapter 6, s is set to 0. This value requires the value of $P_1$ to be at least 9 dB above that of $P_2$ before a reply is initiated.

Equation (5.64) requires merely that the directional antenna pulses be sensed by the transponder. Equations (5.65) and (5.66) set the conditions for side-lobe suppression. If equation (5.65) is satisfied, the directional signal is sufficiently high to initiate a reply; otherwise, transponder action is suppressed. If equation (5.66) is satisfied, the omnidirectional pulse cannot be sensed, and a reply occurs. Since the interference protection mechanisms of the transponder described in Chapter 2 are not of

importance to the objectives of this thesis, they are not modeled. Instead, the minimum triggering level of the transponder, a constant, is used as the transponder sensitivity.

## 5.9 Receiver Side-Lobe Suppression

In order to evaluate the effect of receiver side-lobe suppression (RSLS) and secondarily to investigate the effects of the various antenna patterns with regard to performance in the presence of external interference, a simple interference model was created. The model consists of a specified number of aircraft replying at a specified average rate and located at random azimuths and at a range selected at random from a uniform distribution from 0 to 200 nm. Since aircraft interrogation rates in such high-density areas as New York and Los Angeles tend to average about 100 interrogations per second and are not expected to increase appreciably, the average reply rate used for the numerical examples of Chapter 6 is 100 per second.

Upon determining a valid reply at a particular slant range, the model checks for interference in the following manner. First, the range of the valid reply is compared with the effective range of each potential interfering pulse. This effective range is a random number uniformly distributed between 0 and the distance that can be traveled by a reply between transmissions at the specified average reply rate for interference (100 per second in Chapter 6). For the rate of 100 per second, the effective range is thus in excess of 800 nm. This process allows a ground-based

interrogator/receiver with a 200-nm range the opportunity to capture approximately one-fourth of the transmitted replies as potential interference over its entire range; that is to say, on the average, one of every four sweeps of the radar of interest will involve a reply from an interfering aircraft replying at an average rate of 100 per second. If the effective range of an interfering reply is within 1.65 nm of the valid reply range, then the interference check continues, as the two 20.3-microsecond pulse trains involved may in fact be overlapped. If the ranges are separated by more than 1.65 nm, there can be no interference of the two signals in question, and the interference check is discontinued.

If a potentially interfering reply is identified, the model chooses a random number uniformly distributed between 2 and 14, and multiplies that result by .06. The random number represents the number of pulses in the reply train, which varies from just 2 framing pulses to a completely-filled series of information bits plus the bracket pulses (14 pulses total). Since the region in which an interfering pulse may fall is 40.6 microseconds, corresponding to a range difference of $\pm$ 1.65 nm, the space in the vicinity of each framing pulse ($\pm$.45 microseconds) in which interference can occur is approximately 6% of the total space. This implies that interference is assumed to occur when the edges of the pulses begin to overlap — a worst-case assumption. Thus, the model simply increases the probability of interference in a

linear fashion as a function of the number of reply pulses that are interfering. This assumption of linearity with the number of pulses also results in a higher probability of interference than would be expected to occur in the field, particularly with the aid of advanced degarbling equipment or software. The assumption is suitable, however, for the purposes of the thesis. If a random number between 0 and 1 is greater than the number determined above, the interference check is discontinued. Otherwise, the interfering reply is assumed to be in a position adequate to warrant further investigation of its interference potential.

Finally, a random azimuth for the interfering reply, a range for the aircraft that transmitted the reply chosen from a uniform distribution from 0 to 200 nm, and a random phase for the radio frequency of the reply are chosen. Based on these parameters, values for the electromagnetic field of both the valid reply and the interfering reply are calculated. The square root of previous power calculations gives the strength of the electromagnetic field, while the random phase of the interfering reply determines the manner in which the two signals are to add (or subtract) vectorially. The two signals are added, the result squared, and the final power level returned to the receiver model for subsequent processing. Signals are processed on the omnidirectional antenna as well as the directional if RSLS is on.

After the interfering signal has been added to the valid reply, the receiver is ready to begin its operation. In the

simulation model, the receiver sensitivity-time control functions exactly as described in Section 4.5 and as specified by equation (4.29). If the reply is detected on the directional antenna, that is if the received signal exceeds receiver sensitivity including the effect of the STC, the simulation continues its operation.

Finally, the simulation model checks the RSLS switch. If RSLS is off, a valid reply is recorded and simulation action is advanced to the next sweep of the ATCRBS. If RSLS is on, however, a valid reply can only be recorded if the following equation is satisfied:

$$P_{r_{d\ dB}} > P_{r_{o\ dB}} + k_{dB} \tag{5.67}$$

where $P_{r_d}$ is the power at the receiver from the directional antenna, $P_{r_o}$ is the power at the receiver from the omnidirectional antenna, and k is an adjustable threshold control for RSLS. If equation (5.67) is not satisfied, the reply is rejected as a side-lobe response, and the simulation continues with the next sweep.

## 5.10 Aircraft Flight Profiles

The simulation model determines aircraft elevation angle, slant range, and altitude depending on the particular flight profile specified. In this section, the equations for constant altitude and constant elevation flight profiles are presented.

Over a constant-altitude flight path, an aircraft actually

flies an arc of a circle of radius $R+h_t$ concentric with the sphere of the earth. In the simulation model, the aircraft altitude $h_t$, an initial slant range $p_{d\ max}$, and aircraft velocity are specified. The arc of length s denoting the distance the aircraft has traveled since the start of the flight is set initially to zero. The increments of path length that the aircraft flies from scan to scan of the radar are uniform and are simply the product of the specified aircraft velocity and the scan time of the radar. Each scan of the radar when a new aircraft position is desired, the simulation model increments the path length s and computes slant range according to the following equation:

$$p_d^2 = (R+h_i)^2 + (R+h_t)^2 - 2\,(R+h_i)(R+h_t)\cos\left(\alpha - \frac{s}{R+h_t}\right) \quad (5.68)$$

where

$$\alpha = \cos^{-1}\left[\frac{(R+h_i)^2 + (R+h_t)^2 - p_{d\ max}^2}{2\,(R+h_i)(R+h_t)}\right] \quad (5.69)$$

Elevation angle is computed using the equation presented in the next paragraph for a constant elevation-angle flight.

The constant elevation flight is similar to that described above. The increment in this case, however, is an increment in slant range, since, at constant elevation, the rate of change of position of the aircraft is entirely in the direction of the interrogator/receiver. Thus, in this case an initial $p_{d\ max}$ is specified as before, and an increment of slant range is the pro-

duct of the aircraft velocity and the radar scan time. Each scan of the radar when a new aircraft position is desired, the simulation model increments the slant range from its initial value to a new one closer to the interrogator. This time, however, the altitude of the aircraft must change from its specified initial value $h_{t0}$. Also, the initial value of the elevation angle must be computed. The elevation angle, which remains constant throughout the flight according to the nature of the profile, is determined from the following equation:

$$\theta = \sin^{-1}\left[\frac{(R+h_{t0})^2 - (R+h_i)^2 - p_{d\ max}^2}{2\ p_{d\ max}\ (R+h_i)}\right] \qquad (5.70)$$

The new aircraft altitude is determined after each increment of slant range from this equation:

$$h_t = \left[p_d^2 + 2\ p_d\ (R+h_i)\ \sin\theta + (R+h_i)^2\right]^{1/2} - R \qquad (5.71)$$

In both of these flight profile algorithms, the aircraft is assumed to be stationary while the ATCRBS antenna is pointed at it, and in fact for the duration of one entire scan. The aircraft then moves instantaneously to its new position when the antenna has completed a full revolution.

# CHAPTER 6

# APPLICATIONS OF THE MODELS

## 6.1 Introduction

In this chapter the inputs to and results of several applications of both the simple flat-earth model and the complex spherical-earth simulation are presented. Discussions of the physical implications of the results as well as comparison of actual ATC display photographs taken during field tests with simulated displays generated by the complex model serve to illustrate the validity of the models.

Although there are innumerable applications and numerical examples that could have been performed, the chosen examples are representative of the capabilities of the models and are pertinent both to the immediate objectives of the FAA and to its long-range plans. Both en route and terminal configurations of the standard antenna, the new prototypic antennas described in Chapter 1, and an ideal antenna are modeled in a manner similar to the common current use of the ATCRBS. The results of these applications afford a direct comparison of the antennas using a common baseline configuration.

After the baseline data are presented, the models are focused on adjustment of various system parameters to optimize the performance of each antenna in a terminal configuration. The performance of an antenna system with an integral omnidirectional

radiation pattern is also modeled. Finally, comparisons of the various terminal configurations with and without receiver sidelobe suppression in the presence of several interference environments are made.

Throughout the chapter the correlation of results from the simple flat-earth model and the complex spherical-earth simulation is discussed in detail.

## 6.2 Inputs to the Models

Although many of the model inputs are specific to the particular investigation of interest, some are common for most of the applications. The specific parameters are presented in those sections that describe the results. The more common ones, however, are given here.

Ground receiver sensitivity was held at -88 dBm despite a variety of changes for the different investigations in other interrogator/receiver characteristics such as antenna patterns, antenna heights, interrogator power, antenna gains, and transmission line losses. For most tests in which coverage was the key parameter of interest, transponder sensitivity at the receiver end of the transmission line was held at its lowest value allowed by the National Standard, -72 dBm. Power radiated from the transponder, measured at the antenna, was also kept at the low extreme allowed by the National Standard, 51 dBm for the en route examples and 48.5 dBm for the terminal cases. When contributions or susceptibility to interference were analyzed, the

transponder characteristics were reversed: high sensitivity, -80 dBm at the receiver end of the transmission line, and high power, 500 watts at the antenna.

In all investigations the effect of the aircraft antenna radiation pattern and of shielding by the aircraft was ignored. This was done to separate the airborne equipment characteristics from the phenomena related to the ground-based system whose performance was being analyzed. The comparison of the results of the thesis with those obtained in the field will necessarily be discrepant to some degree because of this inability to control the experiment precisely in the real operational world. Both aircraft antenna gain and transmission line loss, which normally offset each other, were included parametrically in the models, but were assumed to be zero.

The RSLS threshold control k described in equation (5.67) was set at 6 dB after several trials at higher levels. This level allowed a significant reduction in interference without causing false suppression for the cases investigated.

The relative permittivity of the reflecting medium was assumed to be 2, and the conductivity .001 throughout. These values appear to be close to those characteristic of the reflecting medium at the National Aviation Facilities Experimental Center in Atlantic City, New Jersey, from which field test data concerning the new ATCRBS antennas is being obtained. The values used in the models are those of dry, sandy loam and yield depths

of nulls approximately equal to those obtained in experimental flight tests to date. The other characteristic of the reflecting medium, the height H of surface irregularities, is held constant at 3 in, except for an illustrative example of the effect of H on the output of the complex model. In this demonstration, H is increased to 10 ft, a value typical for a site surrounded by small trees.

For the en route configuration, interrogator rotation rate was specified as 6 rpm, interrogation repetition rate as 360 per second, and maximum range for the aircraft flight profile as 240 nm. All aircraft were assumed to begin at an azimuth of $90^{o}$ at the maximum slant range and to proceed toward the interrogator along the $90^{o}$ radial with a heading of $270^{o}$. The flights were terminated when the aircraft reached either its minimum slant range or 1 nm. In the terminal configuration, rotation rate was 15 rpm, interrogation repetition rate 400 per second, and maximum range 60 nm.

The various antenna patterns used in the applications of the models represent the largest body of input data. A complete description of the patterns, which include uplink and downlink radiation from directional and omnidirectional antennas in both horizontal and vertical planes, is included in Appendix C along with computer-generated plots of each. A special switch in the complex simulation model causes the omnidirectional antenna to remain fixed in azimuth, like the standard antenna or the new

Hazeltine open array, or to rotate with the directional antenna, like the separate rotators built by Texas Instruments and Westinghouse.

## 6.3 Model Validation

There are many ways in which models such as those developed in the thesis can be validated. The discussions of the physical implications of the results presented in subsequent sections serve as partial validation as long as the results themselves are consistent with the laws of physics. There are some very specific means of validating, however, that are presented in this section. These consist of a direct comparison of data obtained from experimental field tests at the National Aviation Facilities Experimental Center in Atlantic City, New Jersey, with the same data produced by the simulation model. The data exist from both sources in the convenient form of photographs (or simulated photographs) of an air traffic control display. Validation of the simple model, which involves several simplifying assumptions, is done in the discussion of the results of later sections in this chapter. Validation of the simple model is perhaps better defined as a restriction of the model to applications for which its results are relevant and meaningful. Certainly the simple model cannot be certified or validated for unrestricted use; although the complex model cannot be so certified either, its use is much less restricted than that of the simple model.

There is not much that can be said regarding the performance

comparison between simulation and experimental field tests unless comparisons are made between unusual phenomena. Thus, the phenomena of interest in the figures that follow are discussed in detail. The white-on-black photographs on subsequent pages are those obtained from the experimental flight tests at Atlantic City. Range rings in these photographs are spaced 5 nm apart. The black-on-white graphics are those produced by a Calcomp plotter as the result of output from a CDC 6600 FORTRAN computer program used to implement the model. Range rings in the simulated display are spaced 10 nm apart.

The flight tests chosen to illustrate the validity of the complex model involve the standard FA-8043 antenna and the new Hazeltine open array antenna discussed earlier. Flights at an altitude of 5000 ft at different levels of interrogator power provided the most interesting effects and the most dramatic correlation between the test results and those of the simulation.

Figure 6.1 shows the result of a flight test in which the FA-8043 antenna was operated with SLS at an interrogator power of 300 watts. Note in particular the effect of the null at about 42 nm and the two-hit return in the middle of the "hole" in the coverage. The results of a simulated flight approximating these conditions are shown in Figure 6.2. The simulated display was obtained using improved SLS and an interrogator power of 500 watts. Since improved SLS results in half the interrogator power being radiated from the directional antenna and half from the

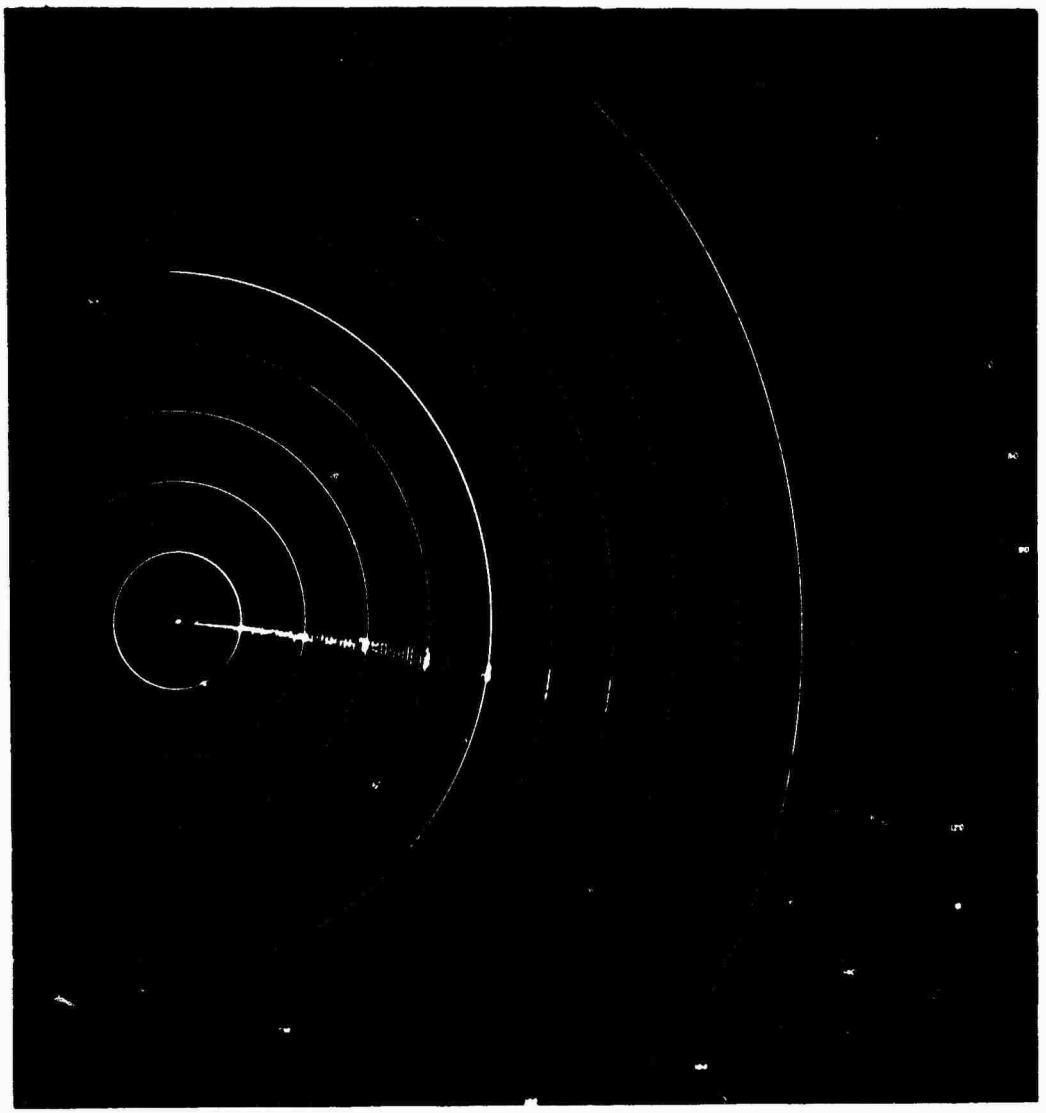

Figure 6.1 5000-Ft Flight Test, FA-8043 Antenna,
Low Interrogator Power

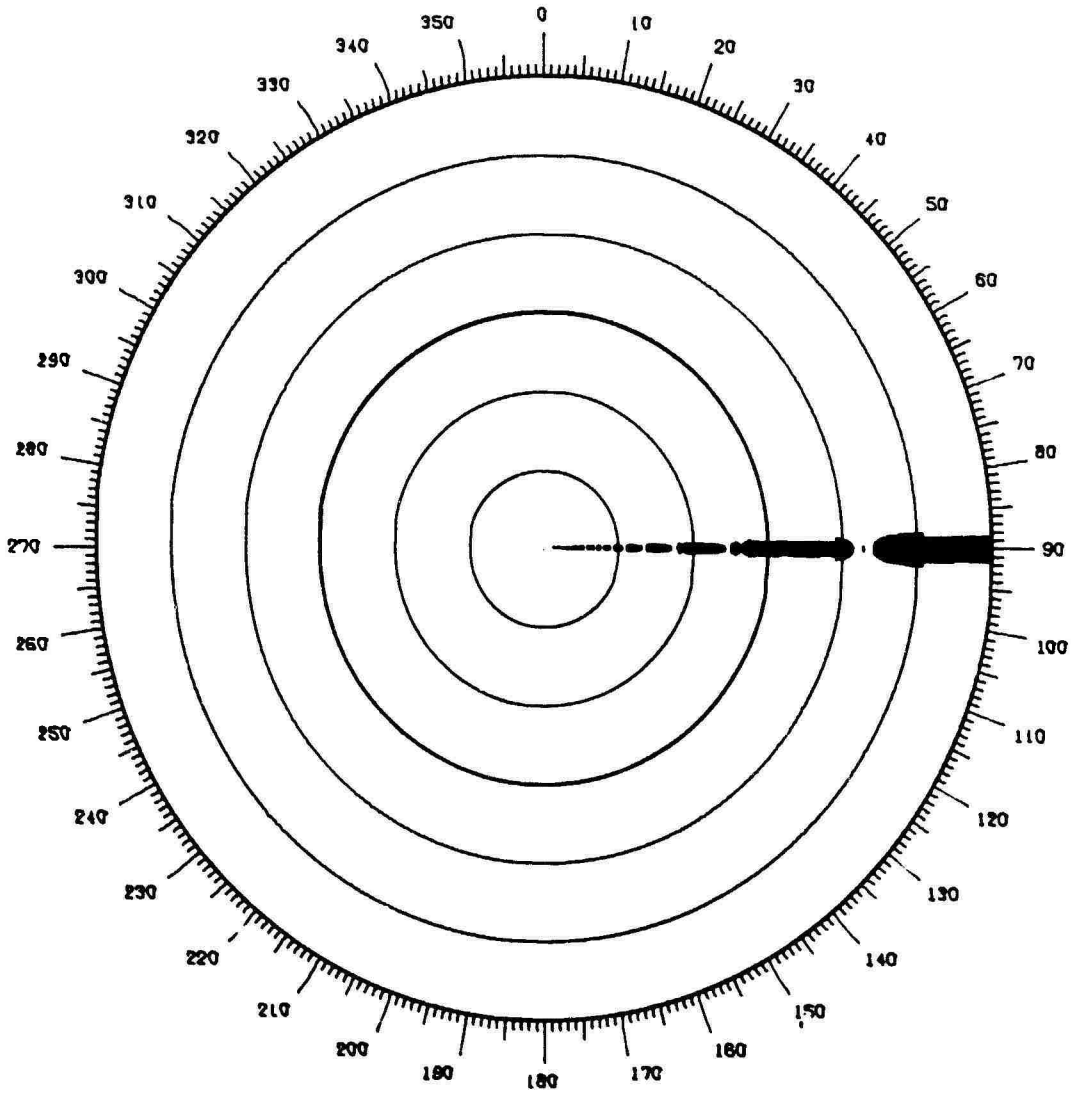


Figure 6.2 Simulated 5000-Ft Flight, FA-8043 Antenna, Low Interrogator Power

omnidirectional antenna, only 250 watts is being radiated directionally in the simulation. This amount of power certainly approximates the 300 watts in the experimental test to within the uncertainties of both the simulation and the test configuration. In the simulation, the large hole in coverage appears at the same range (42 nm), and the same short series of hits appears in the middle of the hole.

The correlation between the short string of hits in the middle of the coverage hole, two in the case of the flight test and five for the simulation, is certainly more than a chance occurrence. The detailed output of the model shows that the portion of the hole beyond the short series of hits in the middle is caused by the inability of the receiver to detect the replies of the aircraft, which was in fact interrogated. Thus, the hole in coverage in this region is due to a null in the 1090 MHz (downlink) pattern. On the side of the hole closer to the interrogator, on the other hand, the uplink power is insufficient to allow detection by the aircraft due to a null in the 1030 MHz pattern. The few hits that manage to be detected in the middle result from the crossing of the two nulls into their respective zones of insensitivity. The fact that nulls closer to the interrogator result in a total loss of the target in the simulation can be explained partially by the fact that the test aircraft in the simulation is slightly less sensitive (as insensitive as the National Standard allows) and much less powerful than the actual

test aircraft. The reasons for the choice of the simulated aircraft transponder's characteristics are explained in the previous section.

More fine details of correlation are presented in the next three figures. Figures 6.3 and 6.4 show the results of boosting power to the FA-8043 over the same flight path in an attempt to close the coverage hole. The flight test result used 950 watts of interrogator power, while the simulated result involved 1000 watts; both tests used normal SLS. Again the location of the hole is the same in range, but of much greater significance is the shape of the pattern in the vicinity of the hole. As one examines the pattern from approximately 50 nm in toward the interrogator, a paraboloidal shape up to the start of the hole is apparent. The last scan before the hole involves a short series of hits that is characteristically similar in both instances.

The coverage hole is then followed by a suddenly wide trace followed immediately by a narrower target in both cases. The flight test appears to result in an asymmetry in the first wide target after the hole. This asymmetry could be due to a slight turning motion of the aircraft or some other anomaly. Nevertheless, the wide slash followed by the narrow one is apparent in both cases. The physical reasons for this phenomenon are the same as those explained in the low-power test. By increasing power, however, the inner portion of the hole begins to be covered, since it is sensitive to uplink power. The outer portion of the

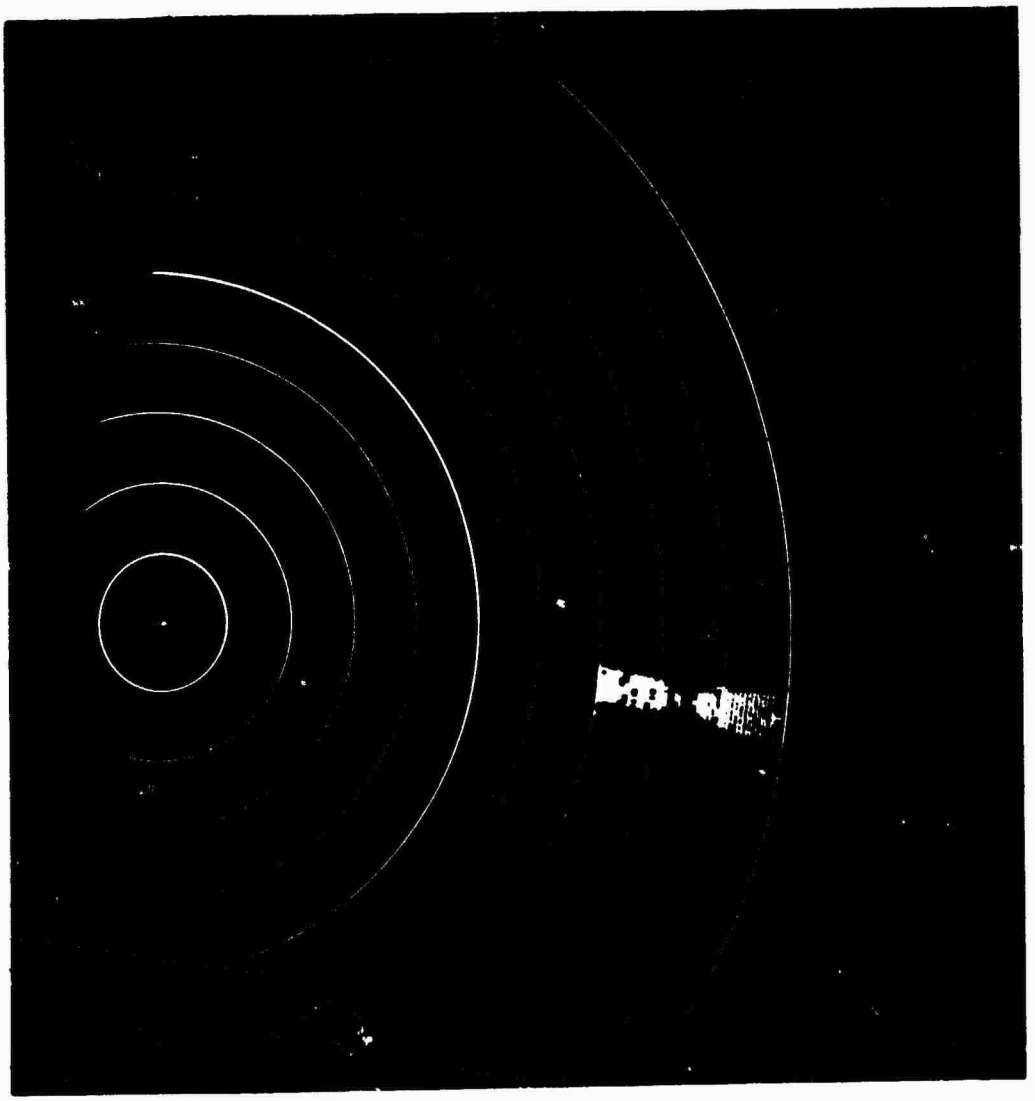

Figure 6.3 5000-Ft Flight Test, FA-8043 Antenna, High Interrogator Power

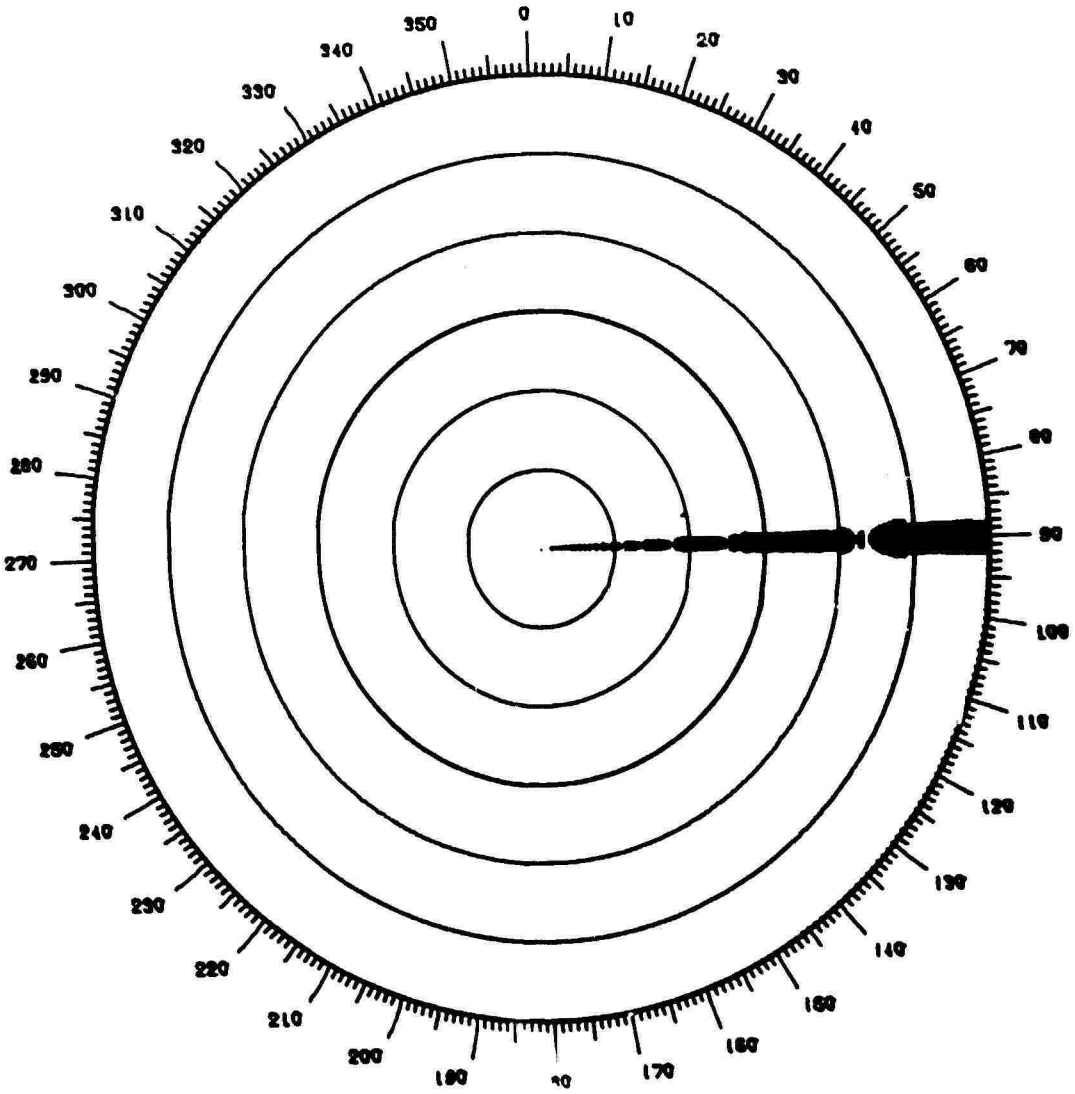


Figure 6.4 Simulated 5000-Ft Flight, FA-8043 Antenna, High Interrogator Power

hole, caused by a downlink null, is unaffected by the change in uplink power.

Figure 6.4 also shows a characteristic rapid drop in target width at increasingly shorter intervals inside 20 nm. The simulation output shows this to be a result of the rapid rate of increase in omnidirectional antenna power due to its lobing characteristics that results in sudden suppression of the outer portion of the target. The same phenomenon is apparent in the flight test shown in Figure 6.5 in the same region inside 20 nm. The larger hole at 25 nm in the flight test is caused by the use of very low power (15 watts) for this particular test. The similarities in these fine structural details add more convincing evidence of the validity of the complex model.

Comparisons of actual and simulated tests of the Hazeltine open array antenna are slightly less dramatic in fine detail, but equally convincing. Figures 6.6 and 6.7 show the results of an actual flight with 100 watts of interrogator power and a simulated flight with 250 watts of power, respectively. Coverage gaps are again located in the same places and are approximately 4 to 5 nm long. The cigar-shaped coverage pattern between 27 and 42 nm is apparent in both illustrations, as is the slight flaring of target width just before the null at 27 nm. The cigar shapes of Figure 6.7 are also visible in the flight test photograph of Figure 6.5.

Figures 6.8 and 6.9 depict the results of increasing power

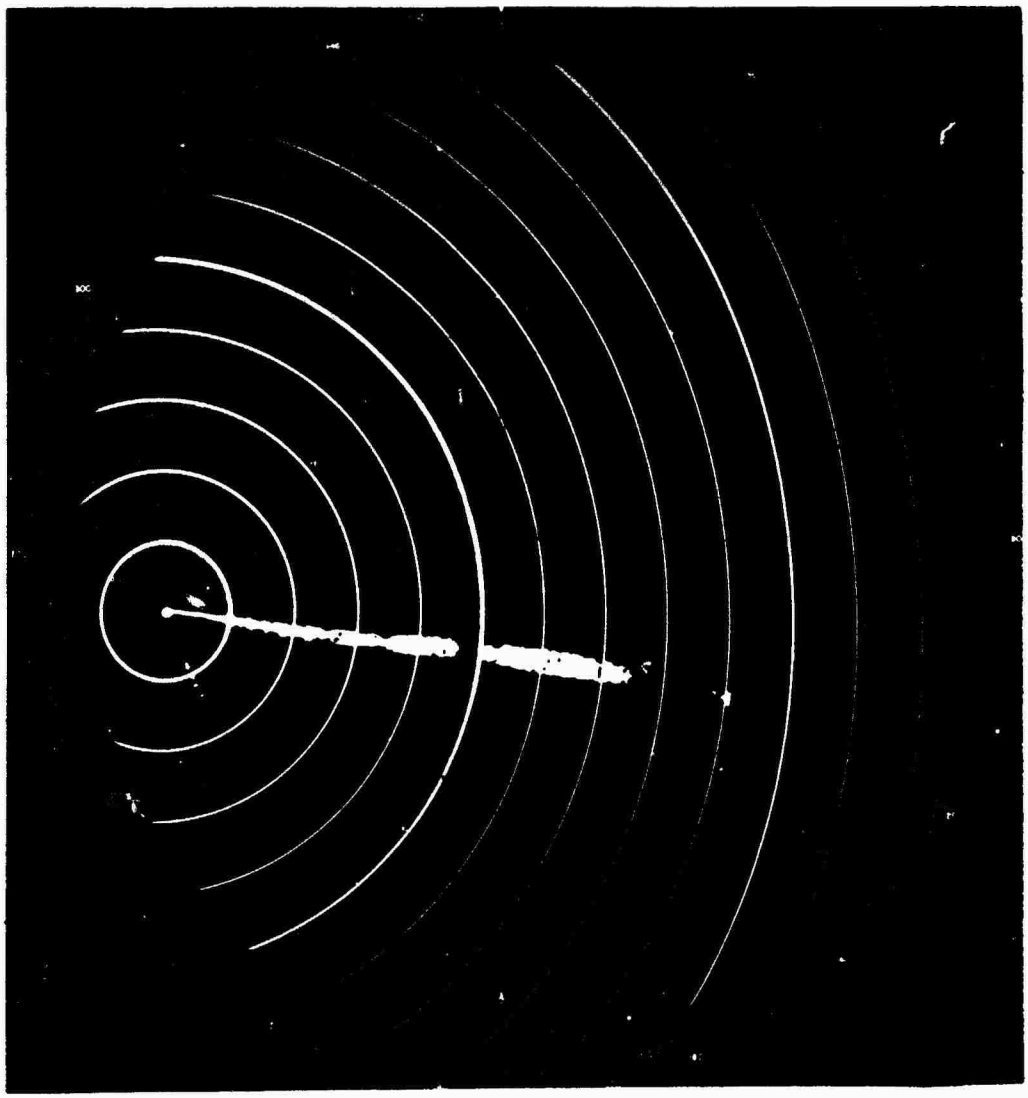

Figure 6.5 5000-Ft Flight Test, FA-8043 Antenna,
Showing Target Detail Inside 25 NM

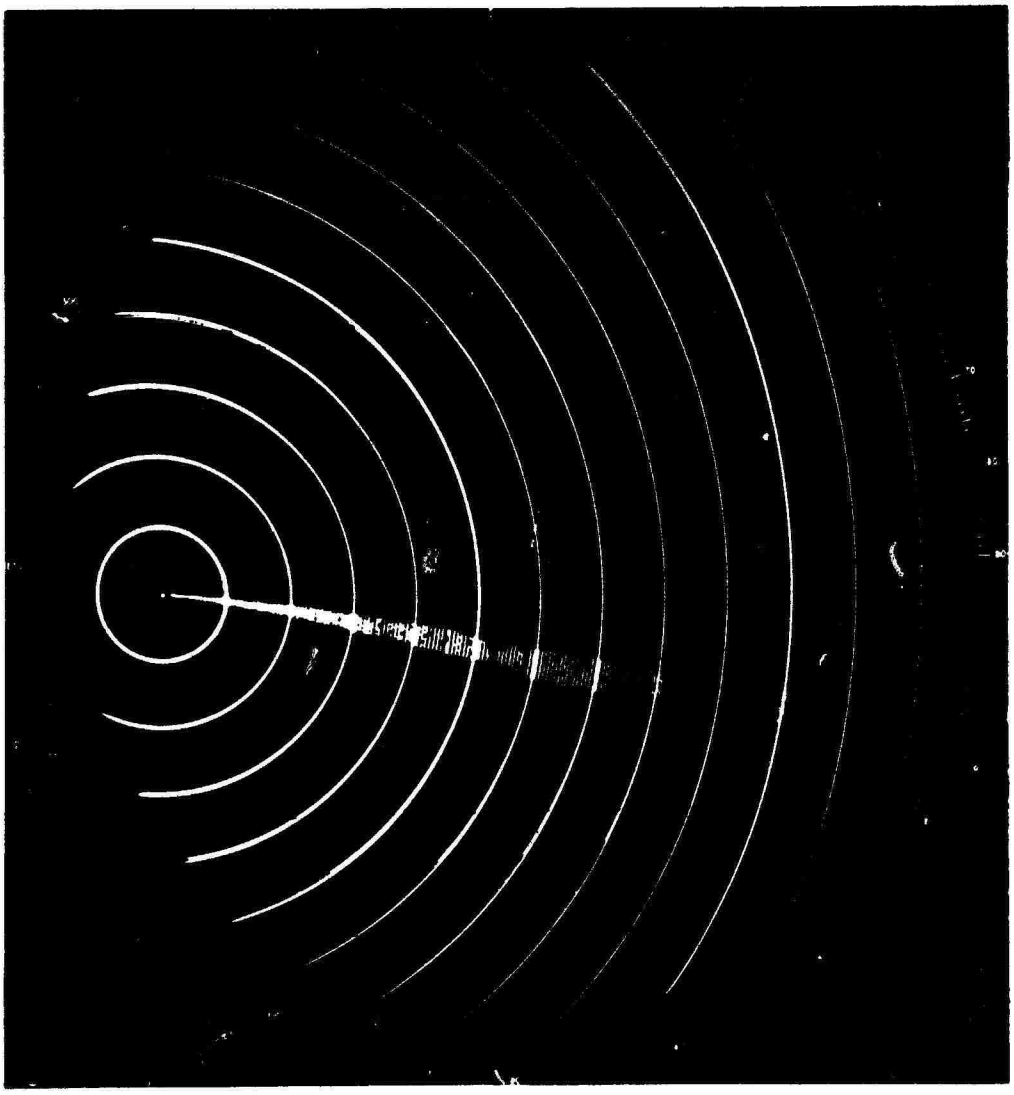

Figure 6.6 5000-Ft Flight Test, Hazeltine Antenna, Low Interrogator Power

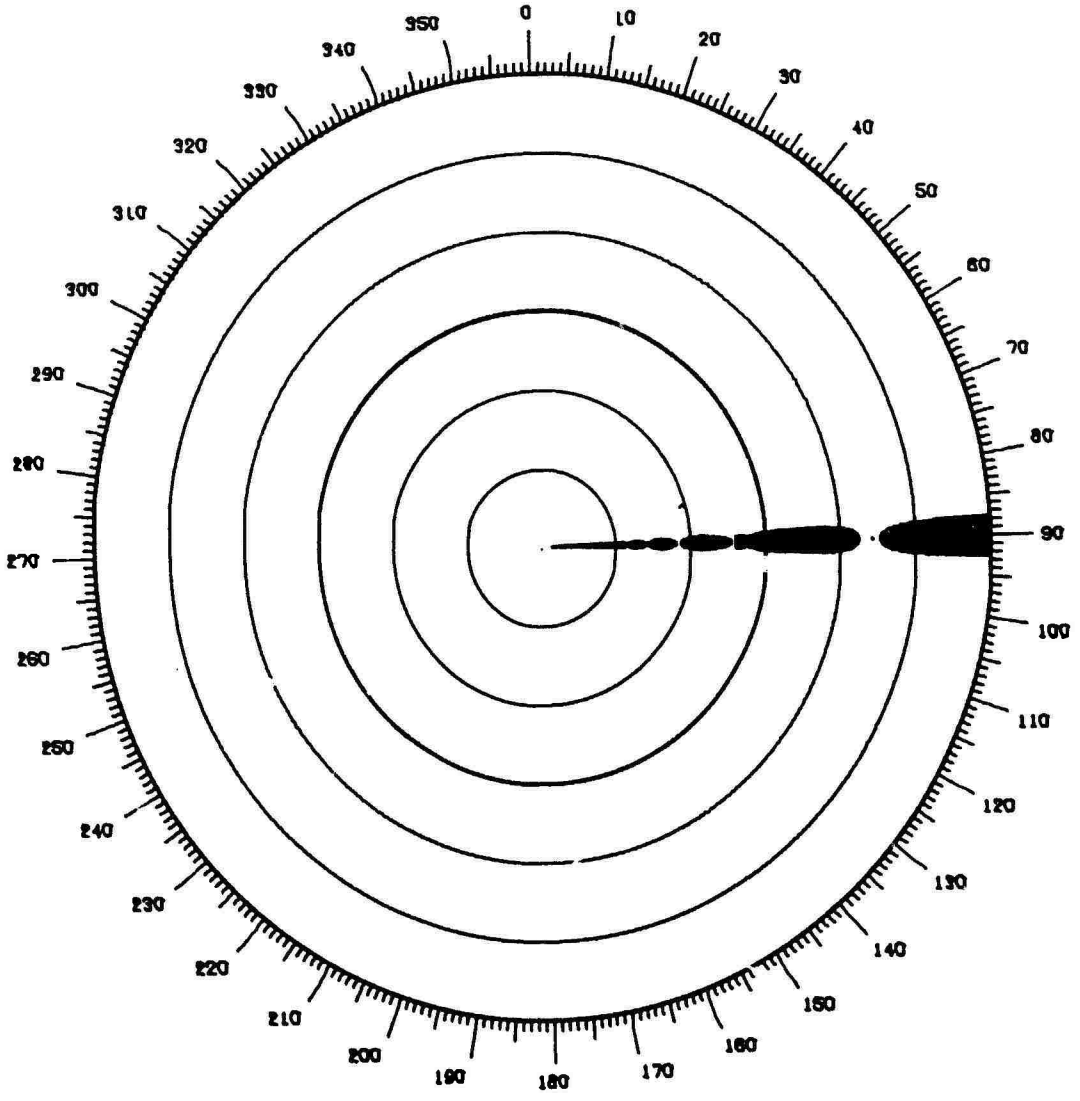


Figure 6.7 Simulated 5000-Ft Flight, Hazeltine Antenna, Low Interrogator Powe:

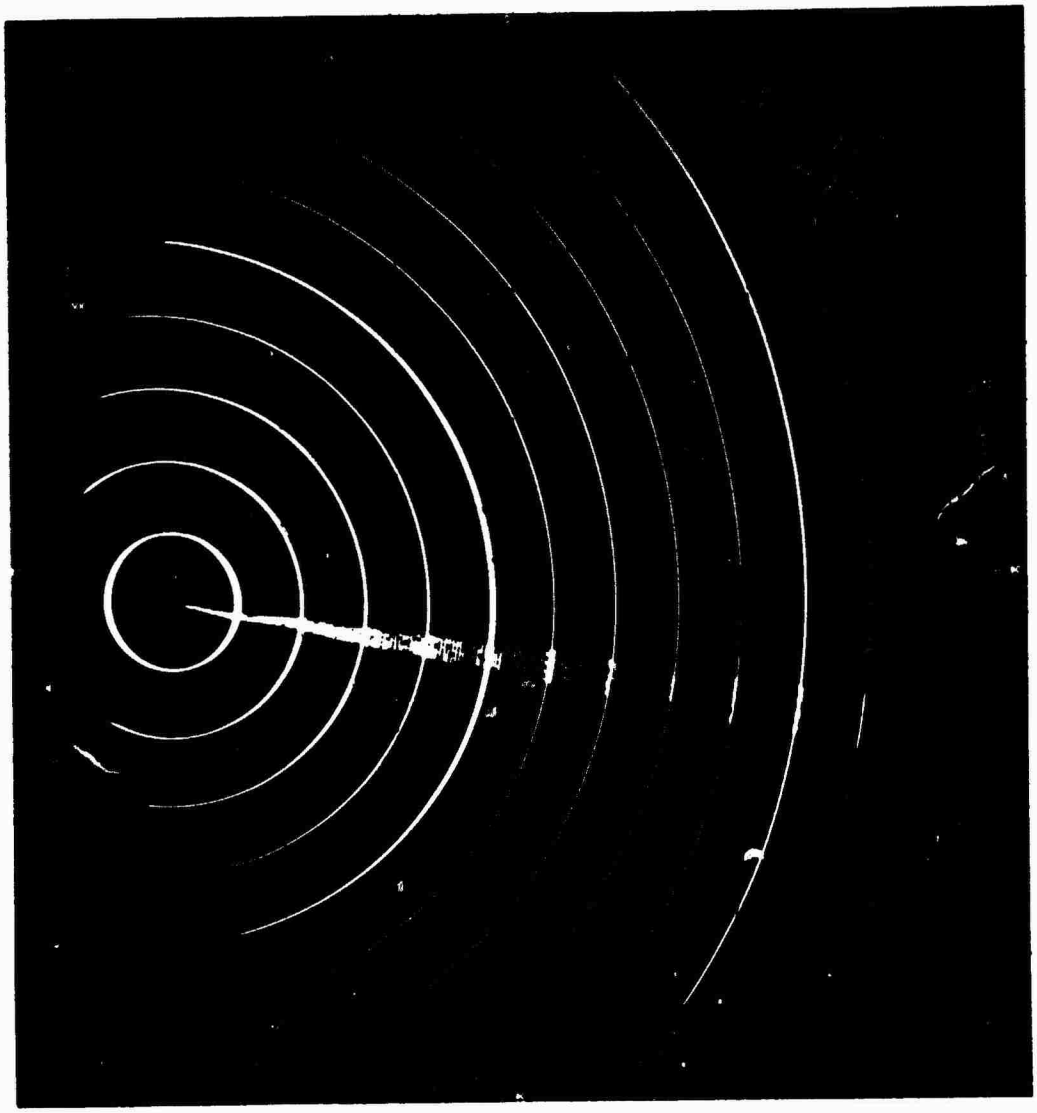

Figure 6.8 5000-Ft Flight Test, Hazeltine Antenna, High Interrogator Power

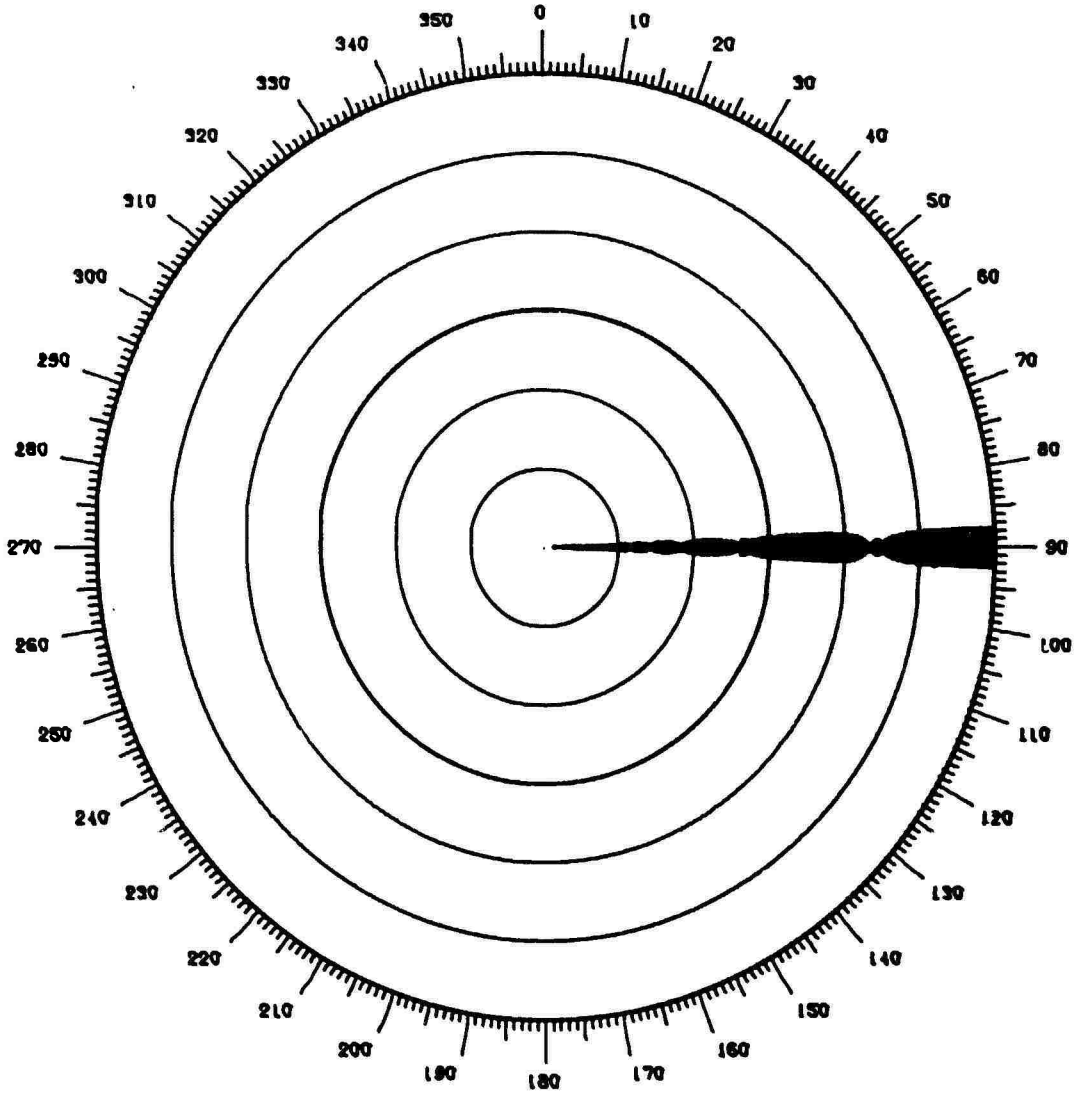


Figure 6.9 Simulated 5000-Ft Flight, Hazeltine Antenna, High Interrogator Power

to the open array to an actual 575 watts and a simulated 630 watts, respectively. Coverage gaps are just closed in each case.

The effect of the surface roughness parameter H, discussed in Section 5.7, is shown in Figure 6.10. Whereas all other simulated flight tests in this chapter use a value of 3 in for H, including those simulated display photographs already shown in this section, surface irregularities are assumed to be 10 ft for the purposes of Figure 6.10. Clearly, the vertical lobing effects observed in Figure 6.2 have vanished; in all other respects, however, the two simulations were the same. The sudden reduction in target width at 37 nm is due to the fact that the transponder becomes sensitive to the omnidirectional antenna power at that range and begins to suppress a few hits on the outer edges of the target.

## 6.4 Antenna Performance in a Standard En Route Configuration

To assess the relative performance of five en route antenna systems according to some basic ground rules, a common test configuration was developed for both the simple flat-earth and complex spherical-earth models. The tests would entail utilization of most of the characteristics of the ATCRBS as it is currently used en route, including 1500 watts of interrogator power, a 42 dB STC curve, and improved SLS. An aircraft traveling at 550 knots was flown over two profiles, one at a constant altitude of 12,000 ft from a maximum range of 120 nm on in to the interrogator, and the other at a constant altitude of 40,000 ft from a

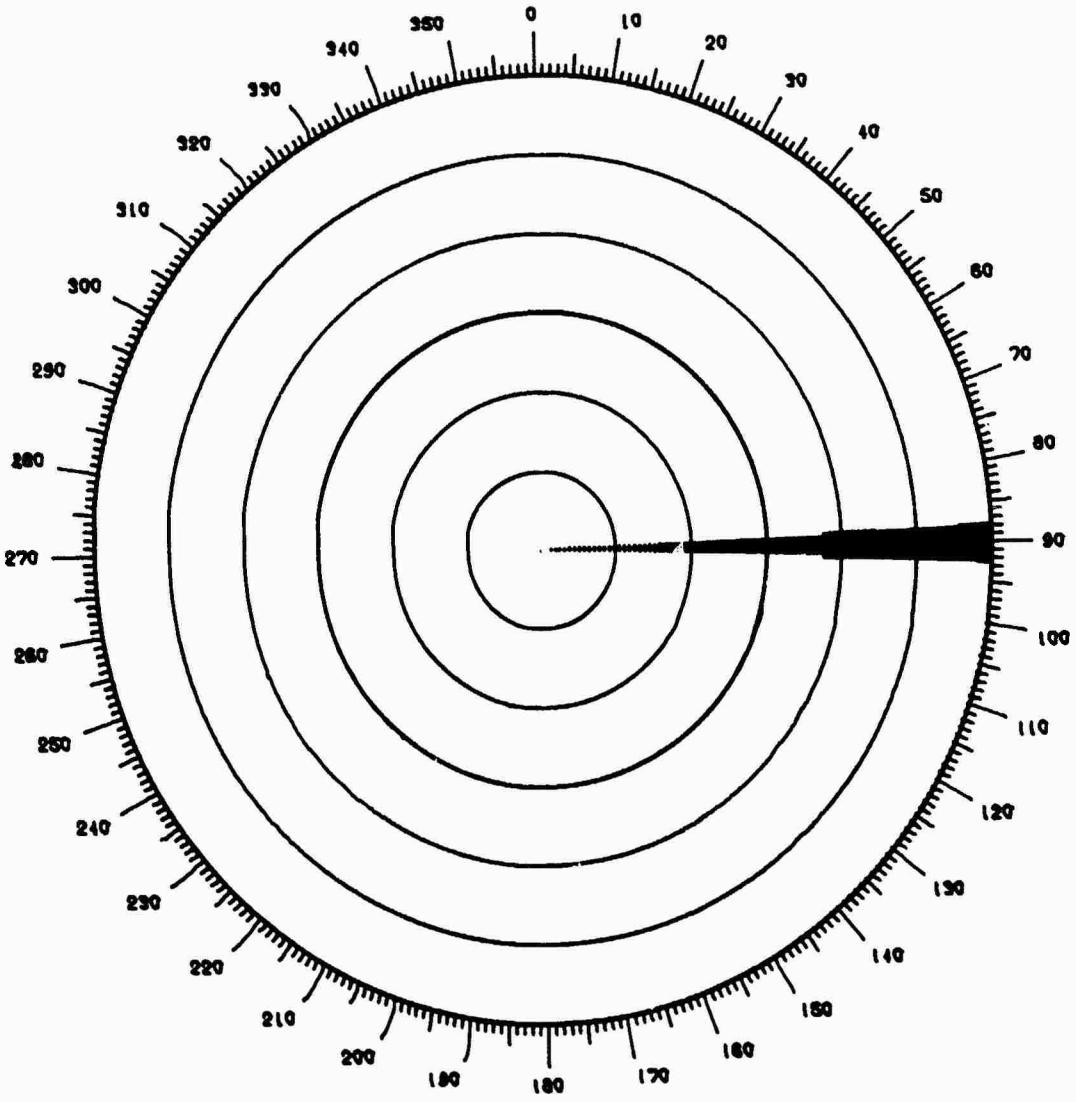


Figure 6.10 Simulated 5000-Ft Flight, FA-8043 Antenna, Roughness Parameter H=10 Ft

maximum range of 240 nm.

The five antenna systems tested in the en route configuration are listed in Table 6.1. Each of these systems was described in

Table 6.1 En Route Antenna Systems Modeled

| SYSTEM | DIRECTIONAL ANTENNA | OMNIDIRECTIONAL ANTENNA |
|---|---|---|
| 1 | FA-8043 | FA-8045 |
| 2 | ARSR Beacon Feed | FA-8045 |
| 3 | ARSR Beacon Feed | TI ARSR Omni |
| 4 | TI Separate Rotator | TI Separate Rotator Omni |
| 5 | Westinghouse Separate Rotator | Westinghouse Separate Rotator Omni |

Chapter 2 with the exception of System 2, which is also of current interest to the FAA. System 2 is typical of a system currently being used by the FAA called the NADIF (NAFEC Dipole Feed). The TI ARSR Beacon Feed has a radiation pattern similar for the most part to that of the NADIF. Of primary concern is the use of the present omnidirectional antenna, the FA-8045, with any kind of beacon feed arrangement for the directional antenna. Since there is a significant mismatch in the two patterns, the results of their interaction is of significant interest.

In addition to the differences in the antenna radiation patterns for each of these systems, there are several other differences in their characteristics that were taken into account in

parametric inputs to the models. These characteristics are shown in Table 6.2.

Table 6.2 En Route Antenna System Characteristics

| PARAMETER | SYSTEM 1 | 2 | 3 | 4 | 5 |
|---|---|---|---|---|---|
| Directional antenna: | | | | | |
| height (ft) | 105 | 93 | 93 | 84 | 84 |
| line loss (dB) | 6 | 12 | 12 | 6 | 6 |
| gain (dB) | 23 | 29 | 29 | 25 | 23 |
| Omnidirectional antenna: | | | | | |
| height (ft) | 110 | 110 | 110 | 93 | 92 |
| line loss (dB) | 6 | 6 | 6 | 6 | 6 |
| gain (dB) | 4 | 4 | 6 | 5 | 5 |

Contours showing coverage nulls due to vertical lobing, analogous to the curves explained in Figure 3.1, and those depicting false suppression in the main beam, analogous to Figure 3.2, appear on the following pages for each of the five systems as produced by the simple flat-earth model. Figures 6.11 through 6.15 are coverage curves for Systems 1 through 5, respectively; Figures 6.16 through 6.20 are false suppression contours for Systems 1 through 5, respectively. The areas under these curves as determined by the simple model are contained in Table 6.3

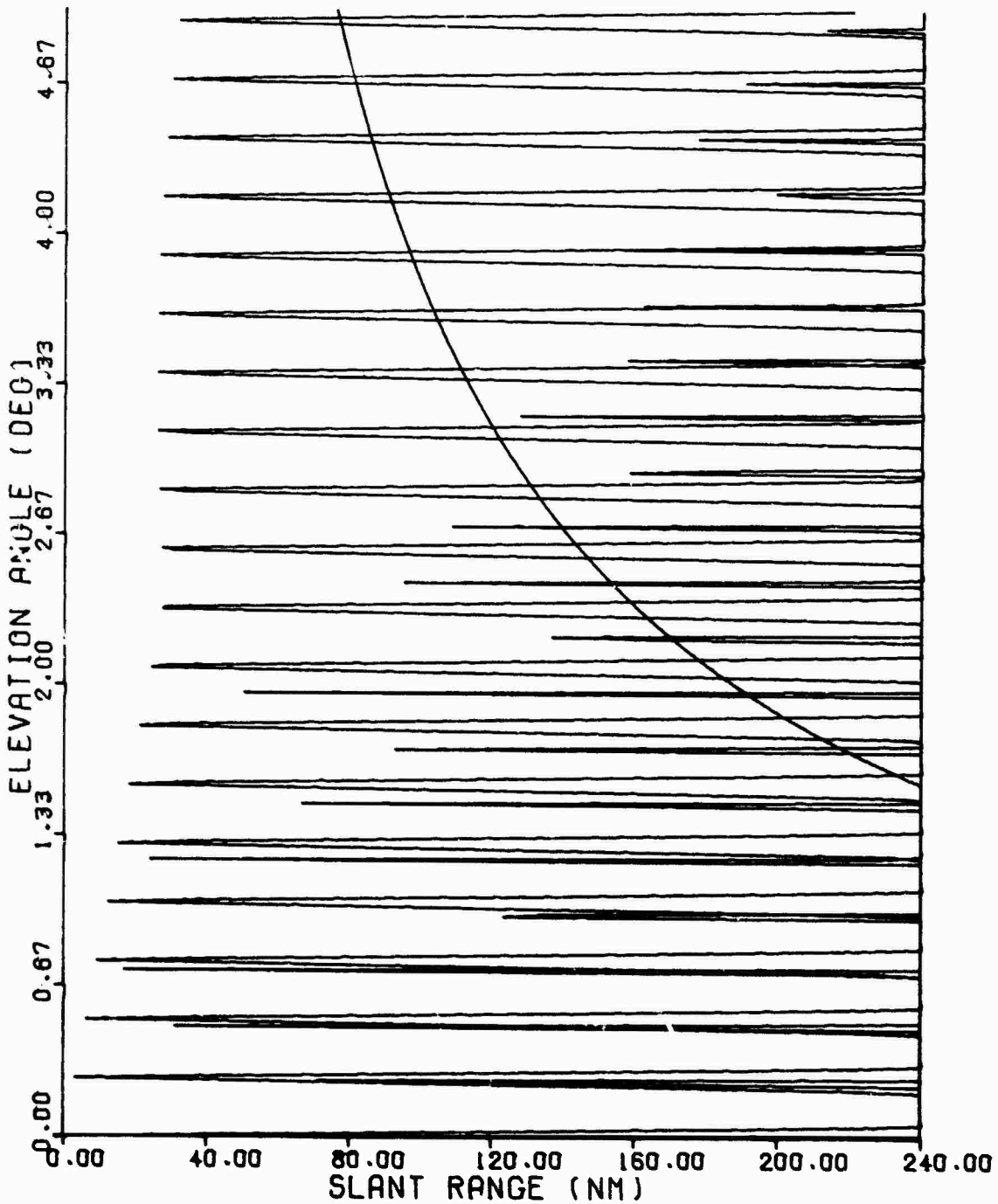


Figure 6.11 Vertical Lobing Contours, System 1

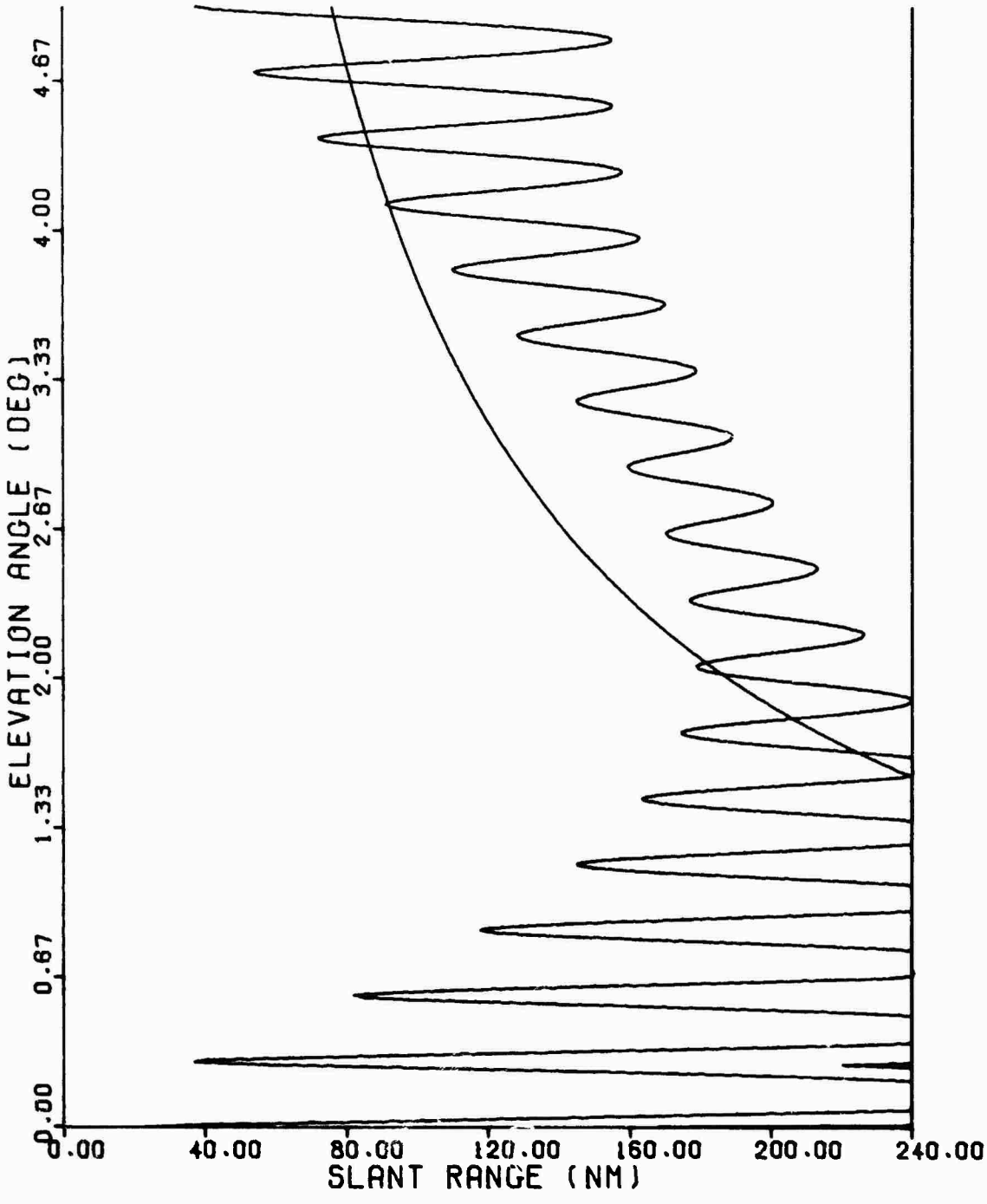


**Figure 6.12 Vertical Lobing Contours, System 2**

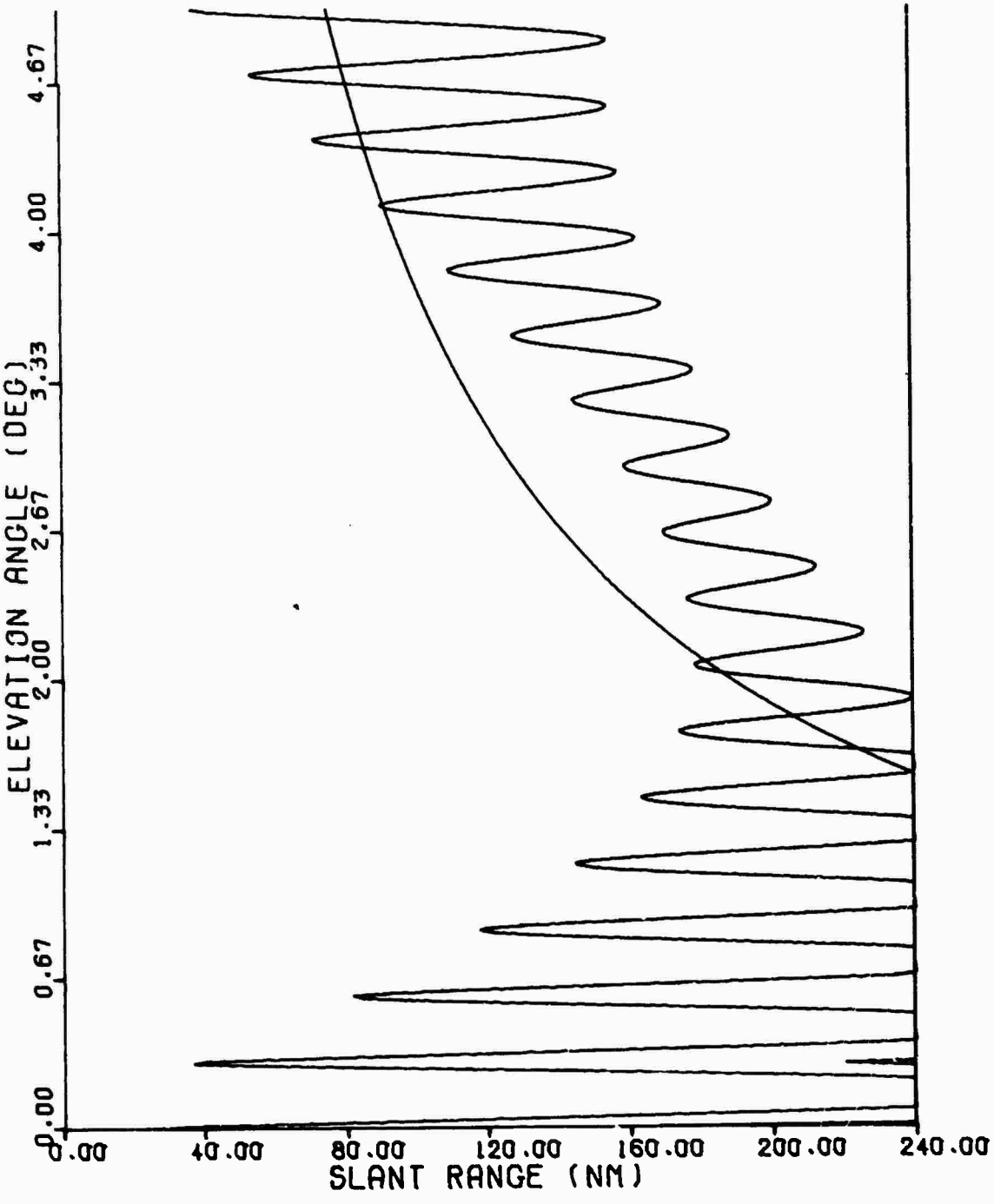


Figure 6.13 Vertical Lobing Contours, System 3

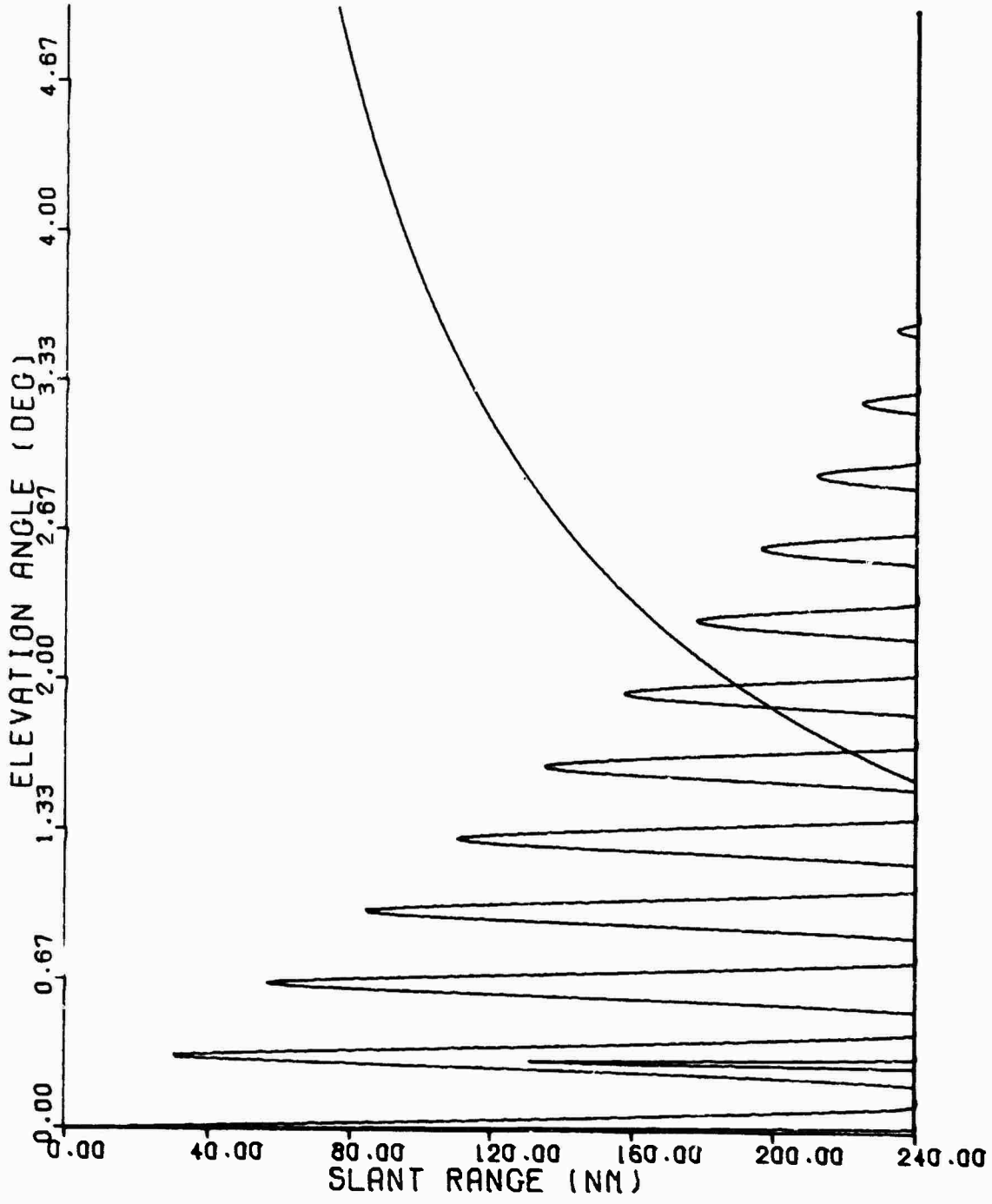


Figure 6.14 Vertical Lobing Contours, System 4

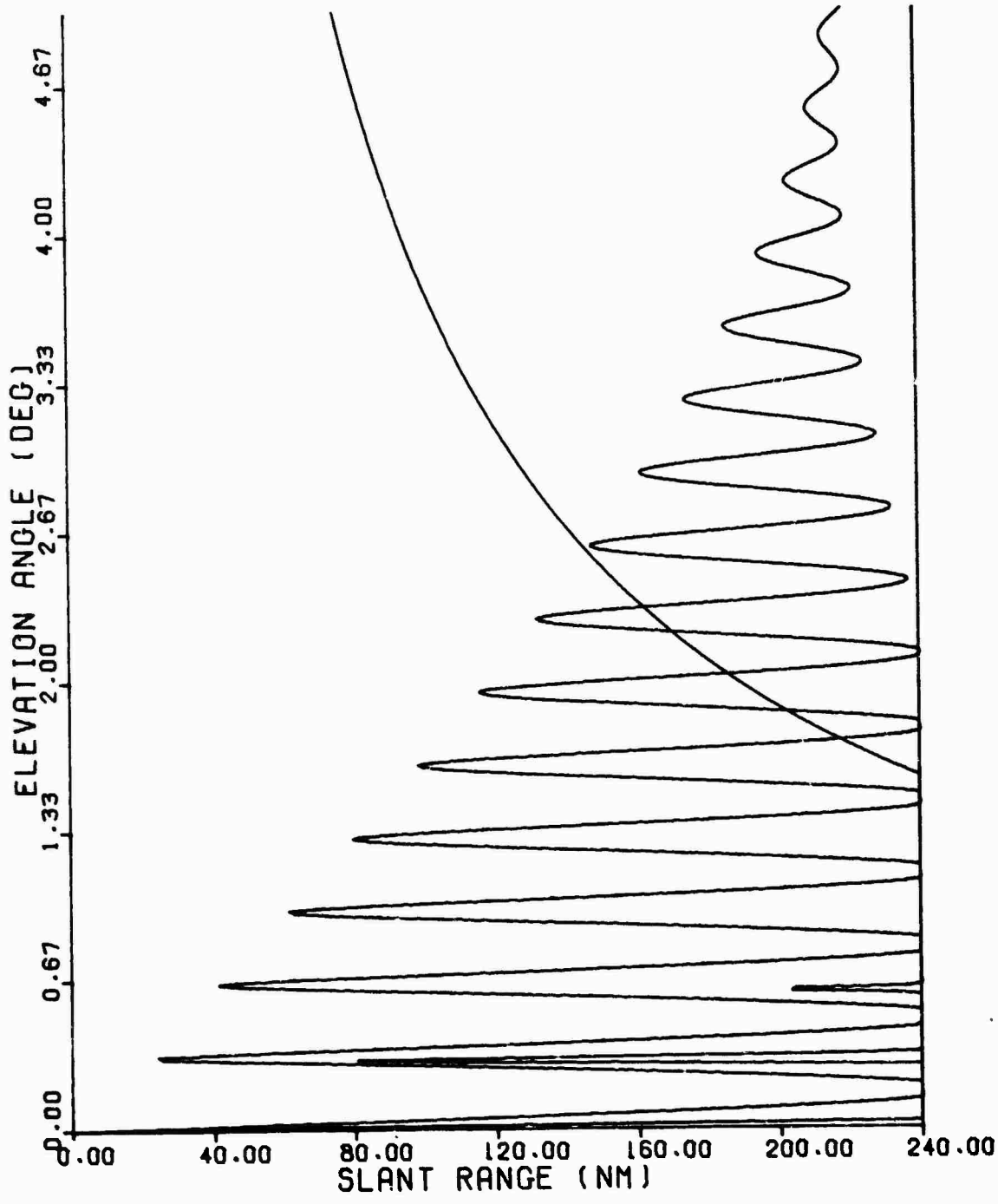


Figure 6.15 Vertical Lobing Contours, System 5

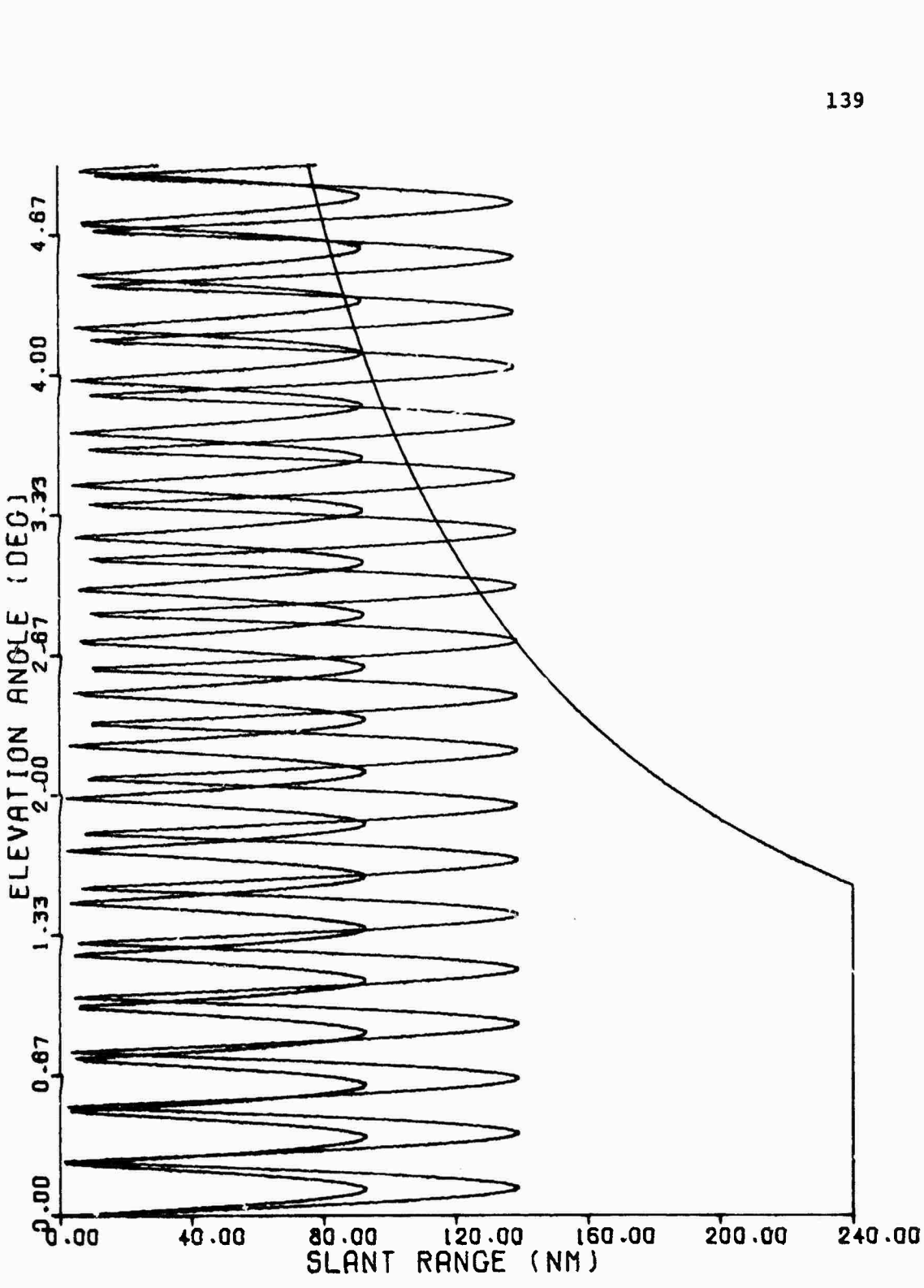


Figure 6.16 False Suppression Contours, System 1

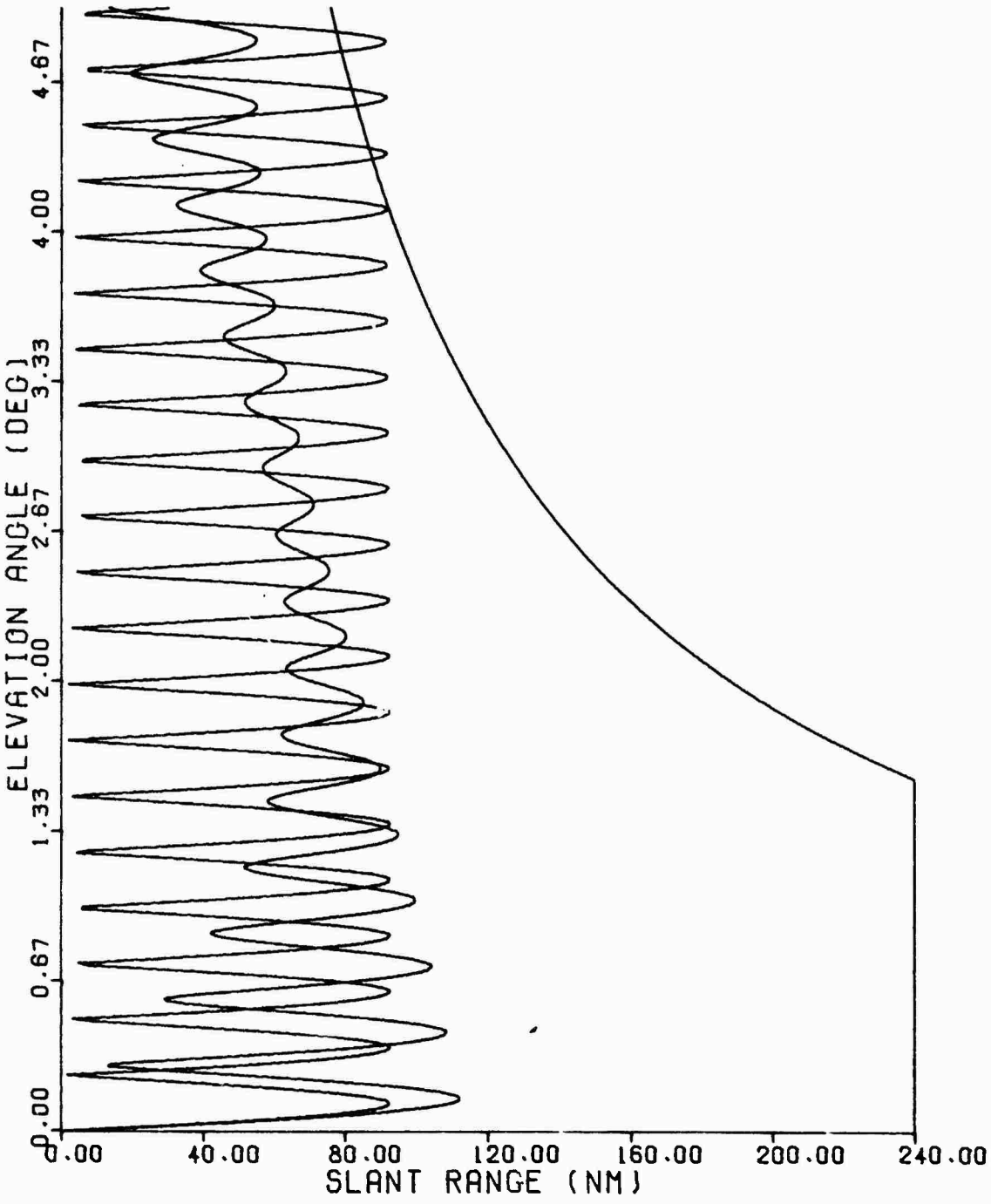


Figure 6.17 False Suppression Contours, System 2

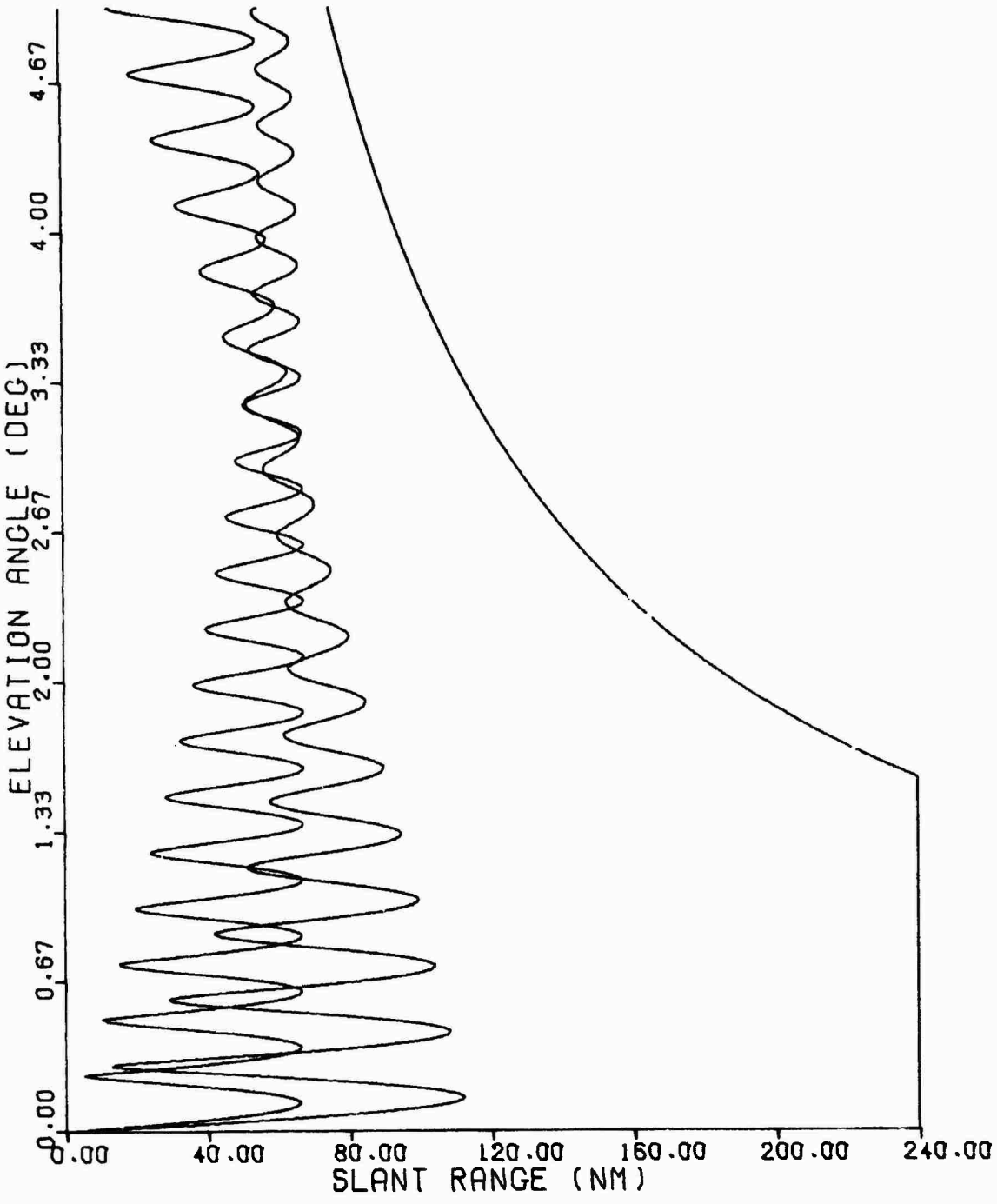


Figure 6.18 False Suppression Contours, System 3

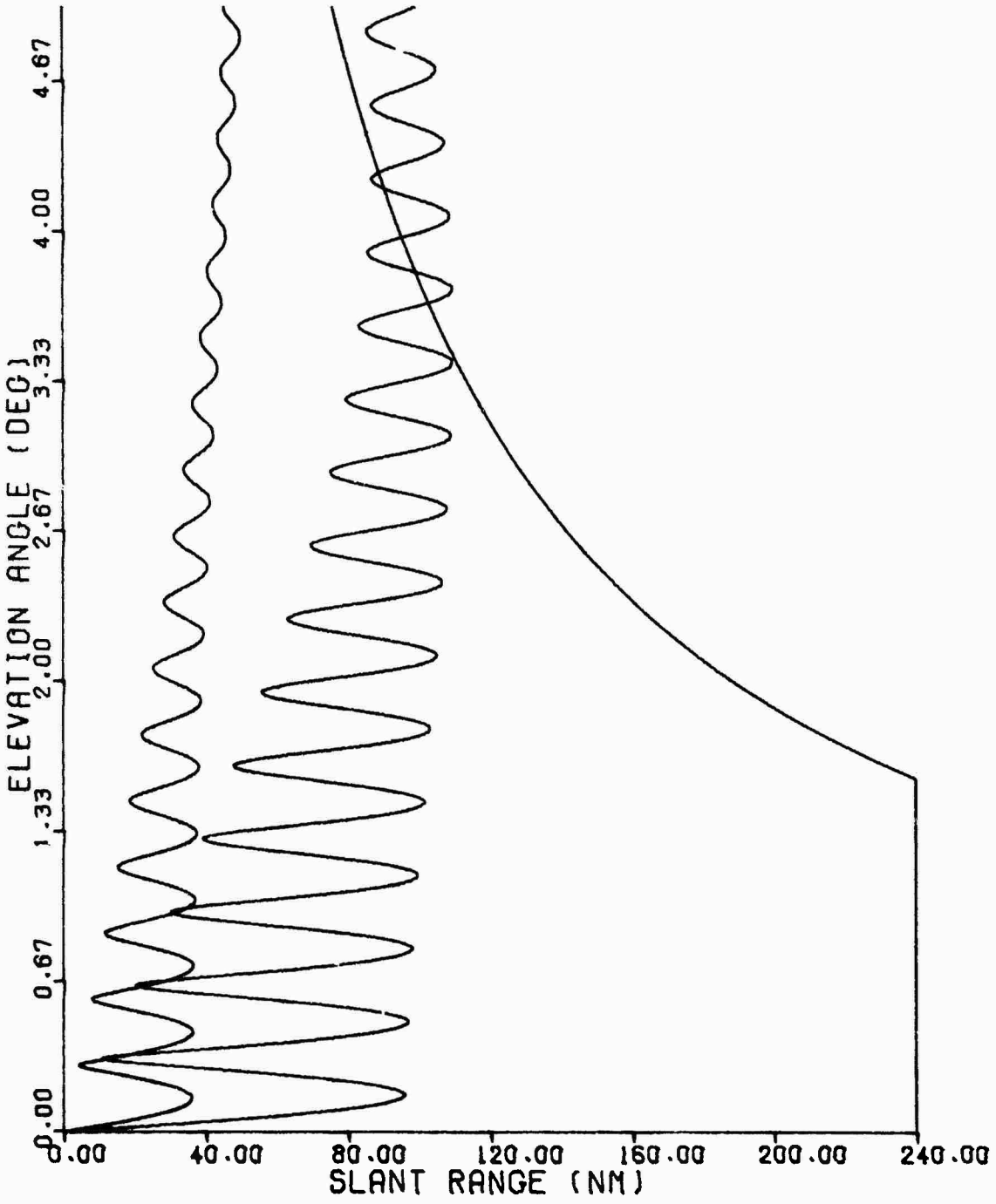


Figure 6.19 False Suppression Contours, System 4

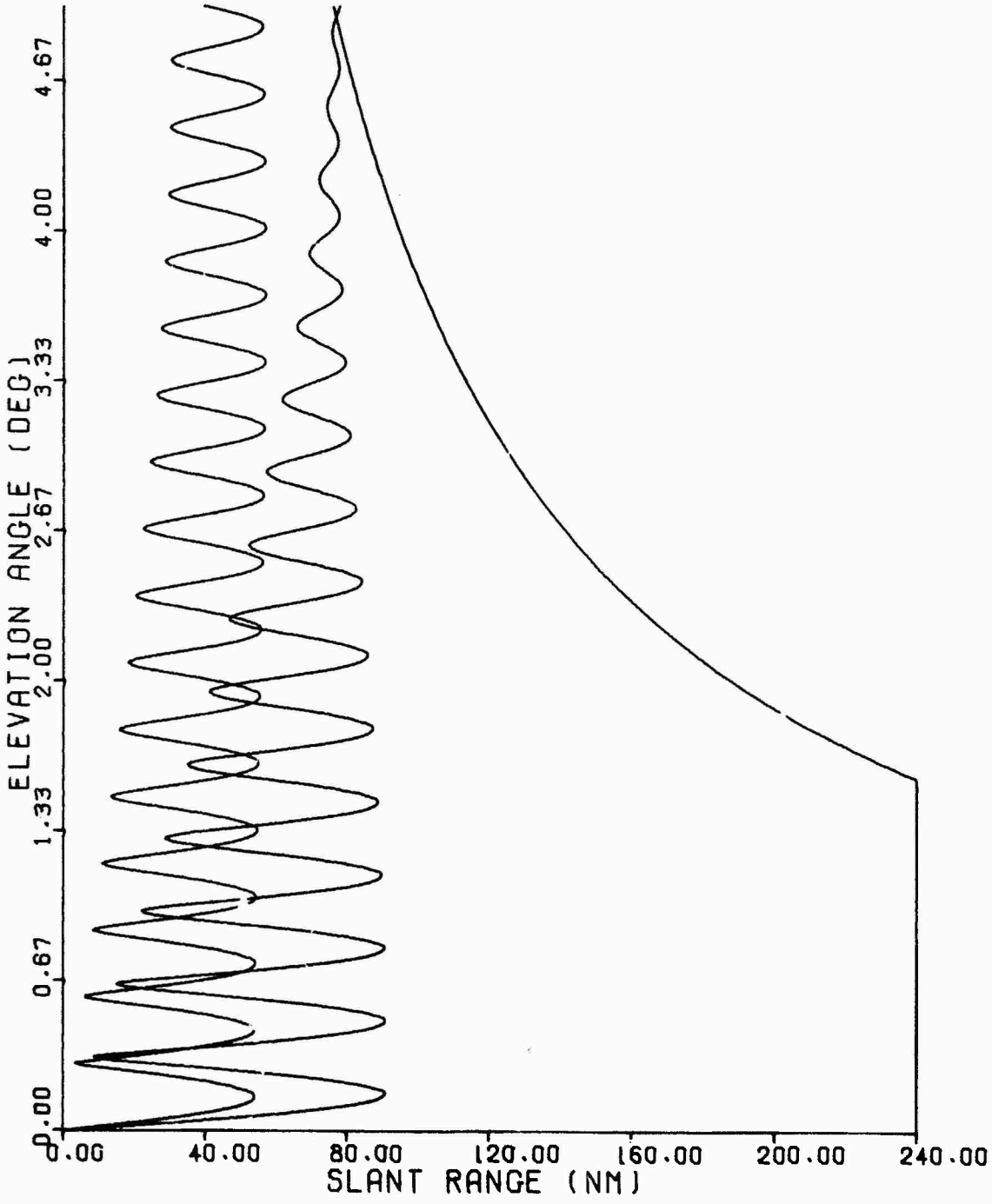


Figure 6.20 False Suppression Contours, System 5

according to the various types of performance criterion which

Table 6.3 En Route Antenna System Performance, Simple Model

| CRITERION (areas in $nm^2$) | SYSTEM 1 | 2 | 3 | 4 | 5 |
|---|---|---|---|---|---|
| Uncovered uplink | 307.4 | 197.5 | 197.5 | 311.4 | 402.5 |
| False suppression | 116.8 | 137.1 | 73.9 | 0.5 | 10.9 |
| Uncovered downlink | 52.4 | 1.4 | 1.4 | 13.8 | 28.3 |
| Over-interrogation | 107.4 | 111.5 | 111.5 | 103.9 | 100.2 |
| Interference susceptibility | 118.8 | 115.8 | 115.8 | 111.5 | 111.2 |

they influence. In Figures 6.11 through 6.15, the uplink nulls are always deeper than the downlink contours. Similarly, in Figures 6.16 through 6.20, the directional antenna contours are the contours with the higher peaks at the lower elevation angles.

The total area in a "slice" of vertical coverage 40,000-ft high out to a range of 240 nm is 1330 sq nm. Of this amount, then, the simple model says that 307 sq nm (up to $5^{o}$ elevation) is uncovered when the present system is in use under the given conditions. Systems 2 and 3, both of which involve the beacon feed have an extremely sharp underside cut-off of the radiation pattern and reduce lobing substantially. This effect can be seen in Figures 6.13 and 6.14, and is evidenced in the reduction in

uncovered uplink area shown in Table 6.3. The TI separate rotator has about the same uncovered uplink area, while the performance of the Westinghouse antenna in this regard is considerably worse. Figures 6.14 and 6.15 give some indication of the reason for this apparently poor performance. The nulls for both of the separate rotators are considerably wider (in elevation) than those of the FA-8043, but not nearly as deep. Also, by the time an elevation of $3^{o}$ is reached, the separate rotators have ceased their lobing effects within the desired coverage area, but the FA-8043 continues its uplink holes above $5^{o}$ elevation. If the simple model had been applied above $5^{o}$, the uplink coverage holes would have continued to add for the FA-8043, while the separate rotators' uncovered uplink areas would have remained constant.

The combination of large vertical aperture and matched omnidirectional antennas shows its advantages in the false suppression areas. As might be expected, the mismatch of the present omni pattern with that of a beacon feed causes even more false suppression than does the FA-8043 with its own "matched omni". The primary trouble with the mismatched system occurs at higher elevation angles where the pattern of the beacon feed begins to drop much more rapidly than that of the omni. When, as in System 3, the matched omni is introduced, the falsely suppressed area is halved. The separate rotators experience very little false suppression as is evident from Figures 6.19 and 6.20.

The downlink does not appear to be too serious a problem for

any of the systems, as the nulls are out of the desired coverage area even for the FA-8043 by $3^{\circ}$ elevation. Similarly, there is little difference in the areas of over-interrogation or susceptibility to interference for any of the systems. This is true primarily because most of the area between the desired coverage area and that in which interference is involved must be covered in the main beam if coverage at the desired slant range is to be obtained. Further examples in this chapter will continue to support this hypothesis that control of interrogation range and reception range in the main beam beyond the desired coverage range is difficult to effect. Even control of interrogator power will be shown later to have little effect. The primary reason for control of power and sensitivity, then, must relate more to reflections and side-lobe phenomena than to effects of the main beam.

Figures 6.21 through 6.25 show simulated displays produced by the complex model for 120-nm flights at 12,000 ft using Systems 1 through 5, respectively; range rings are spaced 25 nm apart, with accentuated rings 50 nm apart. Similarly, Figures 6.26 through 6.30 show the result of simulated flights at 40,000 ft from a range of 240 nm. Range rings for the longer-range flights are also spaced 25 nm apart and accentuated every 50 nm. The displays correlate well with the results of the simple model already presented. The standard FA-8043 antenna gives the poorest performance over the longest range with frequent misses

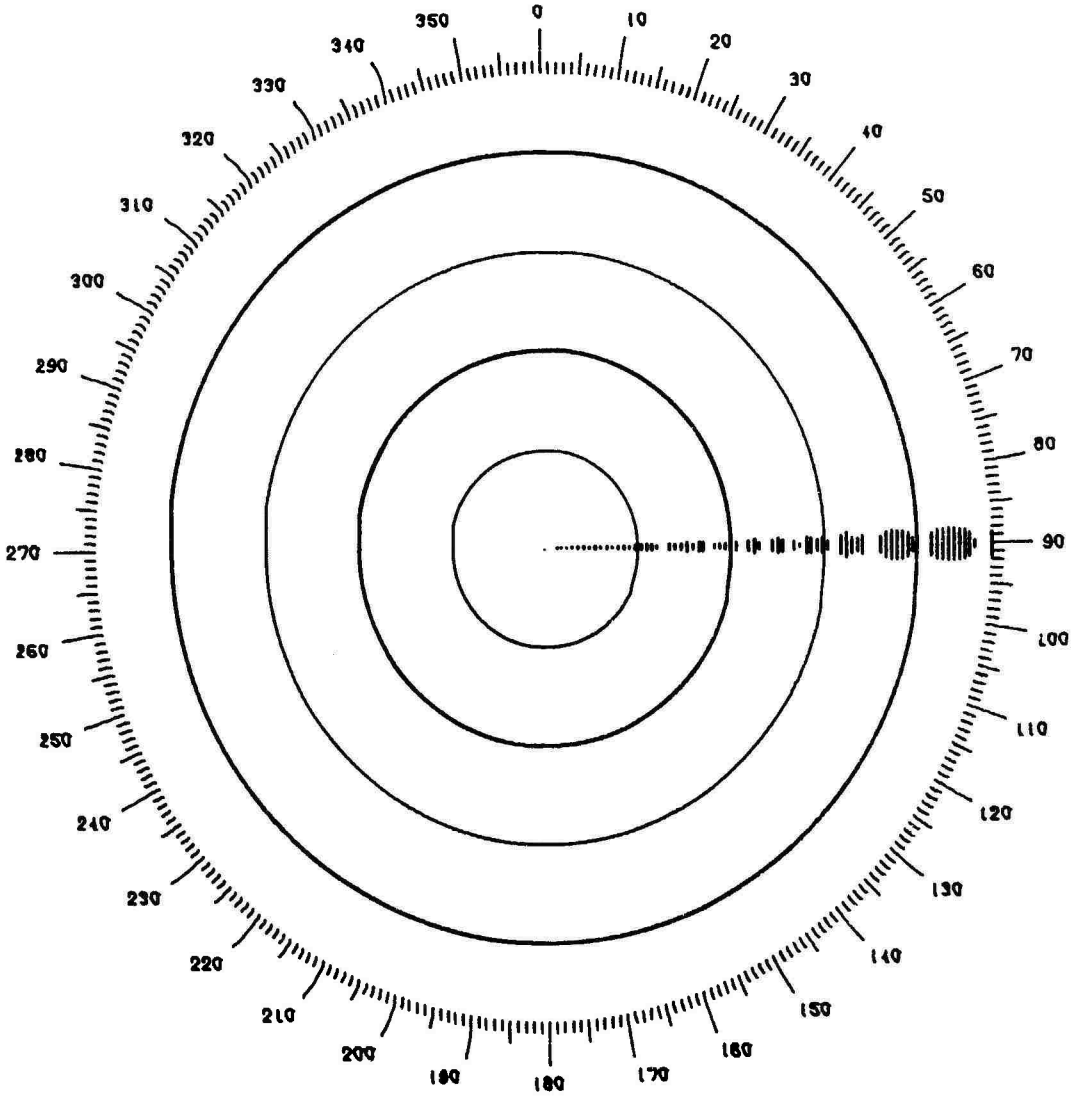


Figure 6.21 Simulated Flight at 12,000 Ft, System 1

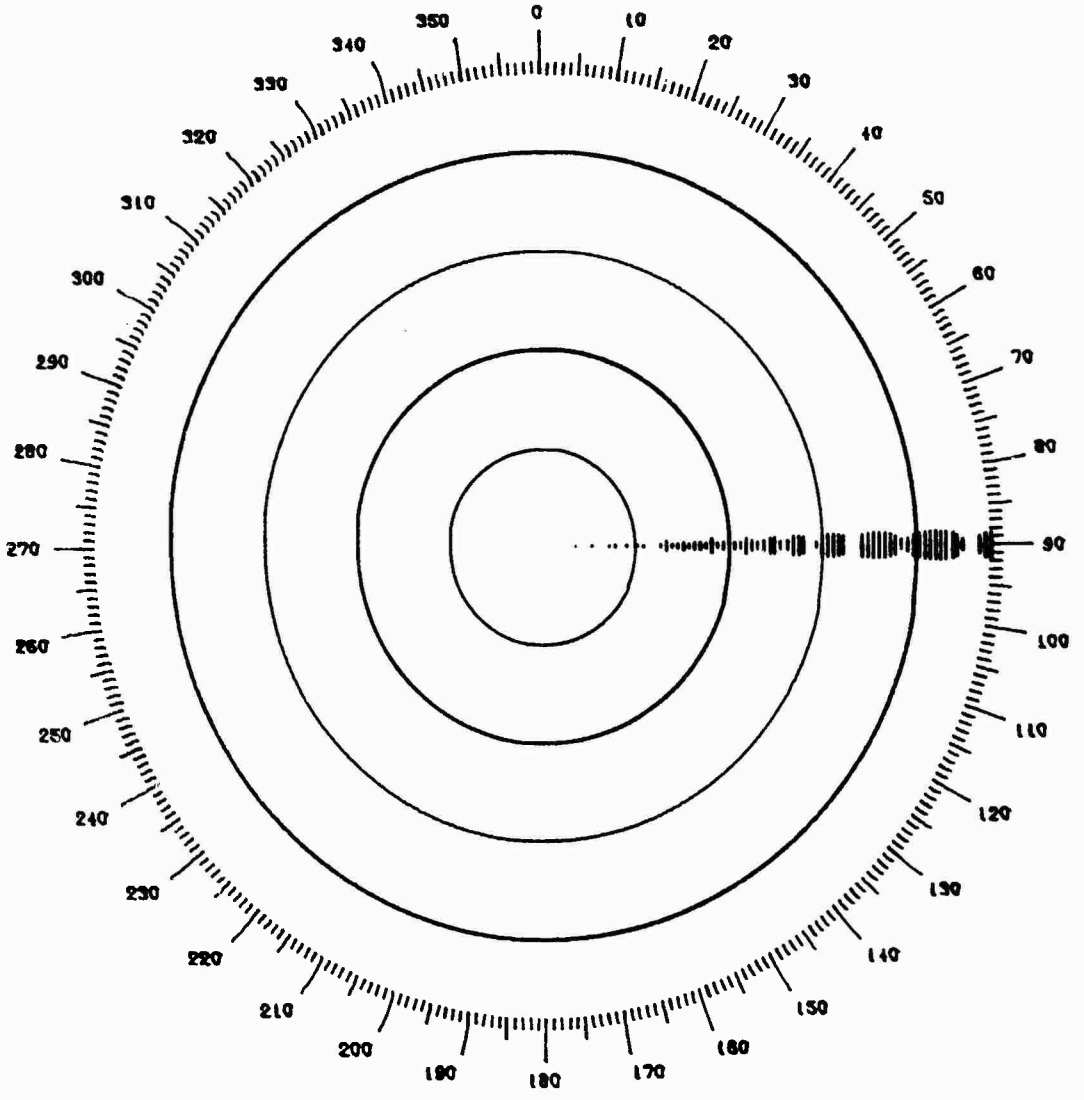


Figure 6.22 Simulated Flight at 12,000 Ft, System 2

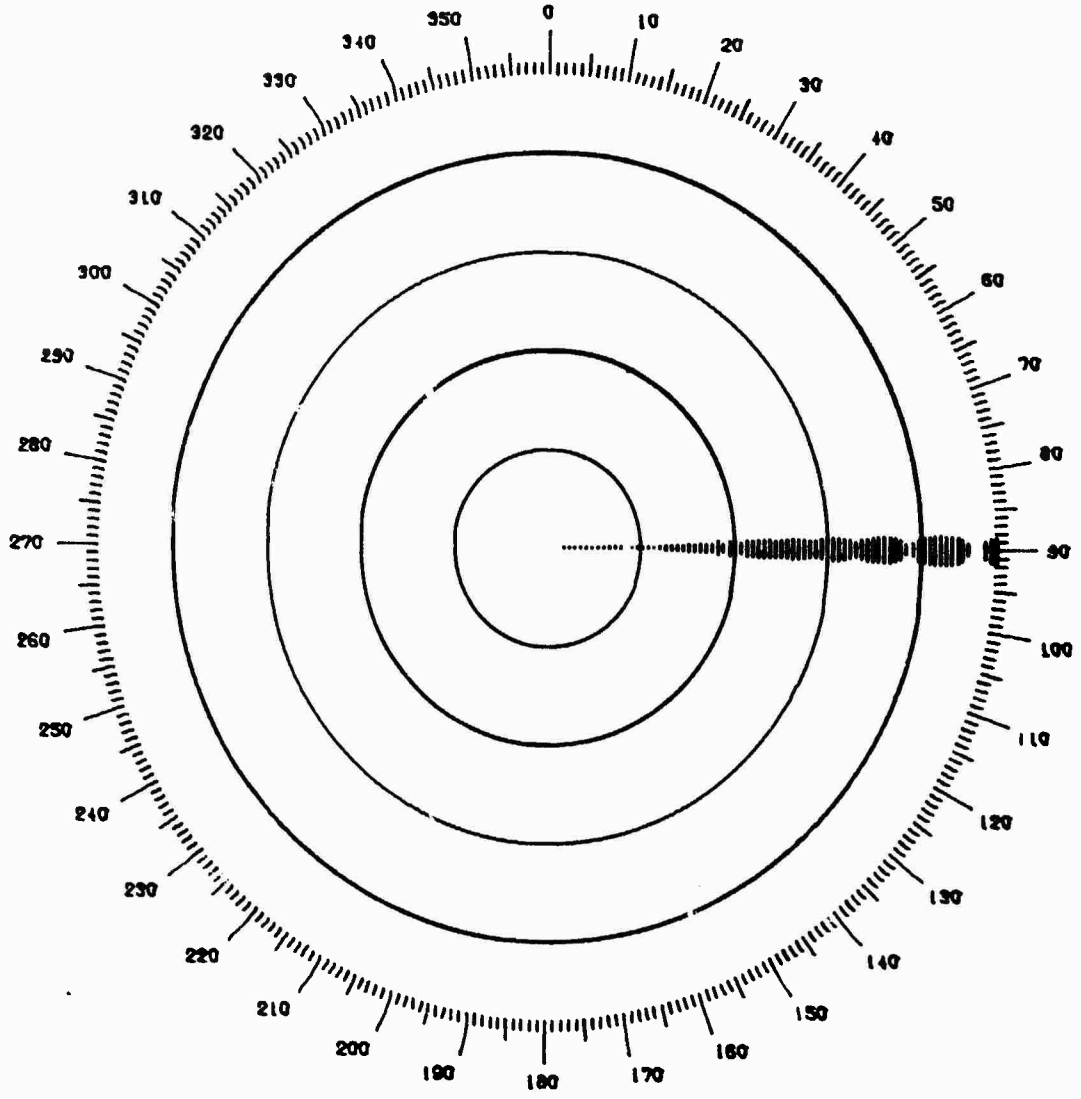


Figure 6.23 Simulated Flight at 12,000 Ft, System 3

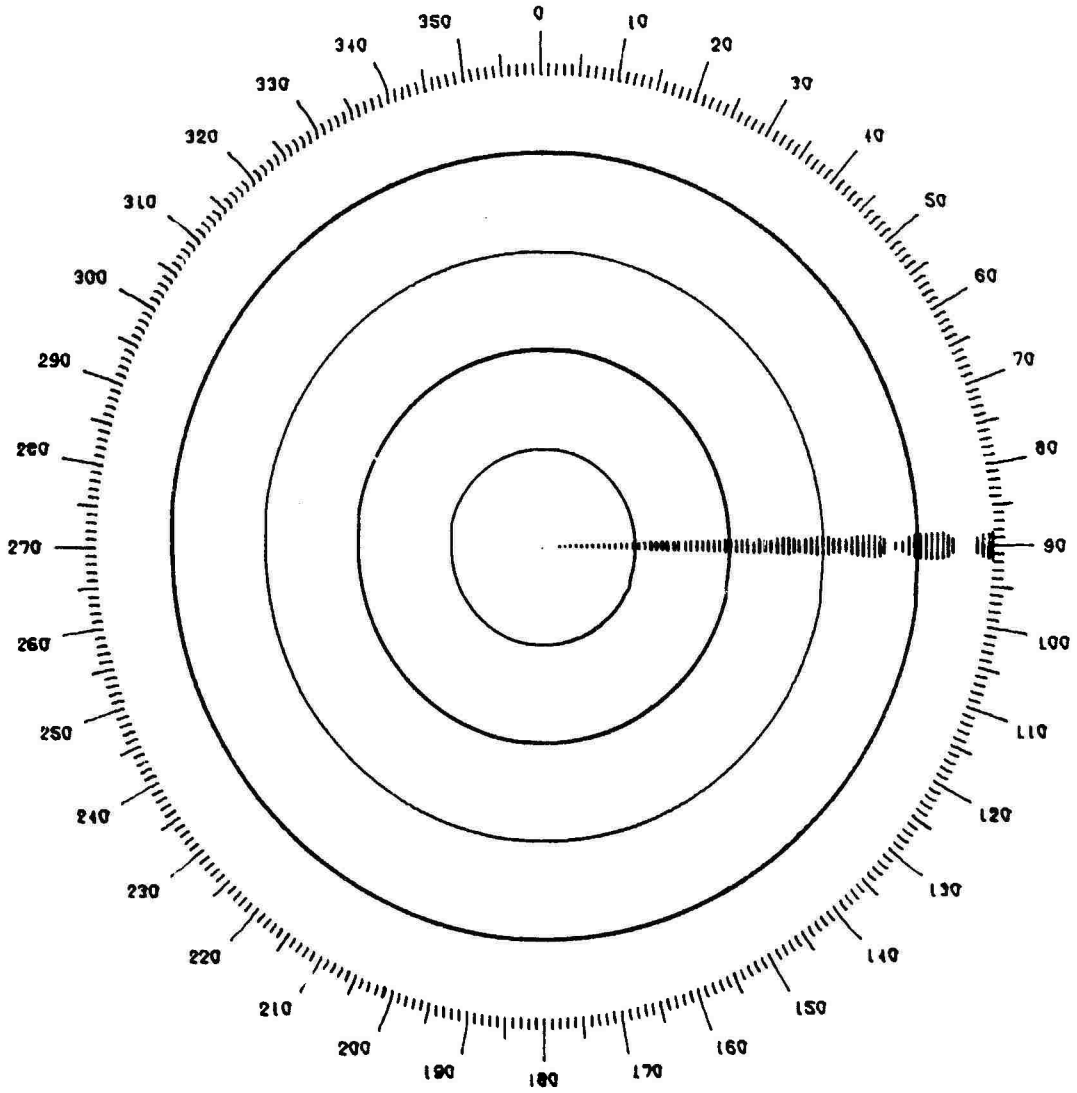


Figure 6.24 Simulated Flight at 12,000 Ft, System 4

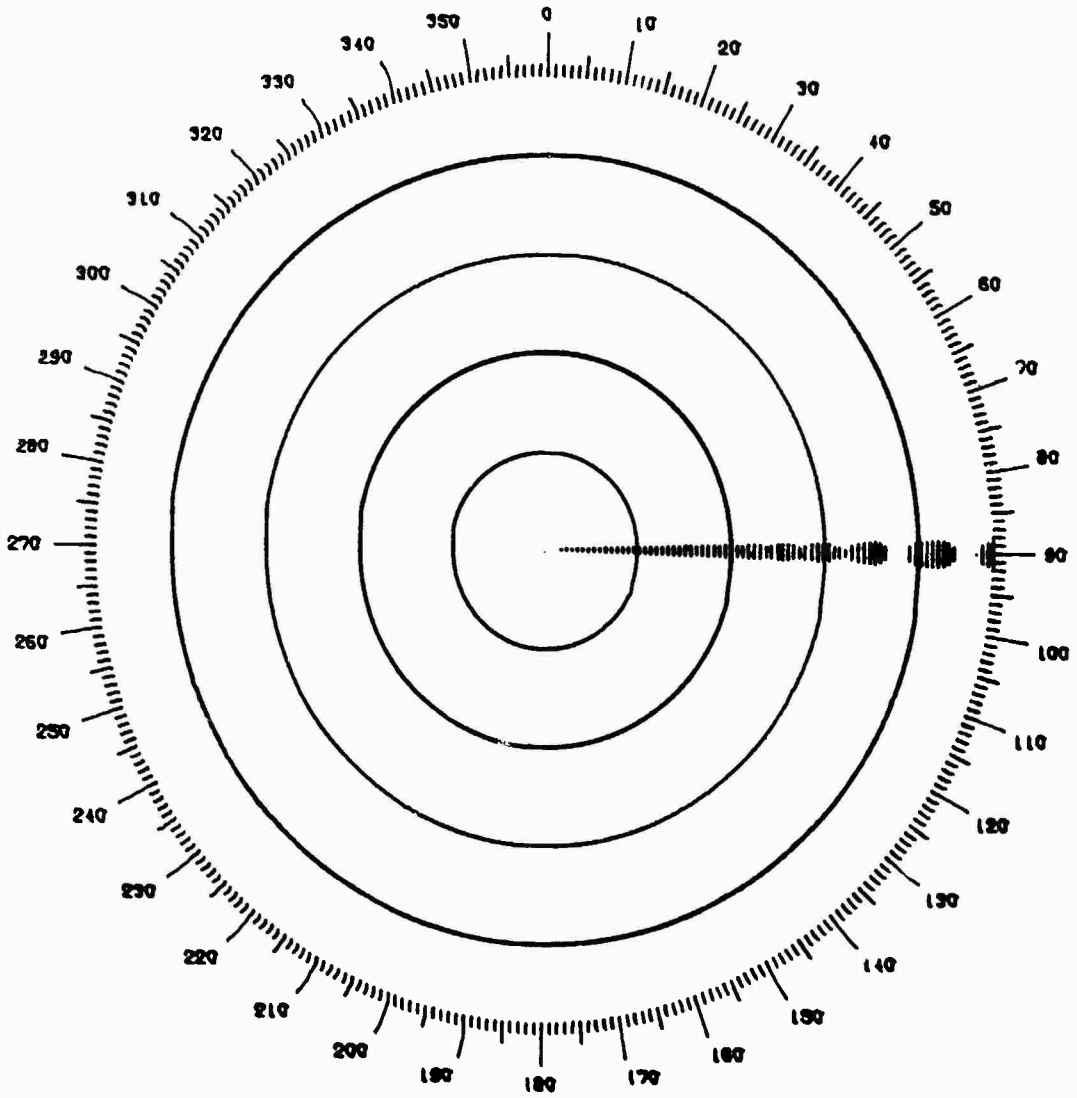


Figure 6.25 Simulated Flight at 12,000 Ft, System 5

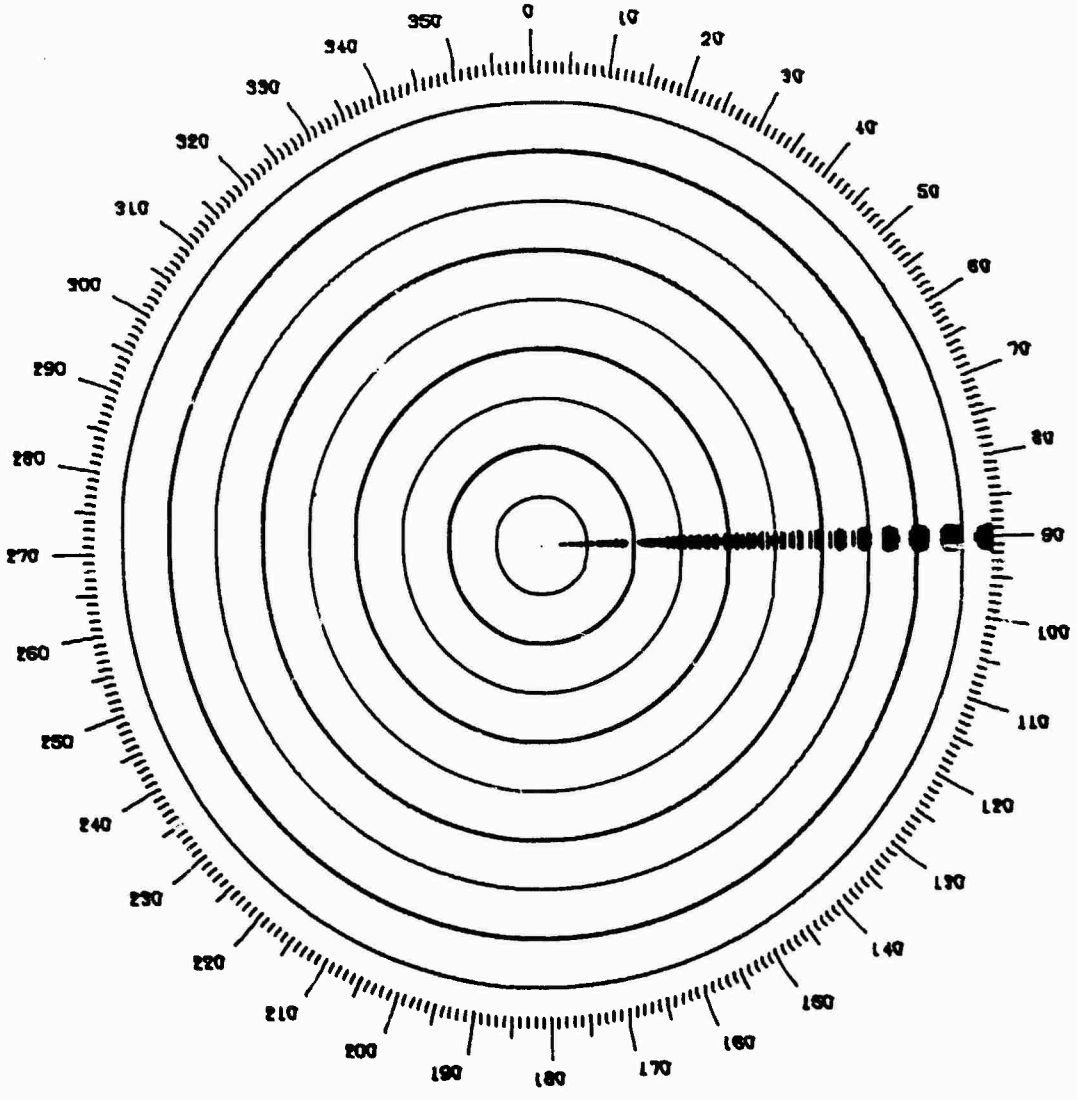


Figure 6.26 Simulated Flight at 40,000 Ft, System 1

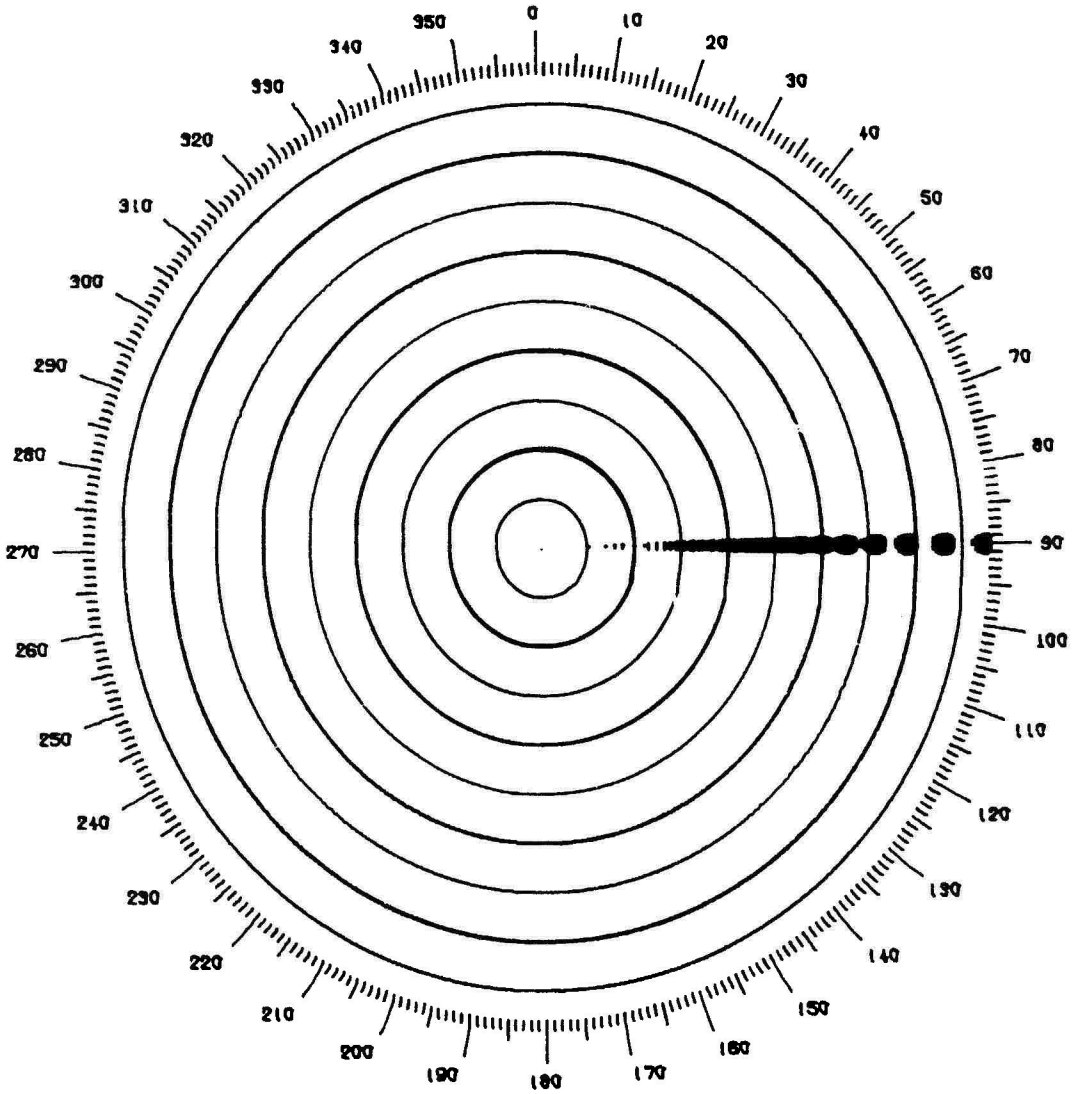


Figure 6.27 Simulated Flight at 40,000 Ft, System 2

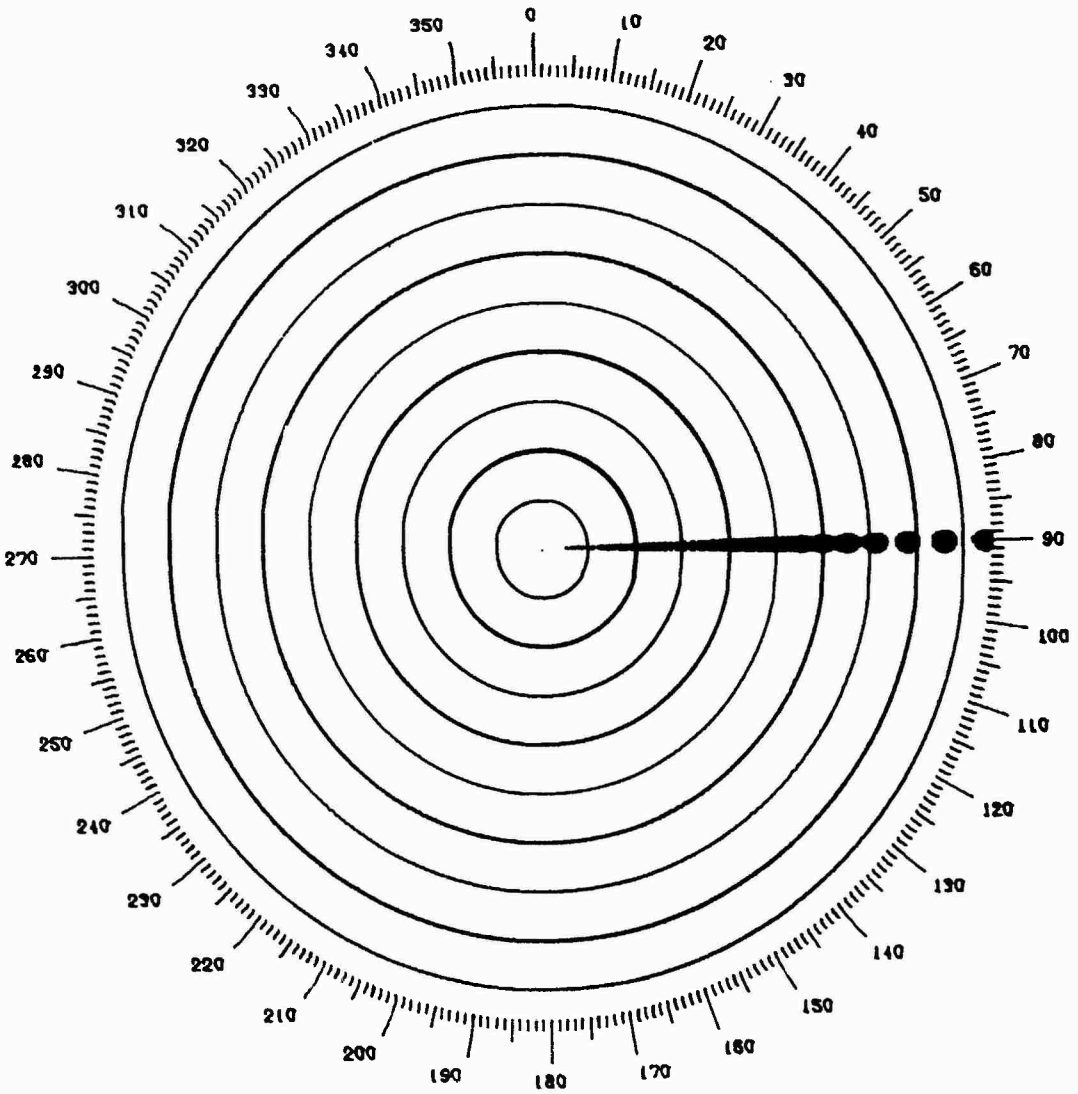


Figure 6.28 Simulated Flight at 40,000 Ft, System 3

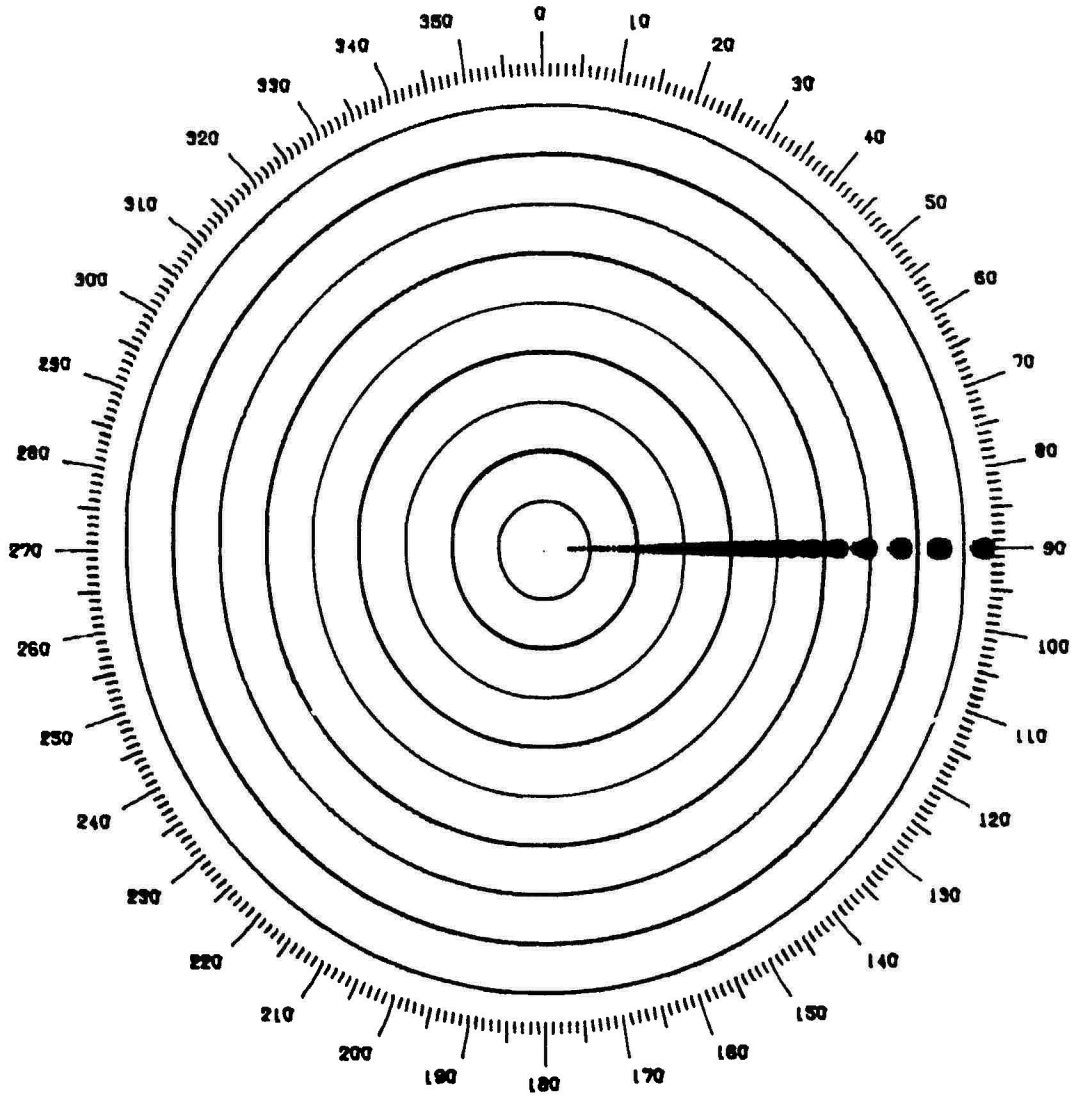


Figure 6.29 Simulated Flight at 40,000 Ft, System 4

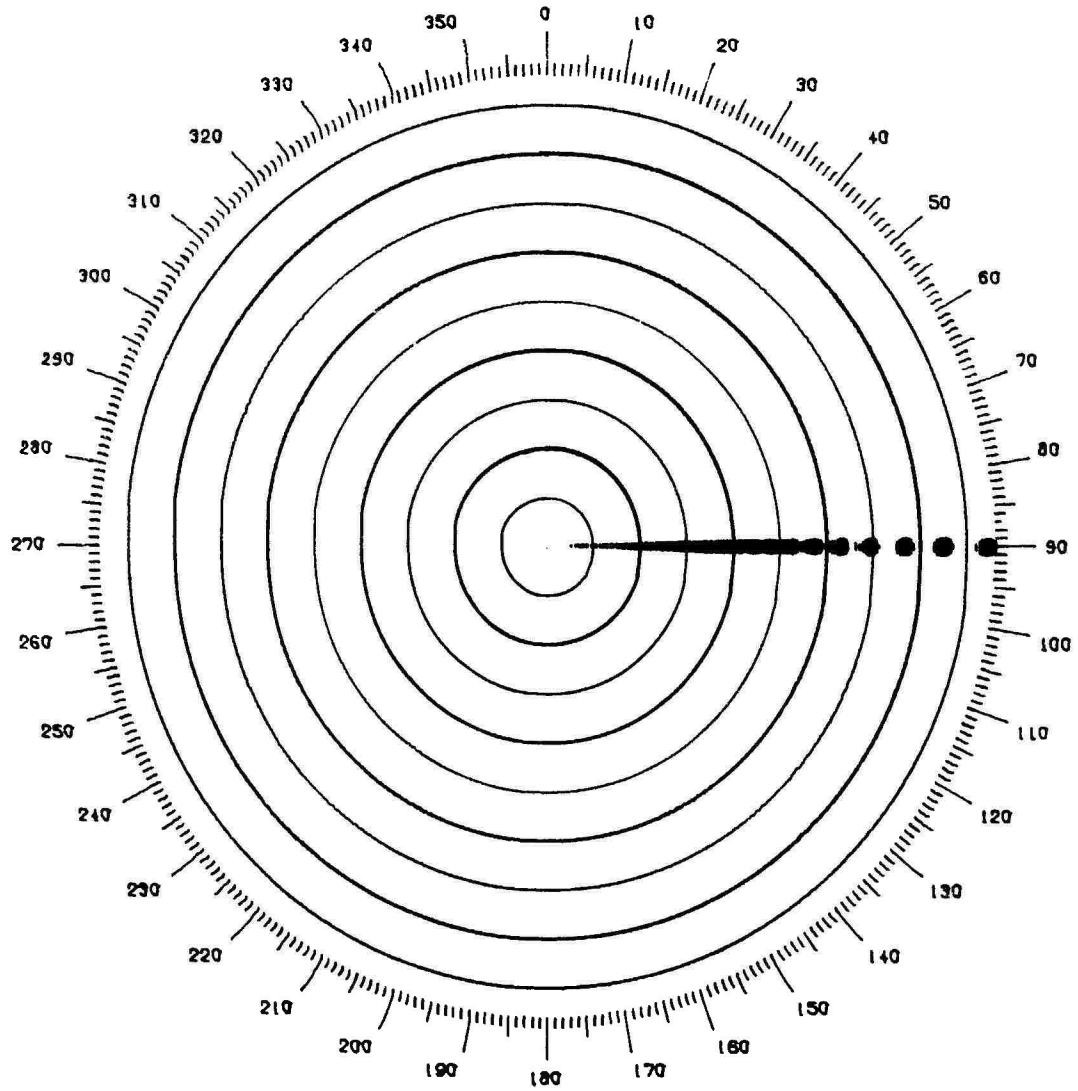


Figure 6.30 Simulated Flight at 40,000 Ft, System 5

of several consecutive scans. (Precise data is tabulated in the next paragraph.) Very wide gaps at high elevation angles close to the interrogator are apparent in the simulations of System 2 because the omni antenna pattern does not fall off as rapidly as the directional pattern and causes appreciable false suppression as explained in the discussion of the results of the simple model. Addition of a matched omni in System 3 solves the false suppression problem and appears to produce the most desirable display at both altitudes. The separate rotators give similar performance, each producing two coverage holes for the 12,000 ft flight and four holes for the 40,000 ft case. The holes produced by the TI separate rotator are slightly smaller than those of the Westinghouse antenna, as would be expected due to the taller aperture (10 ft vs 8 ft) of the TI antenna, and hence the sharper underside pattern roll-off. The much sharper roll-off of the ARSR beacon feed of System 3, due to the 22-ft aperture of the ARSR dish, causes a further reduction in the size of the holes, and even closes entirely the hole at 163 nm present in the flights of both separate rotators. These figures are useful in visualizing the data that follow.

Table 6.4 summarizes the performance criteria tabulated in the execution of the complex model for the 12,000-ft flight. The total flight consists of 78 scans of the antenna. The number of hits used to distinguish a valid target from a weak or missing target is 7, the number commonly used in ARTS target processing

Table 6.4 En Route Antenna System Performance, Complex Model, 12,000-Ft Flight

| CRITERION | SYSTEM 1 | 2 | 3 | 4 | 5 |
|---|---|---|---|---|---|
| Number of holes | 10 | 7 | 2 | 2 | 2 |
| Most consecutive scans with fewer than 7 hits | 2 | 2 | 2 | 3 | 4 |
| Total scans with fewer than 7 hits | 13 | 18 | 5 | 5 | 8 |
| Total scans with no hits | 13 | 17 | 4 | 5 | 7 |
| Average replies per scan | 26.7 | 24.3 | 31.9 | 32.2 | 31.0 |
| Standard deviation of replies per scan | 14.6 | 16.5 | 12.6 | 9.8 | 11.7 |
| Total single $P_2$ pulses | 928 | 987 | 644 | 364 | 339 |
| Total number of suppressions | 2823 | 3302 | 2238 | 1536 | 1478 |
| Total number of interrogations | 2482 | 1900 | 2532 | 2943 | 2924 |
| Total number of replies | 2084 | 1897 | 2488 | 2515 | 2421 |

algorithms. The number of holes is the number of times a succession of consecutive scans with fewer than 7 hits was initiated. The remainder of the criteria have been discussed previously or are self-explanatory.

Clearly, the new antennas with matched omnis are the most successful in minimizing the number of holes. The slightly wider holes of the separate rotators discussed previously are evident in

the additional consecutive scans with fewer than 7 hits. Again, the superiority of the new antennas with matched omnis is apparent in the number of scans with few hits. The new antennas also yield 5 to 7 more hits, on the average, than Systems 1 or 2. System 1, of course loses its average simply on coverage, while most of the reduction in width using System 2 is caused by its tendency to suppress falsely in the main beam. The standard deviation of replies per scan is perhaps one of the best indicators of antenna system performance. The fluctuations of System 1 and the wide false suppression gap of System 2 account for their appreciable deviations from the average. The display of the flight using System 3 shows extreme target narrowing as the aircraft approaches the interrogator. The ARSR beacon feed pattern even for this "matched" system rolls off at high elevation angles more rapidly than the omni pattern and causes some of this reduction in target width. This shows up in the tabulated results as a deviation from the normally wider target. The separate rotators thus show the most consistent target width by their relatively small deviation and large number of average replies per scan.

The total number of $P_2$ pulses, suppressions, interrogations, and replies will be of greater interest in subsequent sections. Note, however, the correlation between the number of suppressions and the performance criteria discussed above. System 2 in particular shows evidence of its false suppression characteristic. The total number of replies, as would be expected, is also an

indicator of total system performance.

Table 6.5 is analogous to Table 6.4 for the 40,000-ft flight. The total number of scans in this longer flight is 156.

Table 6.5 En Route Antenna System Performance, Complex Model, 40,000-Ft Flight

| CRITERION | SYSTEM 1 | 2 | 3 | 4 | 5 |
|---|---|---|---|---|---|
| Number of holes | 14 | 8 | 3 | 3 | 4 |
| Most consecutive scans with fewer than 7 hits | 4 | 6 | 3 | 7 | 8 |
| Total scans with fewer than 7 hits | 32 | 41 | 15 | 21 | 26 |
| Total scans with no hits | 32 | 40 | 15 | 19 | 24 |
| Average replies per scan | 25.7 | 21.5 | 27.5 | 27.7 | 26.9 |
| Standard deviation of replies per scan | 15.1 | 14.2 | 10.7 | 12.5 | 14.1 |
| Total single $P_2$ pulses | 553 | 651 | 801 | 696 | 340 |
| Total number of suppressions | 2621 | 3382 | 201 | 1729 | 1024 |
| Total number of interrogations | 4636 | 3364 | 4500 | 4821 | 4673 |
| Total number of replies | 4008 | 3359 | 4293 | 4327 | 4197 |

For this high-altitude flight, many of the effects that occur at larger elevation angles become evident in the tabulated data.

The low number of average replies per scan for System 2, for example, is due to the fact that there is no coverage at all from 30 nm out all the way in to the interrogator. Once again, the 40,000-ft flight shows the new antennas to be superior in their greater number of replies, greater average replies per scan, and smaller deviation from the average. Although the number of holes is reduced with the use of Systems 3, 4, and 5, the separate rotators still present a difficulty in that their few holes are longer in terms of the number of consecutive scans than are the holes produced by the FA-8043. This result, which is in direct agreement with the vertical lobing contours obtained with the simple model, could have a serious impact on target tracking. Successive scans of weak targets numbering 7 or 8 would be nearly certain to result in the dropping of target tracks by most conventional algorithms.

The results presented in this section are meant to provide a general indicator of the type of performance that can be expected from several different en route antenna configurations, given a common baseline. Since it is difficult to establish a common baseline or procedure with which to evaluate several different systems, the procedure used here can be called representative at best. In the section that follows, another group of antennas is evaluated in a similar fashion. The section after that, however, undertakes another procedure that attempts to optimize the best features of each antenna system.

## 6.5 Antenna Performance in a Standard Terminal Configuration

As a first step in the assessment of the relative performance of five terminal antenna systems according to some basic ground rules, a common test configuration was developed for both the simple flat-earth and complex spherical-earth models. The tests would entail utilization of most of the characteristics of the ATCRBS as it is currently used at terminal sites, including 500 watts of interrogator power, a 36 dB STC curve, and improved SLS. An aircraft traveling at 200 knots was flown over three profiles, one at a constant altitude of 2,000 ft, another at 5,000 ft, and the third at 10,000 ft, all from a maximum range of 60 nm on in to the interrogator.

The five antenna systems tested in the terminal configuration are listed in Table 6.6. Each of these systems was described in

Table 6.6 Terminal Antenna Systems Modeled

| SYSTEM | DIRECTIONAL ANTENNA | OMNIDIRECTIONAL ANTENNA |
|---|---|---|
| 6 | FA-8043 | FA-8044 |
| 7 | Hazeltine Open Array | Hazeltine Omni |
| 8 | TI Separate Rotator | TI Separate Rotator Omni |
| 9 | Westinghouse Separate Rotator | Westinghouse Separate Rotator Omni |
| 10 | Ideal (FA-8043 azimuth, ideal elevation) | Ideal (FA-8044 azimuth, ideal elevation) |

Chapter 2 with the exception of System 10, which is discussed in Appendix C. System 10, a so-called ideal antenna system, has the azimuth patterns of the FA-8043 and FA-8044, but "ideal" elevation patterns with no attenuation above the horizon and 36 dB of attenuation below the horizon. Such a pattern affords an evaluation of an ultimate system that could not be tested in the real world.

In addition to the differences in the antenna radiation patterns for each of these systems, there are several other differences in their characteristics that were taken into account in parametric inputs to the models. These characteristics are shown in Table 6.7.

Table 6.7 Terminal Antenna System Characteristics

| PARAMETER | SYSTEM 6 | 7 | 8 | 9 | 10 |
|---|---|---|---|---|---|
| Directional antenna: | | | | | |
| height above ground (ft) | 31.5 | 33 | 26 | 26 | 31.5 |
| line loss (dB) | 3 | 3 | 6 | 6 | 3 |
| gain (dB) | 23 | 23 | 25 | 23 | 23 |
| Omnidirectional antenna: | | | | | |
| height above ground (ft) | 33 | 37 | 35 | 34 | 33 |
| line loss (dB) | 3 | 3 | 6 | 6 | 3 |
| gain (dB) | 4 | 5 | 5 | 5 | 4 |

Contours showing coverage nulls due to vertical lobing, analogous to the curves explained in Figure 3.1, and those depicting false suppression in the main beam, analogous to Figure 3.2, appear on the following pages for the first four terminal systems as produced by the simple flat-earth model. Figures 6.31 through 6.34 are coverage curves for Systems 6 through 9, respectively; Figures 6.35 through 6.38 are false suppression contours for Systems 6 through 9, respectively. The areas under these curves as determined by the simple model are contained in Table 6.8 according to the various types of performance criterion which

Table 6.8 Terminal Antenna System Performance, Simple Model

| CRITERION (areas in $nm^2$) | SYSTEM 6 | 7 | 8 | 9 |
|---|---|---|---|---|
| Uncovered uplink | 11.1 | 7.1 | 3.4 | 5.7 |
| False suppression | 25.6 | 13.0 | 0.2 | 3.8 |
| Uncovered downlink | 0.9 | 0.4 | 0.5 | 0.8 |
| Over-interrogation | 1152.5 | 1141.2 | 1159.6 | 1116.1 |
| Interference susceptibility | 1244.6 | 1252.2 | 1245.7 | 1241.1 |

they influence. In Figure 6.31, the uplink nulls are always deeper than the downlink nulls, of which only two fall inside the area of desired coverage. Vertical lobing has been reduced for

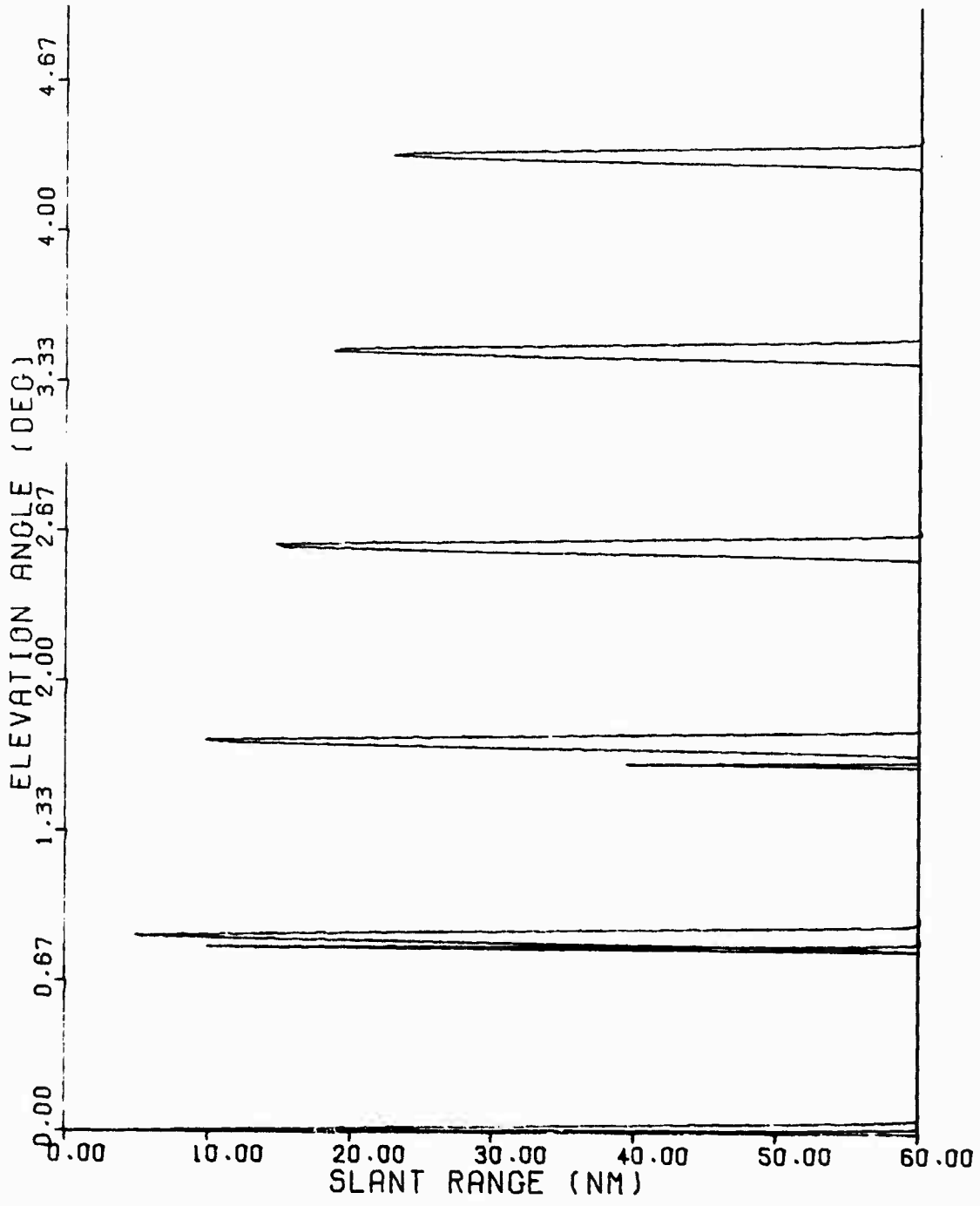


Figure 6.31 Vertical Lobing Contours, System 6

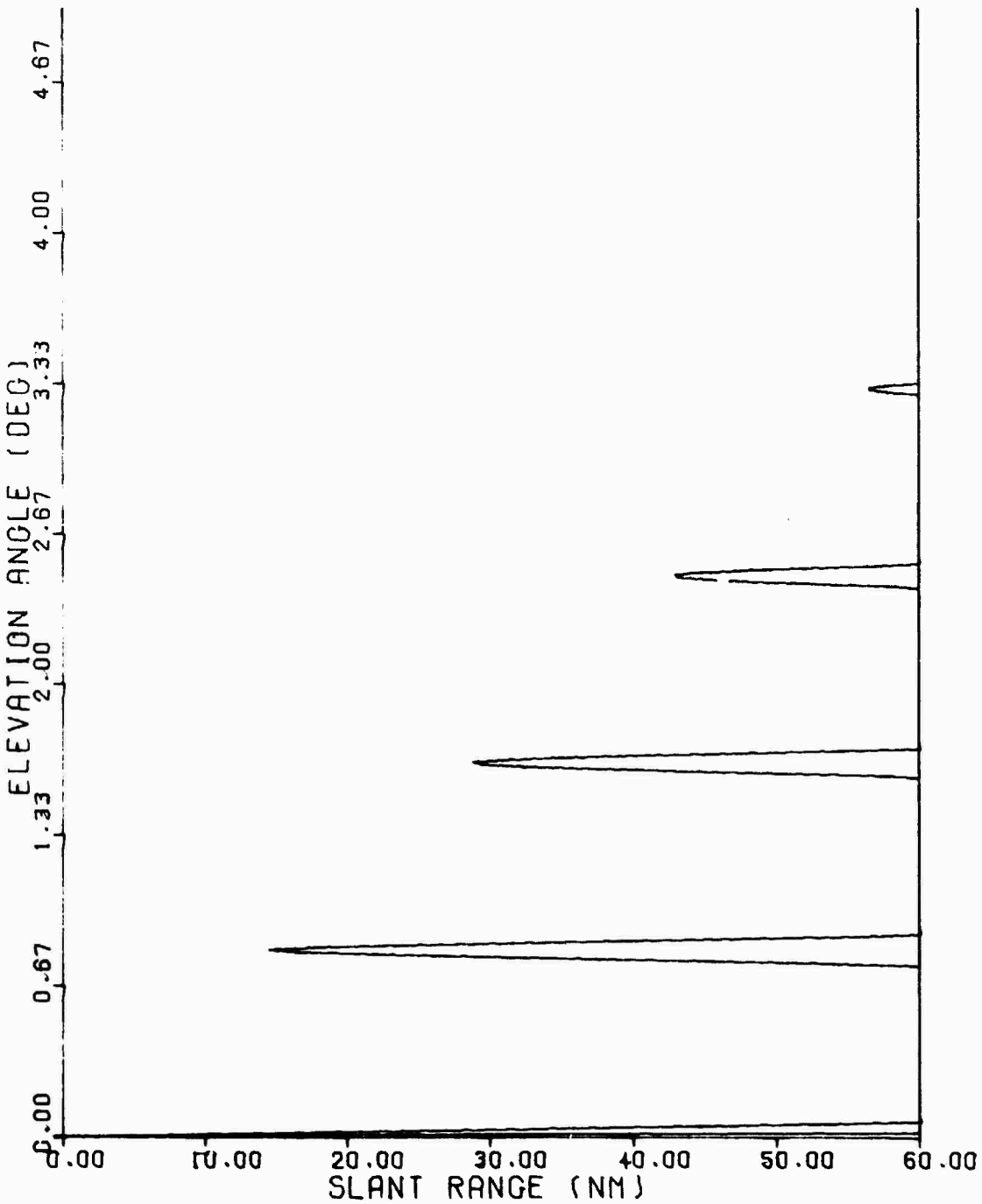


Figure 6.32 Vertical Lobing Contours, System 7

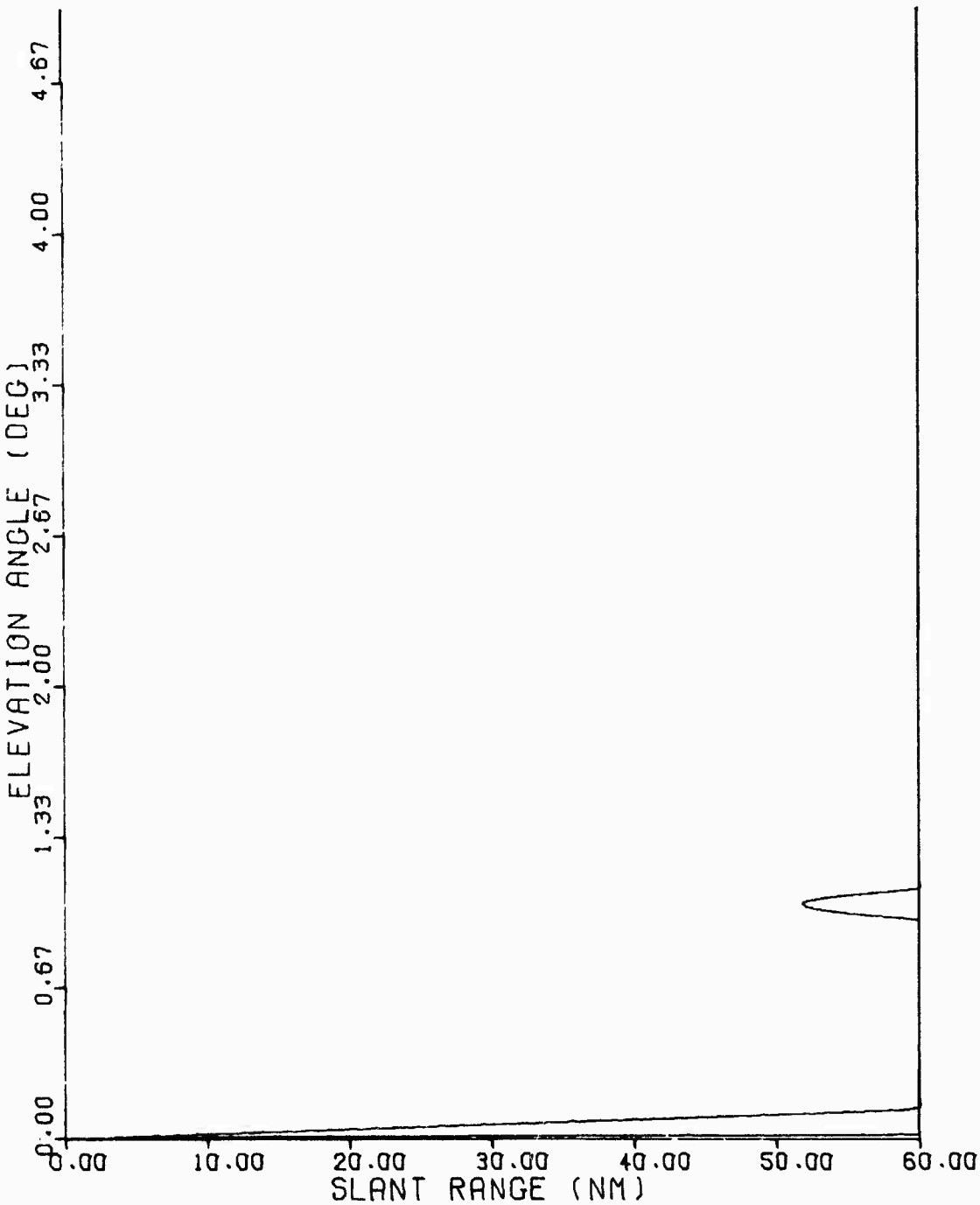


Figure 6.33 Vertical Lobing Contours, System 8

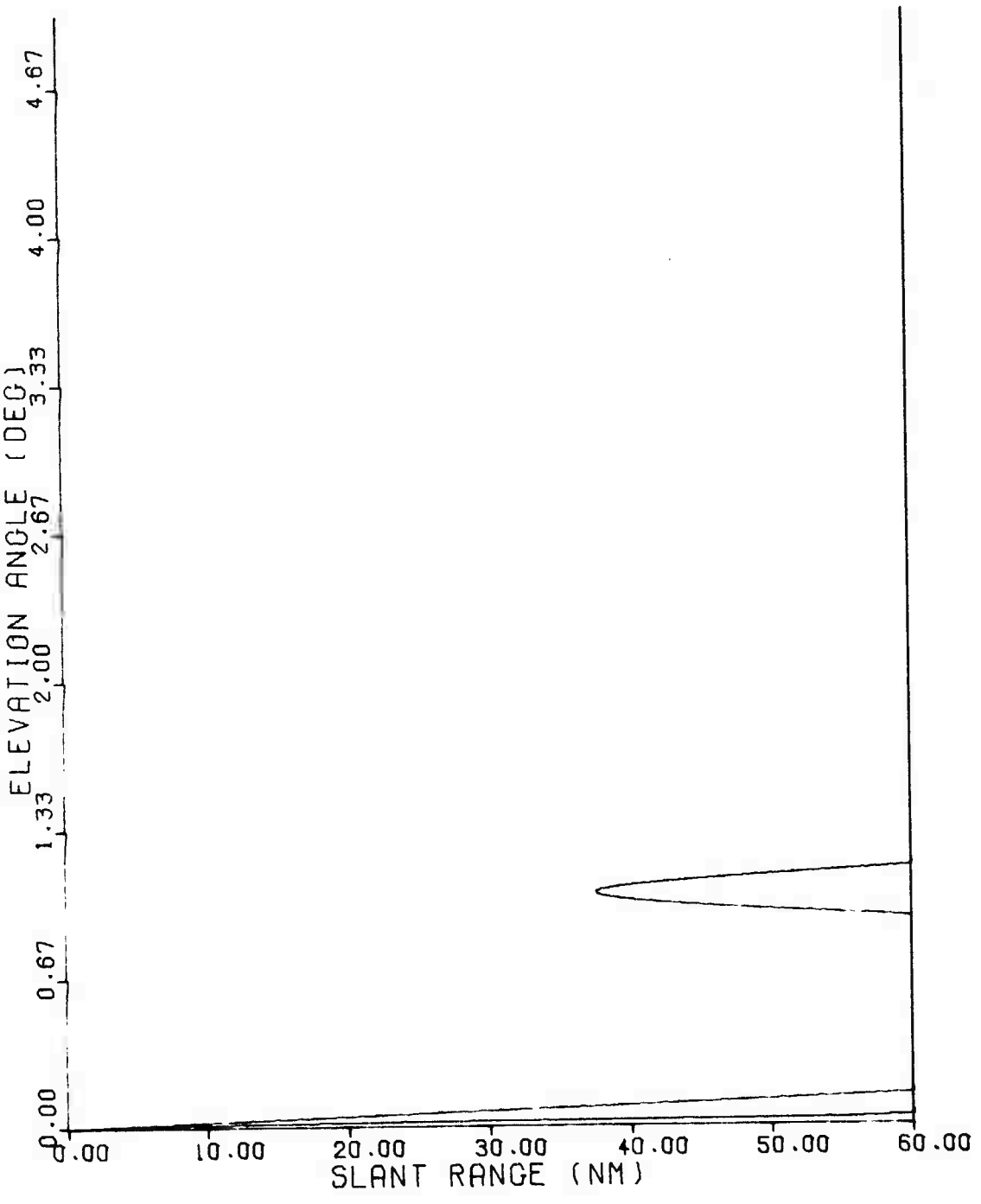


Figure 6.34 Vertical Lobing Contours, System 9

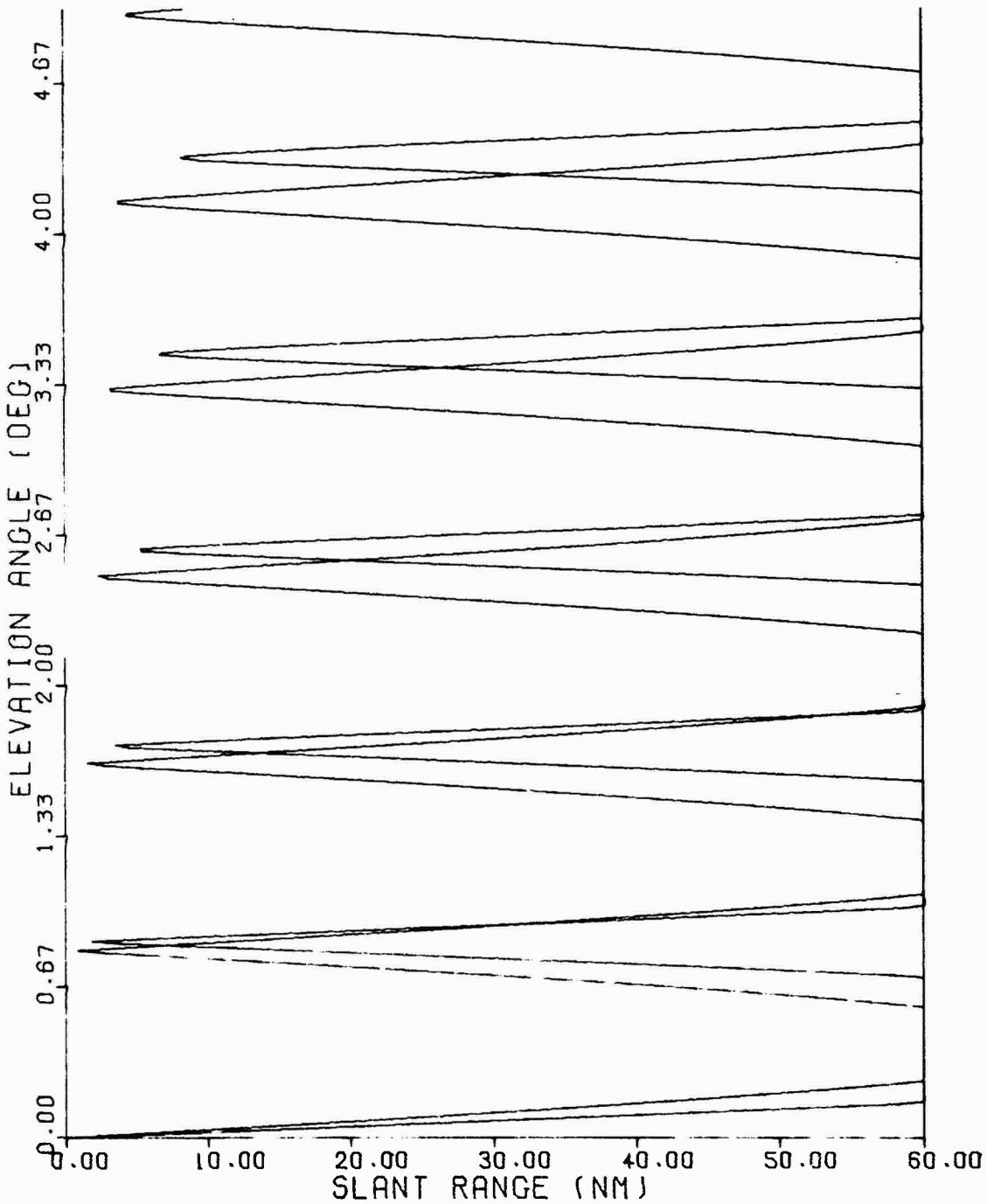


Figure 6.35 False Suppression Contours, System 6

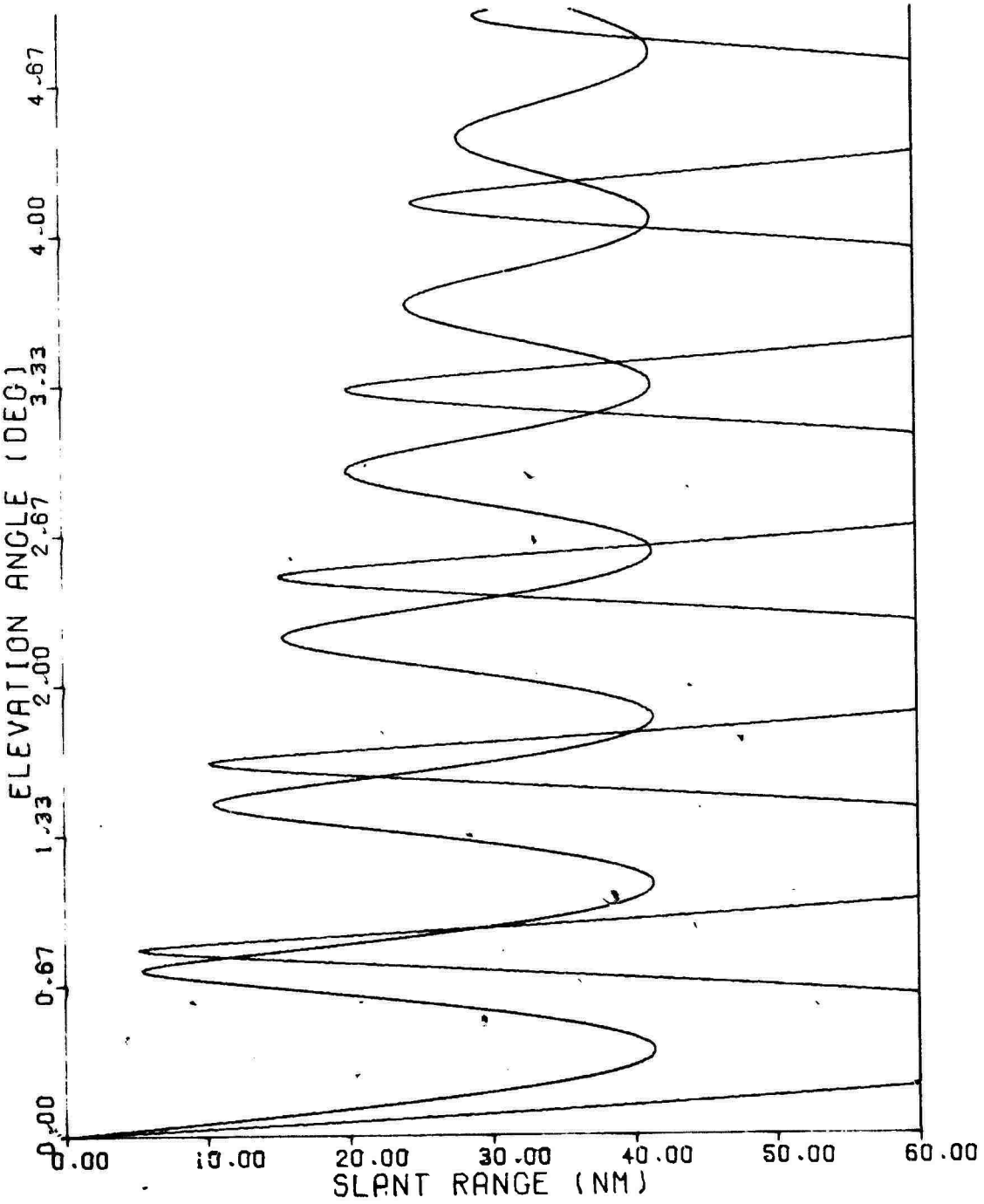


Figure 6.36 False Suppression Contours, System 7

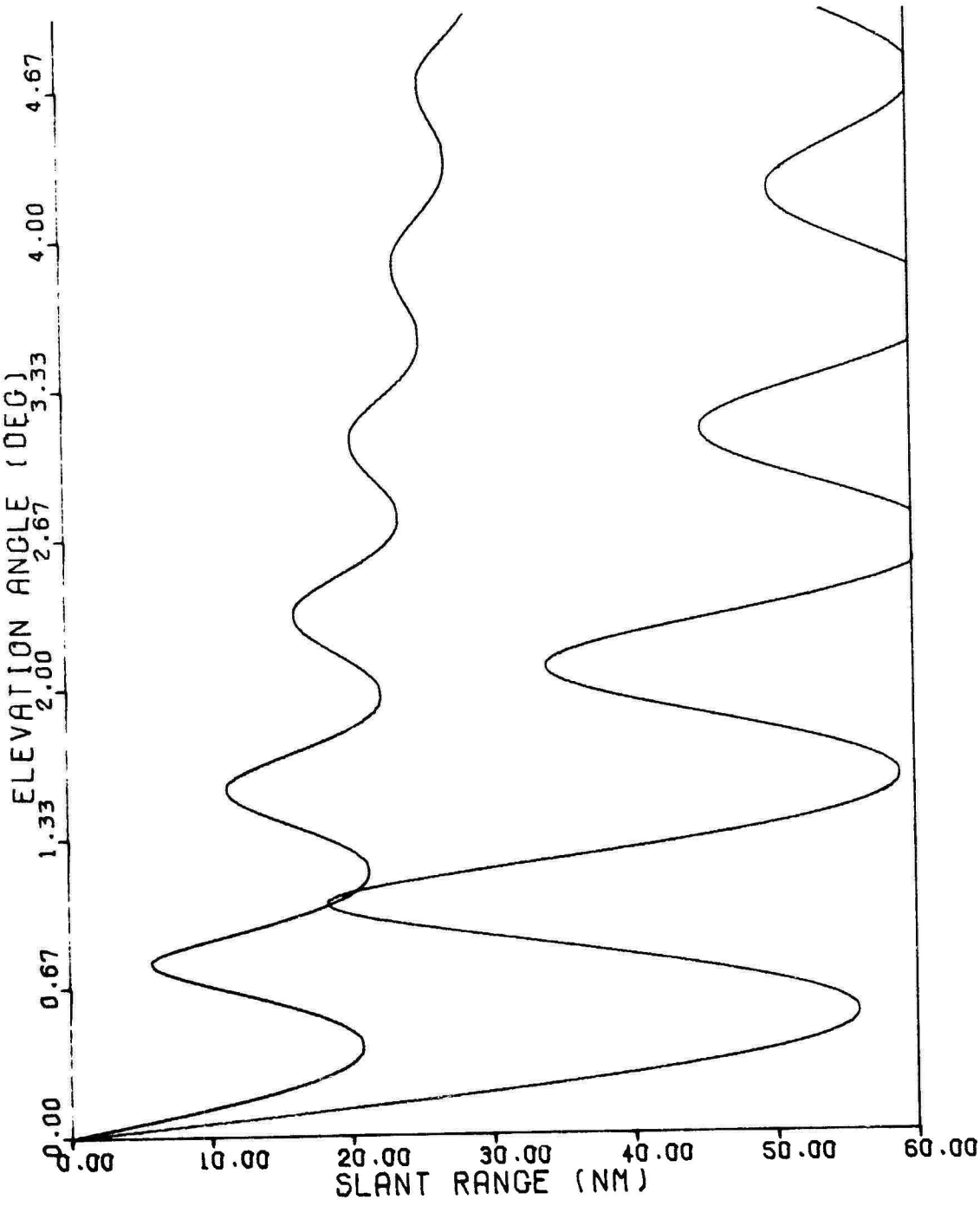


Figure 6.37 False Suppression Contours, System 8

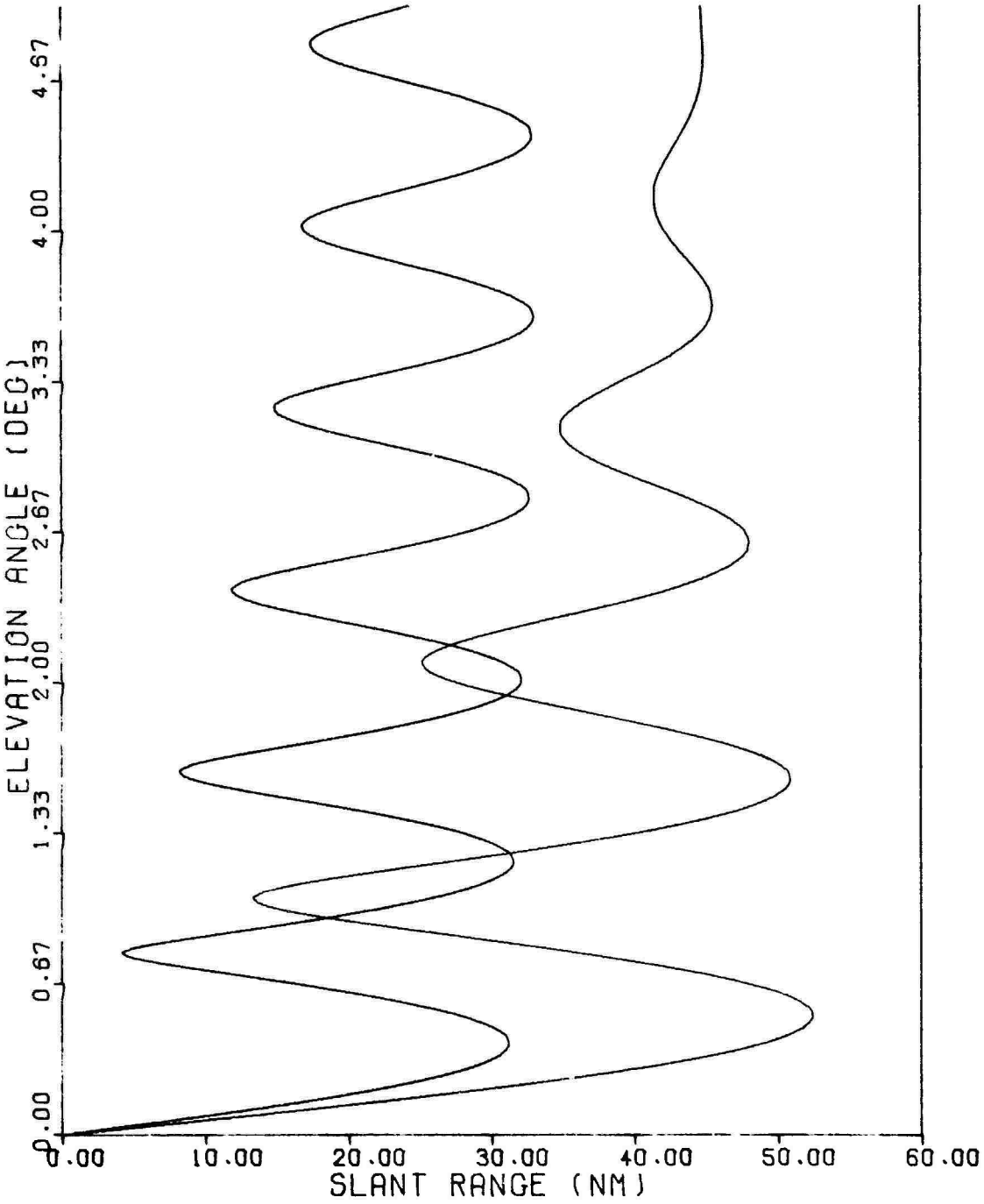


Figure 6.38 False Suppression Contours, System 9

the three new antennas with larger vertical apertures to the point at which no downlink nulls fall into the area of desired coverage. In Figure 6.35, the omni antenna contour is the one whose null is the lower in each pair of nulls. The lower peaks in Figures 6.36 through 6.38 are those of the omni antenna contours also.

The total area in a "slice" of vertical coverage 40,000-ft high out to a range of 60 nm is 157 sq nm (up to $5^{o}$ elevation). Of this amount, then, the simple model says that 11 sq nm of airspace are not covered when the present system is in use under the given conditions. The three new antennas of Systems 7, 8, and 9 reduce this uncovered airspace as one might expect in relation to the sharpness of their underside pattern slopes.

As in the en route configuration, the new antennas show an even more significant reduction in the area of false suppression within the main beam. The uncovered downlink area is, as before, not a serious problem.

Both the over-interrogation and interference susceptibility regions are nearly equal, regardless of the antenna system used. As in the en route examples presented in the previous section, nearly all of the area between the desired coverage area and the spherical-earth-horizon barrier is covered by the main beam, both uplink and downlink, to ensure coverage at the desired range. Thus, the terminal case supports further the hypothesis that control of interrogation range and reception range for reduction of interference is difficult to implement.

Figures 6.39 through 6.43 show simulated displays produced by the complex model for 60-nm flights at 2000 ft using Systems 6 through 10, respectively. Similarly, Figures 6.2, 6.7, and 6.44 through 6.46 show the result of simulated flights at 5000 ft for the five standard terminal systems, while Figures 6.47 through 6.51 depict flights at 10,000 ft using Systems 6 through 10, respectively. Range rings for all terminal configuration flights are spaced 10 nm apart and accentuated every 30 nm.

At approximately 52 nm, the grazing angle is below the minimum grazing angle described in Section 5.6 for the series of 2000-ft flights. Thus, the information outside 52 nm should be disregarded in Figures 6.39 through 6.43. This is an academic point, since aircraft at 2000 ft would not normally be under the control of a terminal site whose interrogator was more than 52 nm away. The ideal pattern of Figure 6.43 shows precisely where the range corresponding to $0^{o}$ elevation lies, as the aircraft drops instantly from the display as it passes below the local horizontal plane of the interrogator. Just as the simple model indicated progressively better performance by the antennas with larger vertical apertures, the displays of simulated 2000-ft flights show the same correlation. The FA-8043 and Hazeltine antennas some holes in coverage, while the TI and Westinghouse antennas manage to close the gaps inside 50 nm. Quantitative data is presented in the tables that follow.

The sequence of 5000-ft flights is similar. The FA-8043 and

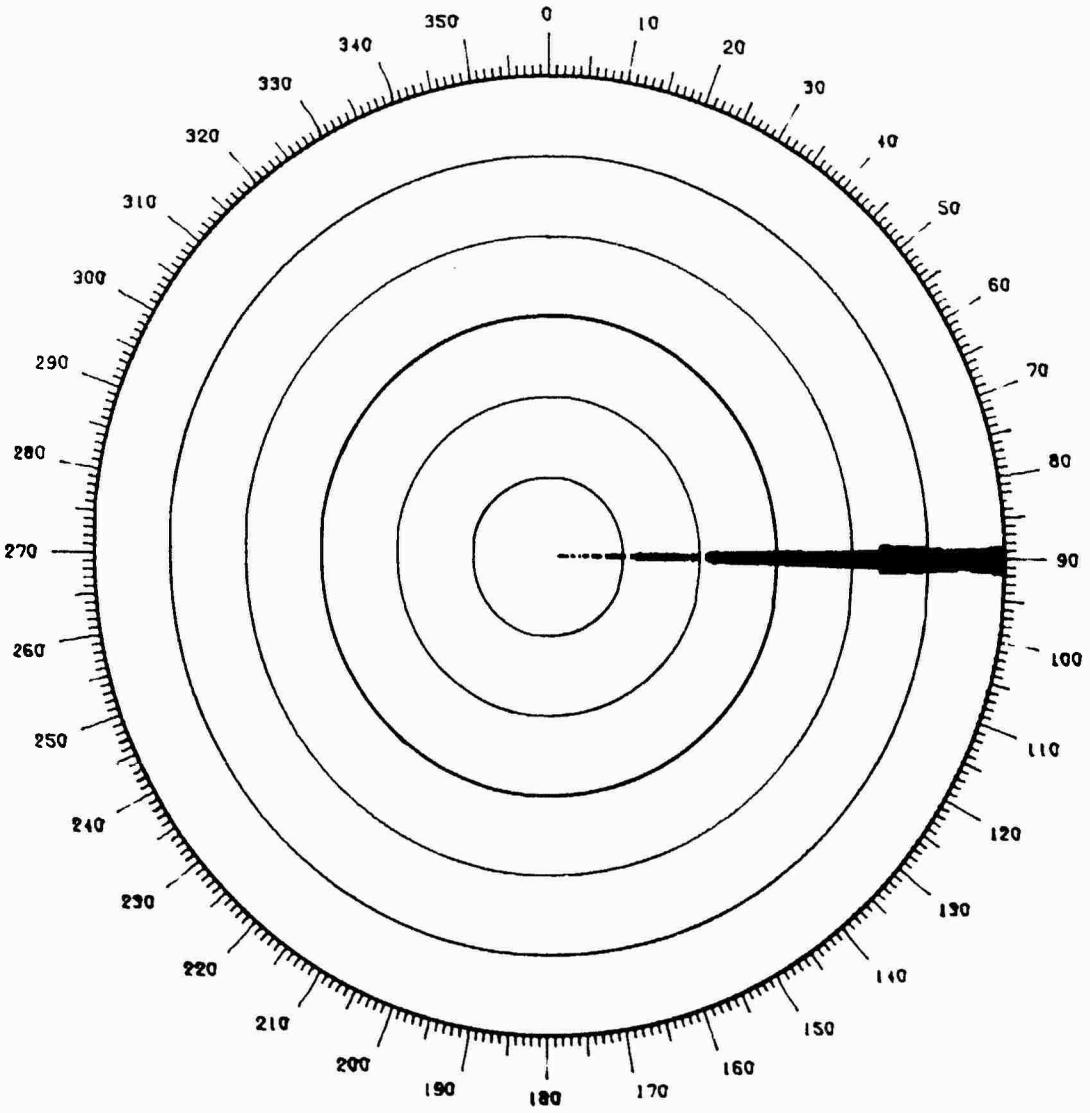


Figure 6.39 Simulated Flight at 2000 Ft, System 6

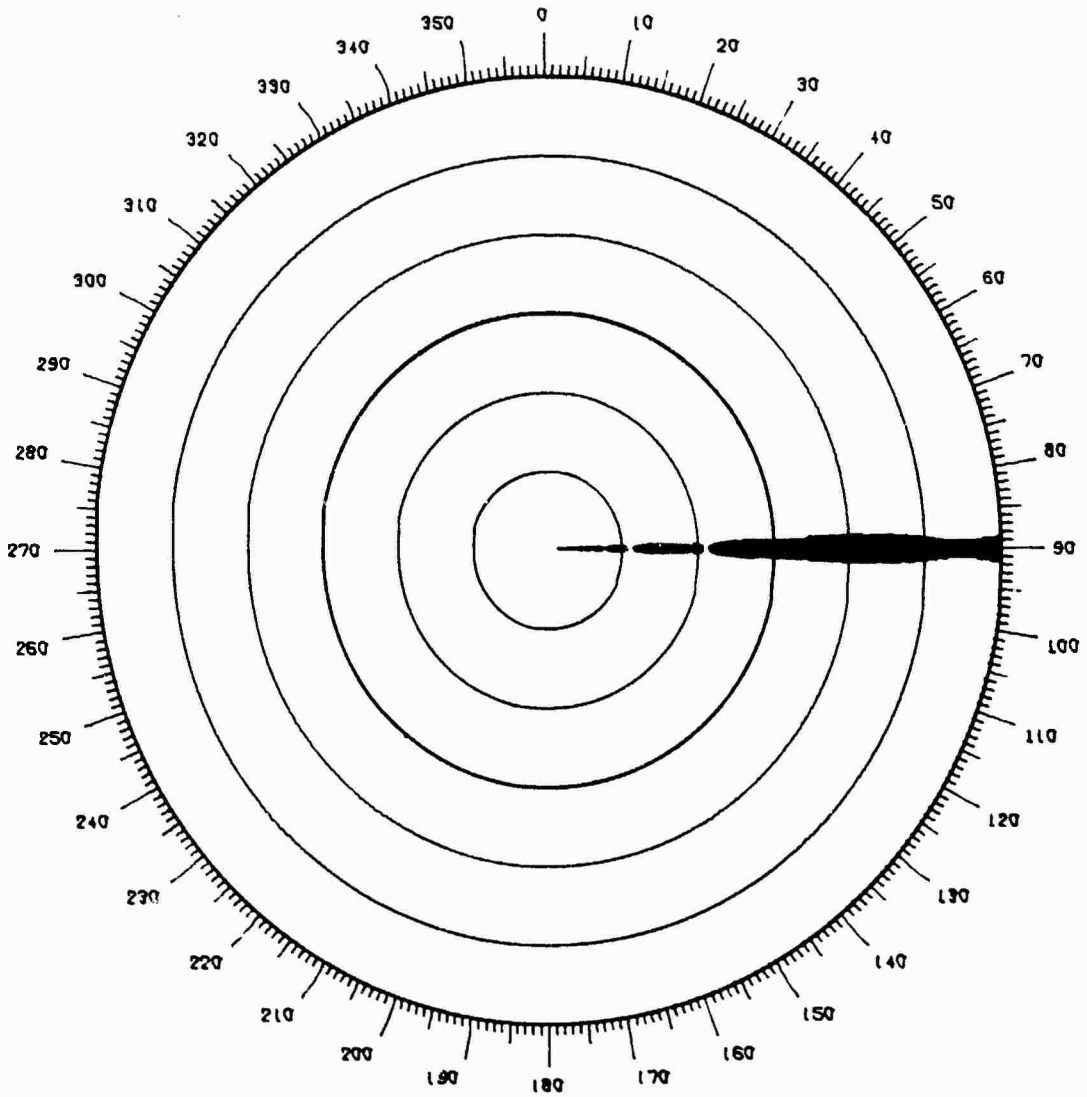


Figure 6.40 Simulated Flight at 2000 Ft, System 7

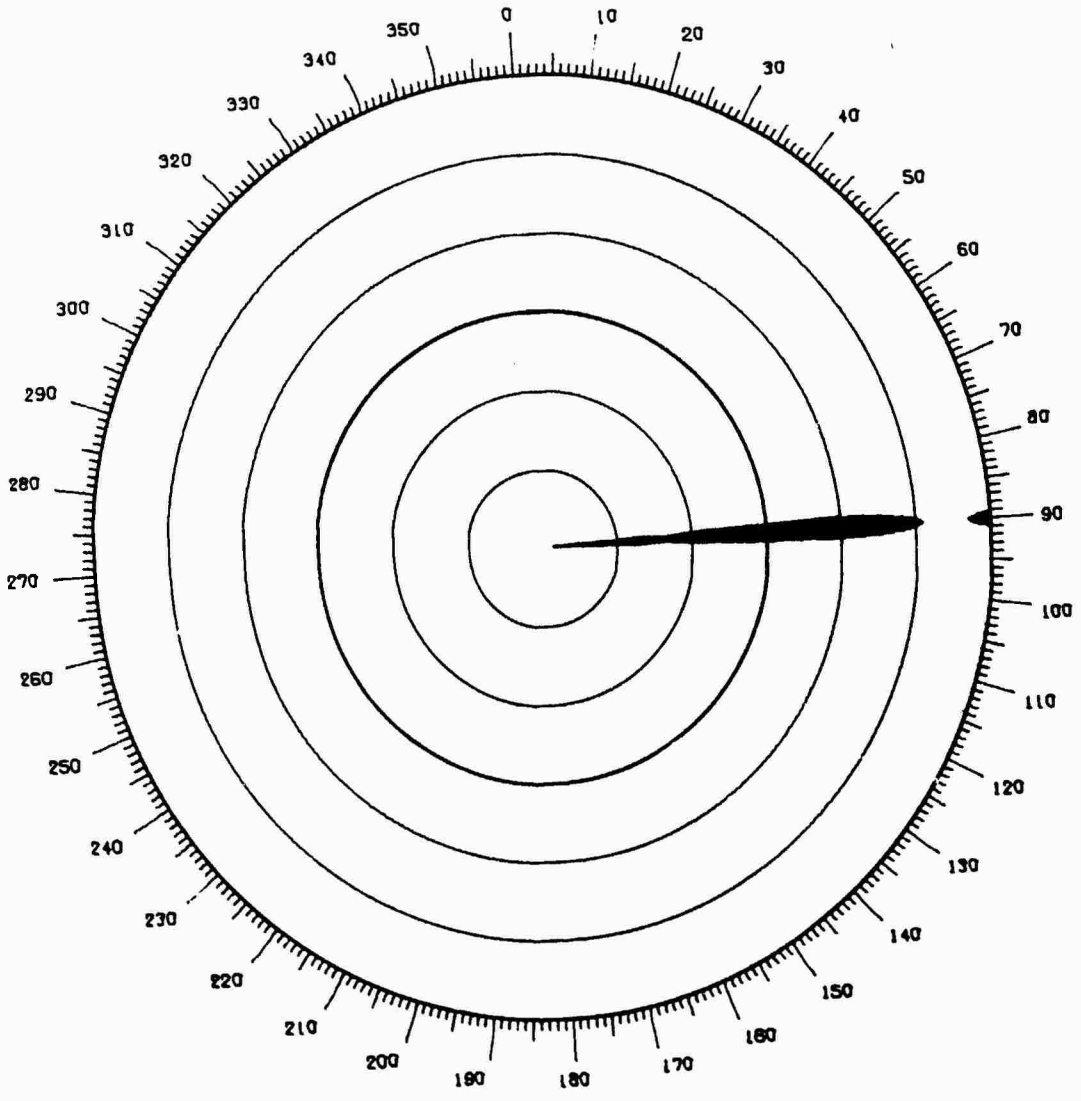


Figure 6.41 Simulated Flight at 2000 Ft, System 8

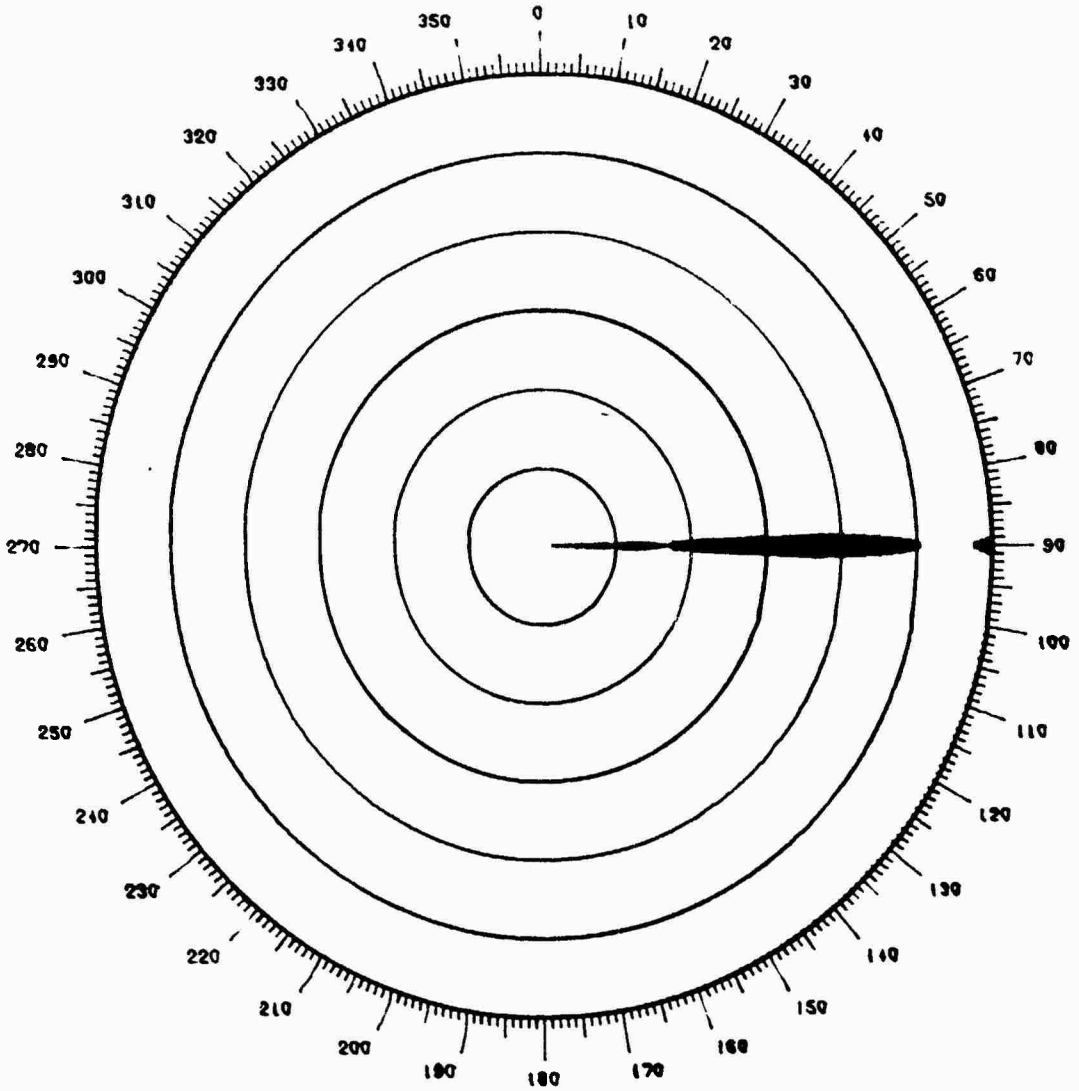


Figure 6.42 Simulated Flight at 2000 Ft, System 9

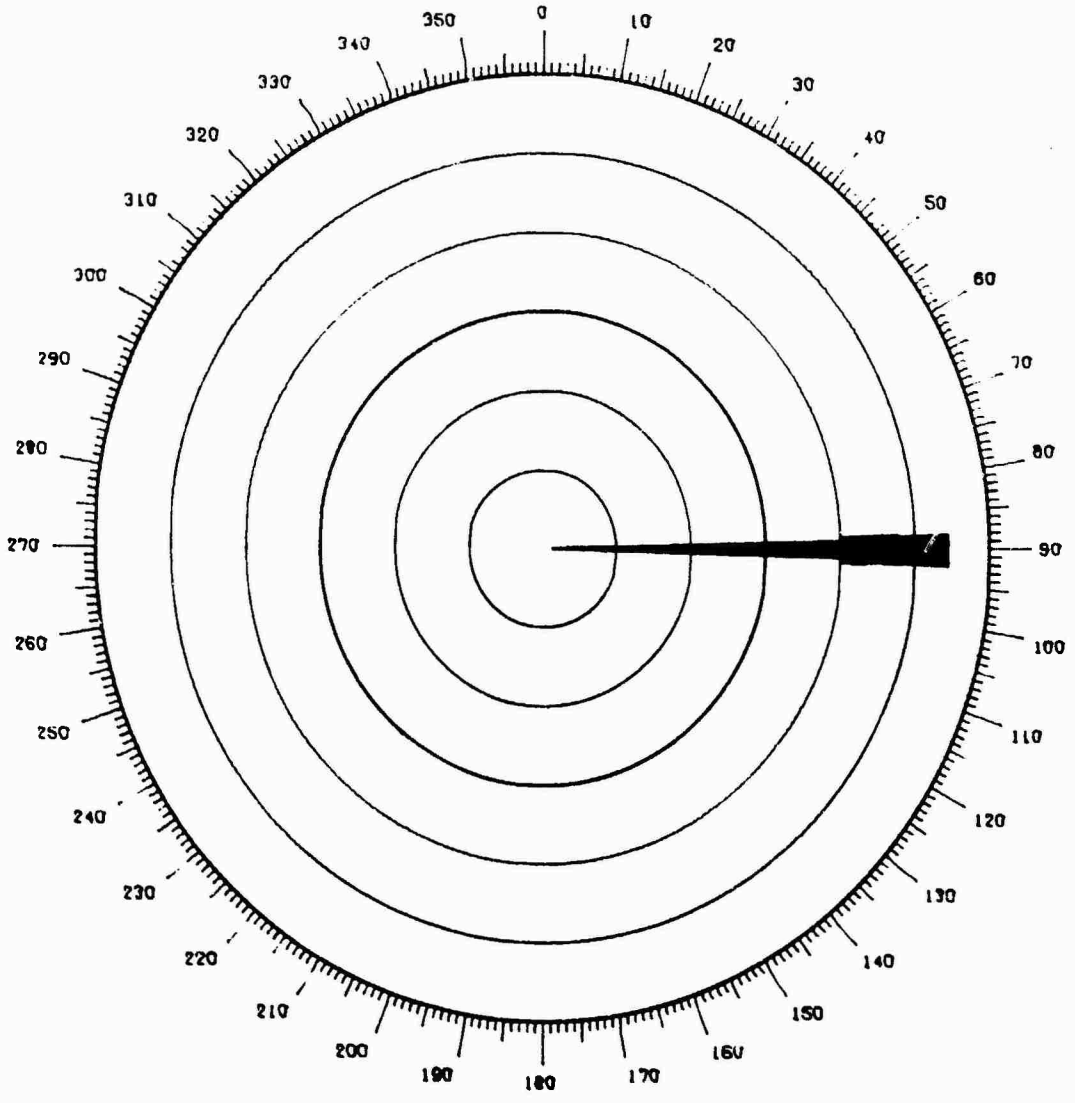


Figure 6.43 Simulated Flight at 2000 Ft, System 10

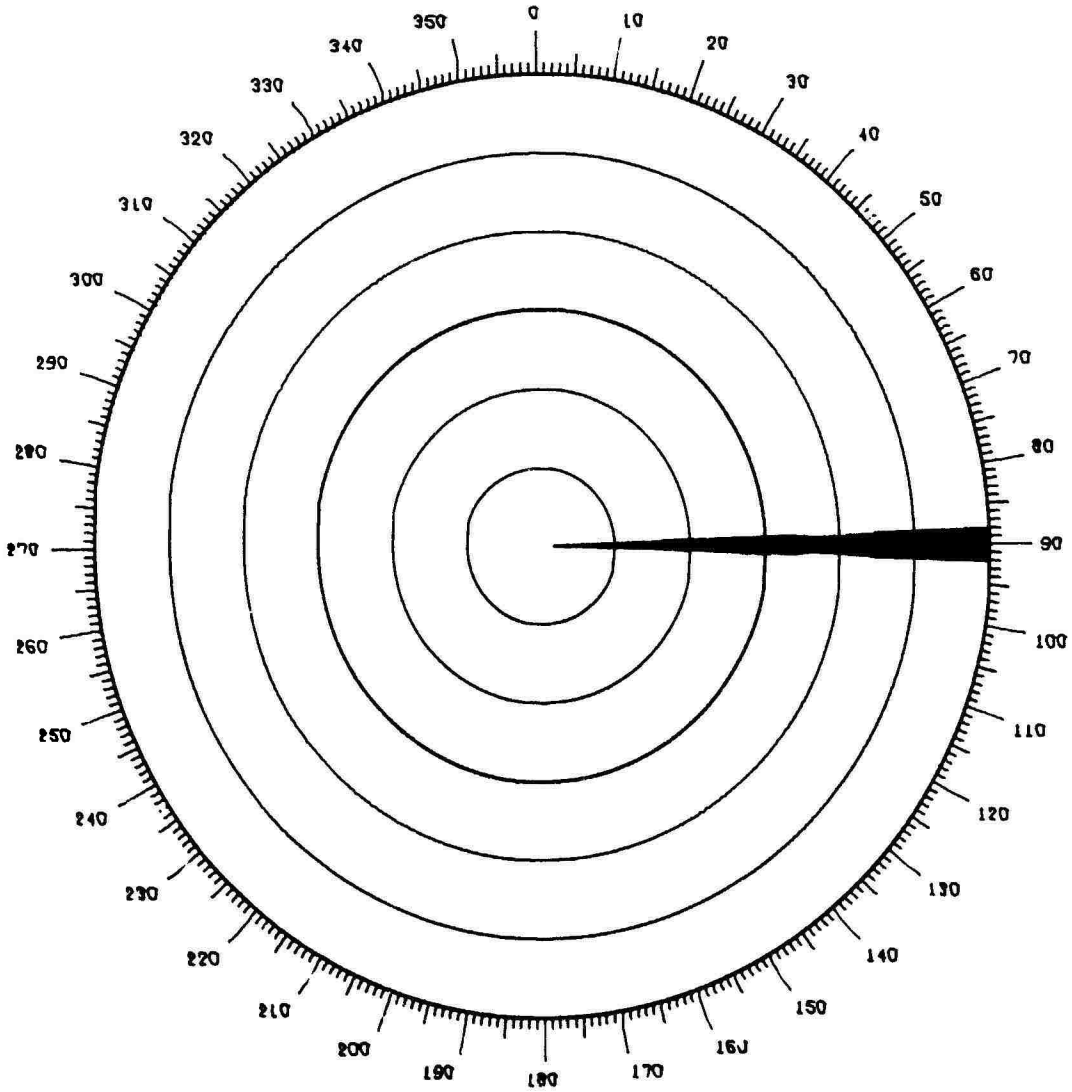


Figure 6.44 Simulated Flight at 5000 Ft, System 8

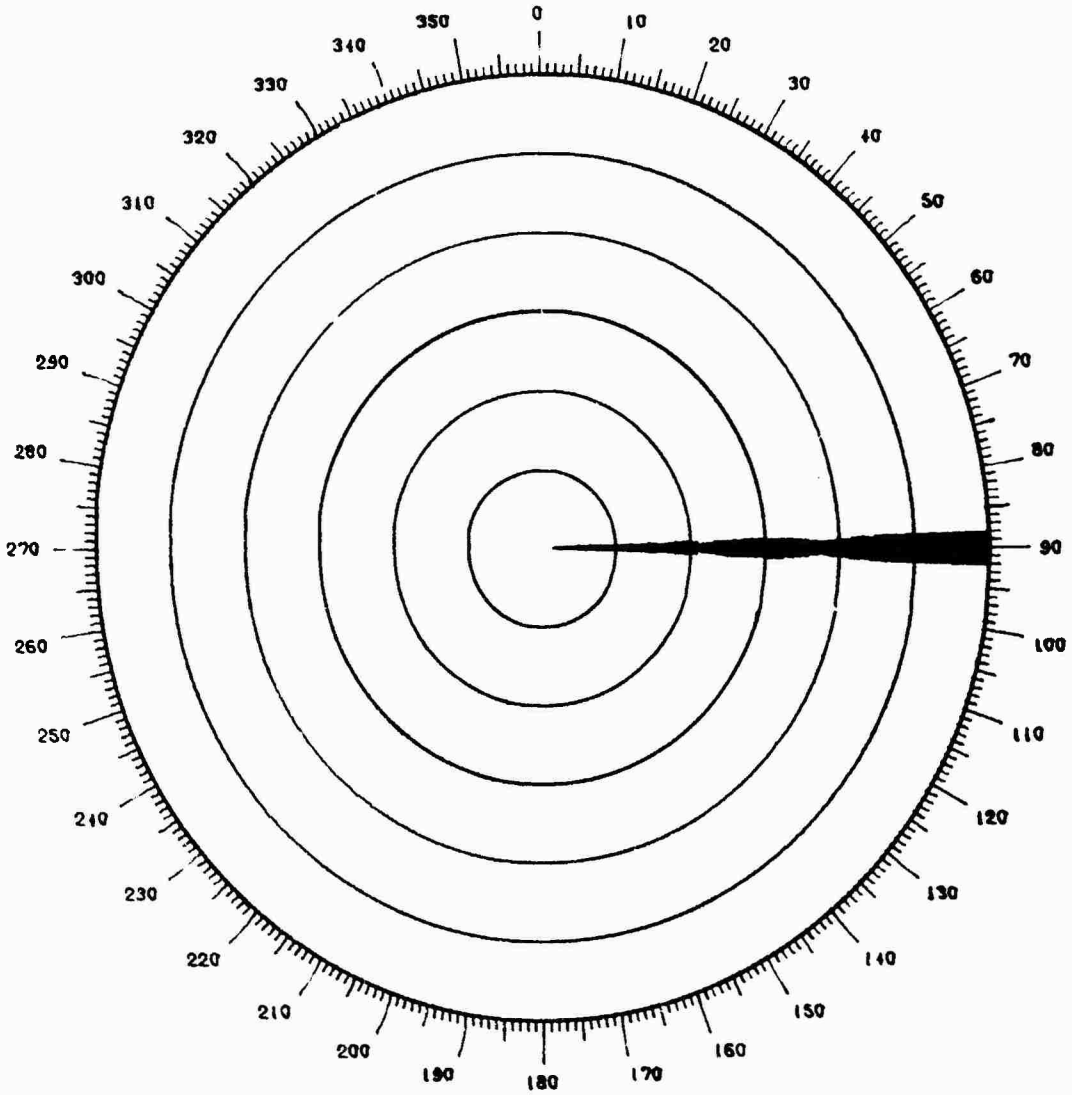


Figure 6.45 Simulated Flight at 5000 Ft, System 9

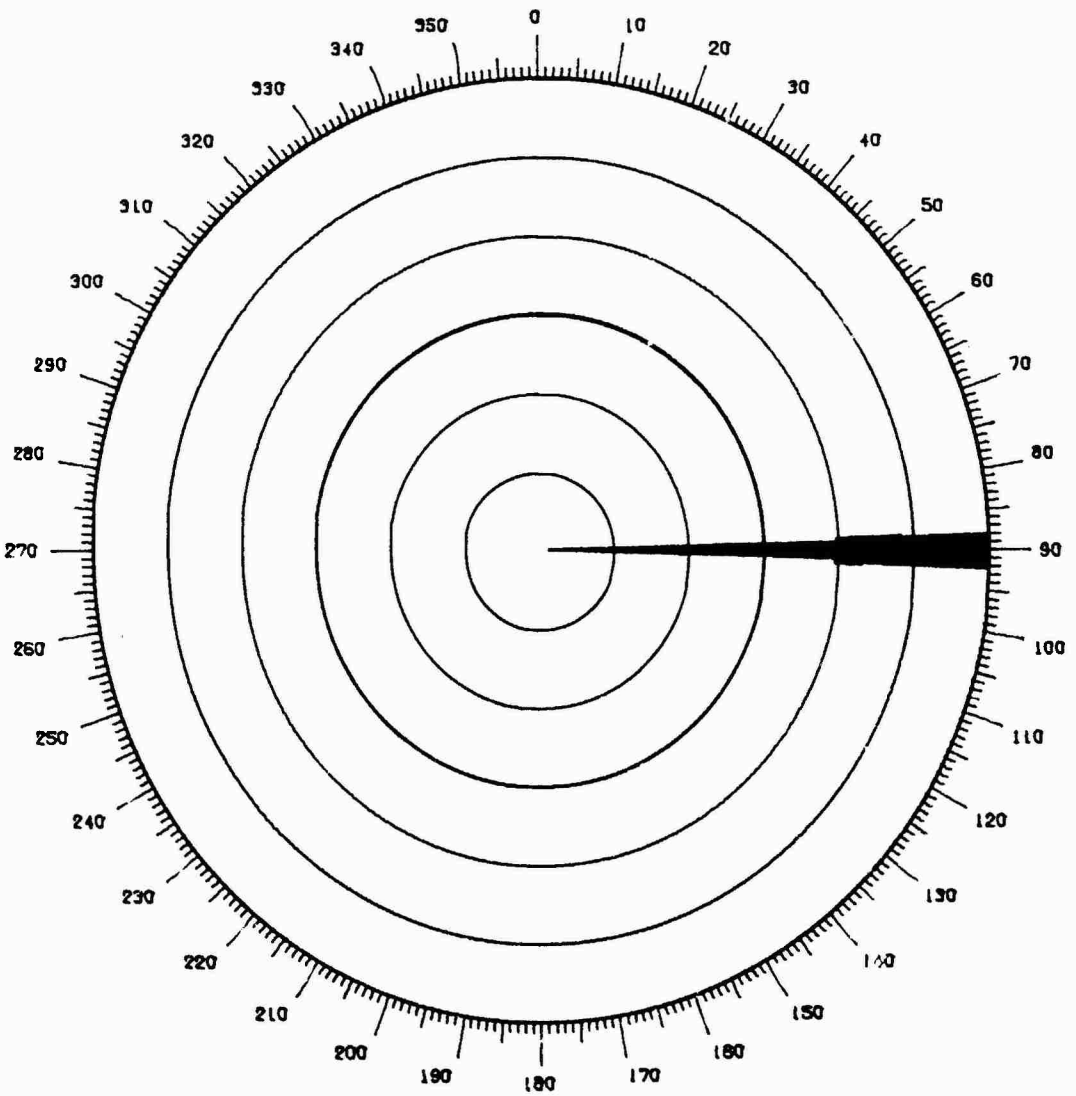


Figure 6.46 Simulated Flight at 5000 Ft, System 10

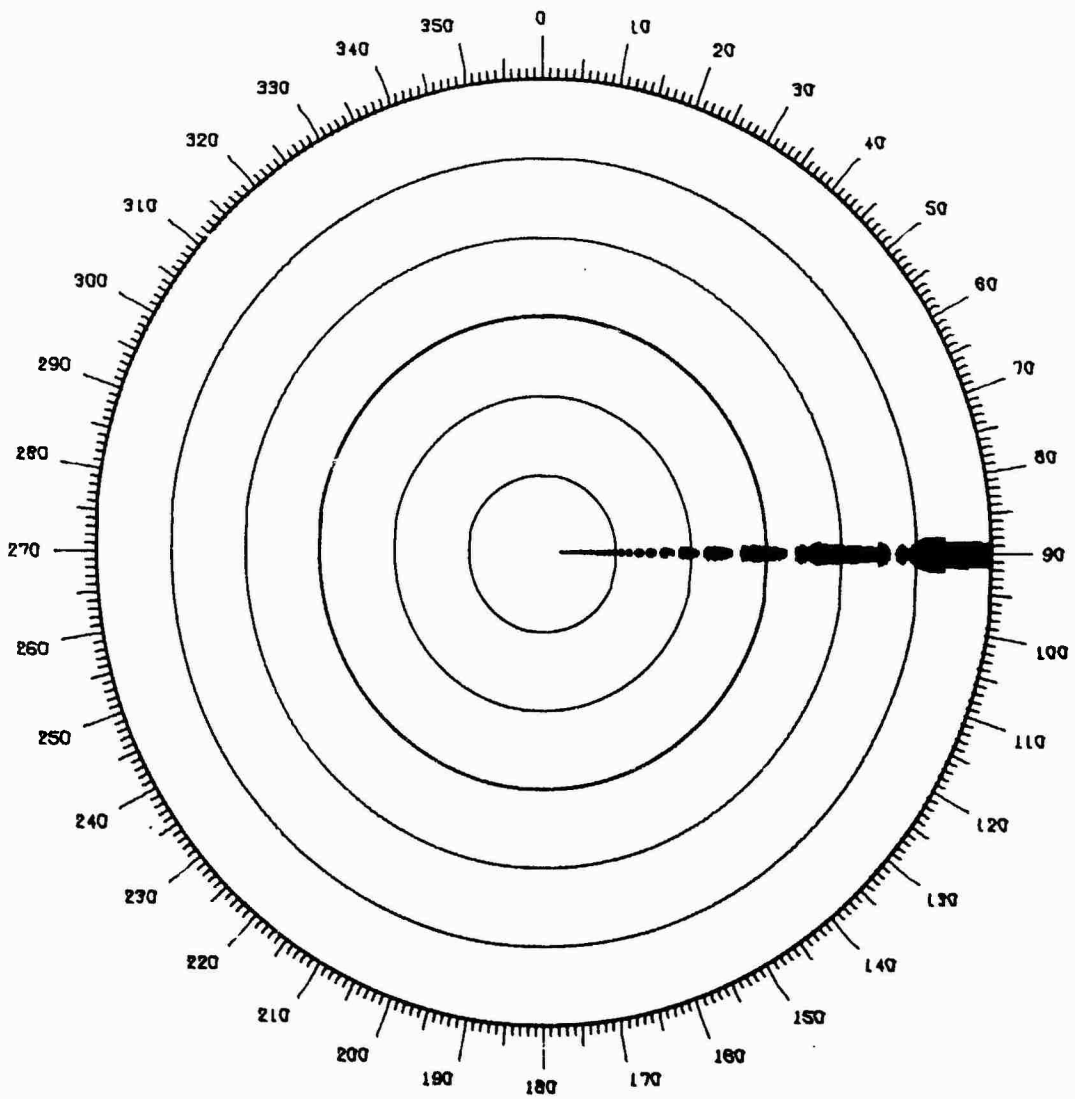


Figure 6.47 Simulated Flight at 10,000 Ft, System 6

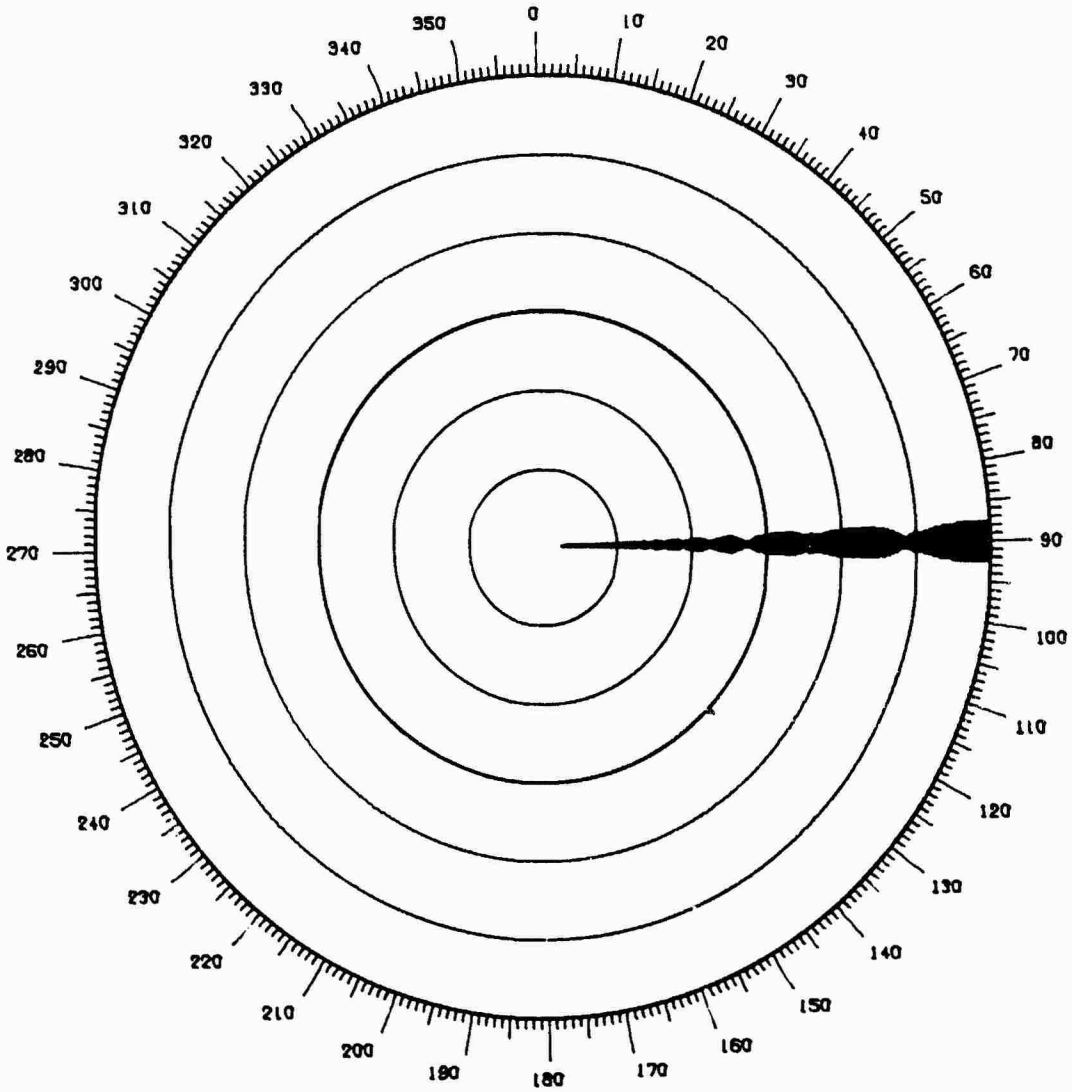


Figure 6.48 Simulated Flight at 10,000 Ft, System 7

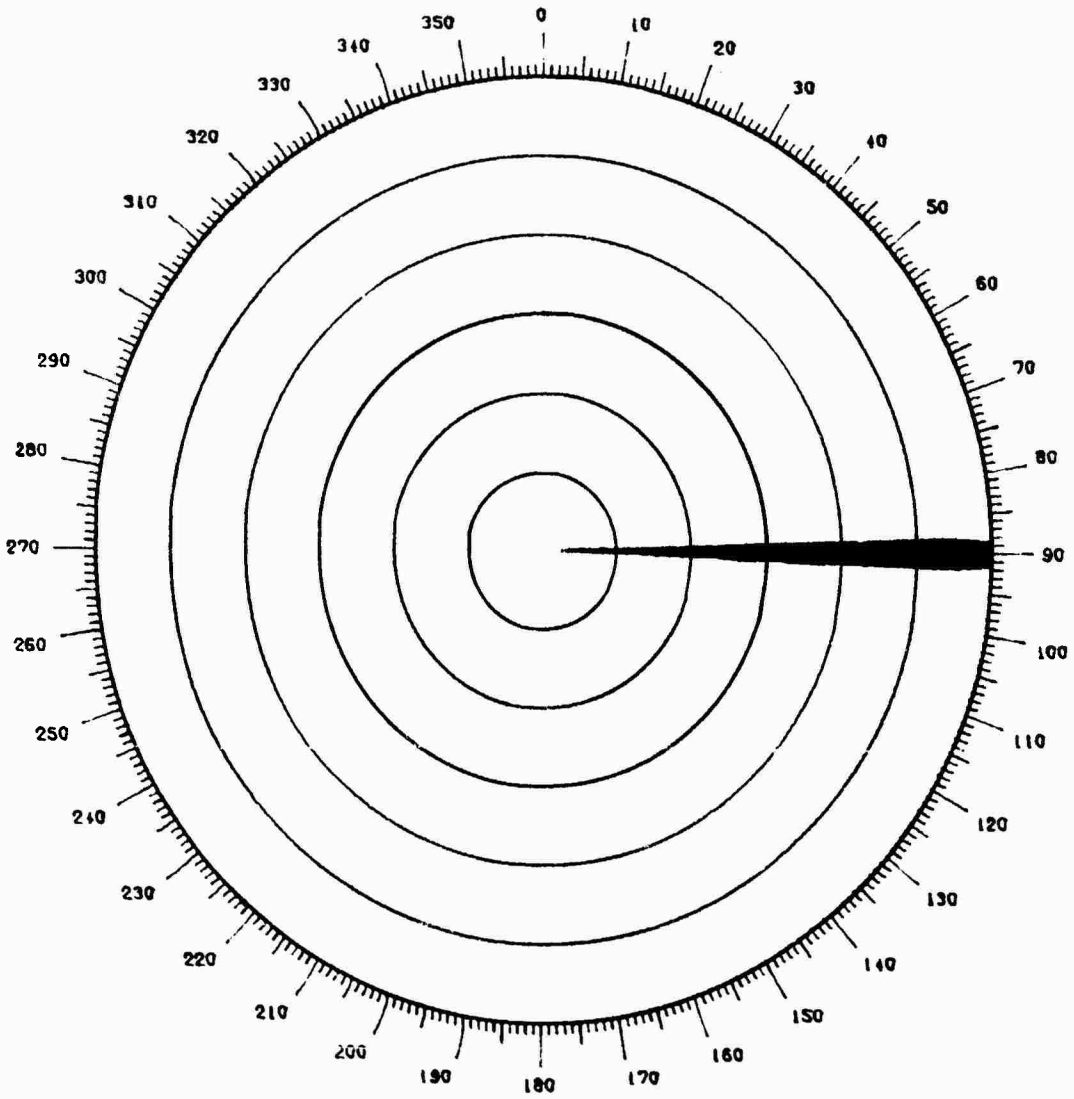


Figure 6.49 Simulated Flight at 10,000 Ft, System 8

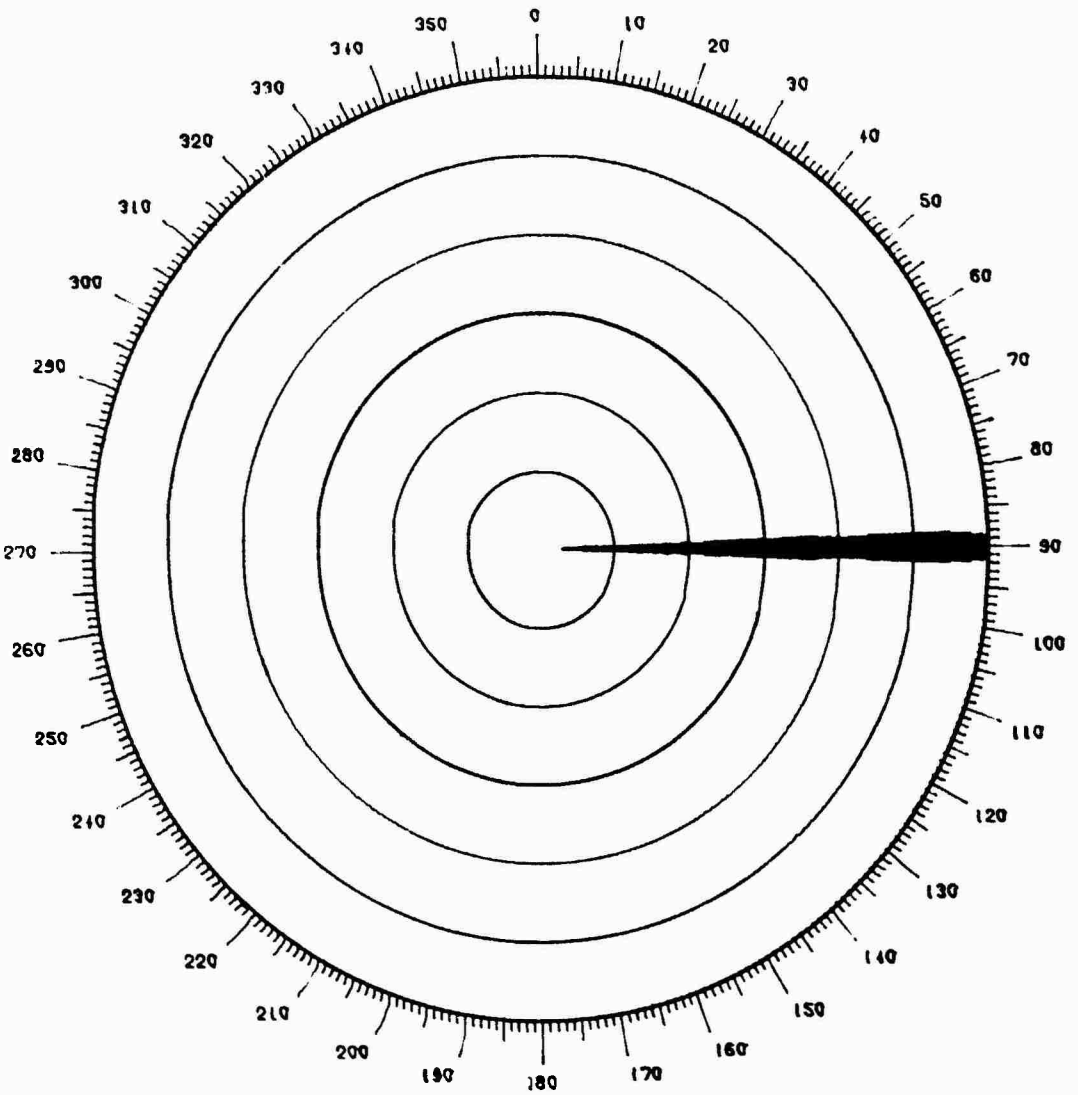


Figure 6.50 Simulated Flight at 10,000 Ft, System 9

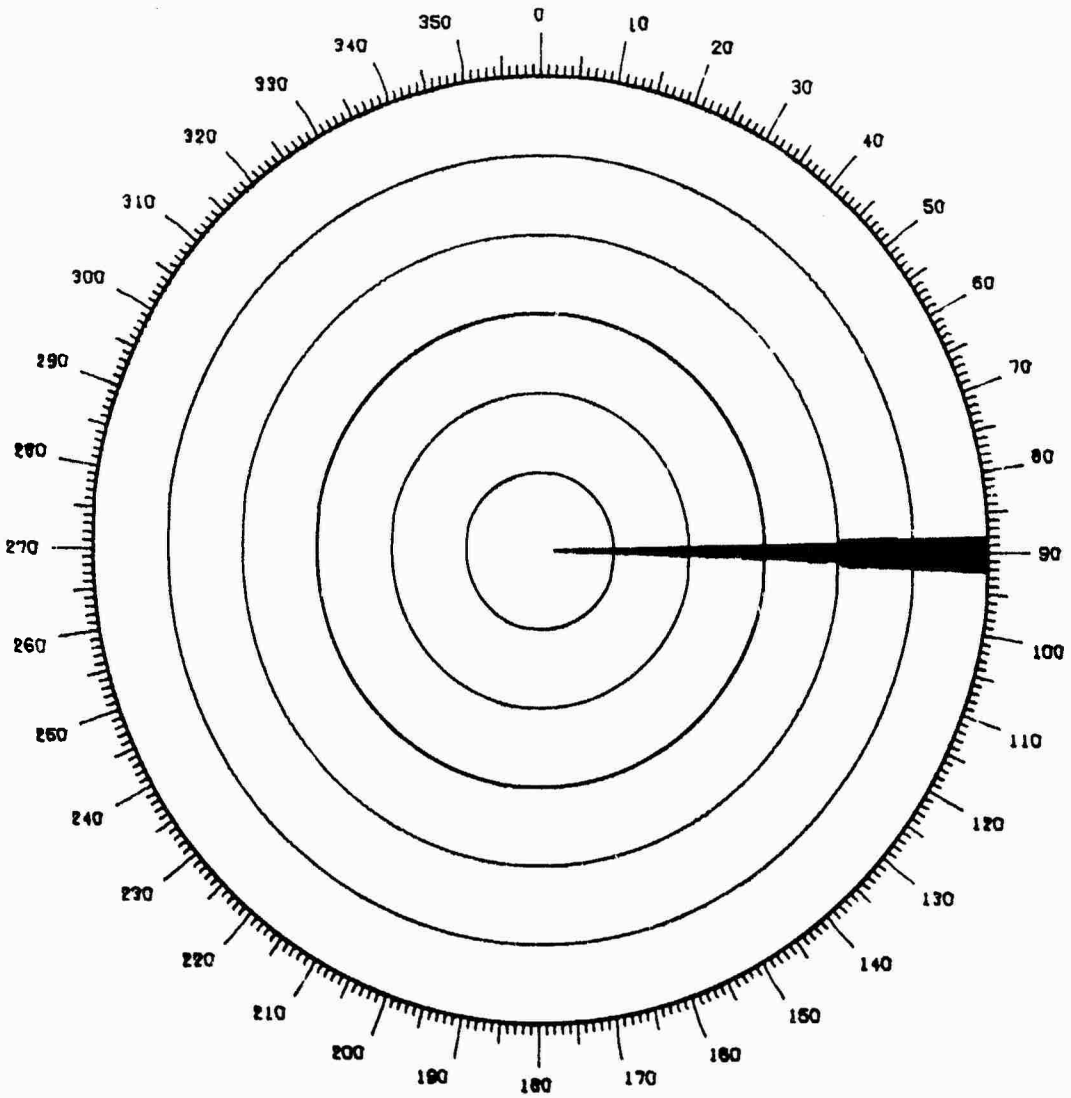


Figure 6.51 Simulated Flight at 10,000 Ft, System 10

Hazeltine antennas still show holes in coverage, while the TI and Westinghouse antennas, and, of course, the ideal antenna, show rather solid coverage all the way in.

At 10,000 ft, even the Hazeltine antenna system results in a closing of the coverage holes, although performance of the FA-8043 is still relatively poor. The TI and Westinghouse antennas yield even better coverage than at 5000 ft, with the former's performance practically indiscernible from that of the ideal antenna. The sudden decrease in target width for tests of the ideal antenna at about 40 nm is due to the acquisition of the omnidirectional signal at that range by the aircraft transponder. This sudden suppression of the outer interrogations narrows the target.

Tables 6.9 through 6.11 summarize the performance criteria tabulated in the execution of the complex model for the 2000-ft, 5000-ft, and 10,000-ft flights, respectively. There are 266 scans of the terminal ATCRBS in each flight of the 2000-ft series, and 268 scans in each of the higher-altitude series. Explanations of the various performance criteria produced by the complex model were given in Section 6.4.

The results given in Table 6.9 are somewhat distorted by the fact that they include the information beyond 52 nm which is past the lower limit of the grazing angle. Thus, Systems 8, 9, and even the ideal 10 contain one large hole according to the data. This factor also accounts for the relatively short target length and the large deviation from the average length. It should also

Table 6.9 Terminal Antenna System Performance, Complex Model, 2000-Ft Flight

| CRITERION | SYSTEM 6 | 7 | 8 | 9 | 10 |
|---|---|---|---|---|---|
| Number of holes | 9 | 3 | 1 | 2 | 1 |
| Most consecutive scans with fewer than 7 hits | 3 | 4 | 38 | 39 | 25 |
| Total scans with fewer than 7 hits | 13 | 8 | 38 | 43 | 25 |
| Total scans with no hits | 10 | 4 | 27 | 31 | 25 |
| Average replies per scan | 14.4 | 17.7 | 14.5 | 14.4 | 15.1 |
| Standard deviation of replies per scan | 3.9 | 4.9 | 6.3 | 6.8 | 5.5 |
| Total single $P_2$ pulses | 704 | 1064 | 752 | 336 | 1550 |
| Total number of suppressions | 6104 | 2750 | 1803 | 2161 | 5052 |
| Total number of interrogations | 3988 | 5020 | 4146 | 4171 | 4012 |
| Total number of replies | 3834 | 4714 | 3859 | 3831 | 4012 |

be noted that, although the standard deviation of replies from the average is 1 reply per scan greater for the Hazeltine antenna than for the FA-8043, the Hazeltine antenna's average target width is more than 3 hits greater per scan. It would seem in this case that the 3-hit wider target is a desirable benefit despite a slight increase in the fluctuation of the target width over the entire flight range. The ideal system exhibits perfect downlink

Table 6.10 Terminal Antenna System Performance, Complex Model, 5000-Ft Flight

| CRITERION | SYSTEM 6 | 7 | 8 | 9 | 10 |
|---|---|---|---|---|---|
| Number of holes | 10 | 3 | 0 | 0 | 0 |
| Most consecutive scans with fewer than 7 hits | 13 | 14 | 0 | 0 | 0 |
| Total scans with fewer than 7 hits | 31 | 19 | 3 | 2 | 0 |
| Total scans with no hits | 25 | 15 | 3 | 2 | 0 |
| Average replies per scan | 13.7 | 17.8 | 17.7 | 17.8 | 17.1 |
| Standard deviation of replies per scan | 5.5 | 6.1 | 2.5 | 2.8 | 2.7 |
| Total single $P_2$ pulses | 1807 | 633 | 496 | 717 | 1576 |
| Total number of suppressions | 5943 | 3231 | 2372 | 2380 | 5009 |
| Total number of interrogations | 3926 | 5095 | 4983 | 4899 | 4573 |
| Total number of replies | 3674 | 4783 | 4736 | 4758 | 4573 |

performance by receiving all replies from the transponder.

Table 6.10 is more representative of true system performance. The ideal antenna's performance appears truly ideal in terms of the tabular data, showing no scans in which at least 7 hits were not received. The existence of several total scans with few hits but no holes for Systems 8 and 9 indicates that the scans with few hits occurred at the very end of the flight when the aircraft was

Table 6.11 Terminal Antenna System Performance, Complex Model, 10,000-Ft Flight

| CRITERION | SYSTEM 6 | 7 | 8 | 9 | 10 |
|---|---|---|---|---|---|
| Number of holes | 9 | 0 | 1 | 0 | 0 |
| Most consecutive scans with fewer than 7 hits | 5 | 0 | 1 | 0 | 0 |
| Total scans with fewer than 7 hits | 29 | 5 | 7 | 7 | 0 |
| Total scans with no hits | 22 | 4 | 7 | 6 | 0 |
| Average replies per scan | 13.6 | 18.3 | 17.2 | 18.0 | 17.0 |
| Standard deviation of replies per scan | 5.5 | 4.4 | 3.4 | 3.4 | 2.5 |
| Total single $P_2$ pulses | 1732 | 744 | 738 | 1025 | 1703 |
| Total number of suppressions | 6302 | 3589 | 3024 | 2216 | 5011 |
| Total number of interrogations | 3878 | 5145 | 4872 | 4943 | 4568 |
| Total number of replies | 3632 | 4898 | 4617 | 4836 | 4568 |

at a high elevation angle approaching the cone of silence of the interrogators. The low deviation from the average target width for Systems 3, 9, and 10 seems to be an excellent indicator of their performance. A deviation of the order of 2.5 to 3.0 would be representative, therefore, of a good antenna with respect to vertical lobing performance in the terminal area. The narrow average target width for the 5000-ft flight is due apparently to

an excessive amount of false suppression in the main beam. Like the 2000-ft flight, the 5000-ft flight exhibits perfect performance of the downlink of the ideal antenna.

About the same conclusions drawn from the other two series of flights can be drawn about the 10,000-ft flight. The single-scan hole in the test of System 8 is due to an anomaly in the radiation pattern at a high elevation angle just eight scans from the end of the flight. Figures 6.49 through 6.51 tell more about system performance in this case than do the numbers of Table 6.11. Or perhaps it is more correct to state that the displays indicate a way in which to quantize the performance indicated by the deviation of replies in the table and by the oscillations in target width shown in the figures. Whereas the increase in standard deviation of replies from 2.5 for the ideal antenna to 3.4 for the TI and Westinghouse antennas is hardly discernible in the displays, an additional increase to 4.4 is indicative of the significant oscillations shown in Figure 6.49. Nevertheless, there are no holes in coverage for the 10,000-ft flight even for the Hazeltine antenna. This trend toward better performance of the open array at higher altitudes is indicative simply of the fact that the airspace being investigated is more "hole-free", as would be expected at the higher elevation angles involved.

## 6.6 Antenna Performance in an Adjusted Terminal Configuration

Since the antenna systems simulated and discussed in Section 6.5 would not normally be operated at the same power levels nor

with identical STC curves, an effort was undertaken to adjust these parameters in such a way as to improve the performance of each antenna. The 5000-ft series of flights was chosen as the baseline from which to perform the adjustments, as two antennas, the FA-8043 and the Hazeltine open array, still had holes in their coverage at 5000 ft, while the TI and Westinghouse antennas had no holes. The separate rotators, therefore, could actually be adjusted in such a way as to reduce the amount of their coverage and thus to benefit from such other advantages as fewer reflections and false targets.

The adjustments in each antenna system's configuration were made on the basis of plots of uplink and downlink power received by and from the aircraft on both directional and omnidirectional antennas during the flight. These plots, shown in Figures 6.52 through 6.55 for Systems 6 through 9, respectively, indicate the relative adjustments that can be made in order to ensure that levels of received power remain above or below certain limits. In the figures, the four curves of similar shape are, from top to bottom, uplink directional power at the aircraft, downlink directional power at the ground receiver, uplink omni power at the transponder, and downlink omni power at the ground receiver. The curve that decreases with range is the STC curve, which eventually limits when it reaches -88 dBm (full recovery).

To ensure that uplink interrogations would reach the transponder, the top curve was examined for protrusions below the level

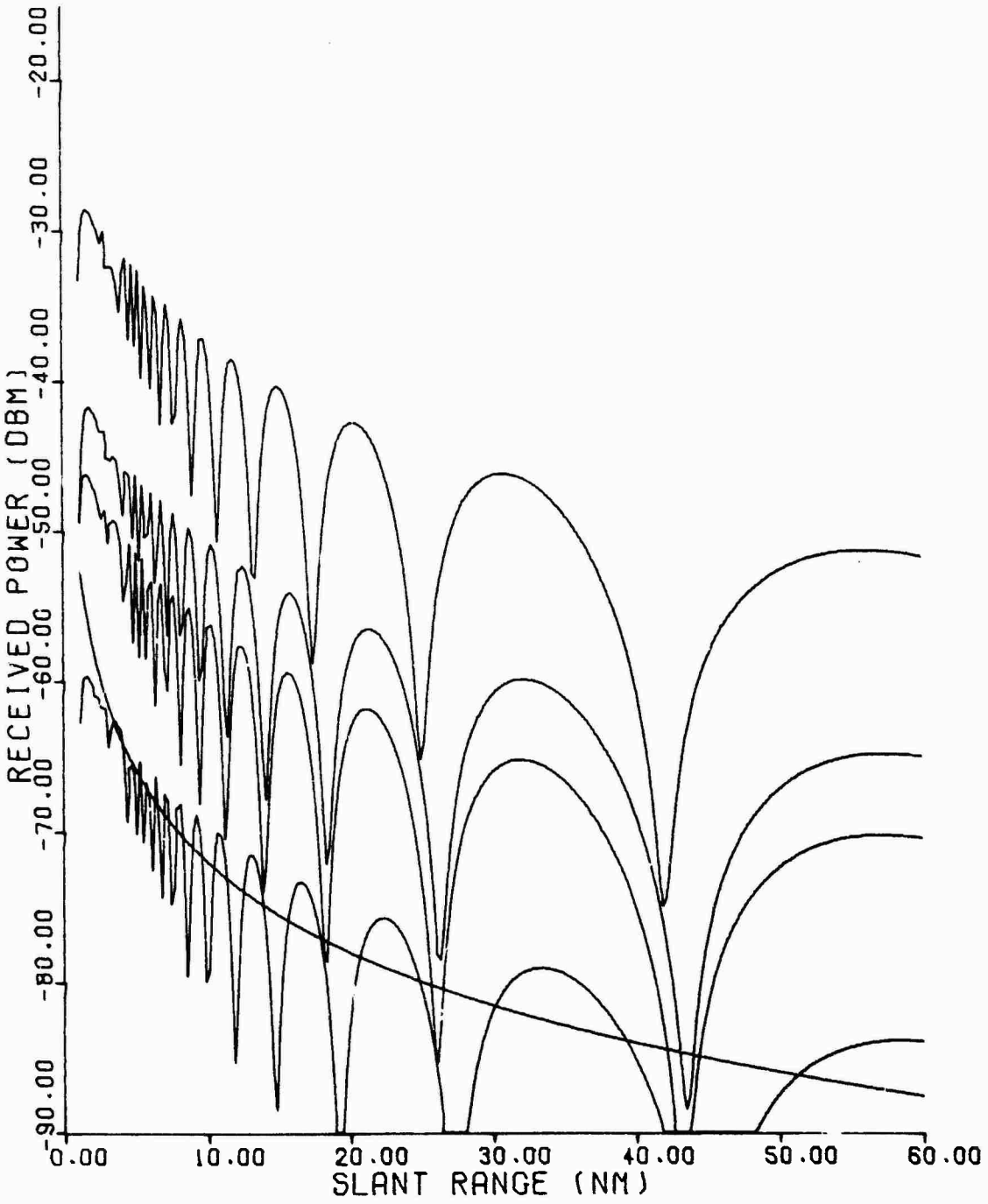


Figure 6.52 Simulated Power Levels for 5000-Ft Flight, System 6

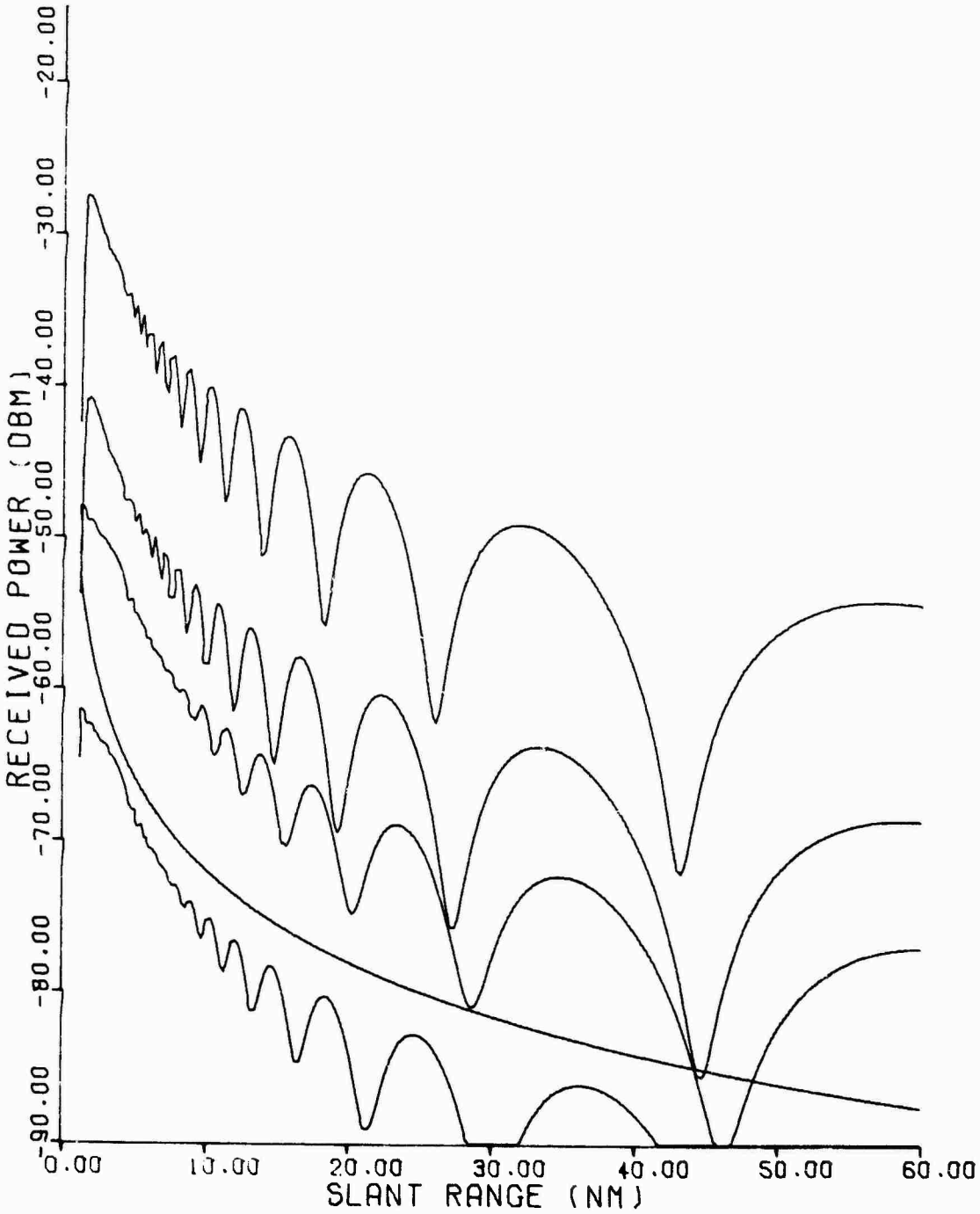


Figure 6.53 Simulated Power Levels for 5000-Ft Flight, System 7

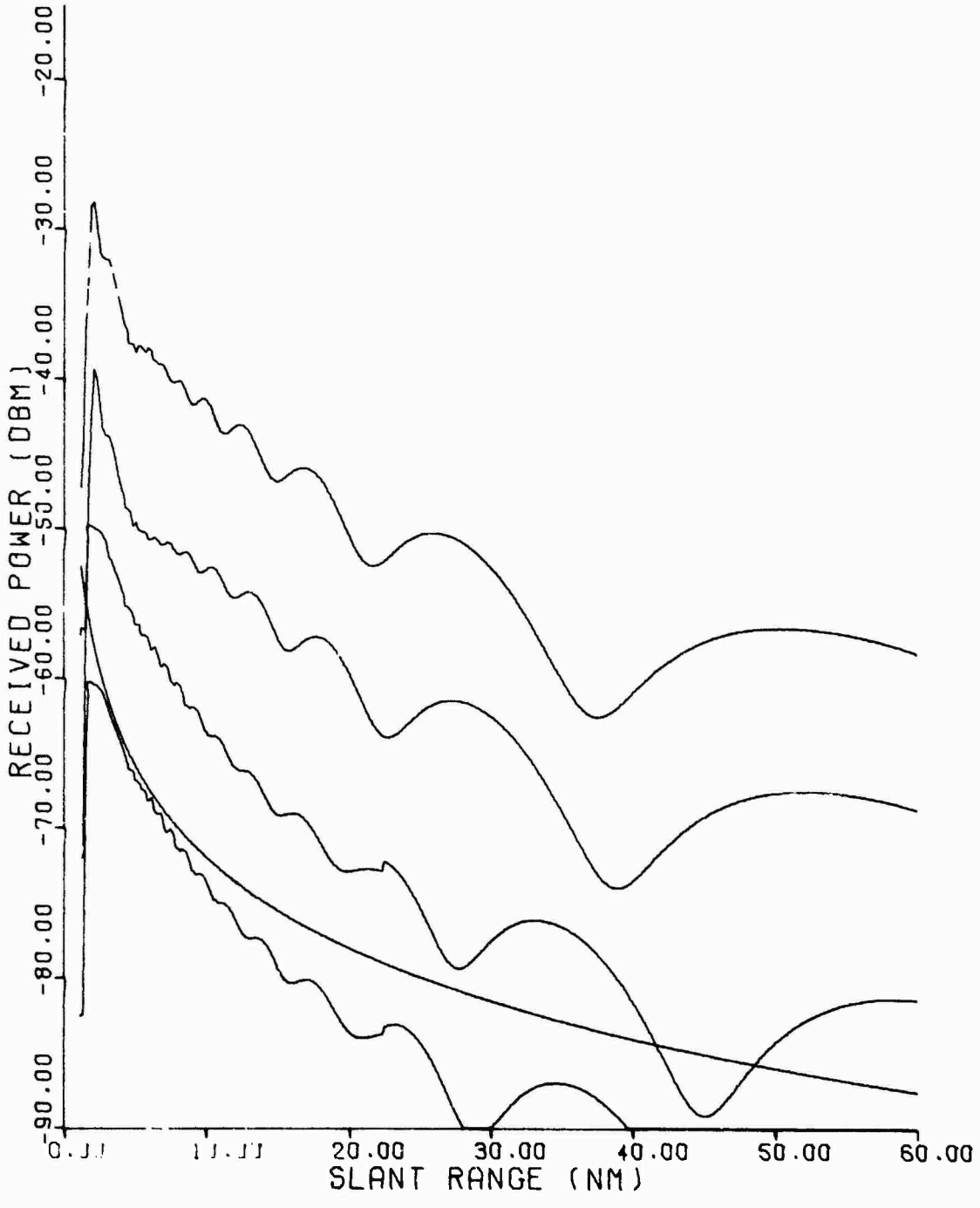


Figure 6.54 Simulated Power Levels for 5000-Ft Flight, System 8

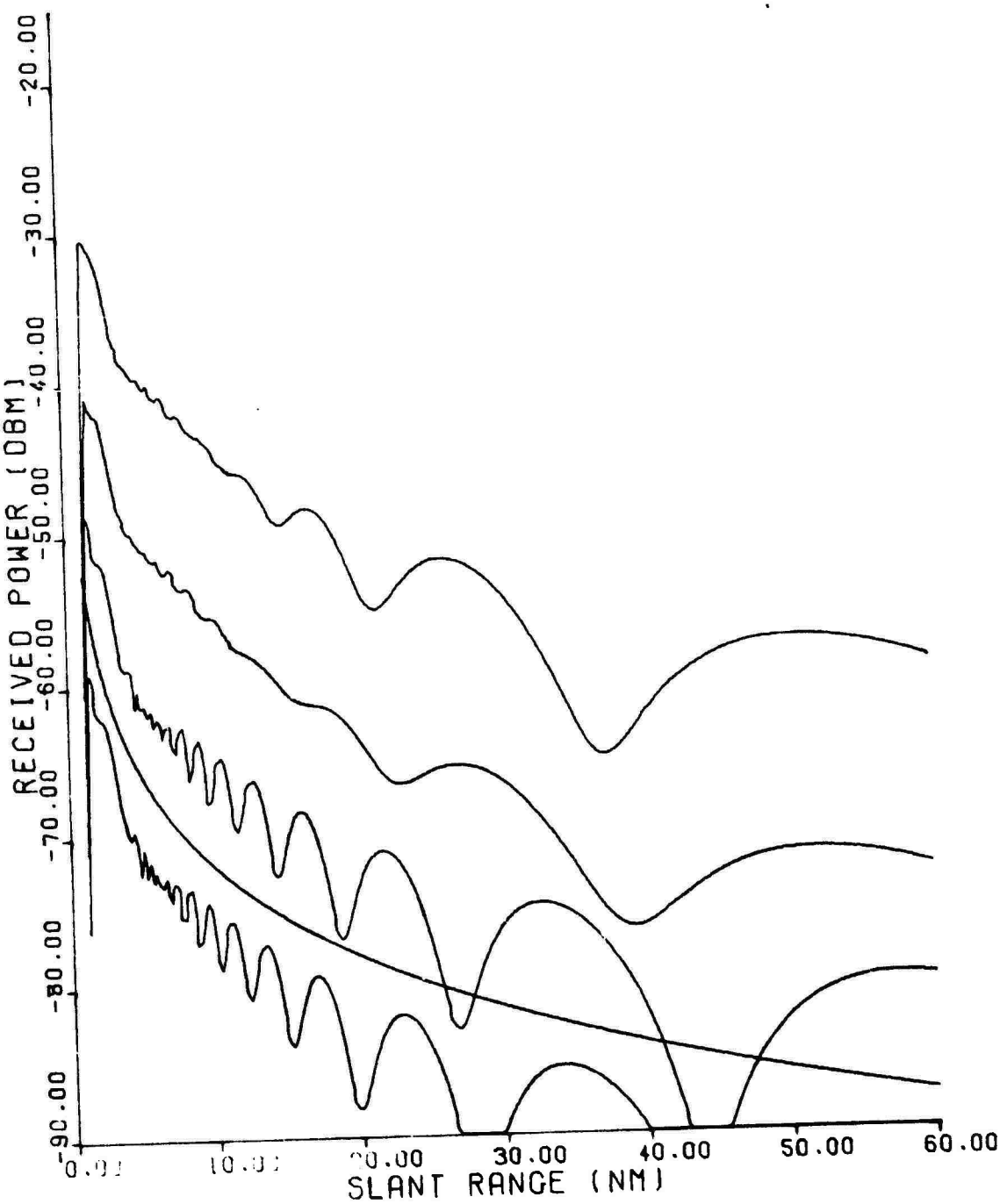


Figure 6.55 Simulated Power Levels for 5000-Ft Flight, System 9

of minimum transponder sensitivity (-69 dBm). The power budget had to ensure that this level was reached, either through an upward or downward revision of interrogator power. In the case of the Hazeltine and FA-8043 antennas, of course, power would have to be increased to fill the holes. In the case of the separate rotators, on the other hand, power could be reduced to lower the amount of radiation through the side lobes while still retaining coverage. Such adjustments would only ensure the desired performance, of course, at the altitude for which the adjustment was being made.

Once the uplink directional signal's detection was assured, the omni level was examined in an attempt to keep it below the level necessary to avoid false suppression in the main beam. A further adjustment could thus be made by placing a pad (attenuator) in the omni line if the difference between the directional and omni signals became less than 9 dB.

Finally, the downlink directional signal's nulls were examined for protrusions below the STC curve. The STC was adjusted either downward (less sensitive) in the case of the separate rotators to allow as much interference rejection as possible without blocking the downlink signal, or upward (more sensitive) in the case of Systems 6 and 7 to enable the receiver to detect those replies that had not been sensed in the initial flight.

In each case, a margin of 3 dB was added to ensure that the desired reply was detected not only on the boresight of the beam,

but also anywhere within the 3-dB beamwidth. An attempt was made to adjust the parameters in a way that could be performed easily in the field as well as in the computer. Table 6.12 lists the changes made in Systems 5 through 9 to achieve the adjustments.

Table 6.12 Characteristics of Adjusted Terminal Systems

| NEW SYSTEM | FORMER SYSTEM | INTERROGATOR POWER | SIDE-LOBE SUPPRESSION | STC | OMNI PAD |
|---|---|---|---|---|---|
| 11 | 6 | 1000 watts | normal | 29 dB | 1.5 dB |
| 12 | 7 | 630 watts | normal | 32 dB | 1.0 dB |
| 13 | 8 | 140 watts | improved | 43 dB | 0 |
| 14 | 9 | 250 watts | improved | 40.5 dB | 0 |

The ATC displays resulting from simulation of these adjusted antenna configurations are shown in Figures 6.4, 6.9, 6.56, and 6.57 for Systems 11 through 14, respectively. The performance criteria tabulated by the complex model are included in Table 6.13.

The same adjustments were inserted into the simple model to investigate the performance that might be expected over a wider range of airspace if the adjustments for a level 5000-ft flight were used. The numerical results of the simple model's assessment of Systems 11 through 14 appear in Table 6.14.

The missing scan at 43 nm for the simulation of System 11 is due to the fact that the maximum ground receiver sensitivity was insufficient, even with the STC curve reduced considerably, to allow detection of the signal transmitted from the transponder.

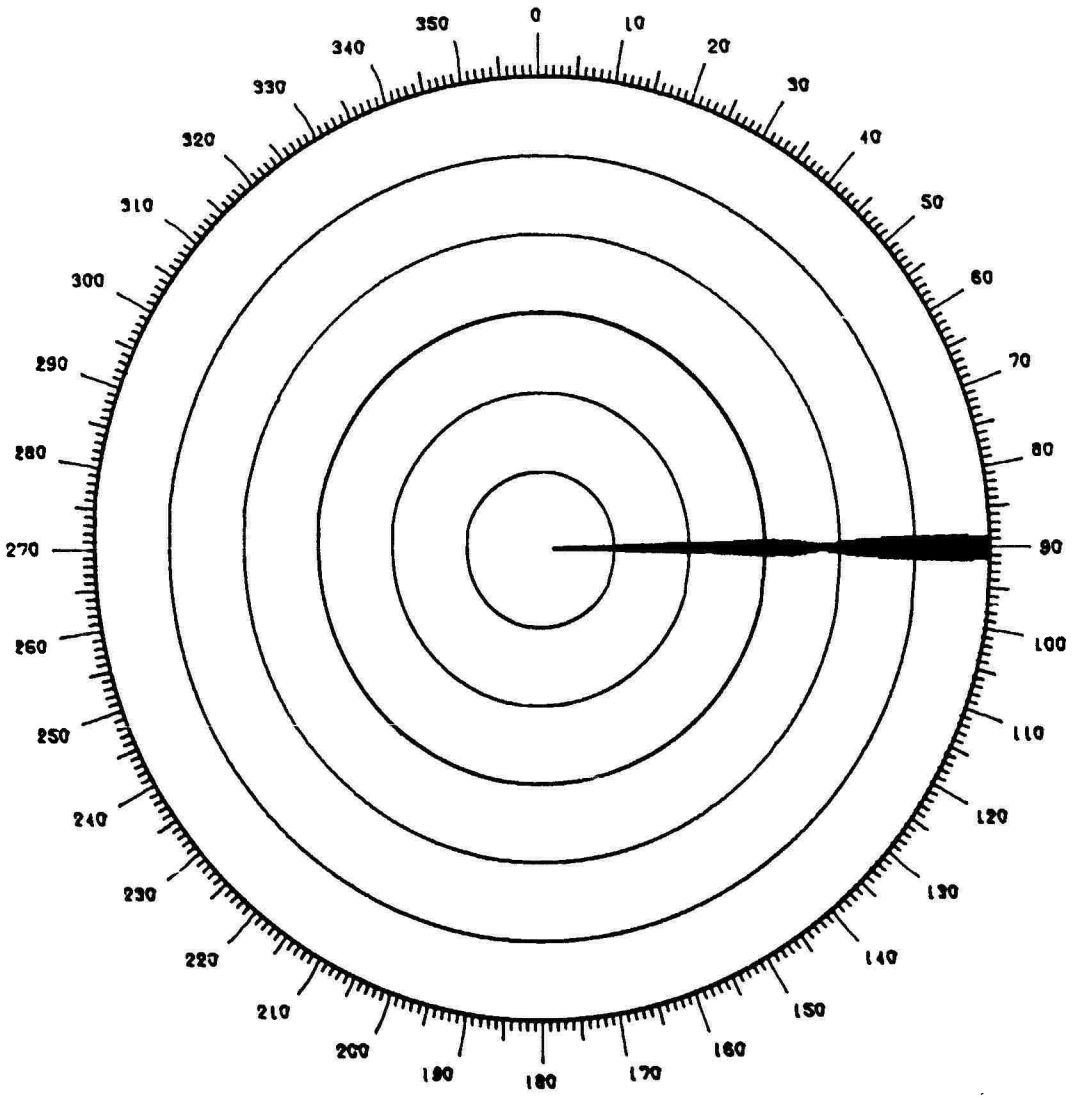


Figure 6.56 Simulated Flight at 5000 Ft, System 13

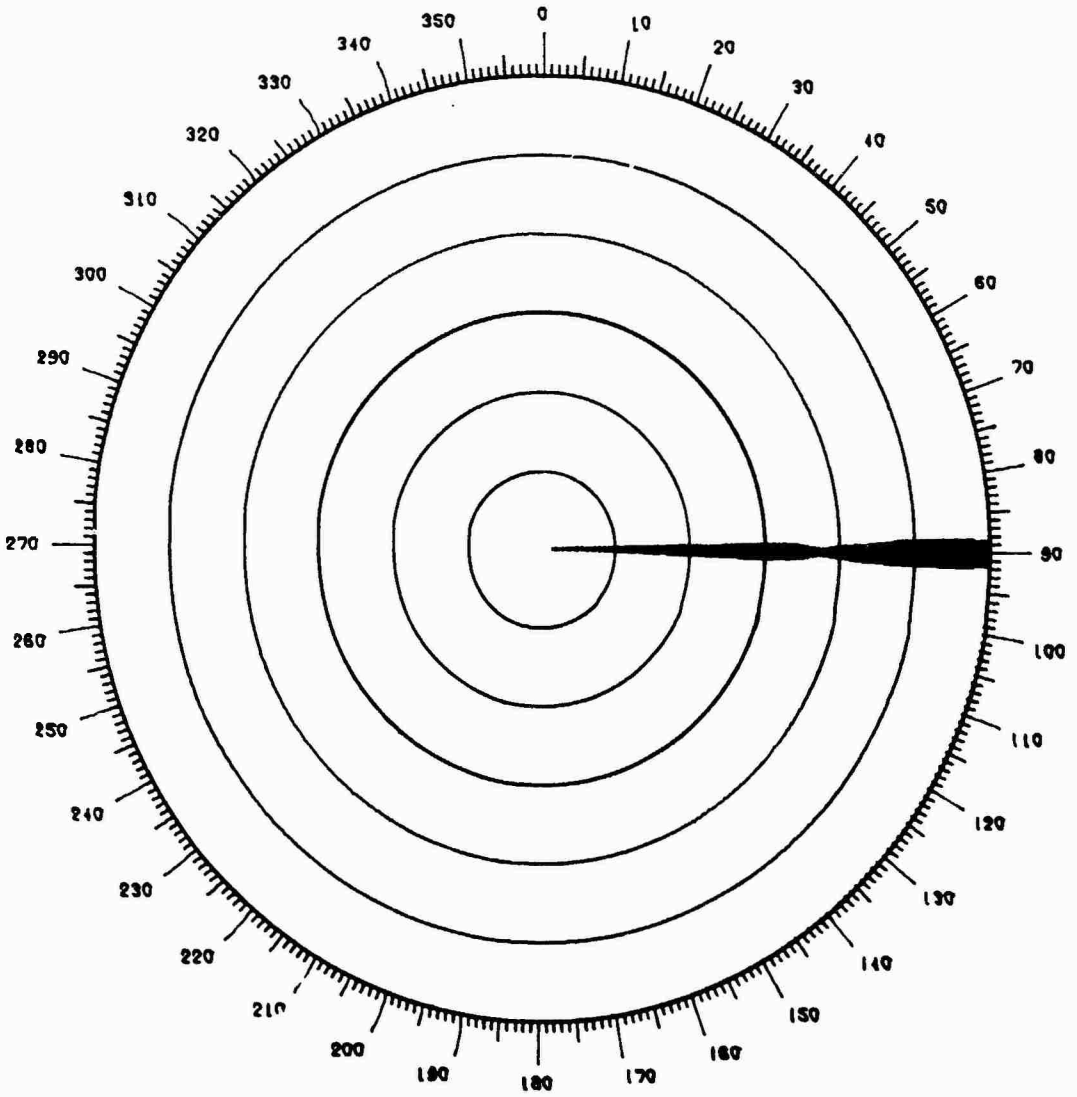


Figure 6.57 Simulated Flight at 5000 Ft, System 14

Table 6.13 Adjusted Terminal Antenna System Performance, Complex Model, 5000-Ft Flight

| CRITERION | SYSTEM 11 | 12 | 13 | 14 |
|---|---|---|---|---|
| Number of holes | 4 | 0 | 1 | 0 |
| Most consecutive scans with fewer than 7 hits | 2 | 0 | 4 | 0 |
| Total scans with fewer than 7 hits | 5 | 1 | 6 | 2 |
| Total scans with no hits | 1 | 0 | 2 | 1 |
| Average replies per scan | 18.0 | 20.8 | 14.3 | 15.8 |
| Standard deviation of replies per scan | 4.1 | 4.0 | 3.1 | 3.0 |
| Total single $P_2$ pulses | 520 | 256 | 120 | 144 |
| Total number of suppressions | 1890 | 804 | 576 | 590 |
| Total number of interrogations | 3356 | 3997 | 2817 | 3045 |
| Total number of replies | 3223 | 3720 | 2555 | 2828 |

The single "hole" for System 13 is somewhat misleading, as it consists of a string of 4 consecutive scans of 6 returns. Because the target beamwidth is very sensitive to adjustments in power, this particular case happened to fall a few tenths of a decibel short of that required to produce a string of 7 hits. The most important point to note is that the holes in coverage of the Hazeltine antenna were able to be filled, while those of the

FA-8043 were not.

Table 6.14 Adjusted Terminal Antenna System Performance, Simple Model

| CRITERION (areas in $nm^2$) | SYSTEM 11 | 12 | 13 | 14 |
|---|---|---|---|---|
| Uncovered uplink | 4.2 | 2.8 | 14.7 | 12.1 |
| False suppression | 11.1 | 4.8 | 0.1 | 1.9 |
| Uncovered downlink | 0.7 | 0.3 | 0.7 | 1.0 |
| Over-interrogation | 1209.6 | 1198.5 | 954.7 | 1018.2 |
| Interference susceptibility | 1244.6 | 1252.2 | 1245.5 | 1241.0 |

From the results of the simple model, it is clear that the reduction of power to the two separate rotators caused them to lose some low angle coverage. Their false suppression area is still very low, however. The total of false-suppressed and uncovered uplink areas is, in fact, less for either of the two separate rotators as adjusted than for the FA-8043 with its power turned up in an attempt to cover holes that still remain. To improve upon the adjustment scheme, therefore, the power curves shown earlier in this section should be obtained for the flight profile that produces the minimum elevation angles expected to occur in the terminal area of interest.

A final series of flight simulations was made with the

adjusted terminal antenna systems to investigate the parameters that affect system interference characteristics. Whereas the previous simulations involved a scan limit of $4^{\circ}$ in azimuth on either side of the target (to save computer time during the investigation of main-beam phenomena), the scan limit was removed and the 5000-ft flights repeated using an aircraft with a 500-watt, 77-dBm transponder. This series of simulations, of course, would not show coverage problems, but would indicate the relative contributions to interference of the various adjusted antenna systems. ATC displays for this series of runs appear in Figures 6.58 through 6.61. Tabular data is presented in Table 6.15.

With the sensitivity of the transponder now high and its output power also increased, it is not surprising to see very few scans with narrow targets nor a nearly perfect record of reception of replies by the ground receiver. The most noticeable coverage effect is a rather serious false suppression problem experienced by the Westinghouse antenna. Once again, the smoothness of target width is indicated by the variation of 2.5 replies per scan for the TI antenna.

Of particular note for this series of simulated flights should be the number of single $P_2$ pulses and suppressions experienced by the transponder. Using the FA-8043 numbers as a reference, the Hazeltine antenna manages to nearly halve the number of suppressions while radiating only about 10% more single $P_2$ pulses. This is an appreciable reduction of the amount of trans-

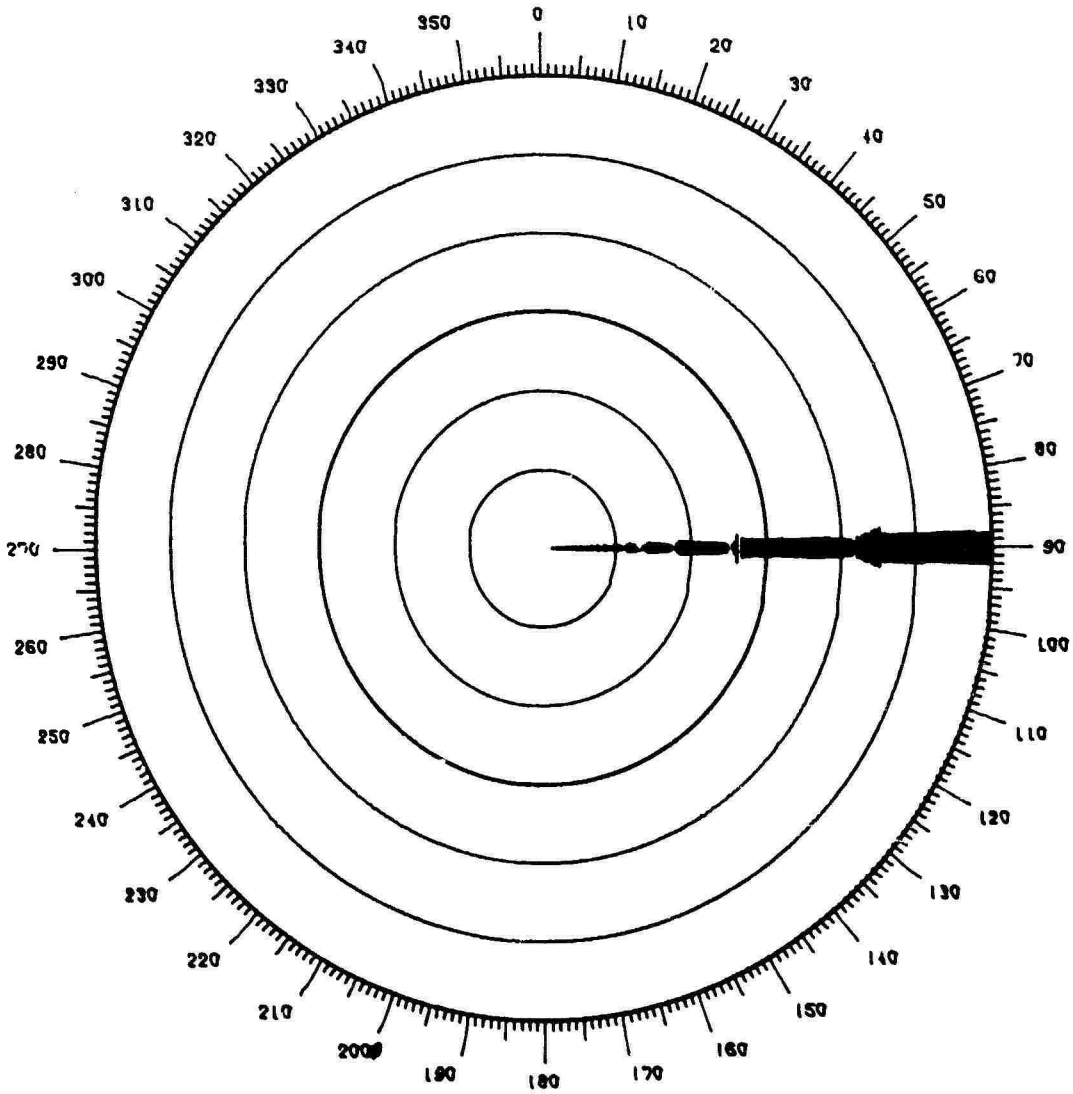


Figure 6.58 Simulated Flight at 5000 Ft, System 11, Sensitive, High-Power Transponder

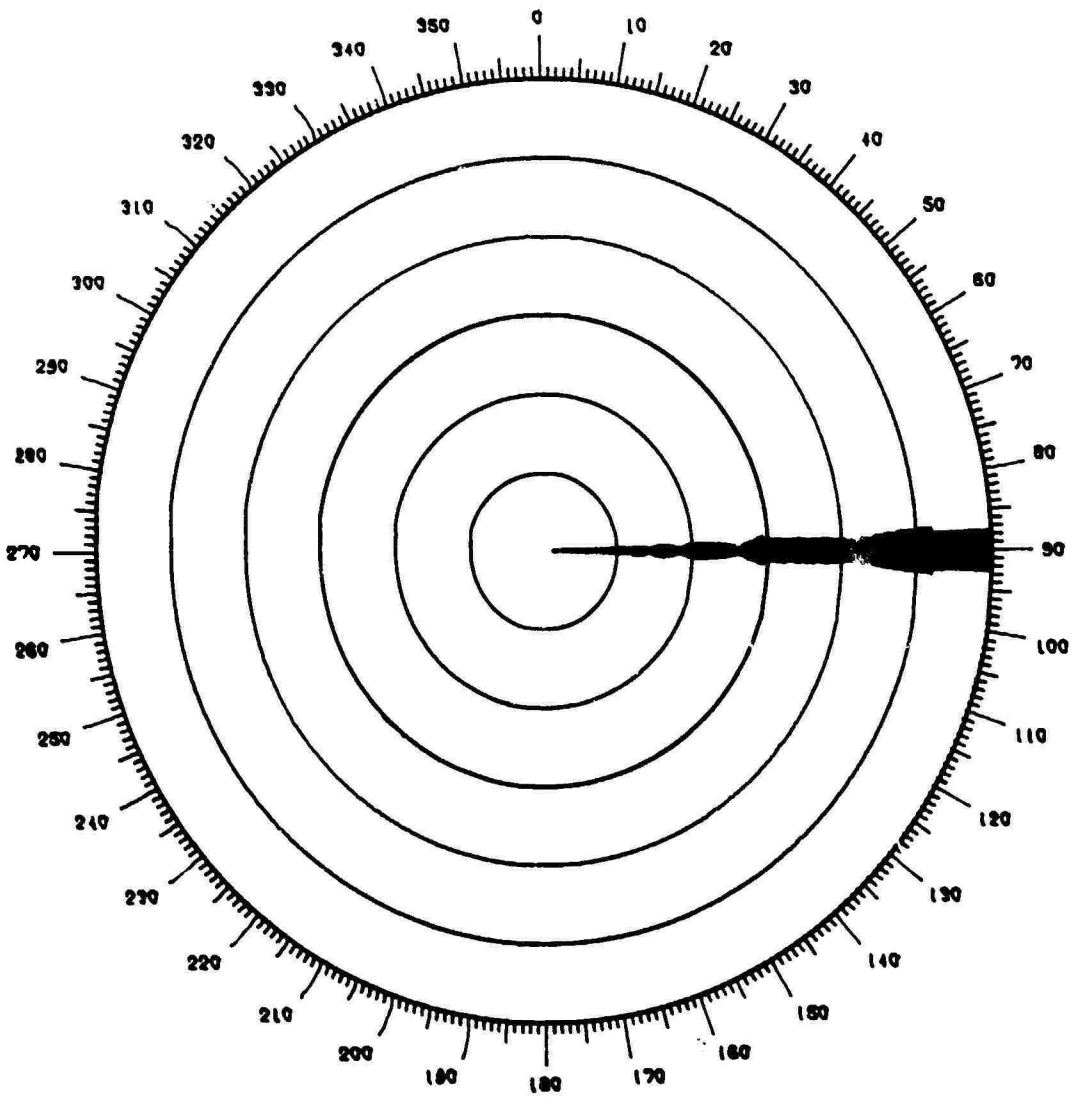


Figure 6.59 Simulated Flight at 5000 Ft, System 12, Sensitive, High-Power Transponder

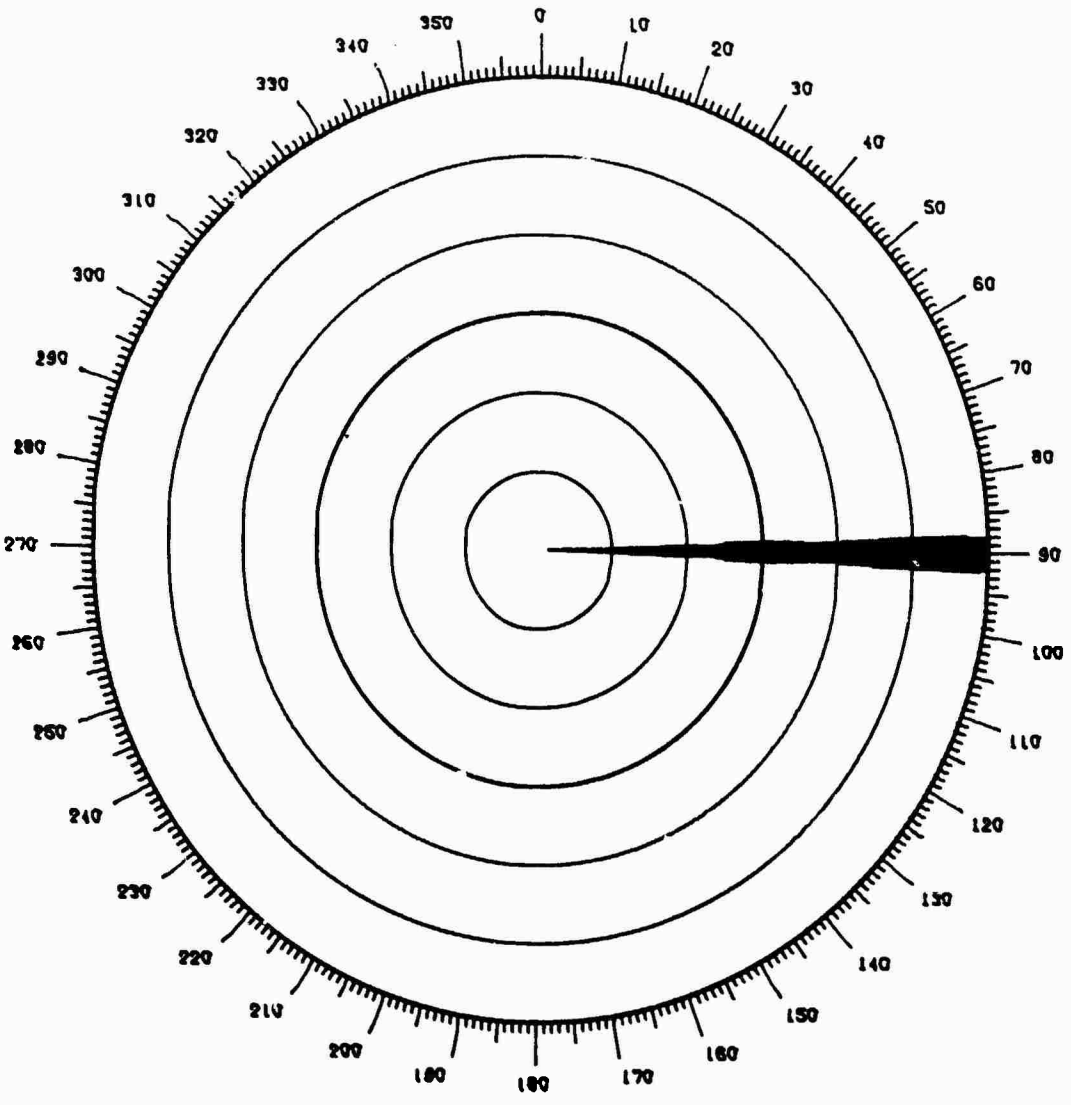


Figure 6.60 Simulated Flight at 5000 Ft, System 13, Sensitive, High-Power Transponder

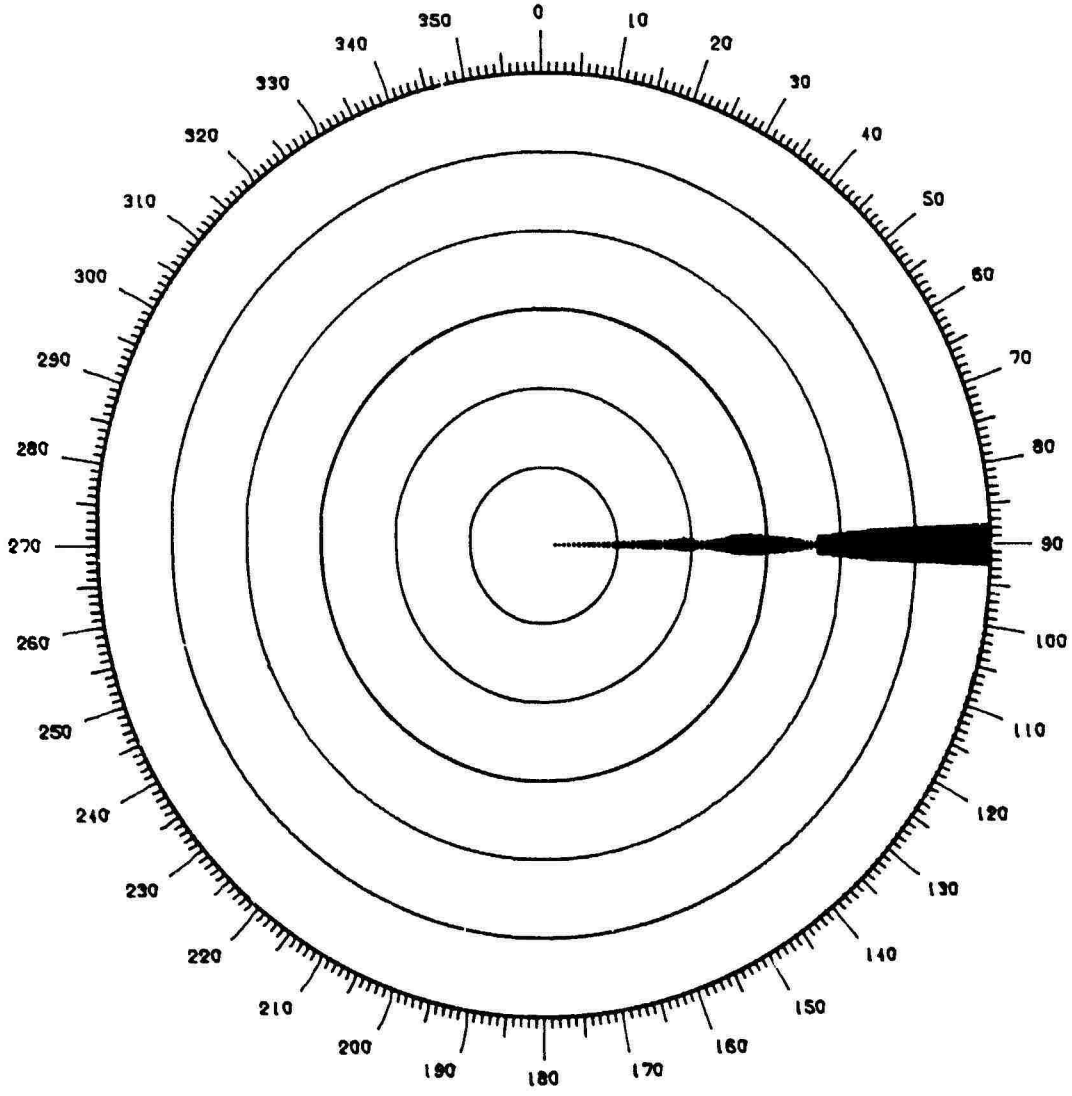


Figure 6.61 Simulated Flight at 5000 Ft, System 14, Sensitive, High-Power Transponder

Table 6.15 Adjusted Terminal Antenna System Performance, Complex Model, 5000-Ft Flight, 500-watt/77-dBm Transponder

| CRITERION | SYSTEM 11 | 12 | 13 | 14 |
|---|---|---|---|---|
| Number of holes | 2 | 0 | 0 | 1 |
| Most consecutive scans with fewer than 7 hits | 1 | 0 | 0 | 2 |
| Total scans with fewer than 7 hits | 2 | 1 | 0 | 3 |
| Total scans with no hits | 0 | 0 | 0 | 1 |
| Average replies per scan | 18.6 | 21.9 | 19.0 | 18.8 |
| Standard deviation of replies per scan | 4.1 | 4.0 | 2.5 | 4.5 |
| Total single $P_2$ pulses | 148815 | 167119 | 20880 | 40208 |
| Total number of suppressions | 115345 | 64983 | 66134 | 117313 |
| Total number of interrogations | 3342 | 3934 | 3404 | 3375 |
| Total number of replies | 3332 | 3927 | 3394 | 3374 |

ponder interference caused by the mechanisms discussed in Chapter 3. The TI antenna, while exhibiting the best coverage performance, also nearly halves the number of suppressions but in addition reduces the single $P_2$ pulses by a factor of more than 7! The Westinghouse antenna under these same conditions does half as well as the TI antenna in reduction of single $P_2$ pulses, but cannot reduce the number of suppressions at all.

System 12 was further modified to investigate the effect of a common aperture for both directional and omnidirectional patterns on system performance. The FAA has initiated a program to develop a version of the Hazeltine antenna from which both patterns will be radiated without a separate omni. Such an antenna can be modeled simply by setting the height of both the directional and omni antennas equal.

The result of the simple model for this "integral omni" antenna is shown graphically in Figure 6.62 and in tabular form in Table 6.16. Despite the occurrence of rather deep nulls in both the directional and omni patterns, the alignment of the patterns as shown in Figure 6.62 prevents the occurrence of false

Table 6.16 Integral SLS Antenna System Performance, Simple Model

| CRITERION (areas in $nm^2$) | WITHOUT INTEGRAL SLS | WITH INTEGRAL SLS |
|---|---|---|
| Uncovered uplink | 2.8 | 2.8 |
| False suppression | 4.8 | 0.0 |
| Uncovered downlink | 0.3 | 0.3 |
| Over-interrogation | 1198.5 | 1198.5 |
| Interference susceptibility | 1252.2 | 1252.2 |

suppression.

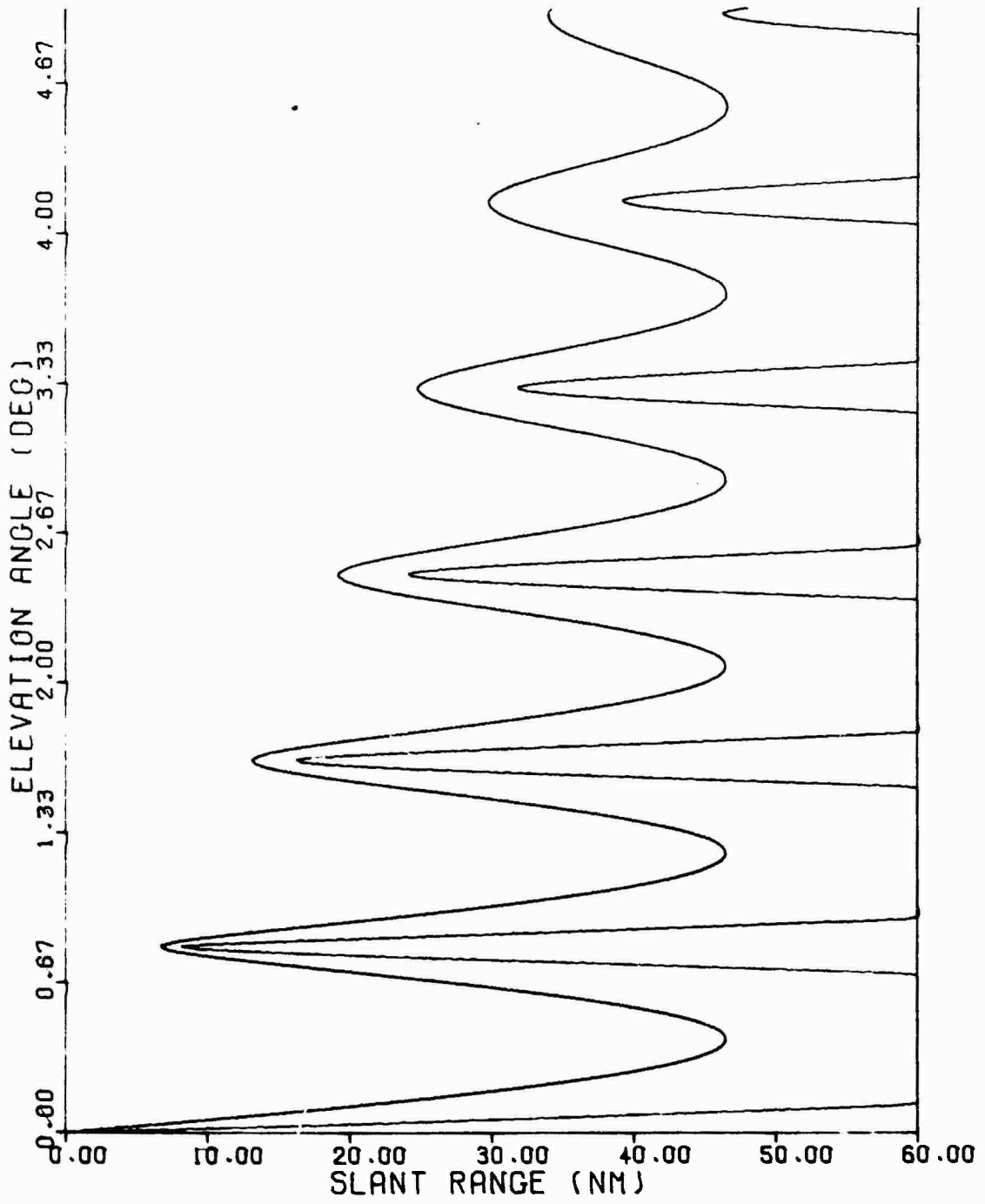


Figure 6.62 False Suppression Contours, Integral SLS

An ATC display analogous to that of Figure 6.9, but with the integral SLS feature incorporated, is shown in Figure 6.63. For this run of the complex simulation, the average target width was reduced slightly from 20.8 to 20.6 replies per scan, while the standard deviation from the average dropped from 4.0 without integral SLS to 3.5 replies per scan with integral SLS. The reduction in the deviation from the average, of course, is due to the elimination of false suppression that previously caused oscillation of the target width.

## 6.7 Performance of Receiver Side-Lobe Suppression

The RSLS model was evaluated for several interference environments using the adjusted FA-8043/8044 terminal antenna system. When RSLS was switched on, the STC was made inoperative; with RSLS off, the STC was set to its adjusted value as described in the previous section. For four aircraft populations, 100, 200, 500, and 1000 aircraft within 200 nm of the interrogator, fruit counts were recorded as were the ratios of received replies to interrogations that reached the aircraft. The results of these RSLS simulations are recorded in Table 6.17.

Clearly, RSLS was successful for all interference environments in reducing substantially the amount of fruit that could not be removed by the STC. If RSLS did not affect the ratio of replies to interrogations to a great extent, therefore, it would be of extreme value to the ATCRBS with few drawbacks. Unfortunately, the reply ratio does become degraded rather rapidly as the

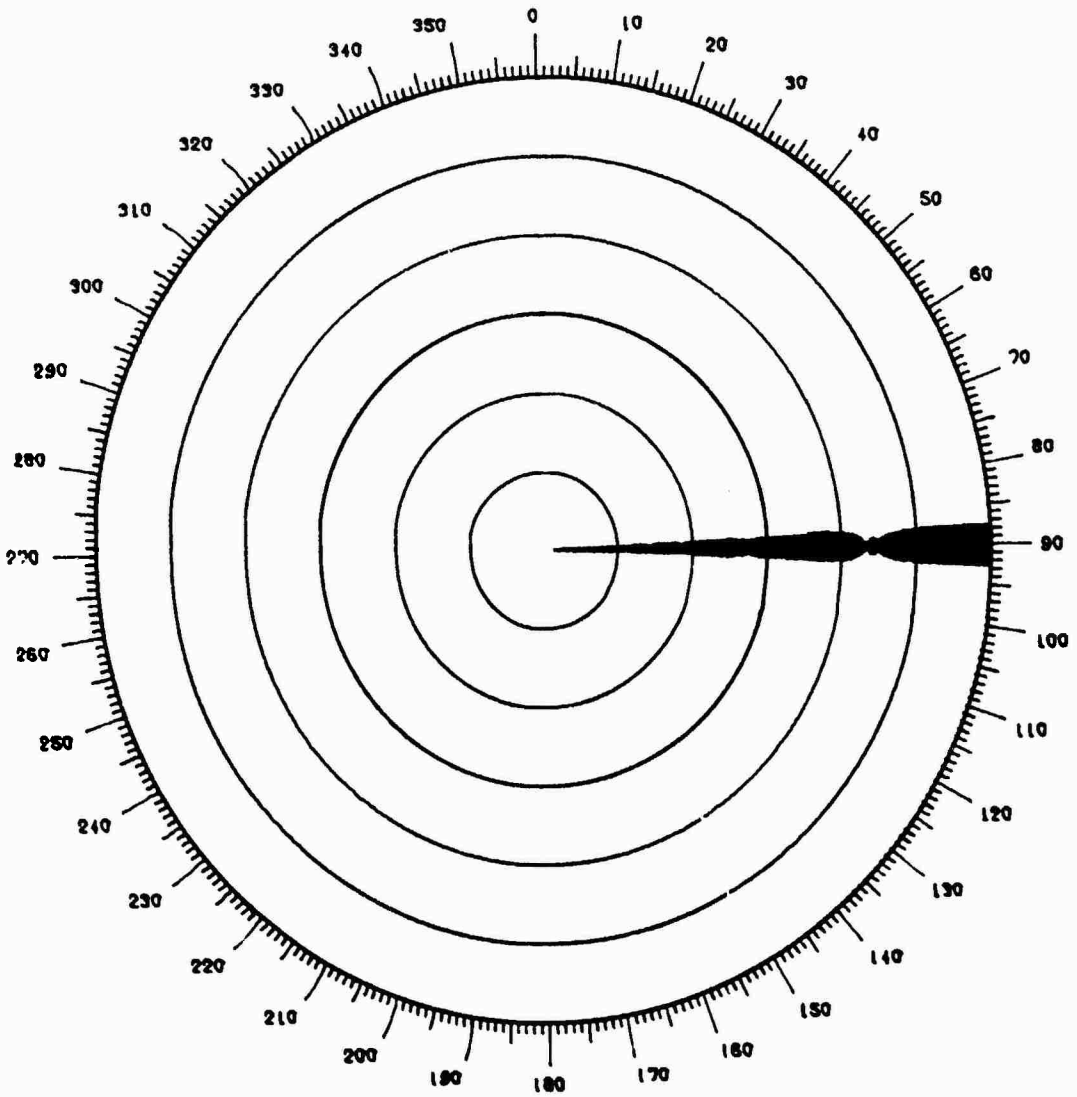


Figure 6.63 Simulated Flight at 5000 Ft, Integral SLS

Table 6.17 RSLS Performance as a Function of Interference

| AIRCRAFT POPULATION | RSLS OFF FRUIT/SEC | RSLS OFF REPLY RATIO | RSLS ON FRUIT/SEC | RSLS ON REPLY RATIO |
|---|---|---|---|---|
| 100 | 742 | .96 | 38 | .89 |
| 200 | 1293 | .96 | 69 | .88 |
| 500 | 3119 | .96 | 180 | .86 |
| 1000 | 6148 | .96 | 365 | .82 |

number of aircraft in the interference environment increases. Since the simulation did not take into account such factors as aircraft maneuvers and capturing of an aircraft transponder by interrogators other than the one of interest, the reply ratio with RSLS on could be reduced appreciably below that shown — quite probably into the 70% - 80% range. Code validation for modern target processors might thus become a difficult task.

RSLS performance was also compared when it was used in conjunction with the four antenna systems described in the previous section. For this comparison, an aircraft population of 500 was chosen as the interference environment. The results of this simulation appear in Table 6.18. Again, it is clear in each case that RSLS is effective in removing fruit from the side-lobe replies. Note also that the fruit rates correlate strongly with the depth of the STC curves used for each adjusted antenna system. The results of the main-beam killing observed in Table 6.17 are quite different in Table 6.18, however. Whereas the STC of the adjusted

Table 6.18 RSLS Performance as a Function of Antenna Systems

| ANTENNA SYSTEM | RSLS OFF FRUIT/SEC | RSLS OFF REPLY RATIO | RSLS ON FRUIT/SEC | RSLS ON REPLY RATIO |
|---|---|---|---|---|
| 11 | 3119 | .96 | 180 | .86 |
| 12 | 2536 | .93 | 189 | .84 |
| 13 | 1064 | .91 | 160 | .95 |
| 14 | 1298 | .93 | 182 | .92 |

FA-8043 system was set to ensure receipt of all downlink replies if possible, the steeper curves of the other antennas tend to reduce the width of the targets as received on the downlink. This steeper STC curve causes the reply ratio with RSLS off (and STC on) to be lower for Systems 12, 13 and 14. When RSLS is switched on, the Hazeltine antenna still experiences a drop of approximately 10% in the reply ratio as does the FA-8043. The separate rotators, on the other hand either decrease slightly or, in the case of the TI antenna, increase the reply ratio. The reason for this is that the exceptionally steep STC curves (greater than 40 dB) for Systems 13 and 14 cause a narrowing of the target on the downlink that offsets losses due to main-beam killing when the STC is turned off and RSLS on. The lost replies are redistributed from the outer edges of the targets with RSLS off to random locations within the target with RSLS on. Another strong influence on the increase in reply ratio is the fact that the removal of the STC causes the TI antenna to have three full

scans at the end of the flight that were formerly in the high-angle cone of silence when the STC was employed. It should also be kept in mind that the transponder employed in these flight tests had minimum sensitivity and power as allowed by the National Standard.

The detail available from the simple and especially the complex models allows an endless variety of data to be obtained. The examples presented in this chapter are representative of the types of problems that can be undertaken, but should not be interpreted as the final answer to any question regarding the systems analyzed. The applications of this chapter do indicate further areas that should be explored, however. The tools used to produce these illustrations are a means for such exploration.

# CHAPTER 7

# CONCLUSIONS AND RECOMMENDATIONS

## 7.1 Conclusions Concerning Methods of the Thesis

The objectives defined at the beginning of the thesis were accomplished. A set of performance criteria were expressed in closed-form that allow the assessment of surveillance system performance over a wide-range of system coverage using a simple-flat earth model. Likewise, a more complex simulation of propagation over a spherical earth was developed using a minimum of simplifying assumptions to facilitate the detailed investigation of the interactions between interrogator and aircraft over a specific flight profile.

Each of the techniques has its unique advantages and applications. The simple, flat-earth model, because of the simplifying assumptions involved, should not be applied without verification of its results by several representative simulations using the complex model over the range of airspace that the simple model covers. If the indications of the simple model are indeed substantiated by several simulated flights, then the results of the simple model can be accepted with confidence over the airspace analyzed. The advantage of obtaining confidence in the main-beam performance criteria with a minimum involvement of the complex model is a significant saving in computer time. The simple model requires approximately the same time to evaluate a vertical slice

of airspace as the complex model requires to simulate a single flight through that airspace. In theory, therefore, an infinity of flight paths through the airspace in question would have to be simulated by the complex model to allow the same conclusions to be drawn from each. In general, it may be said that the simple model allows a quick and comprehensive assessment of relative main-beam phenomena over an entire airspace. There is no danger of omitting that airspace in which an unusual phenomenon, such as false suppression over a narrow band of altitudes, occurs.

The complex model provides a tool for less comprehensive but more specific analysis. The inclusion of side-lobe detail affords the opportunity to investigate reflection phenomena and the effects of external interference on such systems as receiver side-lobe suppression. If reliable input data concerning a particular system configuration can be obtained, the time and cost of running the complex simulation will be well worth the opportunity to gather data that can be interpreted more in an absolute sense rather than relative to the performance of some other baseline system. As in all simulations, however, the quality of output can certainly be no better than the reliability of the inputs with which the computer must work. Because it involves primarily one aircraft and one interrogator, the complex model, despite its level of detail, runs quickly on a high-speed digital computer. Typical simulations of vertical lobing performance ran in 1/50 the time of the aircraft flight on the CDC 6600. Thus, the cost

of a simulated test is approximately $20 per hour of flight test, including aircraft, pilot, controller, and test director. The simulation, of course, can be run independent of the weather, aircraft maintenance, and other factors that all too frequently hamper live tests. Even in a heavy interference environment, the complex model runs in 1/5 the time of an actual flight. The detailed nature of the complex simulation model necessitates the same caution in its use that must be exercised in the process of experimental tests in the field. If vertical nulls are sought, for instance, the aircraft flight profile must be planned carefully and methodically to ensure a thorough searching of the airspace of interest.

The new solutions for the grazing angle over a spherical earth presented in Section 5.4 offer, respectively, a simpler and slightly more accurate solution than the commonly-used form developed nearly thirty years ago, and a much more accurate solution of comparable complexity. Although these new solutions are not expected to result in any major innovations in radar technology, their discovery is evidence that other numerical and analytic techniques in this field and in many others still await development.

The simulation of an air traffic control display as one means of digesting the data produced by the complex model has proven invaluable. Such a form offers a convenient tool for model validation by comparison with actual display photos taken

during field tests. The simulated displays also convey to such non-technical users as air traffic controllers the ultimate meaning of implementation of a new system currently under consideration or development.

## 7.2 Conclusions Concerning Applications of the Thesis

The use of larger vertical apertures for ATCRBS antennas is very dependent upon the particular site under consideration. Although this thesis has concentrated on applications of the various antennas over terrain that results in severe vertical lobing problems, the demonstration of the roughness parameter made it quite clear that there are conditions under which no system improvement is necessary. The first step in any site analysis, therefore, should be a careful assessment and quantization of the terrain over which the system must operate. Then the performance of the system as assessed by the techniques developed herein can be reviewed relative to its cost. Although the performance of the various antennas investigated in Chapter 6 followed rather intuitively the size of the vertical aperture, some quantitative measures of this performance can now be associated with each system. Certainly the most promising development underway is the integral SLS antenna discussed and simulated in Chapter 6.

Receiver side-lobe suppression is very effective in reducing fruit that arrives outside the main beam of the receiver antenna. It does result, however, in a reduction of approximately 10% in the reply ratio due to the phenomenon of main-beam killing. This

reduction in replies is appreciable for moderate interference environments and increases beyond 10% for more severe environments. The reduction of approximately 10% holds both for the current FA-8043 antenna system and for the Hazeltine open array. The larger-aperture antennas of TI and Westinghouse, however, experience no such reduction in reply ratio, apparently because of the better-behaved vertical lobing patterns that are susceptible to fewer interfering replies. The ultimate implementation of RSLS, therefore, may be as dependent upon site selection as is the deployment of new antennas.

## 7.3 Specific Contributions of the Thesis

The following items are believed to be original and unique contributions of the thesis:

1. the development of a set of performance criteria by which the relative performance of a variety of radio frequency surveillance systems for air traffic control, and in particular the Air Traffic Control Radar Beacon System, can be assessed;

2. the closed-form solution of the area under a vertical lobing curve for the case of a flat earth;

3. a new quadratic solution for the grazing angle over a spherical earth that is simpler and, on the average, more accurate than the classical solution of Fishback;

4. a new cubic solution for the grazing angle over a spherical earth that is much more accurate than the classical solution of Fishback and of comparable complexity;

5. the development of a surface roughness criterion that takes into account most of the discrepant criteria used to date in the literature;

6. the development of a complex spherical-earth model of ATCRBS operation that produces a simulated air traffic control display and which is believed to be the most complete, detailed, and accurate model of ATCRBS propagation effects now in existence.

## 7.4 Recommendations for Further Study

The applications of both simple and complex models to the systems and problems discussed in Chapter 6 are merely a beginning of the information that can be obtained. Of signigificant interest would be the adjustment of the en route antenna systems in a manner similar to that used in Section 6.6 to optimize their performance. Antenna height is a parameter that should be investigated further both for en route sites and terminal sites, particularly for those configurations involving a separate rotator antenna whose height is no longer determined by the primary radar that supports it. Antenna height could possibly be adjusted to place critical antenna nulls in unused airspace.

The roughness parameter H and the relative permittivity and conductivity of the reflecting medium were held constant for the applications of the thesis to create a worst-case environment with regard to vertical lobing. These parameters and the sensitivity of various antenna systems and configurations to changes in the parameters deserve further analysis.

The adjustment of parameters in the terminal configuration of Section 6.6 was performed on the basis of a single aircraft flight profile. A similar means of system adjustment to optimize coverage using the simple model could result in improved performance over a wide range of airspace, rather than over a single flight path. Investigation of such an optimization technique is encouraged.

Finally, the RSLS model whose performance was analyzed in Section 6.7 should be combined with a more accurate model or simulation of external system interference, such as that described in Reference 5. The model of interference developed for the thesis contains many random parameters that, under some unique situations in the real world, may not describe accurately the interference that is actually occurring. In this same regard, the garble model used in the thesis could be refined and more closely related to the real world. If the assumptions of randomness used in the simulation cause the performance of RSLS to appear better than it would actually be in the field, the refinement of the interference and garble models would be particularly valuable.

Variations in the RSLS threshold in conjunction with the STC setting, rather than independent of it, may also prove effective in the reduction of interference and minimization of main-beam killing. STC curves should not be restricted to their current form in which sensitivity varies with the square of time. Rather, the use of nonlinear forms of recovery that complement the vertical radiation pattern of the directional antenna should be explored. The complex simulation model will facilitate such exploration and provide an immediate indication of the effect of using such STC curves in conjunction with various antennas.